

The Hong Kong Polytechnic University

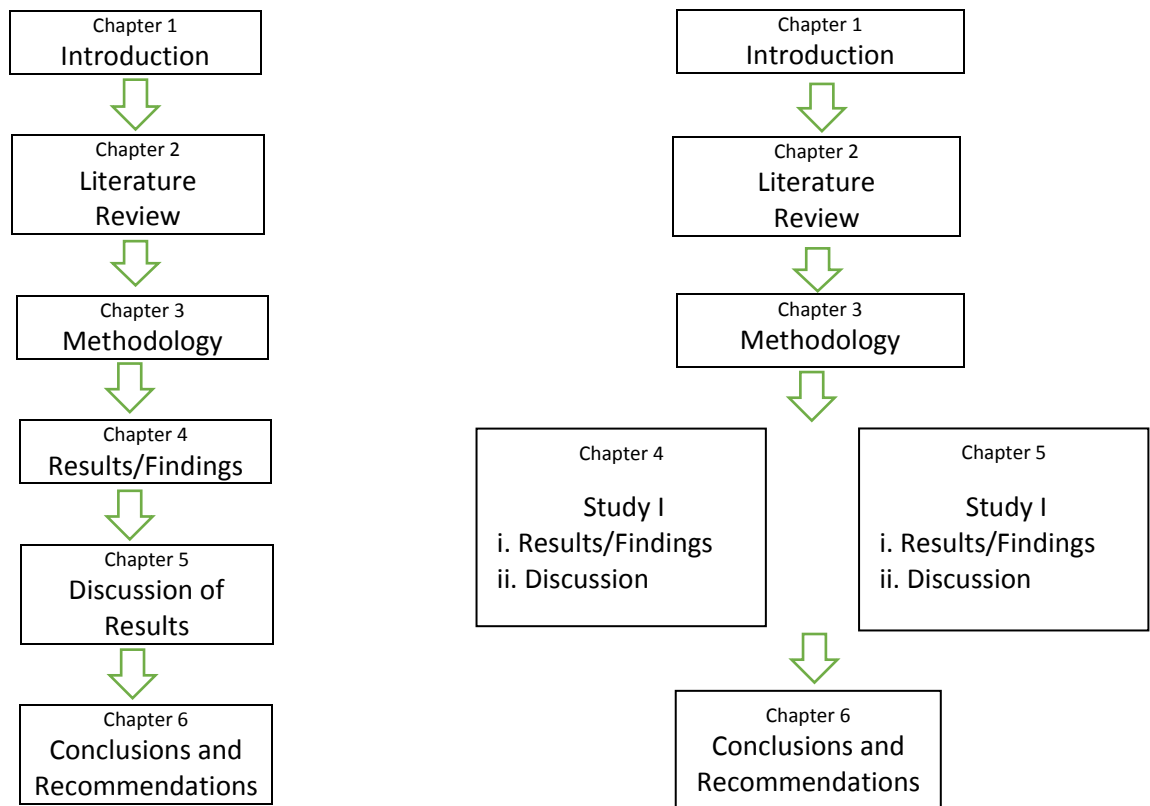
Department of Civil and Environment Engineering

Degradation of Refractory Contaminants in Water by Chemical-Free Radicals Generated by Ultrasound and UV Irradiation

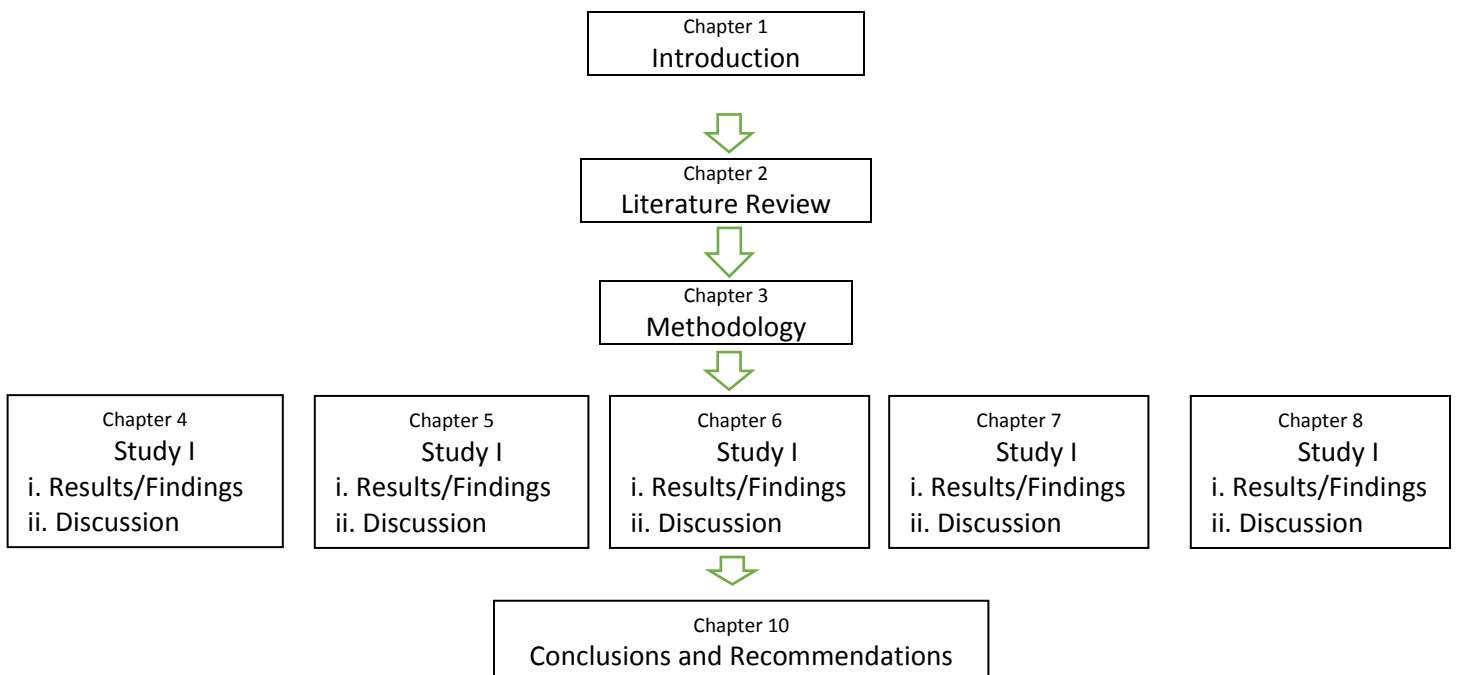
**A thesis submitted in partial fulfillment of the requirements of the
Degree of Doctor of Philosophy**

2014

Theses are usually organised in the following ways:



This thesis is organised as shown here



Abstract

The abstract is the first part of a thesis dissertation and should be a short summary of the entire thesis. Its purpose is to attract people to read your thesis. Abstracts normally include a number of aspects including: the background, the importance of topic, the purpose of the research, the methodology used in the study, the key findings and the implications the findings will have. The abstract should be very short and precise.

This abstract is very effective partly because the writer includes the following:

Structure

Background	↓	paragraph 1, sentence 1-2
Aims	↓	paragraph 1, sentence 3
Methods	↓	e.g. paragraph 2, sentence 1-3
Results	↓	paragraph 2, sentence 4-8

Content

- Describes the background to the topic (e.g. paragraph 1, sentence 1-2)
- Highlights the gap in current understanding of the problem (e.g. paragraph 1, sentence 2)
- Gives the scope of the research (e.g. paragraph 1, sentence 3)
- Describes the methodology used in each investigation (e.g. paragraph 2, sentence 2)
- Describes the main finding of each investigation (e.g. paragraph 2, sentence 2-5)
- Gives details of the important results of each investigation (e.g. paragraph 2, sentence 4)
- Uses and defines key terms (e.g. paragraph 4 sentence 1).
- Introduces abbreviations of key terms that appear in the thesis (e.g. paragraph 1 sentence 2-3)

Language

- Uses present perfect tense when describing the background (e.g. paragraph 1, sentence 1)

- Uses a new paragraph to summarise each investigation
- Provides a topic sentence for each paragraph (e.g. paragraph 3 sentence 1)
- Uses past simple tense and passive voice to describe methodology and findings, e.g. was found (e.g. paragraph 5, sentence 6)

To Consider

In general, this abstract is effective. However, it could be further improved in the following aspects.

- 💡 Highlight how the findings can be used in further research.
- 💡 Explain how the findings will aid the wider community.
- 💡 Explain the limitations of the research.
- 💡 Avoid the overuse of linking words at the start of each paragraph. It is better to incorporate them into the topic sentence, e.g. *A second investigation examined...*
- 💡 Use vocabulary to show the importance of the work, e.g. *contamination has serious negative consequences on human health and clean would potentially improve millions of people's lives.*
- 💡 Use vocabulary to show the success of the research conducted, e.g. *the results clearly demonstrates that...*
- 💡 Avoid including too much detail in the abstract.

ABSTRACT

The contamination of water bodies by endocrine disrupting compounds (EDCs) has drawn increasing attention in recent decades because of their potential adverse effects on aquatic lives and human health. The inefficiency of biological treatment methods in degrading EDCs promoted the development of various kinds of advanced oxidation technologies (AOTs). In this study, a chemical-free AOT by combining high frequency ultrasound and ultraviolet irradiation (i.e. US/UV) was proposed and intensively investigated to degrade different kinds of EDCs, including dimethyl phthalate (DMP), di-*n*-butyl phthalate (DBP), diethyl phthalate (DEP), monomethyl phthalate (MMP), atrazine (ATZ), and nonylphenol (NP).

Initially, a prototype US/UV unit consisting of a 400 kHz ultrasonic system and a photolytic system at 253.7 nm was set up by using DMP as a probe compound. Several important parameters were evaluated, including ultrasonic frequency, ultrasonic power, initial concentration of the probe compound, initial solution pH, UV light intensity, and the effect of H₂O₂, etc. Both the ultrasonic frequency and power density played important roles in ultrasonic process. The optimal performance in this study was obtained by a 400 kHz frequency and the maximum input power of 120 W. In addition, the ultrasonic degradation rate increased directly with power density, and decreased moderately with increasing pH in the range typically found in the environment (pH 5 – 9). Higher initial concentration resulted in a smaller rate constant. The addition of hydrogen peroxide can increase the radical generation to some extent. It was also found that higher UV light intensity was beneficial for both the photolysis and sonophotolysis of DMP.

Furthermore, the synergistic effect and mechanisms of the hybrid process (US/UV) was investigated. The role of ultrasonically generated hydrogen peroxide was examined qualitatively and quantitatively, and its generation and photo-decomposition were found to be the principal reason for the process synergy. The sonolysis and photolysis of the investigated compounds all followed pseudo first-order kinetics, but the sonophotolysis of different compounds exhibited different kinetics. A novel inverted S-curve model was developed and found to successfully describe the sonophotolytic process and the degradation of different compounds. Different compounds also demonstrated different magnitudes of synergistic effect due to their different physicochemical properties (e.g. the hydrophobicity and the photochemical properties).

In addition, the distinct feature of ultrasonic process, i.e. the heterogeneous micro-environment that exists between cavitation bubbles and bulk solution, was investigated by comparing the degradation performance of ATZ in two different ultrasonic processes (20 kHz and 400 kHz). The better heterogeneous distribution of solutes in the 400 kHz ultrasound allowed a faster degradation of hydrophobic compounds than that in the 20 kHz ultrasound. Moreover, the sonophotolytic degradation of a group of phthalate acid esters (PAEs) with different physicochemical properties was compared. It was found that although stronger hydrophobicity was beneficial for the sonochemical degradation of PAEs, it was adverse to obtaining remarkable synergistic effect in the sonophotolytic process due to the less accumulation of H_2O_2 .

Moreover, the influence of some background species (e.g. radical scavengers, ions in wastewater) was also evaluated. The mechanism of sonochemical degradation of the

involved compounds in this study was found all via radical oxidation near the bubble-liquid interfaces and in the bulk solution rather than pyrolysis inside the cavitation bubbles by employing different kinds of radical scavengers. The presence of ferrous ions (Fe^{2+}) in solution gave rise to a homogeneous sono-photo-Fenton (US/UV/ Fe^{2+}) process, and clear synergistic effects were observed in the US/UV/ Fe^{2+} process which led to it having the greatest impact on DBP degradation. The presence of NaCl demonstrated different effects on the 400 and 20 kHz ultrasonic processes, mainly because of the competition between “salting out” effect and surface tension, and they were also influenced by the different heterogeneous environments in different ultrasonic processes. The background total organic carbon (TOC) coming from wastewater effluent hindered the sonophotolysis of PAEs, and PAEs with stronger hydrophobicity experienced less inhibition by background TOC. Nitrate ions (NO_3^-), the most commonly seen constituent in the secondary effluent and the main component of total nitrogen, had a beneficial effect on the sonophotolytic degradation of NP and the main mechanism was found to be acting as a photosensitizer.

Finally, the degradation mechanisms of the investigated compounds and mineralization efficiencies in the US, UV, and US/UV processes were investigated. Results showed that the ultrasonic process was effective in degrading more hydrophobic target compounds, but less efficient in degrading their more hydrophilic intermediates. However, the involvement of UV process could promote the degradation of these less hydrophobic intermediates via direct photolysis or producing additional hydroxyl radicals in the bulk solution by photodissociation of hydrogen peroxide. The combined US/UV process also had the best mineralization performance compared to individual US or UV process.

[REDACTED]

[REDACTED]

[REDACTED]

[REDACTED]

[REDACTED]

[REDACTED]

[REDACTED]

[REDACTED]

[REDACTED]

[REDACTED]

[REDACTED]

[REDACTED]

[REDACTED]

[REDACTED]

[REDACTED]

[REDACTED]

[REDACTED]

[REDACTED]

[REDACTED]

[REDACTED]

[REDACTED]

[REDACTED]

[REDACTED]

[REDACTED]

[REDACTED]

[REDACTED]

[REDACTED]

[REDACTED]

[REDACTED]

[REDACTED]

[REDACTED]

[REDACTED]

[REDACTED]

[REDACTED]

[REDACTED]

[REDACTED]

[REDACTED]

[REDACTED]

[REDACTED]

[REDACTED]

[REDACTED]

[REDACTED]

[REDACTED]

[REDACTED]

[REDACTED]

[REDACTED]

TABLE OF CONTENTS

CERTIFICATE OF ORIGINALITY	I
DEDICATION.....	II
ABSTRACT.....	III
PUBLICATIONS ARISING FROM THE THESIS.....	VI
ACKNOWLEDGEMENTS	VIII
TABLE OF CONTENTS.....	IX
LIST OF FIGURES	XV
LIST OF TABLES AND SCHEMES.....	XXII
LIST OF ABBREVIATIONS	XXIV
1. Chapter One Introduction.....	1
1.1. Background.....	1
1.2. Aims and objectives.....	4
1.3. Structures of this thesis	5
2. Chapter Two Literature Review	8
2.1. Probe compounds.....	8
2.1.1. Dimethyl phthalate.....	8
2.1.1.1. Basic information.....	8
2.1.1.2. Toxicological effects and environmental fate	8
2.1.1.3. Previous studies of DMP degradation	9
2.1.2. Atrazine.....	10
2.1.2.1. Basic information.....	10
2.1.2.2. Toxicological effects and environmental fate	10

2.1.2.3.	Previous studies of ATZ degradation	11
2.1.3.	Di- <i>n</i> -butyl phthalate	13
2.1.3.1.	Basic information	13
2.1.3.2.	Toxicological effects and environmental fate	13
2.1.3.3.	Previous studies of DBP degradation	14
2.1.4.	Nonylphenol	14
2.1.4.1.	Basic information	14
2.1.4.2.	Toxicological effects and environmental fate	15
2.1.4.3.	Previous studies of NP degradation	16
2.2.	Advanced oxidation processes	18
2.2.1.	Sonochemical process	18
2.2.1.1.	Theories of acoustic cavitation	18
2.2.1.2.	Sonochemical reaction systems	20
2.2.1.3.	Sonochemical process applied in water pollution remediation	24
2.2.2.	UV photolysis	26
2.2.2.1.	Photochemical principles	26
2.2.2.2.	Photochemical reactions	28
2.2.2.3.	UV photolysis applied in water pollution remediation	29
3.	Chapter Three Materials and Methodology	31
3.1.	Chemicals and reagents	31
3.2.	Apparatus and experimental conditions	33
3.2.1.	Ultrasound units	33
3.2.2.	Photo-reactor	35
3.2.3.	The sonopholytic reaction unit	36

3.2.4.	Other experimental conditions and procedures.....	37
3.3.	Analytical methods	38
3.3.1.	Quantification of target compounds.....	38
3.3.2.	Hydrogen peroxide determination	41
3.3.3.	Calorimetric measurement	41
3.3.4.	Intermediates identification.....	41
3.3.5.	TOC and TN measurement	45
3.3.6.	Other analytical methods	45
4.	Chapter Four Degradation of Dimethyl Phthalate Using a High-Frequency Ultrasonic Process	46
4.1.	Overview.....	46
4.2.	Results and discussion	47
4.2.1.	Ultrasonic frequency optimization.....	47
4.2.2.	Effect of power density	49
4.2.3.	Effect of initial DMP concentration	53
4.2.4.	Effects of initial solution pH on DMP sonolytic degradation.....	56
4.2.5.	Effect of addition of hydrogen peroxide on DMP decomposition	58
4.2.6.	Identification of reaction intermediates from DMP sonolysis	60
4.3.	Chapter summary.....	67
5.	Chapter Five Sonophotolytic Degradation of Dimethyl Phthalate: Analysis of the Synergistic Effect and Modeling	68
5.1.	Overview.....	68
5.2.	Results and discussion	69
5.2.1.	Effect of UV light intensity.....	69

5.2.2.	Formation of H ₂ O ₂ during sonication	72
5.2.3.	DMP degradation by UV/H ₂ O ₂ process	73
5.2.4.	Effect of initial solution pH	76
5.2.5.	Sequential and simultaneous tests of US and UV	78
5.2.6.	Modeling the sonopholytic degradation of DMP	81
5.3.	Chapter summary	86
6.	Chapter Six Atrazine Degradation Using Chemical-Free Process of US/UV: Analysis of the Heterogeneous Micro-Environments and the Degradation Mechanisms..	87
6.1.	Overview.....	87
6.2.	Results and discussion	88
6.2.1.	Kinetics of individual UV, US processes	88
6.2.2.	Kinetics of sonopholytic degradation of ATZ.....	90
6.2.3.	Mechanisms of sonolytic degradation of ATZ	94
6.2.4.	Salt effect on sonolytic degradation of ATZ	98
6.2.5.	UV absorption spectra.....	103
6.2.6.	Identification of intermediates and degradation pathways	105
6.2.7.	Mineralization	112
6.3.	Chapter summary	114
7.	Chapter Seven Degradation of Di-<i>n</i>-butyl Phthalate by a Homogeneous Sono- Photo-Fenton Process with In-Situ Generated Hydrogen Peroxide.....	116
7.1.	Overview.....	116
7.2.	Results and discussion	118
7.2.1.	Comparison of US/UV/Fe ²⁺ and related processes.....	118

7.2.2.	H ₂ O ₂ formation in US, UV, and US/UV processes	120
7.2.3.	Properties of Sono-Fenton (US/Fe ²⁺) process.....	123
7.2.4.	Synergistic effect of UV/Fe ²⁺	125
7.2.5.	Effect of initial pH	129
7.2.6.	Effect of Fe ²⁺ dosage.....	131
7.3.	Chapter summary	135
8.	Chapter Eight Sonophotolytic Degradation of Phthalate Acid Esters in Water and Wastewater: Effects of Physicochemical Properties of the Compounds and Degradation Mechanisms	136
8.1.	Overview.....	136
8.2.	Results and discussion	138
8.2.1.	Effect of physicochemical properties on PAE sonolysis.....	138
8.2.2.	Effect of radical scavengers on sonolytic degradation of PAEs	143
8.2.3.	Effect of physicochemical properties on PAE sonophotolytic degradation	144
8.2.4.	Sonophotolytic degradation of PAEs in real wastewater	147
8.2.5.	Degradation mechanisms of DBP	150
8.3.	Chapter summary	155
9.	Chapter Nine Efficient Degradation of Hydrophobic Nonylphenol in Solution by a Green Technology of Sonophotolysis.....	156
9.1.	Overview.....	156
9.2.	Results and discussion	156
9.2.1.	Optimization of synergistic effect.....	156
9.2.2.	Effect of initial solution pH	159
9.2.3.	Effect of nitrate on sonophotolysis of NP.....	161

9.2.4. Reaction mechanism and degradation product of NP sonophotolysis under different conditions	166
9.3. Chapter summary.....	171
10. Chapter Ten Conclusions and Recommendations.....	172
10.1. Conclusions.....	172
10.2. Limitations of this study and recommendations for future work.....	175
Appendix I: Mass spectra of DMP and its major intermediates	177
Appendix II: Mass spectra of ATZ and its major intermediates	180
Appendix III: Mass spectra of DBP and its major intermediates	183
Appendix IV: Mass spectra of NP and its major intermediates.....	188
References	191

LIST OF FIGURES

Figure 2-1: Three reaction zones in the cavitation process, adapted from (Adewuyi 2001).	24
Figure 2-2: The primary routes to loss of electronic excitation (the use of symbols [*] , [‡] , and [†] is only intended to illustrate the presence of electronic excitation and not necessarily differences in states), adapted from (Wayne and Wayne 1996)...	27
Figure 3-1: Schematic diagram of the ultrasonic apparatus at the frequencies of 400, 800, and 1200 kHz.....	33
Figure 3-2: Schematic diagram of the 20 kHz ultrasonic apparatus (applied in Chapter Six).	35
Figure 3-3: The set-up diagram of the sonopholytic reaction unit.....	36
Figure 3-4: The HPLC system (Waters) used for quantification of the target compounds.	39
Figure 3-5: The UV absorption spectra of 0.01 mM DMP, DEP, DBP, and MMP.	39
Figure 3-6: The UV absorption spectra of 0.02 mM ATZ.....	40
Figure 3-7: The UV absorption spectra of 0.5 mM NP dissolved in ACN.	40
Figure 3-8: The Thermo Quest Finnigan LCQ Duo HPLC/MS system.	43
Figure 3-9: The Bruker amaZon SL UPLC/MS system.....	43
Figure 3-10: The composition and gradient programmes of the mobile phase used for the detection of DBP and its degradation intermediates in Chapter Eight.	44
Figure 3-11: The composition and gradient programme of the mobile phase used for the detection of NP and its degradation intermediates in Chapter Nine.	44
Figure 4-1: Temporal variation of DMP concentrations in the sonolytic processes with	

	different ultrasonic frequencies and powers ($[DMP]_0 = 0.1 \text{ mM}$).	47
Figure 4-2:	Temporal variation of DMP concentration in the sonolytic processes with different solution volumes ($[DMP]_0 = 0.1 \text{ mM}$; ultrasound: 400 kHz–120 W).	50
Figure 4-3:	Initial temperature increase of pure water in the 400 kHz ultrasound with 125 mL water volume.....	50
Figure 4-4:	Variation of DMP degradation rate and power density with solution volume ($[DMP]_0 = 0.1 \text{ mM}$; ultrasound: 400 kHz–120 W).....	51
Figure 4-5:	Effect of initial DMP concentrations on DMP degradation (ultrasound: 400 kHz–120 W).....	54
Figure 4-6:	Effect of initial solution pH on DMP sonolysis ($[DMP]_0 = 0.05 \text{ mM}$; ultrasound: 400 kHz–120 W).....	57
Figure 4-7:	Influence of hydrogen peroxide dose on the DMP degradation rate (ultrasound: 400 kHz–120 W).....	58
Figure 4-8:	The concentration evolution of DMP and the detected sonolysis intermediates of DMP (ultrasound: 400 kHz–120 W; $C_0 = 0.25 \text{ mM}$).....	60
Figure 4-9:	HPLC/ESI-MS chromatogram of DMP and its degradation intermediates after 4 h sonolysis (ultrasound: 400 kHz–120 W; $C_0 = 0.25 \text{ mM}$).....	65
Figure 5-1:	Effect of UV light intensity on DMP photolytic degradation ($C_0 = 0.05 \text{ mM}$, UV: $\lambda = 253.7 \text{ nm}$).....	71
Figure 5-2:	Effect of UV light intensity on DMP sonophotolytic degradation ($C_0 = 0.05 \text{ mM}$, UV: $\lambda = 253.7 \text{ nm}$, US: 400 kHz–120 W).	71
Figure 5-3:	Variation of H_2O_2 concentration over sonication time (US: 400 kHz–120 W).	72

Figure 5-4: Degradation of DMP by UV/H₂O₂ process with different initial H₂O₂ concentrations and degradation of DMP by stepwise UV/H₂O₂ process (UV: $\lambda = 253.7$ nm, 6 lamps, [DMP]₀ = 0.05 mM). 73

Figure 5-5: Effect of initial solution pH on DMP sonophotolytic ([DMP]₀ = 0.05 mM, UV: $\lambda = 253.7$ nm, 6 lamps, US: 400 kHz–120 W). 77

Figure 5-6: DMP degradation performance of sequential and simultaneous experiments using US: 400 kHz–120 W and UV: 253.7 nm, 6 lamps, [DMP]₀ = 0.05 mM. 80

Figure 5-7: The variation of H₂O₂ concentration during the sequential and simultaneous tests using US: 400 kHz–120 W and UV: 253.7 nm, 6 lamps, [DMP]₀ = 0.05 mM. 80

Figure 5-8: Modeling DMP degradation in the process of US/UV and comparison with the experimental data. (UV: 253.7 nm, 6 lamps; US: 400 kHz–120 W; $k_{US} = 0.0076 \text{ min}^{-1}$, $k_{UV} = 0.0015 \text{ min}^{-1}$, $k_3 = 0.5060 \text{ min}^{-1} \cdot \text{mM}^{-1}$, $k_1 = 6.97 \times 10^{-4} \text{ mM} \cdot \text{min}^{-1}$, $C_0 = 0.0484 \text{ mM}$). 84

Figure 6-1: Performance of the photolytic, sonolytic, and sonophotolytic degradation of ATZ ([ATZ]₀ = 0.02 mM; UV: 253.7 nm, 1 lamp; US: 400 kHz, 0.03 W mL⁻¹). 88

Figure 6-2: H₂O₂ formation in ultrasonic process in the presence or absence of ATZ. 92

Figure 6-3: ATZ degradation in the UV/H₂O₂ process with different [H₂O₂]₀ ([ATZ]₀ = 0.02 mM). 92

Figure 6-4: The application of kinetics model for the sonophotolytic degradation of ATZ (IE = -0.0706t; SE = $-1.14 \times 10^{-4} t^2$; 400 kHz). 93

Figure 6-5: The application of kinetics model for the sonophotolytic degradation of DMP

	(IE = -0.0091t; SE = -1.76×10 ⁻⁴ t ² , detailed data are shown in Chapter Five, 5.2.6).....	93
Figure 6-6:	Effect of different radical scavengers on the sonodegradation of ATZ ([ATZ] ₀ = 0.02 mM). (a) Fenton process (reference); (b) 400 kHz ultrasound; (c) 20 kHz ultrasound.	96
Figure 6-7:	Effect of NaCl addition on ATZ sonodegradation (400 kHz and 20 kHz US processes). Inset: variation of ATZ partition (between aqueous and <i>n</i> -octanol phases) and surface tension with [NaCl] ([ATZ] ₀ = 0.02 mM).....	99
Figure 6-8:	The determination of CMC value of Triton X-100.	102
Figure 6-9:	Variation of the UV absorption spectra of the reaction solution in the individual process of UV or US ([ATZ] ₀ = 0.02 mM).	104
Figure 6-10:	Temporal profiles of ATZ degradation and formation of principal intermediates in the photolytic process ([ATZ] ₀ = 0.1 mM). Inset: OIET degradation under US, UV, US/UV processes ([OIET] ₀ = 0.02 mM).....	109
Figure 6-11:	Mass spectra of HIET.	111
Figure 6-12:	Temporal profiles of ATZ degradation and formation of principal intermediates in the sonolytic process ([ATZ] ₀ = 0.1 mM).....	111
Figure 6-13:	The separated HPLC peaks of the sonolytic degradation intermediates at the early, middle, and end stages.	112
Figure 6-14:	Evolution profiles of TOC concentration in the UV, US, and US/UV processes ([ATZ] ₀ = 0.1 mM).	113
Figure 7-1:	DBP degradation performance under different processes (conditions: [DBP] ₀ = 0.01 mM; [Fe ²⁺] ₀ = 0.1 mM; [pH] ₀ = 6.5 ± 0.05).	119
Figure 7-2:	(a) Variation of H ₂ O ₂ concentration with reaction time in the processes of US,	

	UV, and US/UV ($[\text{DBP}]_0 = 0.01 \text{ mM}$; $[\text{Fe}^{2+}]_0 = 0.1 \text{ mM}$; $[\text{pH}]_0 = 6.5 \pm 0.05$);	
	(b) Variation of H_2O_2 concentration under UV irradiation with different $[\text{H}_2\text{O}_2]_0$ ($[\text{DBP}]_0 = 0.01 \text{ mM}$; $[\text{Fe}^{2+}]_0 = 0.1 \text{ mM}$; $[\text{pH}]_0 = 6.5 \pm 0.05$; $[\text{H}_2\text{O}_2]_0 = 0.025 - 0.2 \text{ mM}$).....	122
Figure 7-3:	Variation of DBP and Fe^{2+} concentrations with reaction time in the US/ Fe^{2+} process and conventional Fenton process (conditions: $[\text{DBP}]_0 = 0.01 \text{ mM}$; $[\text{Fe}^{2+}]_0 = 0.1 \text{ mM}$; $[\text{pH}]_0 = 6.5 \pm 0.05$; $[\text{H}_2\text{O}_2]_0$ in conventional Fenton is 0.065 mM).....	123
Figure 7-4:	(a) Variation of DBP concentration in UV/ Fe^{2+} and related processes with/without radical scavengers; (b) Variation of $[\text{Fe}^{2+}]$ in the UV/ Fe^{2+} and related processes ($[\text{DBP}]_0 = 0.01 \text{ mM}$; $[\text{Fe}^{2+}]_0 = 0.1 \text{ mM}$; $[\text{pH}]_0 = 6.5 \pm 0.05$; $[\text{MeOH}]_0 = 10 \text{ mM}$; $[\text{KBr}]_0 = 10 \text{ mM}$; Six UV ₂₅₄ lamps; quartz beaker). ...	128
Figure 7-5:	Effect of initial solution pH on DBP degradation in the processes of (a) US/ Fe^{2+} ; (b) UV/ Fe^{2+} ; (c) US/UV/ Fe^{2+} (conditions: $[\text{DBP}]_0 = 0.01 \text{ mM}$; $[\text{pH}]_0 = 2.08 - 9.21$; $[\text{Fe}^{2+}]_0 = 0.1 \text{ mM}$).	131
Figure 7-6:	Effect of initial Fe^{2+} concentration on DBP degradation in the processes of (a) US/ Fe^{2+} ; (b) UV/ Fe^{2+} ; (c) US/UV/ Fe^{2+} (conditions: $[\text{DBP}]_0 = 0.01 \text{ mM}$; $[\text{pH}]_0 = 6.5 \pm 0.05$; $[\text{Fe}^{2+}]_0 = 0 - 0.5 \text{ mM}$).....	134
Figure 8-1:	Temporal variation of PAE concentrations during the sonolysis process ($C_0 = 0.01 \text{ mM}$, solid points: separate reaction, hollow points: mixed reaction). .	138
Figure 8-2:	Correlation between the physicochemical parameters and the pseudo first-order rate constants of different PAEs ($C_0 = 0.01 \text{ mM}$, solid points: separate reaction, hollow points: mixed reaction).....	142
Figure 8-3:	Effect of radical scavengers (100 mM tert-butanol or 2 mM KBr) on the	

sonolytic degradation of PAEs ($C_0 = 0.01$ mM).....	143
Figure 8-4: Temporal variation of PAEs concentrations during the photolytic and sonophotolytic processes ($C_0 = 0.01$ mM).	146
Figure 8-5: Formation of hydrogen peroxide in solution during the sonochemical reaction with the presence of either 0.01 mM MMP or 0.01 mM DBP.	147
Figure 8-6: Variation of pseudo first-order rate constants (k) of different PAEs in the sonophotolytic process mediated by different dissolved TOC concentrations from wastewater (inset: correlation between TOC inhibiting index K and K_{ow} of different PAEs).	149
Figure 9-1: Temporal variation of NP concentrations in the sonolytic, photolytic and sonophotolytic degradation processes ($C_0 = 0.01$ mM, UV: 2 lamps).	158
Figure 9-2: Effect of initial solution pH on the sonophotolytic degradation of NP ($C_0 = 0.01$ mM; UV: 2 lamps).	160
Figure 9-3: The extracted ion chromatogram of nonanoic acid ($[M-H]^- = 157.2$) of the 60 min reaction solution in the sonophotolytic process at $pH_0 = 11.12$ and $pH_0 = 6.5$ (control experiment) conditions.	161
Figure 9-4: Effect of nitrate on NP degradation in sonophotolytic, sonolytic, and photolytic processes.	164
Figure 9-5: The UV absorption spectra of nitrate in different concentrations.	165
Figure 9-6: Effect of hydroxyl radical scavenger on NP photolytic degradation under different conditions ($C_0 = 0.01$ mM, $[NO_3^- - N] = 10$ mg L ⁻¹ , $[MeOH] = 20$ mM).	165
Figure 9-7: Temporal profiles of NP degradation and formation of primary intermediates in the sonophotolytic process ($[NP]_0 = 0.015$ mM, UV: 2 lamps, $pH_0 = 6.5$).	

LIST OF TABLES AND SCHEMES

Table 2-1:	Summary of the characteristic parameters of DMP, ATZ, DBP, and NP at 25 °C (unless otherwise stated) (USNLM).....	17
Table 2-2:	Summary of the sonochemical reactions in the cavitation events (Adewuyi 2001).....	23
Table 3-1:	List of chemicals and reagents used in this study.....	31
Table 3-2:	HPLC conditions for the quantification of different target compounds.....	38
Table 4-1:	Calorimetric results of 400 kHz – 120 W ultrasound ($[DMP]_0 = 0.1 \text{ mM}$)... ..	52
Table 4-2:	Information of the identified intermediates from DMP sonolysis determined by LC/ESI-MS.....	63
Table 6-1:	Details of the identified intermediates of ATZ degradation.	107
Table 7-1:	The pseudo first-order rate constants of different processes	119
Table 8-1:	Summary of the physicochemical properties of the investigated PAEs ($\log K_{ow}$: octanol-water partition coefficient; S_w , water solubility at 25 °C; V_p : vapor pressure at 25 °C; K_H : Henry's law constant at 25 °C; k_{OH} : •OH reaction rate constant at 25 °C) (USNLM, http://toxnet.nlm.nih.gov/).....	140
Table 8-2:	The pseudo first-order rate constants and removal rate in 90 min of different PAEs in the sonolytic process, either in separate reaction or in mixed reaction ($C_0 = 0.01 \text{ mM}$ for each PAE).	141
Table 8-3:	The pseudo first-order rate constants (k_{us}) of different PAEs in the sonolytic degradation with or without the presence of KBr (2 mM) as a radical scavenger.	144
Table 8-4:	The pseudo first-order rate constants of PAEs degradation in the sonolytic,	

	photolytic, and sonophotolytic processes, and the synergistic index for different PAEs in the sonophotolytic processes.	146
Table 8-5:	Parameters of secondary effluent of domestic wastewater used in this study.	149
Table 8-6:	Information of the identified intermediates from DBP degradation.	150
Table 9-1:	Pseudo first-order rate constants of NP degradation in photolytic and sonophotolytic processes and the corresponding synergistic index at different UV light intensities (ref. $k_{US} = 0.0264 \text{ min}^{-1}$).	158
Table 9-2:	Summarization of the identified intermediates of NP sonophotolysis determined by LC/ESI-MS.	166
Scheme 4-1:	Degradation pathways of sonochemical degradation of DMP (Dashed arrows indicate reactions that require more than one step).	66
Scheme 6-1:	Degradation pathways of ATZ for the UV, US, and US/UV processes. The double arrow denotes reaction more than one step.	110
Scheme 8-1:	Degradation pathways of DBP for the US, UV, and US/UV processes (the double arrow denotes reaction requiring more than one step).	154
Scheme 9-1:	Degradation pathways of NP sonophotolysis under different conditions (normal condition: neutral pH_0 without NO_3^- ; $\text{pH}_0 = 11.15$ without NO_3^- ; neutral pH_0 with $10 \text{ mg L}^{-1} \text{ NO}_3^-$).	170

LIST OF ABBREVIATIONS

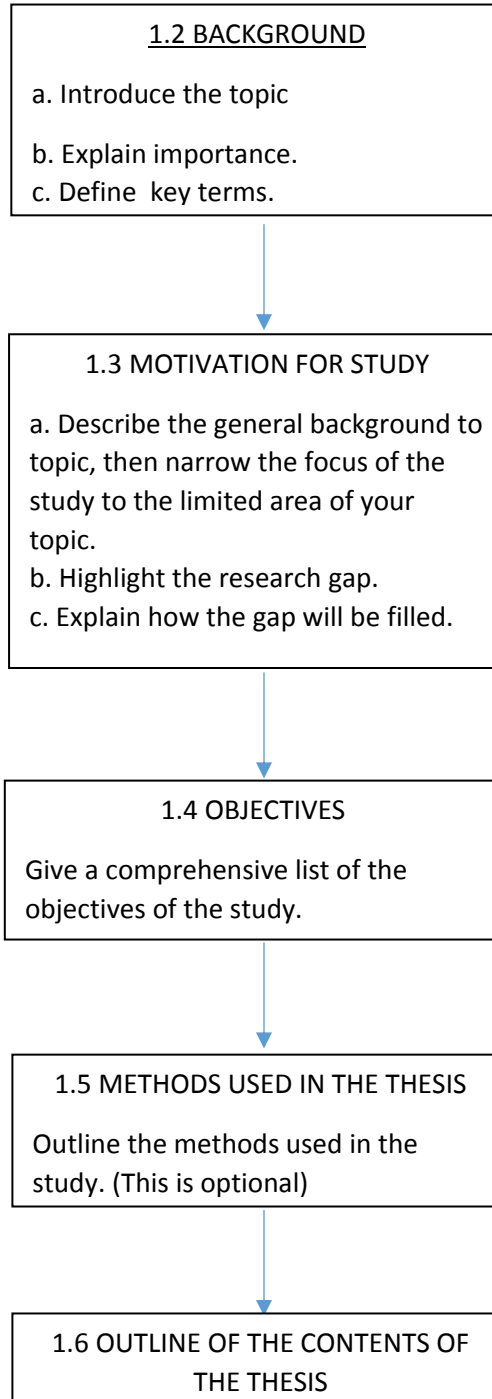
EDCs	Endocrine disrupting compounds
WWTPs	Waste water treatment plants
COD	Chemical oxygen demand
AOTs	Advanced oxidation technologies
NHE	Normal hydrogen electrode
UV	Ultraviolet irradiation
US	Ultrasonic irradiation
US/UV	Sonophotolytic process
DMP	Dimethyl phthalate
DBP	Di- <i>n</i> -butyl phthalate
NP	Nonylphenol
ATZ	Atrazine
APEOs	Alkyl phenol ethoxylates
PAEs	Phthalate acid esters
EPA	Environmental protection agency
OIET	2-hydroxyatrazine
EC50	The half maximal effective concentration
IC50	The half maximal inhibitory concentration
NPEOs	Nonylphenol ethoxylates
HFUS	High-frequency ultrasonic system
MMP	Monomethyl phthalate

PA	Phthalic acid
DEP	Diethyl phthalate
HPLC	High performance liquid chromatography
DDW	Deionized-distilled water
ACN	Acetonitrile
ESI	Electrospray ionization
TOC	Total organic carbon
TN	Total nitrogen
VUV	Vacuum ultra violet
LC/MS	Liquid chromatography tandem mass spectrometry
PDA	Photo diode array
TBA	<i>t</i> -butanol
CMC	Critical micelle concentration
UPLC	Ultra-high performance liquid chromatography
TIC	Total ion chromatogram
SI	Synergistic index

The Introduction

The Introduction chapter is usually organised in the following way:

1.1 INTRODUCTION




1.7 SUMMARY

Chapter 1: Introduction

The introduction chapter is designed to help the reader better understand the technical sections of the thesis by giving an overview. It normally includes the following: the reasons for the research, the scope of the research and its scientific importance, the introduction, explanation and definition of key terms, an introduction of the most important current studies in your field, an overview of the methodology used and an overview of the way the thesis is organized, with a short summary of each chapter.

This introduction is very effective partly because the writer includes the following:

Structure

(Introduction)		Not included
Background		Section 1.1
Objectives		Section 1.2
Outline of the Thesis		Section 1.3
(Conclusion/summary)		Not included

Content

- Introduces the problem (e.g. Section 1.1, paragraph 1, sentence 2)
- Defines key terms and introduces their abbreviations (e.g. Section 1.1, paragraph 1, sentence 3)
- Describes the current situation (e.g. Section 1.1, paragraph 2, sentence 2-5)
- Cites key studies on the topic (e.g. Section 1.1, paragraph 2, sentence 3)
- Discusses possible solutions (e.g. Section 1.1, paragraph 3)
- Evaluates the suggested solutions (e.g. Section 1.1 paragraph 4)
- Identifies a gap in knowledge (e.g. Section 1.1, paragraph 4, final sentence)
- Defines the scope of the research (e.g. Section 1.1, paragraph 5, sentence 4)

Language

- Sums up section 1.1 with a short paragraph (e.g. Section 1.1, paragraph 6)
- Lists aims in point form (e.g. Section 1.2)
- Introduces each point form using the same grammatical structure (e.g. Section 1.2)

- Uses one paragraph for each chapter (e.g. Section 1.3 paragraph 4)
- Uses a range of styles to introduce each paragraph in section 1.3 (e.g. Section 1.3 paragraph 2-4, sentence 1)
- Gives short clear subheadings titles and numbers

To Consider

This chapter of the thesis is effective. However, it could be further improved in the following aspects.

💡 Include the page number in the citation when using a direct quote (e.g. Section 1.1, paragraph 1, sentence 1).

💡 State the contribution the research will make.

💡 Avoid spoken expressions, e.g. *great* (e.g. Section 1.1, paragraph 5, sentence 1).

💡 Provide a short summary paragraph at the end of the chapter which links to the next chapter.

1. Chapter One Introduction

1.1. Background

In recent years, various kinds of organic pollutants, natural or synthetic, have been identified in surface water, groundwater, and other aqueous resources. Some of these organic contaminants can mimic natural hormones in the endocrine systems of animals, which are now collectively known as endocrine disrupting compounds (EDCs) (Snyder et al. 2003). By definition, the EDCs are “as exogenous agents that interfere with the synthesis, secretion, transport, binding, action, or elimination of natural hormones in the body that are responsible for the maintenance of homeostasis, reproduction, development, and/or behavior” (U.S. Environmental Protection Agency 1997). The major source of surface water contamination with EDCs is sewage effluent from both domestic and industrial facilities (Gultekin and Ince 2007). Increasing attention has been paid to EDCs contamination because of their potential adverse effects on environment and human health via drinking water and/or cyclic processes of biotransformation and bioconcentration.

Most wastewater treatment plants (WWTPs) employ conventional treatment processes (coagulation, sedimentation, filtration, activated sludge technology, etc.) due to the cost effective advantages and the capacity of simultaneous removal of chemical oxygen demand (COD) and other nutrients (e.g. nitrogen and phosphorus) from the aqueous phase (Chan et al. 2009). Nevertheless, the fast growth of microbes may also arise the problem of further sludge treatment. In addition, some of the organic substances cannot achieve successful degradation by conventional processes, and the metabolic intermediates or even the intact

original compounds transferring from the aqueous phase to the solid phase may still pose environmental pollution problems. In addition, many studies have shown that the conventional treatment processes were ineffective in eliminating the refractory EDCs (Rahman et al. 2010, Stackelberg et al. 2007, Ternes 1998, Vieno et al. 2007). Therefore, the EDCs present in the final effluent, even at low concentrations, are still toxicologically significant.

The advanced oxidation technologies (AOTs) have attracted considerable interests in the wastewater treatment processes, which have been applied successfully for the degradation of recalcitrant pollutants, either as tertiary treatment methods or as pretreatment methods to convert pollutants into shorter-chain compounds so as to facilitate their further treatment (Wang and Xu 2012). The mechanisms of the AOTs are mainly based on the generation of highly reactive radical species, among which the hydroxyl radical ($\bullet\text{OH}$) is the most frequent and principal species (Esplugas et al. 2007). Due to its high standard potentials (1.8 – 2.7 V) versus normal hydrogen electrode (NHE), the hydroxyl radical is highly reactive and nonselective that can oxidize and mineralize numerous organic compounds and inorganic ions (Guan et al. 2011, Wang and Xu 2012). Various AOTs have been proposed and evaluated within the research community, including stand-alone AOTs, such as ozonation (Derco et al. 2013), ultraviolet irradiation (UV) (Chen et al. 2009a), ultrasonic irradiation (US) (Petrier et al. 1996), Fenton process (Chan and Chu 2003), and hybrid AOTs, such as UV/Fenton (Molkenthin et al. 2013), ozone/ H_2O_2 (Molkenthin et al. 2013), sonopholytic process (US/UV) (Duran et al. 2013).

However, many of these AOTs involve the dosing of chemicals (e.g. O_3 , H_2O_2) and/or

catalysts, which will increase additional operational costs and complexity related to chemical purchase, storage and final disposal or recycle. The undesired leaching of heavy metals from the catalyst surface will also arise potential hazard to the aqueous environment. Therefore, there is growing concern among water utilities to move away from processes requiring the dosing of chemicals towards “chemical-free” treatment, trying to apply environmental friendly and sustainable AOT measures. Among various AOTs, US and UV are two viable processes without dosing of chemicals. The successful degradation of many refractory organic compounds by US, UV, and their combination, US/UV, has been reported in previous studies (Chen et al. 2009a, He et al. 2011, Joseph et al. 2011, Petrier et al. 1994, Song et al. 2005, Torres et al. 2008). Nonetheless, there are still many unknown or conflicting aspects, especially the potential synergistic effect and synergistic mechanism by combining US and UV, and also the applicability of these three concerned processes for the degradation of different target compounds.

Among numerous EDCs, the industrially and agriculturally important chemicals have been brought to the forefront due to their massive production and widespread application. Three major classes of industrial endocrine disruptors have received the most intensive interests recently, which are bisphenols, alkylphenols and phthalates (Gultekin and Ince 2007). The agricultural herbicides are also widely employed, such as to control weeds so as to avoid competition with crop plants for water and nutrients, to maintain roadways free of vegetative obstructions (Short and Colborn 1999). In this thesis, four EDCs were selected as the probe compounds, these being dimethyl phthalate (DMP), di-*n*-butyl phthalate (DBP), nonylphenol (NP), and atrazine (ATZ). DMP and DBP are the most common phthalate acid esters (PAEs), widely used as plasticizers in the manufacture of commercial

products (Chen et al. 2008, Cheung et al. 2007, Lau et al. 2005, Staples et al. 2011). NP is mainly used in the production of nonylphenol ethoxylates (NPEOs), the most widely used non-ionic surfactants, and it is also a commonly seen incomplete degradation product of NPEOs (Soares et al. 2008). ATZ is a widely used herbicide of great environmental concern (de la Casa-Resino et al. 2012, Graymore et al. 2001).

Hence, in this thesis, systematic and intensive studies have been taken to examine the sonolytic, photolytic, and sonophotolytic processes in the degradation of DMP, DBP, NP and ATZ.

1.2. Aims and objectives

The broad aim of this study is to assemble and evaluate a prototype US/UV unit which can be used to degrade various kinds of organic compounds in water and wastewater mediated conditions. The specific objectives of this study are shown as follows:

- 1) To examine the feasibility of degrading four typical EDCs (i.e. DMP, DBP, NP, and ATZ) by employing sole-US, sole-UV, and the hybrid process of US/UV.
- 2) To examine the influence of various parameters on the degradation performance of target compounds, such as US frequency, power density, UV intensity, solution pH, initial concentration of the probe compound, background ions and species (e.g. H_2O_2 , Fe^{2+} , NaCl , KBr , NO_3^-). The optimal operating conditions will be determined thereby.

- 3) To investigate the mutual influence between US and UV in the hybrid process of US/UV. To evaluate the potential synergistic effect in the US/UV process and examine the synergistic mechanisms.

- 4) To examine the degradation kinetics of different organic compounds in the US, UV, and US/UV processes. To establish a kinetics model of general relevance to describe the degradation of different target compounds in the US/UV process.

- 5) To explore the degradation mechanisms and mineralization efficiencies of four probe compounds in the US, UV, and US/UV processes, respectively, and to propose the possible degradation pathways.

1.3. Structures of this thesis

This thesis is composed of ten chapters. The present chapter includes the background information, the objectives and the structures of this thesis.

Chapter Two provides a comprehensive literature review of related theories and issues. In particular, four involved EDCs as the major probes are introduced in detail, including their basic information, toxicological effects and environmental fate, and previous studies of their degradation. In addition, theories of the sonochemical AOT and UV process are summarized and discussed in depth.

In Chapter Three, the specific descriptions of the experimental materials and methodologies

used in this thesis are provided.

The work shown in Chapter Four reports a systematic study of the sonolytic degradation of DMP by high-frequency ultrasound. The significance of various parameters on DMP sonolysis is evaluated. Mechanisms of DMP sonolysis is analyzed based on LC/MS analysis results, and a degradation pathway is proposed.

In Chapter Five, the merits of the combined process of high-frequency ultrasound and catalyst-free UV irradiation have been evaluated with DMP as the probe compound. The synergistic effect and synergistic mechanism of the combined process are investigated. Furthermore, a proper model is proposed to successfully describe the US/UV process and DMP degradation.

In Chapter Six, the effectiveness of sonolysis, photolysis, and sonophotolysis of ATZ is investigated. The heterogeneous micro-environment of sonochemical process is examined and the degradation mechanisms of ATZ in these three processes are also investigated. The benefits of combining US and UV are investigated from the aspect of promoting the intermediates degradation which are resistant in individual processes.

Chapter Seven discusses the influence of background ion, Fe^{2+} , on the US/UV process using DBP as a probe compound, which gives rise to a sono-photo-Fenton process with the in-situ generated hydrogen peroxide from the US process. The properties and synergistic effects of the constituent processes are investigated, especially the UV/ Fe^{2+} process.

In Chapter Eight, the effects of physicochemical properties of a group of phthalate acid esters on their sonolysis and sonophotolysis are investigated under both pure water and wastewater mediated conditions. The degradation mechanisms of DBP in involved processes are also investigated.

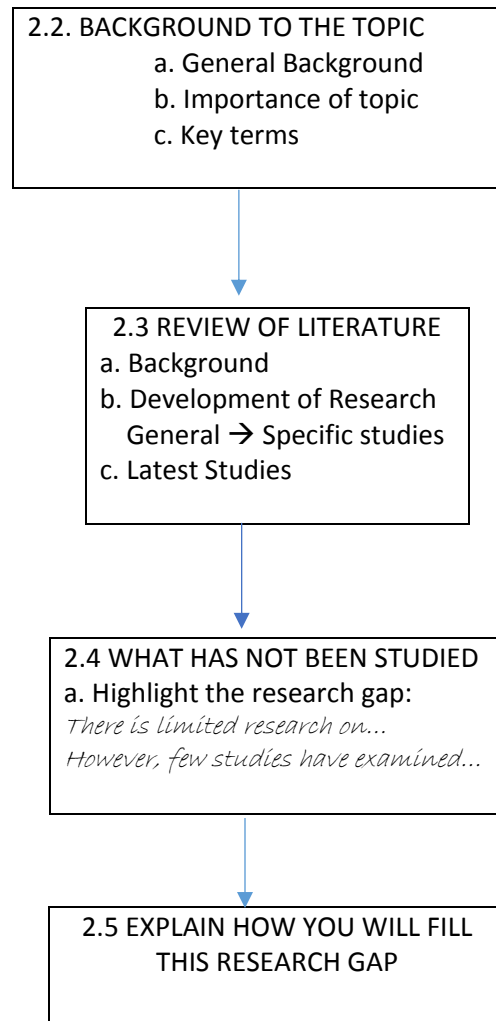
Chapter Nine discusses the sonopholytic degradation of hydrophobic nonylphenol in solution. The critical factor of solution pH and the influence of a commonly seen wastewater constituent, nitrate ion (NO_3^-), on the sonopholytic process were investigated. The degradation mechanisms of NP sonophotolysis at different conditions are also studied.

In the last chapter, conclusions of the whole work present in this thesis are summarized. Moreover, the limitations of the present study and recommendations for the future work are also proposed.

Literature Review

Literature Review is usually organised in the following way:

2.1 LITERATURE REVIEW




2.6 SUMMARY

Chapter 2: Literature Review

A Literature Review discusses previous research in the field. It should be structured in a clear way with the previous studies grouped logically. It should also be organised so as to create a coherent account or a story of existing research and the research gap identified that calls for a solution – the current study. It should include: a summary of important previous findings, a synthesis of studies that are similar, a critical discussion of all current research that is relevant to your topic, an identification of the gap in current research that needs to be addressed and an explanation of how the thesis will fill the research gap.

This Literature Review is very effective partly because the writer includes the following:

Structure

(Introduction)		Not included
Describes for each chemical:		Section 2.1.1 -2.1.4
1. Background		
2. Current Studies		
Theoretical Background		Section 2.2
(Summary)		Not Included

Content

- Has a clear structure for section 2.1. The section is divided into four subsections each reviewing one chemical. These subsections each further contain subsections based on three steps:
 - Background (e.g. Section 2.1.1.1)
 - Problem (e.g. Section 2.1.1.2)
 - Possible Solution (e.g. Section 2.1.1.3)
- Cites sources, grouping studies (e.g. Section 2.1.1.1 sentence 1)
- Critiques studies cited (e.g. Section 2.1.1.3 final sentence 3-4)
- Highlights significance of the topic (e.g. Section 2.1.1.3 final sentence)
- Highlights gaps in current research (e.g. Section 2.1.3.3 final sentence)
- Summarizes main characteristics discussed in the previous section with a table (e.g. Table 2-1)
- Explains key theory (e.g. Section 2.2.1.1)

- Groups similar studies (e.g. Section 2.2.1.3 paragraph 3, sentence 2)
- Explains the scope of the thesis (e.g. Section 2.2.1.3 paragraph 1, last sentence)
- Indicates gap in research (e.g. Section 2.2.1.3 paragraph 3, last sentence)

Language

- Develops paragraphs in a logical way e.g. *three main pathways...the first...the second pathway...however...the third degradation process...* (e.g. Section 2.1.2.3 paragraph 2)
- Sums up longer paragraphs with a final summary sentence (e.g. Section 2.2.1.1)
- Makes statements tentative with the use of adverbs e.g. *generally divided, normally believed mainly responsible* (e.g. Section 2.2.1.1, paragraph 2)
- Numbers equations (e.g. Eq 2.1)
- Uses vocabulary to show importance of topic e.g. *with great interest* (e.g. Section 2.2.1.3, paragraph 1, sentence 2)

To Consider

This chapter of the thesis is effective. However, it could be further improved in the following aspects.

💡 Introduce each chapter with a short introductory paragraph that directs the reader to the content and outlines the way the chapter is organized. Longer sections can also have a short introductory paragraph.

💡 Include the year of each publication cited (e.g. Section 2.1.2.3, paragraph 3 sentence.

💡 Include a transitional statement at the end of the paragraph leading to the next one.

💡 Give a short transitional paragraph at the end of the chapter leading to the next chapter.

💡 Avoid explaining content of figures in the title. It is better to have a short title and explain it in the paragraph (e.g. Figure 2-2).

💡 Include a paragraph at the end of the chapter summarizing the key issues discussed in it.

2. Chapter Two Literature Review

2.1. Probe compounds

The summary of the characteristic parameters of DMP, ATZ, DBP and NP is provided in Table 2-1.

2.1.1. Dimethyl phthalate

2.1.1.1. Basic information

Dimethyl phthalate (DMP) is the simplest and most common member of the phthalate acid esters (PAEs), which are a group of industrially important chemicals, widely employed as plasticizers and additives to improve the mechanical properties and flexibility of various products (Chen et al. 2008, Cheung et al. 2007). DMP is typically used in cellulose ester-based plastics (Staples et al. 1997b). DMP has been listed as a priority pollutant by the U.S. Environmental Protection Agency (USEPA) owing to its toxicological properties (Xu et al. 2010b). Substantial quantities of DMP are released into environmental water bodies through the discharge of manufacturing wastewater and from direct leaching from plastic products, leading to its widespread occurrence and potential risks on the health of humans and wildlife. DMP demonstrates a relatively high water solubility and it is more hydrophilic compared to other PAEs.

2.1.1.2. Toxicological effects and environmental fate

DMP was reported to be acutely and chronically toxic to aquatic lives at concentrations below its aqueous solubility. Studies with algae, invertebrates, and fish showed that the

acute toxicity concentration ranged from 29 to 377 mg·L⁻¹, and the chronic toxicity concentration ranged from 9.6 to 11.0 mg·L⁻¹ (Staples et al. 1997a). Experiments with rats demonstrated that, treatment with 5% DMP resulted in increased liver weight and decreased body weight (Field et al. 1993). So far, the U.S. EPA has classified the cancer risk of DMP as Group D, i.e. not classifiable as to human carcinogenicity (U.S. Environmental Protection Agency 1999b).

The environmental transformation of PAEs are mainly through hydrolysis, photolysis, and biotic degradation, however at very low rates. The aqueous hydrolysis half life and atmosphere photo-oxidation half life were reported to be 3.2 years and 9.3 – 93 days, respectively (Staples et al. 1997b). Biodegradation is a critical process affecting the environmental fate of PAEs. Whereas, even in lab-scale biodegradation process, several days duration still not fulfilled the complete degradation of DMP (Staples et al. 1997b).

2.1.1.3. Previous studies of DMP degradation

Owing to the environmental significance of DMP, intensive efforts have been made to develop methods to remove DMP from waters and wastewaters. Various AOT methods of treating DMP have been investigated in recent years, such as O₃/H₂O₂ (Xu et al. 2009a), O₃/Ce/SBA-15 (Yan et al. 2013), sono-electrolysis (Souza et al. 2013), O₃/UV (Chen et al. 2008), TiO₂-UV (Chen et al. 2009b), Fe(VI)-TiO₂-UV (Yuan et al. 2008a), O₂/Fe@Fe₂O₃/AC/microwave (Chen et al. 2012), Fe/SBA-15/O₃ (Huang et al. 2011). However, most of these methods are viable only in the presence of catalysts or other chemical inducers. Although a few studies have considered the sonolytic degradation of

DMP, proposing the dominant role of $\bullet\text{OH}$ radical oxidation (Psillakis et al. 2004, Yim et al. 2002), still very limited information concerning the “chemical-free” AOTs of sonolytic, photolytic, and sonophotolytic degradation of DMP has been provided. Therefore, the potential feasibility and benefits of applying US, UV, and US/UV processes in the degradation of DMP are of considerable significance.

2.1.2. Atrazine

2.1.2.1. *Basic information*

Atrazine (ATZ) is a chloro-*s*-triazine herbicide that has been widely used in agricultural and forestry applications to inhibit the photosynthesis of plants (de la Casa-Resino et al. 2012, Graymore et al. 2001). Due to its extensive application and moderately high solubility, ATZ is prone to leaching to groundwater and surface runoff (Graymore et al. 2001). It has been reported that ATZ is 20 times more frequently detected than any other herbicide in groundwater in the United States (Belluck et al. 1991). ATZ is of great environmental concern, mainly because of its endocrine disrupting effects on a variety of living beings (de la Casa-Resino et al. 2012) and it is suspected to be a possible human carcinogen (Chen et al. 2009a). Although it has been banned from use in the European Union since 2007 (Tappin et al. 2012), it is still one of the most frequently used herbicides in the world.

2.1.2.2. *Toxicological effects and environmental fate*

Studies reported that ATZ exhibited endocrine disrupting effects, such as antiestrogenic/antiandrogenic activity, and inhibition of ovulation, accompanied by decreased testosterone production (Orton et al. 2009). In another study, ATZ is classified as

moderately to highly toxic to microorganism (Phyu et al. 2013). ATZ was also found to be toxic to green alga (He et al. 2012). However, based on the review of available scientific studies, EPA determined in 2000 that ATZ is not likely to cause cancer in humans (U.S. Environmental Protection Agency).

The environmental degradation of ATZ generally follows three main pathways. The first pathway is the hydrolysis of the C–Cl bond, leading to the formation of hydroxy-atrazine, which is one of the main degradation products in both the soil and aquatic systems. The second pathway is dealkylation, but both the deethylated-ATZ and deisopropylated-ATZ are phytotoxic products. However, ATZ is significantly more toxic than its degradation products toward many algae. The third degradation process corresponds to the splitting of the triazine ring usually caused by microorganisms (Bintein and Devillers 1996).

2.1.2.3. Previous studies of ATZ degradation

Many studies have evaluated the degradation of ATZ in water by AOTs. These have included stand-alone AOTs (such as UV irradiation (Chen et al. 2009a), sonolysis (Petrier et al. 1996), and Fenton process (Arnold et al. 1995)), and hybrid AOTs (such as US/UV-catalyst (Bahena et al. 2008), ozone/H₂O₂ (Nelieu et al. 2000), and UV/Fenton (Chan and Chu 2005)) to enhance the efficiency. The degradation of ATZ by AOTs was shown to involve several mechanisms: de-chlorination; hydroxylation of the *s*-triazine ring; de-alkylation of the amino groups; oxidation of the amino groups; and de-amination (Chan and Chu 2005, Chen et al. 2009a). The opening of the *s*-triazine ring was considered difficult (Bianchi et al. 2006), and therefore, cyanuric acid, ammelide, and ammeline were generally

recognized as the end products from various studies (Borras et al. 2010, Chan and Chu 2005, Huston and Pignatello 1999, Nelieu et al. 2000, Pelizzetti et al. 1990, Perez et al. 2006). Only a few studies have reported the successful mineralization of ATZ, i.e. the successful degradation of the persistent end product, cyanuric acid, via special laboratory conditions (e.g. diamond electrode, supercritical water) (Garcia-Lopez et al. 2007, Horikoshi and Hidaka 2003, Oturan et al. 2012, Yanagisawa et al. 2008, Zhang et al. 2010). In this respect, an AOT followed by biological treatment can be a feasible way for ATZ mineralization, and preferably an AOT with little or no chemicals used to reduce complexity.

The photolytic degradation of ATZ has been reported before, and 2-hydroxyatrazine (OIET) was found to be the main intermediate (Chan and Chu 2005, Chen et al. 2009a, Torrents et al. 1997), accounting for more than 90% of ATZ decay (Chan and Chu 2005). Further degradation of OIET by photolysis is difficult and additional AOTs are needed to facilitate its degradation. The chemical-free US process may be a possible candidate for this. Information concerning the sonolytic degradation of ATZ is very limited. Petrier et al. have reported some preliminary results of sonolytic degradation of ATZ, but only a few intermediates were identified (Petrier et al. 1996). Hiskia et al. also reported some main intermediates of ATZ sonolytic degradation without giving detailed information (Hiskia et al. 2001). Therefore, the feasibility of applying the US, UV, and US/UV processes to ATZ degradation, and the potential improvement by combining US with UV in ATZ degradation are worth exploring.

2.1.3. Di-*n*-butyl phthalate

2.1.3.1. *Basic information*

Di-*n*-butyl phthalate (DBP) is one of the most common PAEs and mainly used as a plasticizer in the manufacture of non-vinyl commercial products (Lau et al. 2005, Staples et al. 2011). DBP initially attracted attention as a potential EDC since it was found to be a weak estrogen receptor agonist in some cell-based assays (Mylchreest et al. 1999). A recent study evaluating the contamination status of the lower reaches of Yangtze River (China) showed that DBP was present as a key contaminant responsible for thyroid receptor antagonist activities (Xu et al. 2013b), and therefore represented a threat to drinking water safety. DBP was also detected as one of the most frequent PAEs contaminants in the River Seine estuary in France (Dargnat et al. 2009).

2.1.3.2. *Toxicological effects and environmental fate*

Studies showed that DBP not only exhibited potent antiandrogenic activity with the half maximal inhibitory concentration (IC₅₀) of 1.05×10^{-6} M, but also showed the androgenic activity with the half maximal effective concentration (EC₅₀) value of 6.17×10^{-6} M. In addition, DBP was also found to possess thyroid receptor antagonist activity with IC₅₀ of 1.31×10^{-5} M (Shen et al. 2009). Studies by Kim et al. also showed the liver-toxic effect of DBP (Kim et al. 2009). EPA has classified the cancer risk of DBP as Group D, not classifiable as to human carcinogenicity (U.S. Environmental Protection Agency 1999a). However, in general, the most common degradation products, the phthalate monoesters, were found less toxic than the corresponding diesters (Jonsson and Baun 2003).

The environmental transformation of DBP is similar with that of DMP, mainly through hydrolysis, photolysis, and biotic degradation (Staples et al. 1997b). However, the aqueous hydrolysis half life and atmosphere photo-oxidation half life were reported to be 22 years and 0.6 – 6.0 days, respectively (Staples et al. 1997b). It was found that DBP was more susceptible to photolysis compared to that of DMP.

2.1.3.3. Previous studies of DBP degradation

The degradation of DBP using AOTs processes has been reported in several studies in recent years. The majority of these studies were conducted using photocatalytic processes with different kinds of catalysts (Bajt et al. 2001, Bajt et al. 2008, Chiou et al. 2006a, Chiou et al. 2006b, Hasegawa et al. 2001, Kaneco et al. 2006, Li et al. 2005, Sharma et al. 2010, Xu et al. 2010a, Xu et al. 2007). The feasibility of applying ozonation process in DBP degradation was also evaluated (Li et al. 2006, Ren et al. 2012). However, very scarce information concerning the photo-degradation (Lau et al. 2005), sono-degradation (Psillakis et al. 2004) of DBP is provided. In addition, the degradation mechanisms of DBP in the US, UV, and US/UV processes are also hardly found.

2.1.4. Nonylphenol

2.1.4.1. Basic information

Nonylphenol (NP) is used in the manufacture of antioxidants, lubricating oil additives and the production of NPEOs surfactants, which is its major use (65%) (Soares et al. 2008). NPEOs are the most significant alkyl phenol ethoxylates (APEOs), accounting for about 80% of total APEOs used (Ying et al. 2002). NPEOs are widely used in industrial,

agricultural and household applications, including the production of detergents, emulsifiers, dispersing agents, etc. (Soares et al. 2008, Vincent and Sneddon 2009). The annual production of NP reached 154,200 tons in the USA, 73,500 tons in Europe, 16,500 tons in Japan, and 16,000 tons in China (Soares et al. 2008). In addition, due to the extensive use of NPEOs, more than 60% of the total NPEOs produced go into the aquatic environment, where they are incompletely degraded to NP, which is more toxic, more stable compared to its precursors (Li et al. 2013c). Hence, the principal route of exposure to NP for human and wildlife is through water (Ying et al. 2002). NP has been found to be able to mimic the effect of the hormone estrogen, which has caused public concern (Ying et al. 2002).

2.1.4.2. Toxicological effects and environmental fate

In 1991, Soto and his colleagues accidentally found that, NP, which was used in the manufacture of the test tubes in their experiments, was capable of initiating proliferation in breast tumor cells (Soto et al. 1991). From then on, NP was continually reported to initiate a variety of responses in organisms, aquatic lives and human bodies. For example, the semen production and the development of embryos of the rainbow trout was significantly affected by 4-nonylphenol (Lahnsteiner et al. 2005); the NP showed toxic effects on normal hearts of guinea pig and might disrupt the cardio-protective effects (Wang et al. 2013); NP was able to induce respiratory toxicity in cells with EC₅₀ of 1.8 ppm (Argese et al. 1994). In general, the effects of NP are very diverse and sometimes unpredictable.

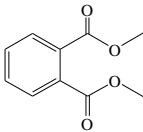
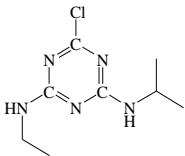
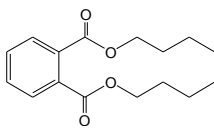
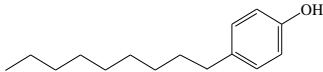
The environmental fate of NP is predominantly determined by its physicochemical properties, which in turn influence its degradation. NP is a hydrophobic compound with the

Log K_{ow} value of 5.71 (average of 3 isomers, see Table 2-1), and therefore it more favorably enters into the organic matters. Thus, NP is prone to adsorption onto the sediment and soil (Ying et al. 2002). In the surface layer of natural waters, NP can be degraded by sunlight photolysis (Ahel et al. 1994). However, the half life of NP in sediments has been estimated to be more than 60 years (Shang et al. 1999). Another important pathway of NP degradation in the environment is via biodegradation, aerobically or anaerobically, with the half life of about several dozen days (Mao et al. 2012). Therefore, reducing the NP concentration in the effluent of WWTPs, which is supposed to be the major sources of NP contamination, may be the most effective method to control NP pollution.

2.1.4.3. Previous studies of NP degradation

The degradation of NP in water by AOTs processes has been reported by relatively few studies, which is probably because of the low solubility of NP in water. In summary, the following processes are involved, including photo-degradation (Li et al. 2013c, Martinez-Zapata et al. 2013, Neamtu and Frimmel 2006), low-frequency ultrasonic degradation (Gultekin et al. 2009, Ince et al. 2009), ozone oxidation (Ning et al. 2007a, b), and photocatalytic degradation (Inumaru et al. 2004, Kohtani et al. 2003). In some studies, in order to increase the solubility of NP in water so as to facilitate its determination, some organic solvents were used (e.g. methanol (Ince et al. 2009, Neamtu and Frimmel 2006)), which however may influence the investigated AOTs processes. Since no information has been provided concerning the NP degradation in high-frequency ultrasonic process and the sonopholytic process, the relevant studies may provide some useful information.

Table 2-1: Summary of the characteristic parameters of DMP, ATZ, DBP, and NP at 25 °C (unless otherwise stated) (USNLM).

Parameters	DMP	ATZ	DBP	NP
Chemical Structure				
Molecular Formula	C ₁₀ H ₁₀ O ₄	C ₈ H ₁₄ N ₅ Cl	C ₁₆ H ₂₂ O ₄	C ₁₅ H ₂₄ O
Molecular Weight	194.18	215.68	278.34	220.35
CAS No.	131-11-3	1912-24-9	84-74-2	25154-52-3
Appearance	Colorless, oily liquid	Colorless powder	Colorless to faint yellow, oily liquid	Pale-yellow, viscous liquid
Specific Gravity	1.189	1.23 (22 °C)	1.05 (20 °C)	0.95 (20 °C)
LogK _{ow}	1.60	2.61	4.9	5.71 (20 °C) (average of 3 isomers)
Solubility (mg·L ⁻¹)	4000	34.7 (26 °C)	11.2	6.35
Henry's Law Constant (atm·m ³ ·mol ⁻¹)	1.97 × 10 ⁻⁷	2.89 × 10 ⁻⁷	1.81 × 10 ⁻⁶	1.10 × 10 ⁻⁶
Vapor Pressure (mm Hg)	3.08 × 10 ⁻³	2.89 × 10 ⁻⁷	2.01 × 10 ⁻⁵	2.36 × 10 ⁻⁵
pKa	–	1.60	–	10.25

2.2. Advanced oxidation processes

2.2.1. Sonochemical process

2.2.1.1. Theories of acoustic cavitation

Ultrasound are waves with the frequencies above the hearing range, i.e. at frequencies above 16 kHz (16,000 cycles per second) (Adewuyi 2001). The ultrasonic wave can produce the alternating compression and rarefaction of the liquid media being irradiated, which is able to break the intermolecular Van der Waals forces which maintains the cohesion of the liquid. Consequently, microbubbles containing the vaporized liquid and/or previously dissolved gas will form because of the sufficiently large negative pressures, (Adewuyi 2001, Cintas and Luche 1999). The microbubbles start growing preferably in the vicinity of inhomogeneities, such as tiny gas bubbles and solid impurities, until they grow to the critical size and then violently collapse and adiabatically implode (Adewuyi 2001, Cintas and Luche 1999). Collapse occurs on a very short time scale, approximately 1/5 of a cycle or less, i.e. $< 10^{-5}$ s for 20 kHz ultrasonic waves, or *ca.* 4×10^{-7} s for 500 kHz ultrasonic waves (Cintas and Luche 1999, Kardos and Luche 2001). The final implosion of the bubbles produces extremely high local temperatures (*ca.* 5000 K) and pressures (*ca.* 1000 atm) (Adewuyi 2001). As a result, under such extreme conditions, volatile molecules (solvent or dissolved gas) vaporized into the gas phase are pyrolyzed to free radicals, followed by very fast cooling ($> 10^9$ K·s⁻¹) (Kardos and Luche 2001, Suslick 1990). Substances of low vapor pressure are unable to penetrate into the gas phase, but they can react with the radical species generated by the volatile molecules (Cintas and Luche 1999). In summary, this series of processes, i.e. nucleation (formation), bubble growth, implosive collapse, is known as the acoustic cavitation (Suslick 1990).

The cavitation can be generally divided into two categories: the transient cavitation and the stable cavitation. A transient cavity is one which exists for only one cycle or a few, and during its existence it expands several times larger than its original size (Henglein 1987, Lorimer and Mason 1987, Thompson and Doraiswamy 1999). Transient cavitation bubbles are filled mainly with vapor and their collapse may be particularly violent because there is little permanent gas to cushion the implosion (Henglein 1987). After the violent collapse, they often split into a mass of smaller bubbles (Henglein 1987). Such transient cavities are normally believed to happen with the ultrasonic intensities in excess of $10 \text{ W}\cdot\text{cm}^{-2}$ (Henglein 1987, Lorimer and Mason 1987). These cavities are mainly responsible for the mechanical activity of ultrasound, which prefer to collapse near extended solid surface and produce shock wave. This property of ultrasound is used for the cleaning purposes and in solid-aqueous reactions to clean the surfaces of the solids (Servant et al. 2001). The maximum temperatures (T_{\max}) and pressures (P_{\max}) within the collapsed cavitation bubbles are proposed by Noltingk and Nepriyas (Eq. 2-1 and 2-2), assuming adiabatic collapse of the bubbles (Adewuyi 2001, Hoffmann et al. 1996, Lorimer and Mason 1987).

$$T_{\max} = T_0 \left[\frac{P_a(\gamma-1)}{P_v} \right] \quad (2-1)$$

$$P_{\max} = P_v \left\{ \frac{P_a(\gamma-1)}{P_v} \right\}^{[\gamma/\gamma-1]} \quad (2-2)$$

where T_0 is the temperature of the bulk solution; γ is the ratio of the specific heats of the cavitation medium (C_p/C_v); P_v is the pressure in the bubble at its maximum size and is assumed to be equal to the vapor pressure of the solvent; P_a is the pressure in the bubble at the moment of transient collapse. It can be concluded that the properties of the cavitation medium (i.e. the solvent, the solute, and the dissolved gas) can significantly influence the

cavitation performance of a specific ultrasound.

The smaller bubbles generated from the disintegration of transient cavities pulsate and oscillate for many acoustic cycles, which are known as the stable cavities (Servant et al. 2001). The stable cavitation bubbles generally form and oscillate at a mean radius and contain mainly permanent gas and some vapor of the liquid (Henglein 1987). The stable bubbles are believed to be generated at lower intensities of $1 - 3 \text{ W}\cdot\text{cm}^{-2}$ (Henglein 1987). Since the time scale of the stable cavitation is much longer compared to the transient cavitation, mass diffusion of gas and other long-term effects may happen (Lorimer and Mason 1987). The stable cavitation bubbles can be divided into different classes: some of them are the “repetitive stable cavitation” where the bubbles either grow by rectified diffusion (cavitation bubbles grow more during expansion than they shrink during contraction due to the unequal diffusion of gases and vapor from the bulk solution to the bubble (Thompson and Doraiswamy 1999)) or dissolve; another class of bubbles concerns which, cycle after cycle, collapse without breaking up into smaller bubbles. The latter bubbles are mainly responsible for the chemical effects of ultrasound and of great interest in aqueous-aqueous reactions (Servant et al. 2001).

2.2.1.2. Sonochemical reaction systems

The acoustic cavitation process is complicated, which is not only dependent on the ultrasonic generator, but also dependent on the properties of solvents, solutes, and gases in the bubbles. The cavities are more readily formed with solvents of high vapor pressure, low viscosity, and low surface tension. However, the intensity of cavitation is more beneficial

by applying solvents of low vapor pressure, high viscosity and surface tension. Simply put, the solvents with higher threshold for cavitation always have more harsh conditions when the cavitation forms (Adewuyi 2001).

The chemical effects induced by the ultrasonic energy are mainly reflected in the following aspects: production of heat, promotion of mass transfer, improvement of material contact, dispersion of chemicals, and production of chemical-free radicals (Adewuyi 2001). So far, four theories have been proposed to explain the sonochemical situations (Adewuyi 2001, Chowdhury and Viraraghavan 2009): (a) hot-spot theory; (b) electrical theory; (c) plasma discharge theory; (d) supercritical theory. In the “electrical theory”, the extreme conditions associated with the collapse are attributed to the intense electrical fields because the homogeneous sonochemistry has numerous analogies with corona chemistry (Lepoint and Mullie 1994, Margulis 1992). The “plasma discharge theory” proposes that the fragmented bubbles act as the microreactors where the microplasma can form, and many analogies between sonochemistry and corona chemistry are proposed (Lepoint and Mullie 1994). The “supercritical theory” suggests that high temperatures and pressures exceeding the critical values of water ($T > T_c = 647$ K and $P > P_c = 221$ bar) occur in the vapor phase of the cavitating bubbles and at the interfaces, which can accelerate the chemical reactions (Hua et al. 1995). In general, the most commonly adopted theory is the “hot spot theory”, which considers the sonochemical reaction as a heterogeneous reaction, and the reactive species and heat are produced from the cavitation bubbles (Serpone and Colarusso 1994).

The “hot spot” model is shown in Figure 2-1, in which three main reaction zones are proposed (Adewuyi 2001, Pang et al. 2011): (a) a hot gaseous bubble interior; (b) an

interfacial region between the cavitation bubble and bulk liquid; (c) the bulk solution. The temperatures of interior and interfacial regions were determined to be $5,200 \pm 650$ K and $\approx 1,900$ K, respectively (Suslick et al. 1986). The extreme conditions within the collapsed bubbles cause the thermal dissociation of water molecules or other vapors and/or gases, leading to the formation of free radicals. These radicals can either serve as oxidants to react with target compounds, or combine mutually or with peripheral water molecules to form other radical species (e.g. HO₂) or molecules (e.g. H₂O₂), which in turn can oxidize organic substrates causing their degradation or even mineralization (Adewuyi 2001, Inoue et al. 2006). Pyrolysis reactions can also occur under such high temperatures. It was found pyrolysis is predominant at high solute concentrations, while at low solute concentrations, free radical reactions are likely to predominate (Adewuyi 2001). Majority of degradation was found to take place in the gas-liquid interfacial regions, which was estimated to extend only about 200 nm thick and have an effective lifetime of less than 2 μs after collapse (Suslick 1990). A small number of free radicals may diffuse into the bulk solution and react with the substrate present therein to form new products.

Some principal reactions identified in the sonochemical processes are summarized in Table 2-2, including the water dissociation reaction (R 2-1), the production of other secondary molecules and/or radicals (R 2-2 – R 2-17), and possible minor reactions due to the presence of dissolved air (R 2-18 – R 2-31).

Table 2-2: Summary of the sonochemical reactions in the cavitation events (Adewuyi 2001).

Reactions	No.	Reactions	No.
$\text{H}_2\text{O} \rightarrow \text{H}\cdot + \cdot\text{OH}$	R 2-1		
$\text{H}\cdot + \text{H}\cdot \rightarrow \text{H}_2$	R 2-2	$\cdot\text{OH} + \cdot\text{OH} \rightarrow \text{H}_2\text{O}_2$	R 2-3
$\text{H}\cdot + \text{O}_2 \rightarrow \text{HO}_2\cdot$	R 2-4	$\text{HO}_2\cdot + \text{HO}_2\cdot \rightarrow \text{H}_2\text{O}_2 + \text{O}_2$	R 2-5
$\text{H}\cdot + \text{HO}_2\cdot \rightarrow \text{H}_2\text{O}_2$	R 2-6	$\text{HO}_2\cdot + \text{HO}_2\cdot \rightarrow \text{H}_2\text{O} + 1.5\text{O}_2$	R 2-7
$\cdot\text{OH} + \cdot\text{OH} \rightarrow \text{H}_2\text{O} + \text{O}\cdot$	R 2-8	$\cdot\text{OH} + \text{HO}_2\cdot \rightarrow \text{H}_2\text{O} + \text{O}_2$	R 2-9
$\text{O}\cdot + \text{O}\cdot \rightarrow \text{O}_2$	R 2-10	$0.5\text{O}_2 + 2\text{H}\cdot \rightarrow \text{H}_2\text{O}$	R 2-11
$\text{H}\cdot + \cdot\text{OH} \rightarrow \text{H}_2\text{O}$	R 2-12	$\text{H}\cdot + \text{H}_2\text{O}_2 \rightarrow \cdot\text{OH} + \text{H}_2\text{O}$	R 2-13
$\text{H}\cdot + \text{H}_2\text{O}_2 \rightarrow \text{H}_2 + \text{HO}_2\cdot$	R 2-14	$\cdot\text{OH} + \text{H}_2\text{O}_2 \rightarrow \text{HO}_2\cdot + \text{H}_2\text{O}$	R 2-15
$\cdot\text{OH} + \text{H}_2 \rightarrow \text{H}_2\text{O} + \text{H}\cdot$	R 2-16	$\text{H}_2\text{O} + \cdot\text{OH} \rightarrow \text{H}_2\text{O}_2 + \text{H}\cdot$	R 2-17
$\text{O}_2 \rightarrow 2\text{O}\cdot$	R 2-18	$\text{N}_2 \rightarrow 2\text{N}\cdot$	R 2-19
$\text{H}\cdot + \text{O}_2 \rightarrow \cdot\text{OH} + \text{O}\cdot$ (or $\text{HO}_2\cdot$)	R 2-20	$\text{N}\cdot + \cdot\text{OH} \rightarrow \text{NO} + \text{H}\cdot$	R 2-21
$\text{O}\cdot + \text{H}_2\text{O} \rightarrow 2\cdot\text{OH}$ (or H_2O_2)	R 2-22	$\text{NO} + \cdot\text{OH} \rightarrow \text{NO}_2 + \text{H}\cdot$	R 2-23
$\text{O}\cdot + \text{H}_2\text{O}_2 \rightarrow \cdot\text{OH} + \text{HO}_2\cdot$	R 2-24	$2\text{NO}_2(\text{aq}) + \text{H}_2\text{O} \rightarrow \text{HNO}_2 + \text{HNO}_3$	R 2-25
$\text{O}\cdot + \text{O}_2 \rightarrow \text{O}_3$	R 2-26	$\text{NO}_2 + \cdot\text{OH} \rightarrow \text{HNO}_3$	R 2-27
$\text{O}\cdot + \text{H}_2 \rightarrow \cdot\text{OH} + \text{H}\cdot$	R 2-28	$\text{N}\cdot + \text{H}\cdot \rightarrow \text{NH}\cdot$	R 2-29
$\text{O}\cdot + \text{HO}_2\cdot \rightarrow \cdot\text{OH} + \text{O}_2$	R 2-30	$\text{NH}\cdot + \text{NH}\cdot \rightarrow \text{N}_2 + \text{H}_2$	R 2-31

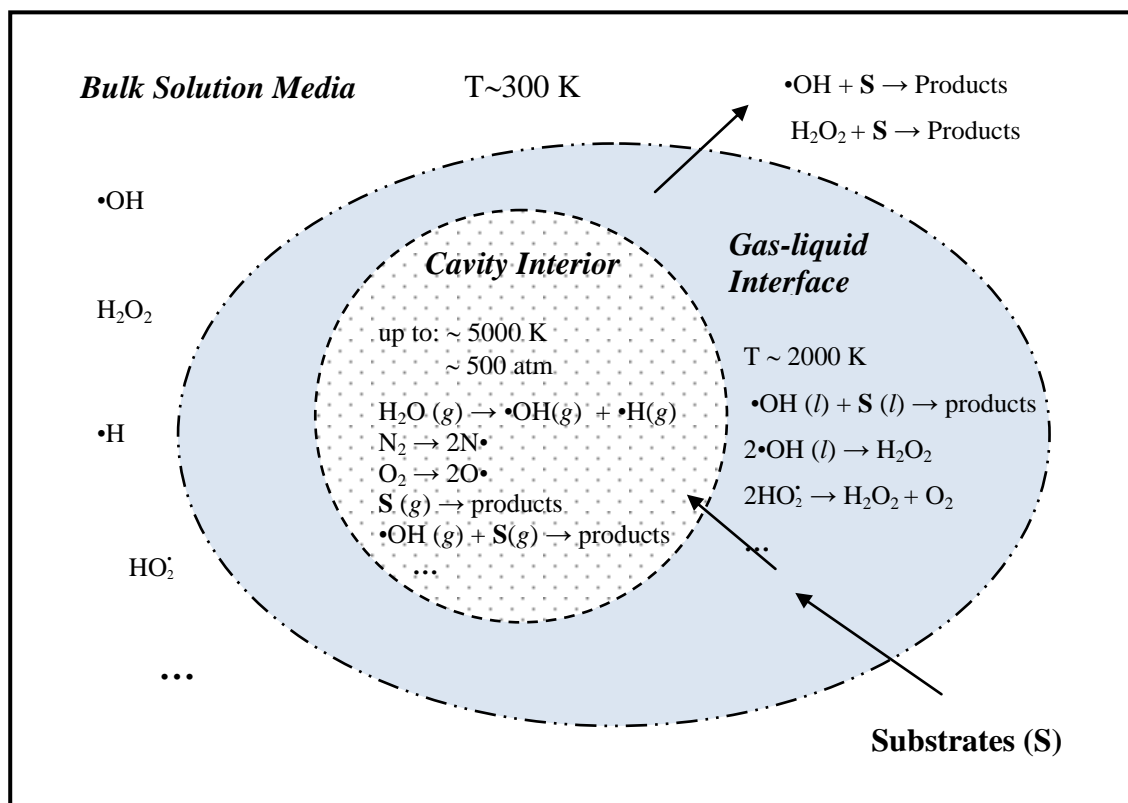


Figure 2-1: Three reaction zones in the cavitation process, adapted from (Adewuyi 2001).

2.2.1.3. Sonochemical process applied in water pollution remediation

Although the application of ultrasound in both industrial and academic areas has long been known, the “green” value of the non-hazardous property has been recognized only recently (Cintas and Luche 1999). Due to its “green” property, ultrasound has been explored with great interest for wastewater treatment of various pollutants in an attempt to establish an environmental-friendly treatment technology, although the efficiency of ultrasound is sometimes lower than many other AOTs. These investigations in water pollution remediation mainly focus on the following aspects: (a) direct degradation of different chemical contaminants (Chiha et al. 2011, Dukkanci and Gunduz 2006, Gao et al. 2013,

Goel et al. 2004, Inoue et al. 2008, Lim et al. 2007); (b) pretreatment of wastewater or sludge (Ayyildiz et al. 2011, Cesaro and Belgiorno 2013, Fernandez-Cegri et al. 2012, Pilli et al. 2011, Yin et al. 2004); (c) disinfection of wastewater (Jin et al. 2013, Li et al. 2012, Madge and Jensen 2002, Naddeo et al. 2009, Wu et al. 2012, Zhao et al. 2013); (d) assisting technology for other AOTs (Gultekin and Ince 2006, Nikolopoulos et al. 2006, Taherian et al. 2013, Zhao et al. 2010). This thesis mainly focuses on the investigation of aspects (a) and (d).

One remarkable advantage of the ultrasonic system as a wastewater treatment technology is its “clean” property, i.e. there is no need to introduce any additives to the US system and no hazardous byproducts generated. Although there is no environmental concerns associated with US technology, the cost effectiveness issue is still an obstacle for its scale-up. Since the ultrasonic system transform the electrical energy into the chemical energy and thermal energy, it requires very high energy input. However, one effective way to reduce the operational cost and make it economically feasible is to use the hybrid process by combining other synergistic AOT processes. A study by Mahamuni and Adewuyi has compared the treatment costs of individual US process with some US-related hybrid processes for 1000 L min⁻¹ capacity treatment plant (Mahamuni and Adewuyi 2010). It was estimated that the cost of wastewater treatment for phenol was \$89 per 1000 gallons for US/UV/O₃ and \$15,536 per 1000 gallons for US alone; the cost for trichloroethylene treatment was in the range of \$25 per 1000 gallons for US/UV to \$91 per 1000 gallons for US alone; the cost for treating azo dyes was in the range of \$65 per 1000 gallons for US/UV/H₂O₂ to \$14,203 per 1000 gallons for US alone. Therefore, the combination of US with other established AOT methods may improve the cost effectiveness for treating

different organic compounds, and the efficiency is also dependent on the property of the target compounds.

The pollutants studied by the use of sonochemical process mainly include (Adewuyi 2001): aromatic compounds, such as phenol, chlorophenol, and nitrophenol; chlorinated aliphatic hydrocarbons, such as trichloroethylene, tetrachloroethylene; organic dyes, such as Remazol Black B. The degradation efficiency and pathway may vary significantly for different contaminants. Very few studies were conducted to investigate the degradation of the selected compounds in this study using the sonochemical process.

2.2.2. UV photolysis

2.2.2.1. Photochemical principles

When a species absorbs a quantum of radiation, it becomes excited. How the species assimilates that energy depends on the wavelength of the incident radiation. The longer the wavelength of electromagnetic radiation, the lower the energy (Eq. 2-3). The energy of radiation in the visible to ultraviolet region is of the right magnitude to induce transitions between the electronic energy levels of a species, leading to electronic transition (Wayne and Wayne 1996).

$$E = h \times \nu = h \times c / \lambda \quad (2-3)$$

where E is the energy of photons, ν is the frequency of radiation, and h is Planck's constant.

The excited state of a species can exhibit a very different reactivity from its ground state because it possesses more energy and it can participate in different reactions due to the new

electronic arrangement. There are several routes the excited species can react or consume its excess energy. Figure 2-2 summarizes some of the most important pathways, where the pathways (1) – (3) strictly are the chemical routes. The eight reaction routes outlined in Figure 2-2 are primary processes. If new products are formed in these reactions, they may then go on to take part in additional secondary thermal reactions, which are photochemical only in the sense that the excited species would not have appeared in the absence of light (Wayne and Wayne 1996).

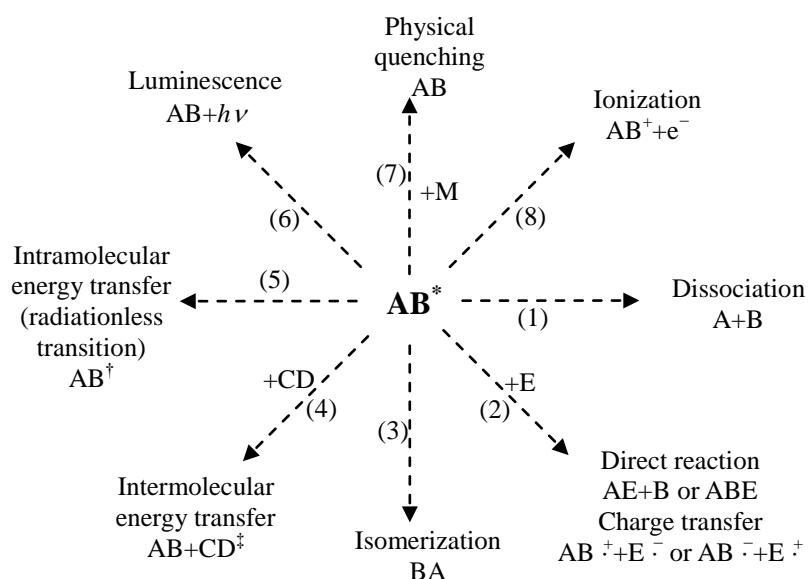


Figure 2-2: The primary routes to loss of electronic excitation (the use of symbols * , ‡ , and † is only intended to illustrate the presence of electronic excitation and not necessarily differences in states), adapted from (Wayne and Wayne 1996).

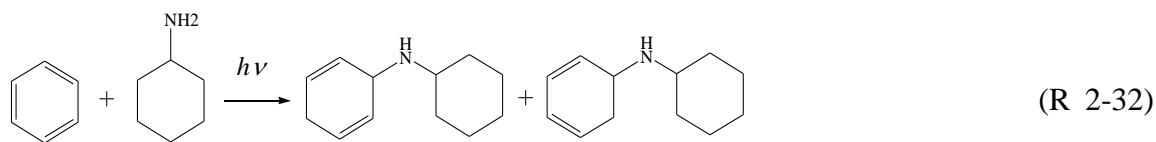
There are two famous laws in photochemistry. The first law of photochemistry, the Grotthus-Draper law, states that only the light absorbed by a molecule can produce photochemical change in the molecule. The second law of photochemistry, Stark-Einstein

law, states that if a species absorbs radiation, then one particle is excited for each quantum of radiation absorbed (Wayne and Wayne 1996). As outlined in Figure 2-2, an excited species could yield new chemical products. For each primary product formed, there may be a number of secondary processes available, so that the overall products of a photochemical reaction can be very diverse. The concept of quantum yield (Φ) is of great value in the photochemistry field to interpret the behaviour, which is defined as “the number of molecules of reactant consumed per photon of light absorbed”. Measured value can range from less than 10^{-6} to more than 10^6 , depending on the reaction system. A quantum yield greater than one suggests the occurrence of secondary reactions, and a value greater than two suggests the operation of a chain reaction mechanism (Wayne and Wayne 1996).

2.2.2.2. *Photochemical reactions*

In general, the photochemical changes come about as a result of photodissociation of the absorbing molecule into fragments, direct reaction of the excited species, or spontaneous isomerization of the excited species (Wayne and Wayne 1996). Photodissociation (route 1 in Figure 2-2) is the most obvious type of photochemical change, in which photoionization (route 8 in Figure 2-2) is a special case of photodissociation. The direct reaction of the excited species (route 2 in Figure 2-2) may be either intermolecular (i.e. reaction with added reactants, solvent, and unexcited molecules), or intramolecular (including intramolecular reductions, additions, etc.). The species may undergo spontaneous isomerization due to the sufficient energy possessed to allow internal rearrangement of the species. Below are examples of some typical types of photoreactions:

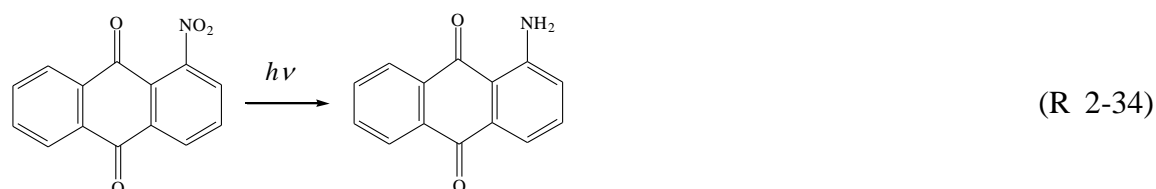
(1) Photoaddition reactions (Wayne and Wayne 1996):



(2) Photocyclization reactions (Wayne and Wayne 1996):



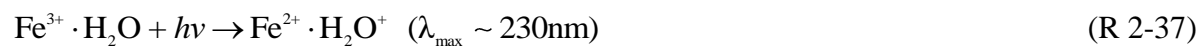
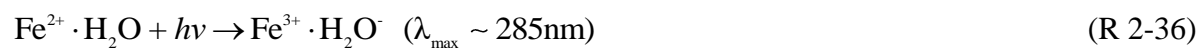
(3) Photoreduction reactions (Gorner 2011):



(4) Photooxidation reactions (Chainikova et al. 2013):



(5) Electron/charge transfer reactions (Wayne and Wayne 1996):



2.2.2.3. UV photolysis applied in water pollution remediation

UV photolysis has long been used as a remediation technology for the degradation of many environmental concerned compounds in water, directly or with photocatalysts (Chu and

Rao 2012, Chu et al. 2011, Rao and Chu 2013). Direct photolysis of organic compounds is realizable or more efficient with the UV-C and vacuum ultra violet (VUV) light sources (Al-Momani et al. 2004, Dantas et al. 2010, Fang et al. 2013, Lau et al. 2005). In addition, the efficiency of the UV AOTs also depends on the structure of the target compounds, and the variation in molecular structures of contaminants sometimes induce significant variations in removal rates, both with respect to direct photolysis and radical reactions (Wols and Hofman-Caris 2012). Many organic compounds have been investigated by using the UV AOTs, such as dyes (Huang et al. 2013, Sadik and Shama 2002), herbicides (Rao and Chu 2010, Wong and Chu 2003), pesticides (Shawaqfeh and Al Momani 2010), plasticizer (Lau et al. 2005). Due to the limitation of direct UV process, i.e. the dependence of molecular structure and the requirement of water transparency, many photocatalysts have been developed to enhance the efficiency of UV AOTs by generating reactive species (Emeline et al. 2012, Kondo et al. 2013, Neppolian et al. 2010, Zhai et al. 2011). Nevertheless, the separation, recovery and recycle of the photocatalysts still arouse complex operational problems and additional costs; the leaching of heavy metal to the aqueous phase will also create environmental hazards, even more serious. Therefore, an environmentally friendly process, which can assist the UV process without generating additional environmental problems, is required, and the high-frequency ultrasound may be a proper candidate.

Chapter 3: Materials and Methodology

The methodology chapter is a description of the methodological approach(es) taken and an explanation of why this was chosen. It often includes: a general introduction restating the central aims, the details of any part of the methodology that may be unfamiliar to the readers, an explanation of how the results will be analyzed, and an explanation of any limitations with the methodology

This description of methodology is very effective partly because the writer includes the following:

Structure

(Introduction)		Not included
Describes the chemicals used		Section 3.1
Apparatus used	↓	Section 3.2
Analytical methods	↓	Section 3.3
Summary		Not Included

Content

- Explains rationale for methods selected (e.g. Section 3.2.2, paragraph 1, sentence 7)
- Refers forward to where the methods are employed (e.g. Section 3.2.4, sentence 4)
- Gives a short closing paragraph linking to the next chapter
- Cites sources that have influenced the choice of the methods used e.g. (e.g. Section 3.3.2, paragraph 1)

Language

- Uses past simple tense and passive voice to add objectivity to the section e.g. *were used* (e.g. Section 3.1, paragraph 1 sentence 2). Gives an introductory section.
- Places the title of tables above the table (e.g. Table 3-1)

- Refers forward to future chapters (e.g. Section 3.2.1, paragraph 1, sentence 8)
- Refers to figures using a range of language e.g. *see Figure 3-1, is shown in Figure 3-2* (e.g. Section 3.2.1)

To Consider

This chapter of the thesis is effective. However, it could be further improved in the following aspect.

- Include an introductory paragraph that gives an overview of the chapter.

3. Chapter Three Materials and Methodology

3.1. Chemicals and reagents

All chemicals used in this study were of analytical standard, solvents used for high performance liquid chromatography (HPLC) and liquid chromatography tandem mass spectrometry (LC/MS) were of HPLC grade and LC/MS grade, respectively. All chemicals were used as received without further purification, and details are summarized in Table 3-1. Deionized-distilled water (DDW) prepared from a Millipore Waters Milli-Q water purification system with resistivity of 18.3 M Ω ·cm was used in this study. The real secondary effluent of domestic wastewater obtained from Tai Po Water Treatment Works, Hong Kong, was also used in Chapter Eight, which was filtered by 0.45 μ m glass fiber filters before use. Acetonitrile (ACN) (\geq 99.9%) of HPLC grade was filtered by 0.22 μ m membrane and degassed before use. Solutions of 0.1 M sulfuric acid and 0.1 M sodium hydroxide were used for pH adjustment.

Table 3-1: List of chemicals and reagents used in this study.

Name	Purity (%)	CAS No.	Molecular Weight (g mol ⁻¹)	Formula	Manufacturer
<i>Target Compounds:</i>					
DMP	99.6	131-11-3	194.18	C ₁₀ H ₁₀ O ₄	Sigma Aldrich Inc.
DBP	98.7	84-74-2	278.34	C ₁₆ H ₂₂ O ₄	Sigma Aldrich Inc.
DEP (Diethyl phthalate)	99.5	84-66-2	222.24	C ₁₂ H ₁₄ O ₄	Sigma Aldrich Inc.

(c.o.)

(b.f.)

ATZ	98.9	1912-24-9	215.68	C ₈ H ₁₄ N ₅ Cl	Chem Service Inc.
4- <i>n</i> -NP	99.9	25154-52-3	220.35	C ₁₅ H ₂₄ O	Sigma Aldrich Inc.

Intermediates:

Phthalic acid	99.5	88-99-3	166.14	C ₈ H ₆ O ₄	Sigma Aldrich Inc.
OIET	> 99.0	2163-68-0	197.24	C ₈ H ₁₅ N ₅ O	Dr. Ehrenstorfer GmbH
Ammeline	–	645-92-1	127.11	C ₃ H ₅ N ₅ O	Dr. Ehrenstorfer GmbH
Monomethyl phthalate	> 98.0	4376-18-5	180.16	C ₉ H ₈ O ₄	Dr. Ehrenstorfer GmbH

Other Chemicals:

Hydrogen peroxide	35	7722-84-1	34.01	H ₂ O ₂	Sigma Aldrich Inc.
Ferrous sulfate heptahydrate	≥ 99.0	7720-78-7	278.05	FeSO ₄ ·7H ₂ O	Sigma Aldrich Inc.
1, 10-phenanthroline	≥ 99.5	5144-89-8	198.22	C ₁₂ H ₁₀ N ₂ O	Riedel-de Haën
Titanium (IV) oxide sulfate hydrate	93.0	13825-74-6	159.94	TiOSO ₄ ·xH ₂ O	International Laboratory USA
Thymol	99.0	89-83-8	150.22	C ₁₀ H ₁₄ O	ACROS ORGANICS
Ammonium sulfamate	ACS	7773-06-0	114.12	H ₆ N ₂ O ₃ S	ACROS ORGANICS
Silver sulfate	ACS	10294-26-5	311.79	Ag ₂ O ₄ S	ACROS ORGANICS
Potassium bromide	–	7758-02-3	119.00	KBr	AJAX Chemicals

(c.o.)

(b.f.)

Methanol	HPLC grade	67-56-1	32.04	CH ₃ OH	Tedia
tert-Butanol	99.5	75-65-0	74.12	C ₄ H ₉ OH	Sigma Aldrich Inc.
Sodium nitrate	> 99.0	7631-99-4	84.99	NaNO ₃	Sigma Aldrich Inc.

3.2. Apparatus and experimental conditions

3.2.1. Ultrasound units

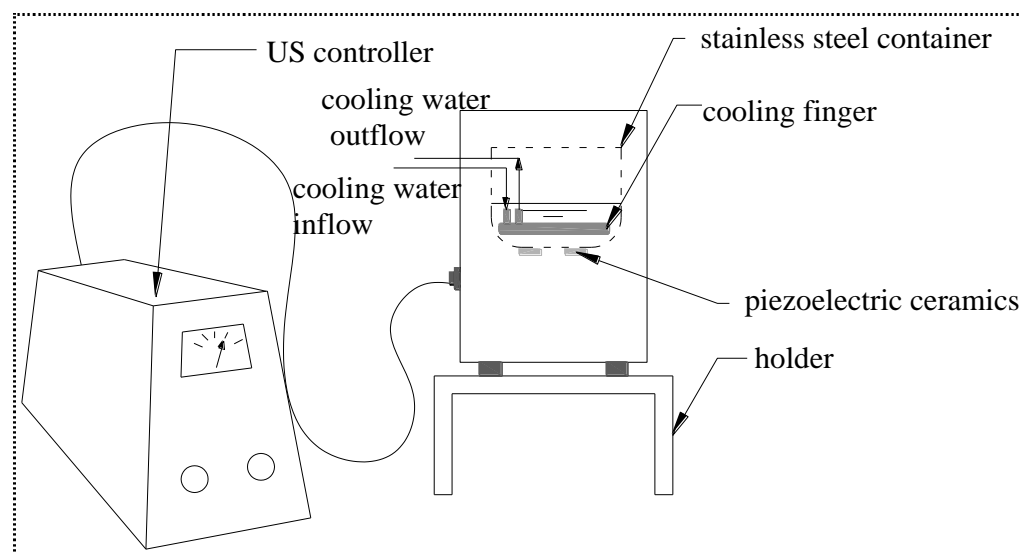


Figure 3-1: Schematic diagram of the ultrasonic apparatus at the frequencies of 400, 800, and 1200 kHz.

Sonolytic experiments were conducted in a cubic stainless steel jacketed reactor with an effective volume of 1.5 L (tailor-made by Ning Bo Scientz Biotechnology Co., China) (see Figure 3-1). Three different frequencies of 400, 800, and 1200 kHz were provided respectively by three independent basins with an identical reactor size. Electrical power

was transduced into ultrasonic vibration by six piezoelectric ceramics stuck uniformly in two rows (i.e. in a 2×3 format) on the back of the basin bottom. The nominal input power was adjustable manually via the control panel. A convolute cooling finger was submerged in the tested water to keep the solution temperature constant at 28 ± 2 °C (not applicable in the calorimetric experiment). A volume of exactly 250 mL reaction solution was used throughout this study, except for the tests relating to different water volumes. The power density applied for the 400 kHz ultrasound in this study was 0.03 W mL^{-1} , unless otherwise stated. In Chapter Four, the 400, 800, and 1200 kHz ultrasounds were employed; in Chapter Five, Seven, Eight, and Nine, only the 400 kHz ultrasound was used; in Chapter Six, the 400 kHz ultrasound and a probe type 20 kHz ultrasound (see below) were used. The sonolysis experiments were conducted without any sparged gas.

A schematic diagram of the 20 kHz probe type ultrasound system (VCX 750, Sonics & Materials Vibra Cell™, used in Chapter Six) is shown in Figure 3-2. In this system, the ultrasonic wave is generated from the cylindrical titanium alloy tip of 13 mm diameter, and the applied input power was 375 W (at 50% amplitude), resulting in a power density of 0.19 W mL^{-1} . The glass beaker as the reaction vessel was thermostated by a water jacket, enabling a constant temperature of 28 ± 2 °C to be maintained by adjusting the flow of cooling water. ATZ solution at the volume of 200 mL was used for the 20 kHz ultrasonic process.

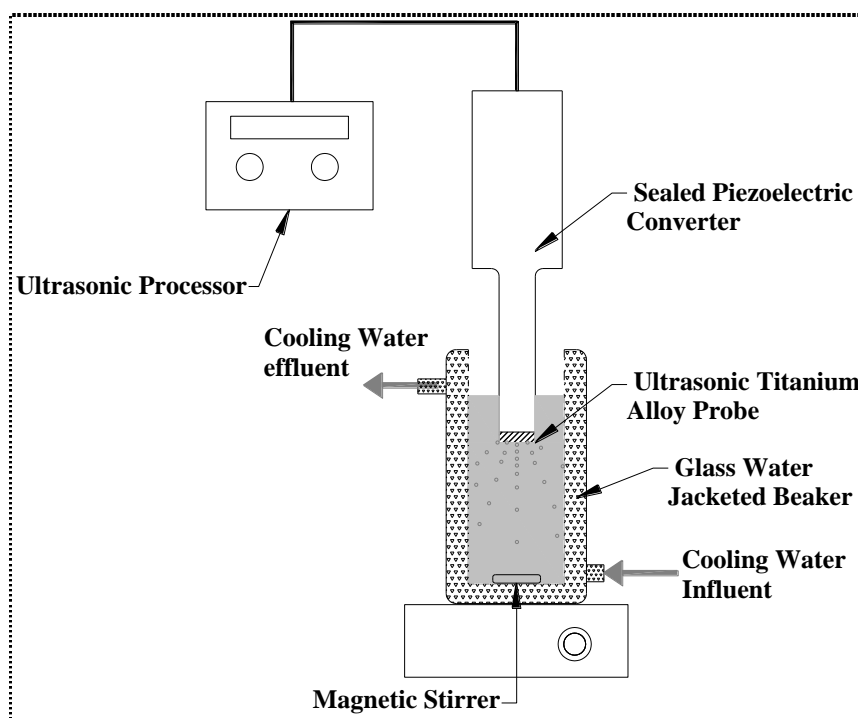


Figure 3-2: Schematic diagram of the 20 kHz ultrasonic apparatus (applied in Chapter Six).

3.2.2. Photo-reactor

An aluminum photoreaction chamber (also tailor-made by Ning Bo Scientz Biotechnology Co.) was employed for the photolytic process, in which six lamps (maximum) can be installed on the ceiling of the chamber. In addition, a ventilation fan was installed in the chamber to prevent heat accumulation. The photolytic experiments were conducted using phosphor-coated low pressure mercury lamps emitting 253.7 nm monochromatic UV light and different UV intensities could be obtained by varying the number of UV lamps. The intensity of incident UV light with 6 lamps was approximately 1.03×10^{-5} Einstein $L^{-1} s^{-1}$ (as cited by the lamp manufacturer, Southern New England Ultraviolet Co., USA). The ultrasonic reactor of 400 kHz without lid is the same reactor (container) used for the

photolytic experiment for fair tests. The reactor was placed in the center of the photo-chamber and the liquid surface was adjusted manually so as to maintain a constant distance of 20 cm from the UV lamps (see Figure 3-3). To ensure a stable UV output, the lamps were allowed to warm up for 10 min before conducting each experiment.

3.2.3. The sonophotolytic reaction unit

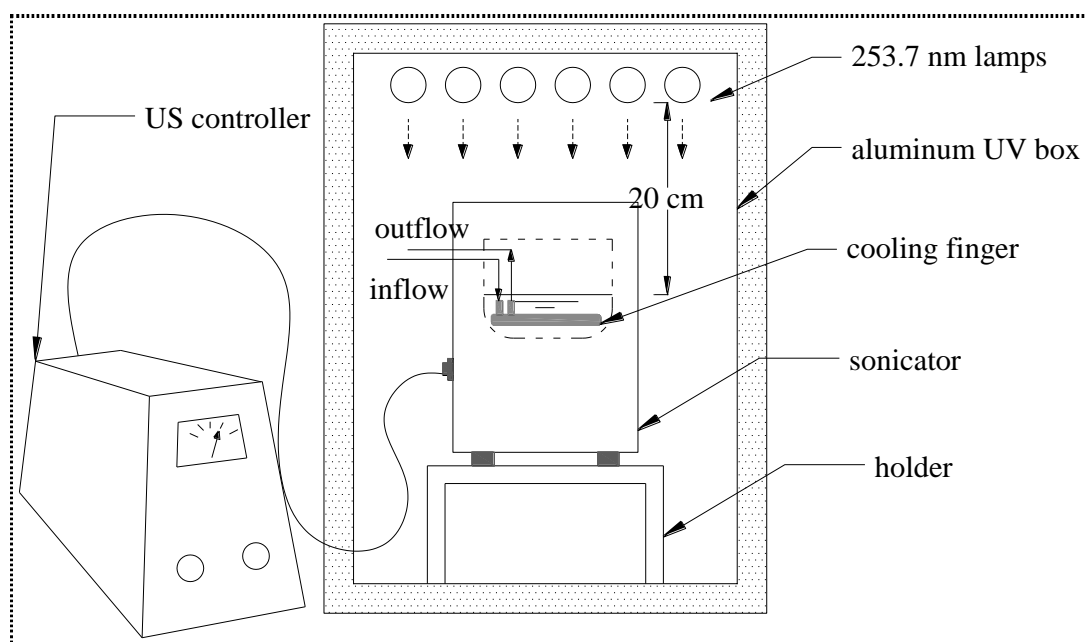


Figure 3-3: The set-up diagram of the sonophotolytic reaction unit.

The 400 kHz ultrasound was used to conduct the sonophotolytic experiments. The simultaneous US/UV (sonophotolytic) reaction was realized by placing the sonicator (i.e. the reactor) inside the photo-chamber, so that both the US and UV could be applied simultaneously (see Figure 3-3). The sequential tests involving either UV followed by US, or vice versa, were carried out by respectively switching on/off either the sonicator or UV lamps, for given time periods. Six lamps were used for DMP degradation (Chapter Five);

one lamp was used for ATZ (Chapter Six) and DBP degradation (Chapter Seven); six lamps were used for PAEs degradation (Chapter Eight); two lamps were used for NP degradation (Chapter Nine).

3.2.4. Other experimental conditions and procedures

All the experiments were conducted at room temperature (air-conditioned at 24 ± 2 °C). The initial pH of the unbuffered solutions (without adjustment) containing different target compounds was maintained at 6.5 ± 0.2 unless stated otherwise (e.g. for the tests at different initial pH levels). The total reduction in solution volume after sampling was kept below 5% of the initial volume. In Chapter Five, the initial concentration of DMP solutions was 0.05 mM in all tests. In Chapter Six, the initial concentration of ATZ solutions was 0.02 mM for all tests except for intermediates identification and total organic carbon (TOC) tests, where 0.1 mM ATZ solution was used (see 3.3.4). In Chapter Seven, DBP solution with an initial concentration of 0.01 mM was used. In Chapter Eight, all PAEs solutions with an initial concentration of 0.01 mM were used. In Chapter Nine, 0.01 mM NP solution was applied throughout except for intermediates and TOC analysis, in which 0.015 mM NP were used to increase detection signals. NP stock solution of 0.015 mM (3.3 mg L^{-1}) was prepared semimonthly and stirred in the thermostatic water bath with constant temperature of 35 °C to ensure the complete dissolution and stable concentration of NP. Stock solutions of other compounds were all prepared under ambient conditions. In Chapter Seven, the Fe^{2+} solution was freshly prepared with degassed DDW before each experiment to prevent precipitation and oxidation. During irradiation, 1.0 – 2.0 mL aliquots were withdrawn from the reactor at predetermined time intervals for further analysis. For the experiments

involving Fe^{2+} , 2 mL sample aliquots were withdrawn from the reactor at predetermined time intervals and quenched immediately with 1 mL methanol. All the experiments were duplicated with an observed deviation of less than 5%.

3.3. Analytical methods

3.3.1. Quantification of target compounds

The concentrations of target compounds were determined by HPLC (Waters, see Figure 3-4), comprising a HPLC pump (Waters 515), a UV-vis detector (Waters 2489), an auto sampler (Waters 717), and a Brava C18-BDS column (5 μm particle size, 250 mm \times 4.6 mm). The HPLC conditions used for different compounds are summarized in Table 3-2, where the maximum absorbance wavelength (λ_{max}) used for compound detection were determined based on UV absorption spectra of the target compounds (see Figure 3-5, Figure 3-6, Figure 3-7).

Table 3-2: HPLC conditions for the quantification of different target compounds.

Compounds	DMP	DEP	DBP	MMP	ATZ	NP
λ_{max} (nm)	230	230	230	230	220	224/280
Mobile phase (ACN ratio)	60%	60%	90%	35%	60%	95%
Flow rate (mL min^{-1})	1	1	1	1	1	1
Injection volume (μL)	10	10	10	10	10	10

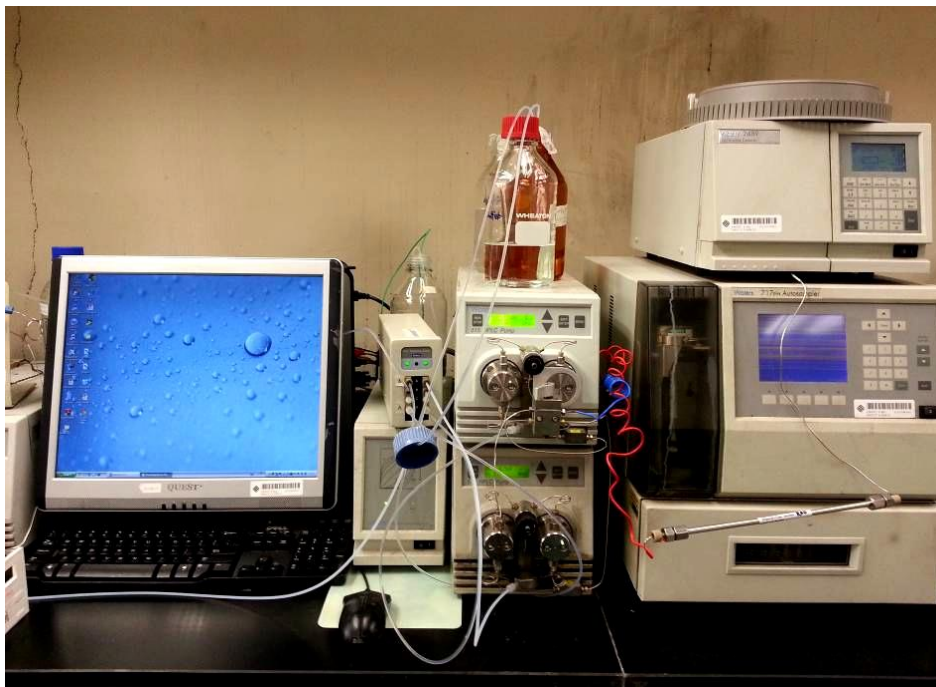


Figure 3-4: The HPLC system (Waters) used for quantification of the target compounds.

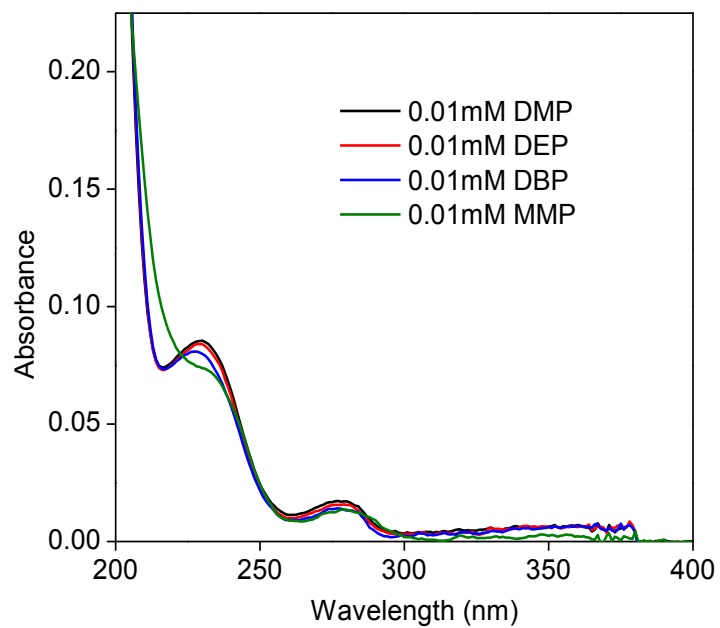


Figure 3-5: The UV absorption spectra of 0.01 mM DMP, DEP, DBP, and MMP.

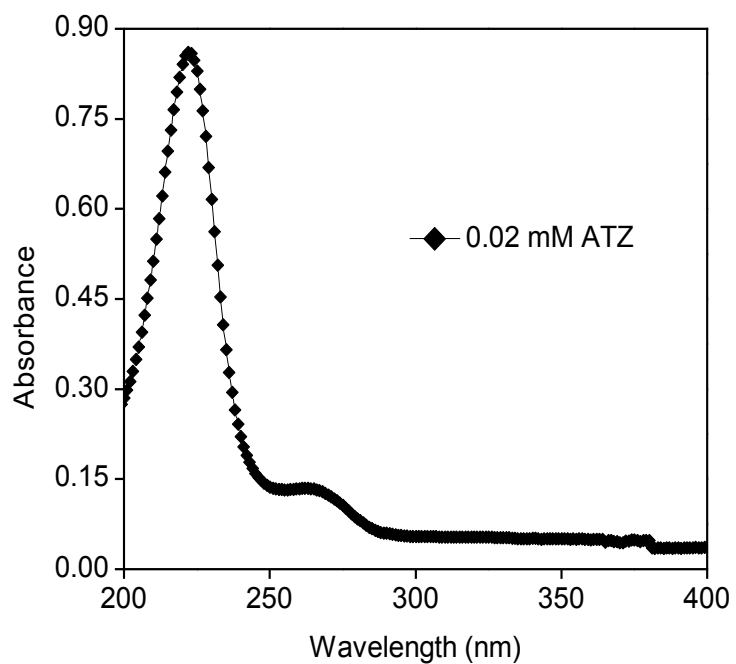


Figure 3-6: The UV absorption spectra of 0.02 mM ATZ.

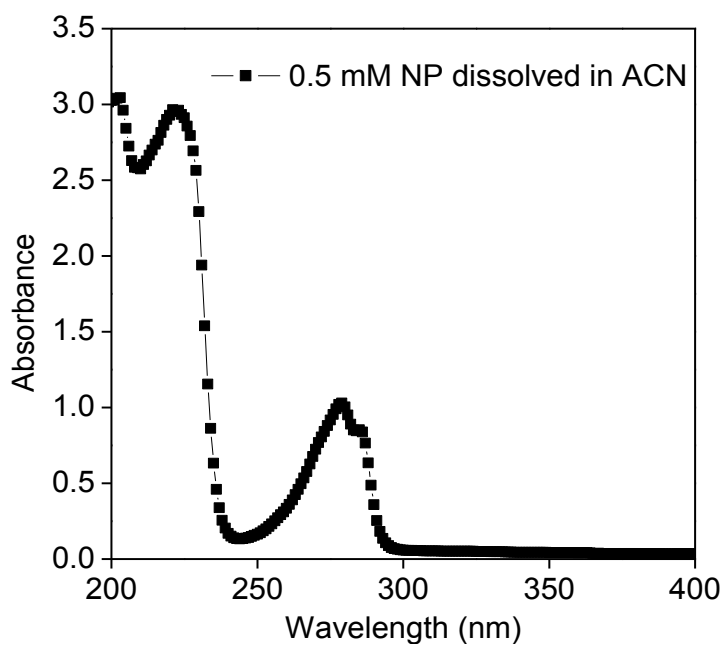


Figure 3-7: The UV absorption spectra of 0.5 mM NP dissolved in ACN.

3.3.2. Hydrogen peroxide determination

The concentration of H_2O_2 was determined by measuring the absorbance of titanium peroxide (TiO_2^{2+}) complex formed from the reaction of TiOSO_4 with H_2O_2 using the Biochrom Libra S12 spectrophotometer at 405 nm (O'Sullivan and Tyree 2007).

3.3.3. Calorimetric measurement

The ultrasonic power dissipated into the liquid was calculated using a calorimetric method (Mason et al. 1992). In the calorimetric experiment, the temperature of the solution was measured by a digital thermometer and recorded at a 15 s interval for the initial 10 min.

3.3.4. Intermediates identification

The identification of intermediates in Chapter Four (DMP) and Chapter Six (ATZ) was performed by a Thermo Quest Finnigan LCQ Duo HPLC/MS system (see Figure 3-8) equipped with a PDA (Photo diode array) detector and a mass spectrometer with an electrospray ionization (ESI) source and a quadrupole ion-trap mass analyzer. In Chapter Four, positive ion mode was applied to detect DMP, while negative ion mode was used to qualitatively detect the intermediates. The mobile phase was a mixture of 100% methanol (A) and 0.1% formic acid (B) at a flow rate of $0.8 \text{ mL}\cdot\text{min}^{-1}$ with a linearly gradient flow from 10%A : 90%B to 90%A : 10%B within 55 min. From 55 min to 60 min, the ratio turned back to the initial composition. The $[\text{DMP}]_0$ for mass analysis was 0.25 mM. The intermediates without commercial standard were quantified by their nominal concentrations using the same response factor of DMP. This approximation is reasonable on the basis that most of the UV absorbance may be derived from the resonance structure of the ring

(Adams and Randtke 1992).

In Chapter Six, ATZ and its degradation intermediates were identified in a positive ion mode. The mobile phase was a mixture of 90% ACN (A) and 5 mM ammonia acetate (pH 5.0) (B) at a flow rate of $0.6 \text{ mL}\cdot\text{min}^{-1}$ with a linear gradient flow from 5%A : 95%B to 70%A : 30%B within 50 min, and back to the initial condition with another 10 min. Argon was used as the collision gas in the MS/MS analysis. The $[\text{ATZ}]_0$ for mass analysis was 0.1 mM. The intermediates were quantified by relative concentration compared to ATZ when standards were not available.

The identification of intermediates in other chapters was performed by a UPLC/ESI-MS system (see Figure 3-9) equipped with Bruker amaZon SL ion trap mass analyzer and Dionex UltiMate 3000 Ultra-high Performance Liquid Chromatography (UPLC). The Thermo Hypersil GOLD column ($1.9 \mu\text{m}$, $50 \times 2.1 \text{ mm}$) was used for UPLC. Positive ion mode was used for DBP detection and both negative and positive ion modes were applied for intermediates detection (Chapter Eight). The composition and gradient programmes of the mobile phase are shown in Figure 3-10. In Chapter Nine, negative ion mode was used for the detection of NP and its degradation intermediates, and the composition and gradient programme of the mobile phase are shown in Figure 3-11. Mobile phase at the flow rate of $0.15 \text{ mL}\cdot\text{min}^{-1}$ was applied for UPLC. Intermediates identified in Chapter Nine were quantified by their relative abundance, which were estimated by comparing their corresponding deprotonated ion intensity to that of the initial NP in solution from mass analysis.



Figure 3-8: The Thermo Quest Finnigan LCQ Duo HPLC/MS system.

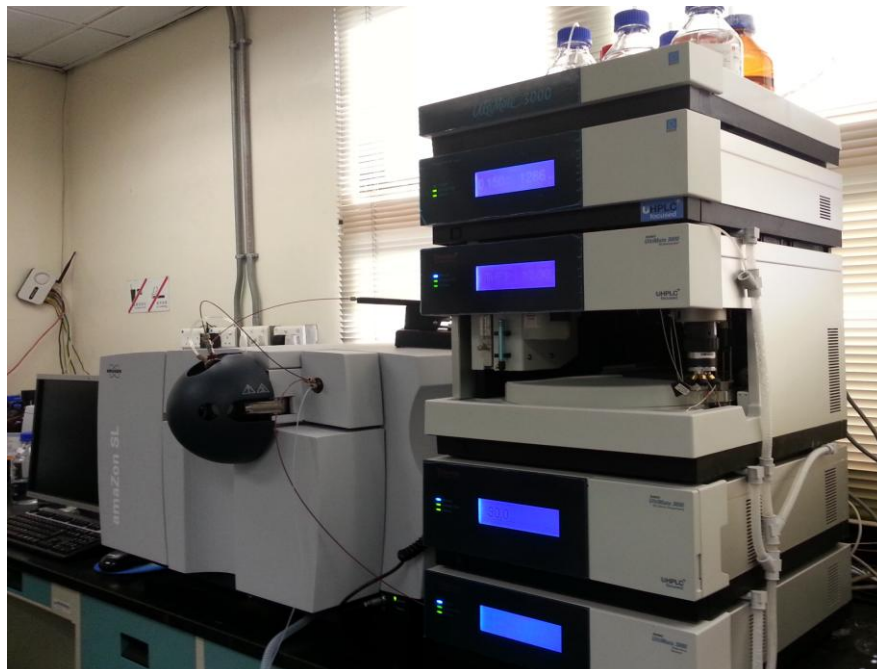


Figure 3-9: The Bruker amaZon SL UPLC/MS system.

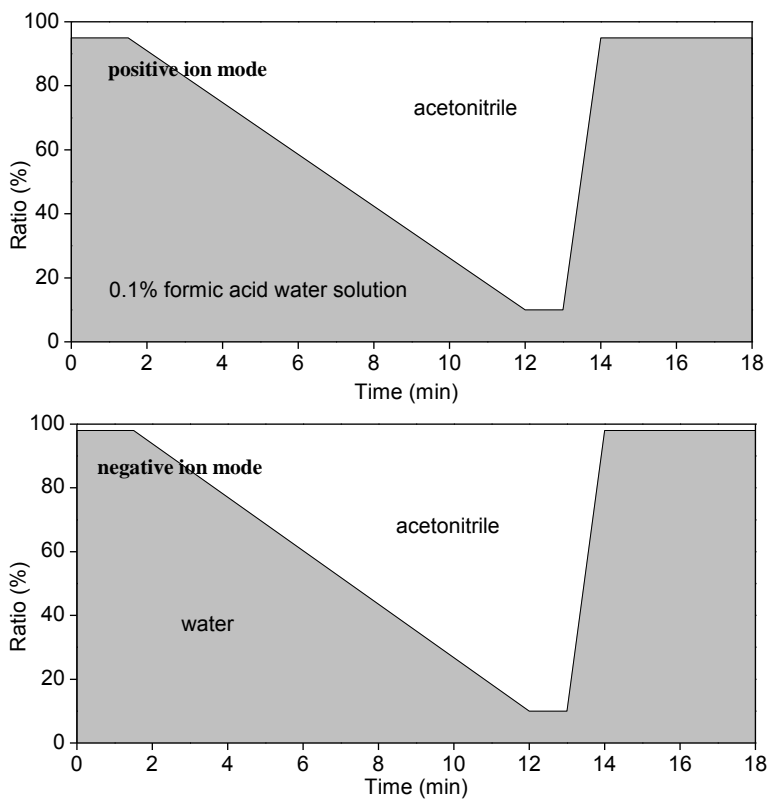


Figure 3-10: The composition and gradient programmes of the mobile phase used for the detection of DBP and its degradation intermediates in Chapter Eight.

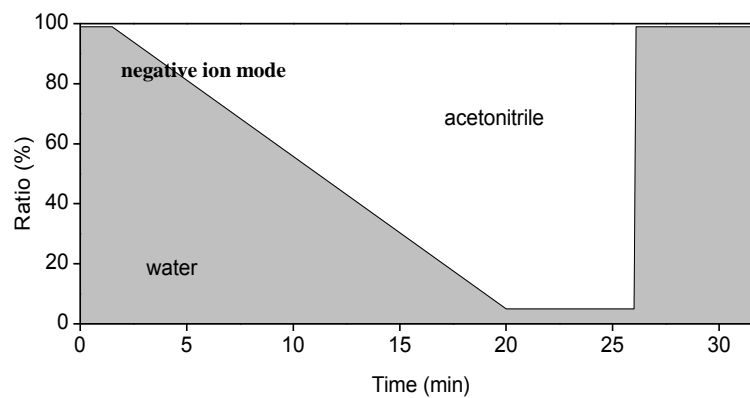


Figure 3-11: The composition and gradient programme of the mobile phase used for the detection of NP and its degradation intermediates in Chapter Nine.

3.3.5. TOC and TN measurement

The TOC measurement in Chapter Four and Six was conducted by Shimadzu TOC-5000A analyzer. The $[ATZ]_0$ for TOC measurement was 0.1 mM (Chapter Six). TOC measurement in other chapters and total nitrogen (TN) measurement were conducted by Shimadzu TOC-L analyzer.

3.3.6. Other analytical methods



The UV absorption spectra of reaction solutions were obtained using a Biochrom Libra S35 UV/Vis Spectrophotometer. Surface tension was measured by DuNouy Tensiometers (CSC Scientific Company, Inc.) with a platinum ring. The concentration of Fe^{2+} was determined by a spectrophotometric method at 510 nm via forming a complex (reddish orange, $\epsilon = 1.1 \times 10^4 \text{ L mol}^{-1} \text{ cm}^{-1}$) with 1, 10-phenanthroline. The concentration of nitrate ions were quantified by spectrophotometric method using thymol and the yellowish complex was measured at 415 nm (Igarashi 1976, SUN Shiping et al. 2007).

Chapter 4: Degradation of Dimethyl Phthalate Using a High-Frequency Ultrasonic Process

The results section of a dissertation is often simply a presentation of results, including tables, diagrams and a description of the findings. It is often done without any interpretation or discussion of the results, which often comes in a separate chapter. This chapter includes a discussion of both the results and the methodology chosen.

This chapter is very effective partly because the writer includes the following:

Structure

Introduction		Section 4.1
Findings and Discussion on each set of parameters in turn		Section 4.2.1-4.2.6
Summary		Section 4.3

Content

- Highlights the need for the investigation (e.g. Section 4.1 paragraph 1)
- Outlines the content of the chapter (e.g. Section 4.1 paragraph 2)
- Presents a clear structure in each subsection, introducing the results and then discusses these results (e.g. Section 4.2.1).
- Compares the results to previous studies (Section 4.2.1, paragraph 2, sentence 1).
- Compares to other studies when discussing results (e.g. Section 4.2.5 paragraph 2, sentence 3).
- Highlights what the study has achieved e.g. *are reported for the first time in this study* (Section 4.2.6, paragraph 2, sentence 8).
- Highlights contribution of findings (Section 4.3 final sentence).
- Summarises the discussion in the chapter (e.g. Section 4.3)

Language

- Uses past simple tense and passive voice to describe the results (e.g. Section 4.2.1, paragraph 1, sentence 3)

- Describes figures present using key numbers from the chart e.g. *the worst performance...* (e.g. Section 4.2.1, paragraph 1, final sentence)
- Uses uncertain language when discusses possible reasons e.g. *may* (e.g. Section 4.2.1 paragraph 2, sentence 9) *most likely* (e.g. Section 4.2.3 paragraph 2, sentence 1).
- Starts section with a clear topic sentence for the whole section (e.g. Section 4.2.2 paragraph 1, sentence 1)
- Structures subsections logically e.g. Introduces a problem → discusses possible causes → highlights problem through the experimental results (e.g. Section 4.2.3)
- Discusses the results in an objective way e.g. *It is believed that these results...* (e.g. Section 4.2.5 paragraph 2, sentence 6)

To Consider

This chapter of the thesis is effective. However, it could be further improved in the following aspects.

💡 Direct readers to tables by giving the page number, if the table is not on the same page as the description, e.g. *in Table 4-2 on page 60*.

💡 Give a transitional statement at the end of the chapter that leads into the next chapter.

4. Chapter Four Degradation of Dimethyl Phthalate Using a High-Frequency Ultrasonic Process

4.1. Overview

Although many studies have been performed using ultrasound to degrade different organic compounds, the information concerning the sonolytic degradation of PAEs is scarce, especially concerning the possible intermediates and products, which is useful to evaluate the process and/or find other proper processes to combine with it. Besides, many studies have focused on improving the efficiency of organic compound degradation by incorporating other AOTs with ultrasound (Peller et al. 2003, Segura et al. 2009, Weavers et al. 2000), which is adverse for scrutinizing the detailed mechanisms of sonolysis due to the faster reaction rate of the combined processes.

In this chapter, the performance of a high-frequency ultrasonic system (HFUS) with DMP as the probe compound was investigated systematically. The effects of several parameters on the efficiency of the ultrasonic system were evaluated, these being the ultrasonic frequency, ultrasonic power, DMP concentration, initial solution pH, and the effect of the presence of H₂O₂. In addition, the main intermediates of DMP sonolysis were identified and the possible degradation pathways were also proposed.

4.2. Results and discussion

4.2.1. Ultrasonic frequency optimization

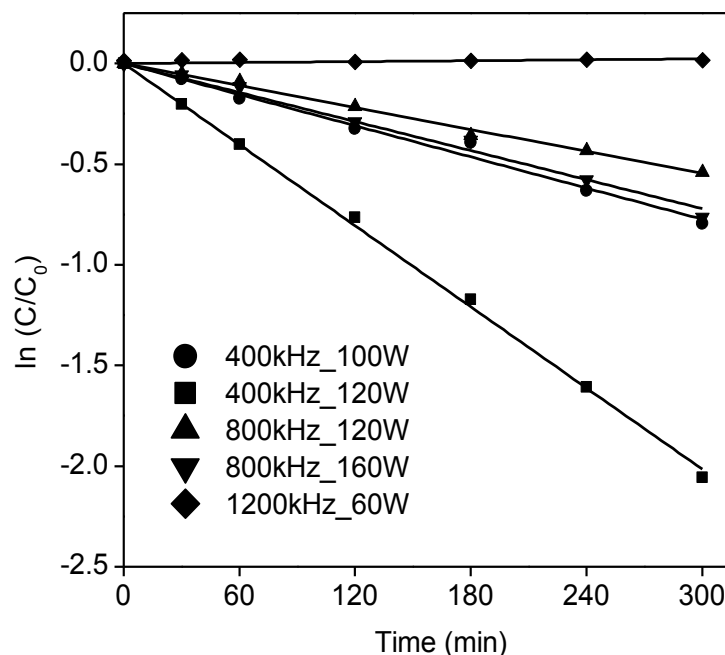


Figure 4-1: Temporal variation of DMP concentrations in the sonolytic processes with different ultrasonic frequencies and powers ($[\text{DMP}]_0 = 0.1 \text{ mM}$).

The DMP degradation performance for different ultrasonic frequencies (400, 800, and 1200 kHz) and powers is shown in Figure 4-1. The results suggested that the DMP sono-degradation follows pseudo first-order kinetics. The greatest degradation performance was obtained from the 400 kHz process using its maximum input power (available) of 120 W. A reaction rate constant (k) of $6.7 \times 10^{-3} \text{ min}^{-1}$ was observed and 87.2% of DMP was removed in 300 min. At the same frequency, the degradation rate decreased substantially when the input power reduced only moderately to 100 W, indicating that the power supplied to the ultrasound system was also a major factor affecting the compound degradation efficiency. Analogously, a similar phenomenon was observed for the 800 kHz process, in which an

increase in the nominal input power from 120 W to its maximum of 160 W produced a corresponding increase in the DMP removal performance. However, the performance at 800 kHz was inferior to that of the 400 kHz-120 W situation, and the magnitude of k of the 800 kHz process was less than one third of the 400 kHz process with the same input power (120 W). The worst performance was evident from the 1200 kHz process at its maximum nominal input power of 60 W, where there was no measurable DMP degradation within 300 min.

The observation from these tests that the most effective frequency for degrading DMP was 400 kHz, agrees with the results reported in other studies (Inoue et al. 2006). The ultrasonic frequency plays an important role in determining the efficacy of the process by influencing the cavitation performance. It is obvious that, the number of acoustic cycles and bubble collapse increases as the frequency increases. However, the critical size of the cavitation bubbles is inversely proportional to the frequency of the ultrasound (Pang et al. 2011). The frequency of the gas bubble pulsation is given by (Henglein 1987):

$$v = \frac{1}{\pi d} \left(\frac{3\gamma P}{\rho} \right)^{1/2} \quad (4-1)$$

where d is the diameter of the bubble; γ is the ratio of the specific heats of the cavitation medium; ρ is the density of the liquid; and P is practically equal to the hydrostatic pressure P_0 . When the bubble has grown to the size where its characteristic frequency (Eq. 4-1) is equal to the frequency of the sound, it shoots (Henglein 1987). For example, the critical diameter of a 100 kHz pulsation bubble is estimated to be 66 μm and 7.6 μm for a frequency of 1 MHz (Henglein 1987). Based on these, the bubbles formed at high-frequency with a correspondingly smaller explosion diameter, release less energy than the

low-frequency bubbles for one single pulsation, since bubbles at the low-frequency ultrasonic field have time to grow and experience more mass transfer to achieve more violent collapse (Henglein 1987, Petrier and Francony 1997). Thus, a higher frequency may compensate for the lower energy release per single bubble explosion by occurring more frequently. However, an above optimal frequency only leads to a small energy release for a single bubble, which could not be accumulated sufficiently by the repeating frequency. The optimal frequency is determined by the comprehensive performance of energy release (bubble sizes and repeating frequency). From the results of these initial tests, the most effective frequency was found to be 400 kHz and this was used in all further tests in this chapter.

4.2.2. Effect of power density

In order to clarify the power effect on sonolysis efficiency, the DMP degradation performance was investigated by varying the solution volume with a constant nominal input power of 120 W. From Figure 4-2, a significant decrease of the degradation rate was observed with the increase of solution volume, indicating the importance of power density (the power applied per unit volume of irradiated liquid (Ning et al. 2009)) on DMP sonolysis.

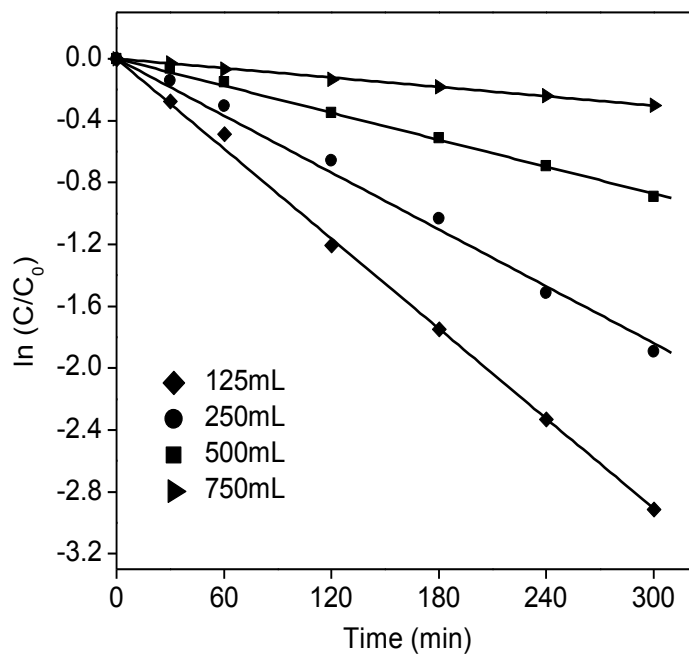


Figure 4-2: Temporal variation of DMP concentration in the sonolytic processes with different solution volumes ($[DMP]_0 = 0.1 \text{ mM}$; ultrasound: 400 kHz–120 W).

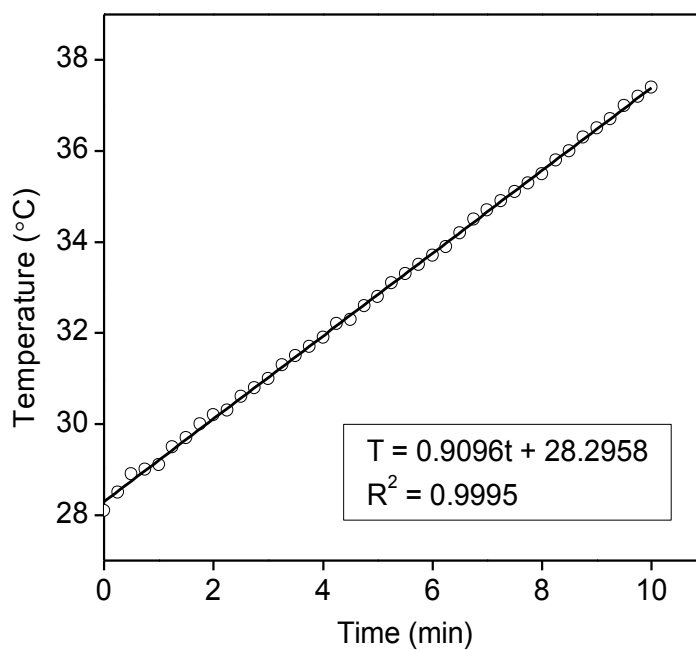


Figure 4-3: Initial temperature increase of pure water in the 400 kHz ultrasound with 125 mL water volume.

The actual power dissipated into the water can influence the amplitude of the ultrasonic wave, causing the cavitation bubbles to oscillate more violently, and thereby giving rise to an increased production of radicals and a greater pyrolysis performance (Xiong et al. 2012). The ultrasonic power actually entering the solution can be determined approximately by measuring the initial rate (10 min, at 15 s intervals) of solution temperature rise, dT/dt , and by Eq. 4-2:

$$\text{Power (W)} = (dT / dt) \cdot C_p \cdot M \quad (4-2)$$

where C_p is the specific heat of water ($4,200 \text{ J} \cdot \text{kg}^{-1} \cdot ^\circ\text{C}^{-1}$), and M is the mass of water (kg).

Figure 4-3 shows the typical tendency of temperature variation over time with water volume of 125 mL, where a good linear correlation ($R^2 = 0.9995$) could be observed in the initial 10 min.

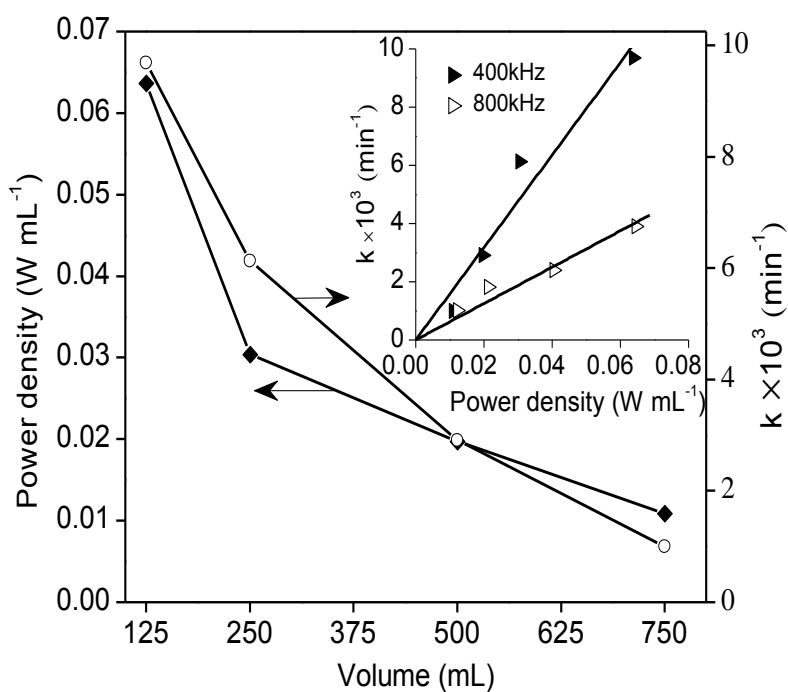


Figure 4-4: Variation of DMP degradation rate and power density with solution volume ($[\text{DMP}]_0 = 0.1 \text{ mM}$; ultrasound: 400 kHz–120 W).

Table 4-1: Calorimetric results of 400 kHz – 120 W ultrasound ($[DMP]_0 = 0.1$ mM).

Volume (mL)	125	250	500	750
dT/dt ($^{\circ}\text{C}\cdot\text{min}^{-1}$)	0.9096	0.4348	0.2815	0.1554
Absorbed power (W)	7.9590	7.6090	9.8525	8.1585
Power density ($\text{W}\cdot\text{mL}^{-1}$)	0.0637	0.0304	0.0197	0.0109
k (min^{-1})	0.0097	0.0061	0.0029	0.0010

The temperature increasing rate (dT/dt), power absorbed and DMP degradation rate (k) with different initial water volumes are summarized in Table 4-1 and Figure 4-4. It was observed that the initial rate of solution temperature rise was inversely related to the solution volume, but the total power absorbed was almost the same for different volumes, accounting for 6.3 – 8.2% of the nominal input power. Kimura et al. also reported that the calorimetrically determined ultrasonic power measurements were independent of the water volume (Kimura et al. 1996). Hence, it was concluded that the variation in solution volume only changed the power density; the power density can be deduced from Eq. 4-2 by incorporating the water density, as follows:

$$\text{Power density (W/mL)} = C_p \cdot \rho \cdot dT/dt \quad (4-3)$$

Since C_p and density ρ (mass/volume) are constants, a higher power density (via less solution volume) leads to a more rapid temperature rise, as observed experimentally.

The relationship between DMP degradation rate and power density is more evident in Figure 4-4, where the power density and k were inversely related to solution volume. An

approximately linear relationship of k as a function of power density was indicated from the results (inset of Figure 4-4), confirming the positive role of power density on DMP degradation. Hwang et al. also investigated the dependence of the reaction rate constant on the power density by varying the input power to obtain different power densities, and the linear relationship was also proposed (Hwang et al. 2011). This positive role of power density can be explained by the extent of the cavitation activity, whereby the number and/or density of the cavitating bubbles increases with increasing power density (Sivakumar and Gedanken 2004).

Comparative tests were conducted using the 800 kHz process and a similar linear trend was observed but with a much lower gradient (inset of Figure 4-4). Thus, the 400 kHz process with a higher gradient displayed a better DMP degradation capability compared to that of the 800 kHz system with the same input power. Hence, in general, the slope can well characterize the sonochemical property among different ultrasonic systems and the linear correlation between k and power density might potentially become a useful tool in predicting the sonochemical process performance if the characterization constant (slope) is predetermined.

4.2.3. Effect of initial DMP concentration

Previous studies have shown that the first-order degradation rate constant of organic compounds by ultrasound is inversely related to the initial compound concentration (e.g. (Weavers et al. 2000)) and similar results were found in this study, where the initial DMP concentration was varied from 0.01 to 0.15 mM (Figure 4-5). The reason for this behavior

has not been fully explained in previous studies, and one hypothesis is proposed here.

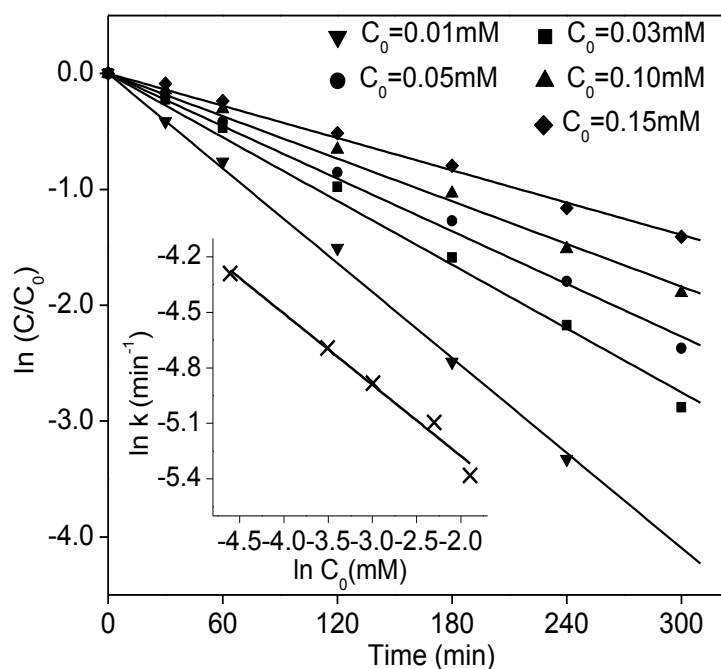


Figure 4-5: Effect of initial DMP concentrations on DMP degradation (ultrasound: 400 kHz–120 W).

In view of the low volatility and hydrophilic nature of DMP, the principal mechanism of DMP degradation in the HFUS is most likely its oxidation by free radicals both at the cavitation bubble interface and in the aqueous phase, rather than by pyrolysis inside the bubble. This was confirmed by conducting tests in the presence of 1.0 M MeOH, an effective radical ($\bullet\text{OH}$) scavenger ($k_{\bullet\text{OH}} = 9.7 \times 10^8 \text{ M}^{-1}\cdot\text{s}^{-1}$ (Buxton et al. 1988)), and no measurable reduction in the DMP concentration was evident for 300 min. Thus, the degradation of DMP by $\bullet\text{OH}$ can be written as follows:



The rate constant k_{DMP} has been reported to be second-order ($x = 1$) with a value of $2.67 \times 10^9 \text{ M}^{-1}\cdot\text{s}^{-1}$ (Wen et al. 2011). During sonication at a constant power input, it can be assumed that the rate of $\bullet\text{OH}$ generation is constant, and that the $\bullet\text{OH}$ concentration in solution during the reaction maintains a steady state, whereby the generation of $\bullet\text{OH}$ radicals equals their consumption by reaction with the target compound and scavengers (Inoue et al. 2006). The main reactions in pure water induced by ultrasonic irradiation have been summarized in Section 2.2.1.2. A prominent product of sonication is hydrogen peroxide (R 2-3, R 2-5, R 2-6, R 2-17, R 2-22), which accumulates linearly in solution during the period of ultrasound irradiation (see 5.2.2) and which also acts as a $\bullet\text{OH}$ radical scavenger (R 2-15; $k_{\bullet\text{OH}} = 2.7 \times 10^7 \text{ M}^{-1}\cdot\text{s}^{-1}$ (Buxton et al. 1988)).

Thus, the net rate of change of $\bullet\text{OH}$ radicals in solution can be expressed as follows:

$$-d[\bullet\text{OH}]/dt = k_g - k_{\bullet\text{OH}} [\bullet\text{OH}]^y [\text{DMP}] - k_{\text{Per}} [\bullet\text{OH}]^w [\text{H}_2\text{O}_2] - k_{\text{Int}} [\bullet\text{OH}]^z [\text{Int}] \quad (4-5)$$

where k_g is the zero-order rate constant for $\bullet\text{OH}$ radical generation; $[\text{DMP}]$, $[\text{H}_2\text{O}_2]$ and $[\text{Int}]$ are respectively the time-dependent concentrations of DMP, hydrogen peroxide, and DMP reaction intermediates; and $k_{\bullet\text{OH}}$, k_{Per} and k_{Int} are the corresponding reaction rate constants. Since under steady state conditions, $d[\bullet\text{OH}]/dt = 0$, and initially ($t \approx 0 \text{ s}$) $[\text{H}_2\text{O}_2]$ and $[\text{Int}]$ can be assumed to be zero, and $[\text{DMP}] = [\text{DMP}]_0$ (initial DMP concentration), Eq. 4-5 can be simplified to give the $[\bullet\text{OH}]$ as follows:

$$[\bullet\text{OH}] = (k_g / k_{\bullet\text{OH}} [\text{DMP}]_0)^{1/y} \quad (4-6)$$

Combining Eq. 4-4 (assuming $x = 1$) and Eq. 4-6, gives the following expression for the sonolytic degradation of DMP:

$$-d[\text{DMP}]/dt = k_{\text{DMP}} (k_g / k_{\bullet\text{OH}} [\text{DMP}]_0)^{1/y} [\text{DMP}] \quad (4-7)$$

Eq. 4-7 represents the first order degradation kinetics for DMP where the pseudo first-order rate constant (k) is equal to $k_{\text{DMP}} (k_g/k_{\text{OH}} [\text{DMP}]_0)^{1/y}$. The results shown in Figure 4-5 are consistent with the inverse dependency of k on $[\text{DMP}]_0$ as indicated by Eq. 4-7, which in general terms can be written as:

$$k = A [\text{DMP}]_0^{-B} \quad (4-8)$$

where $A = k_{\text{DMP}} (k_g / k_{\text{OH}})^{1/y}$, and $B = 1/y$.

The results obtained experimentally (Figure 4-5) were in close agreement with Eq. 4-8 ($R^2 = 0.98$), with the value of B determined to be 0.39 ($y = 2.6$). For the subsequent tests in this chapter, unless otherwise stated, an initial DMP concentration of 0.05 mM was selected in order to shorten the reaction time.

4.2.4. Effects of initial solution pH on DMP sonolytic degradation

The solution pH is generally an important factor influencing the efficiency of the oxidation processes, and the influence of initial pH on the sono-degradation of DMP was studied in the range of pH 2–11; the results are presented in Figure 4-6. It can be seen that the rate constant was not substantially affected by pH, but generally decreased (by 15%) with increasing pH for the range of 4 – 9.

Complementary tests were carried out without ultrasound (only stirring) to determine the direct effect of hydrolysis of DMP at the different pH conditions. No significant hydrolysis was detected for all the pH conditions except for pH 11. Hydrolysis was evident at pH 11 corresponding to a DMP degradation of 49.4% in 240 min, which when compared to the

overall degradation of 85.3% in 240 min with ultrasonic irradiation, indicated the extensive role of DMP hydrolysis in strongly alkaline conditions. Yim et al. have also reported the significant hydrolysis at pH 12 when they examined the sonolysis of another PAEs member, diethyl phthalate (DEP) (Yim et al. 2002). Since the hydrolysis of DMP also followed pseudo first-order kinetics (data not shown), the net degradation rate excluding hydrolysis is also shown in Figure 4-6 (insert figure). By excluding hydrolysis effects, it is clear that the rate of DMP degradation by sonication decreased systematically, and to an increasingly greater extent, between pH 5 and 11. Since DMP is a non-dissociating compound, the most likely reason for this degradation with increasing pH is the effect of increasing hydroxyl radical scavenging by hydroxide ions ($k_{OH} = 1.3 \times 10^{10} \text{ M}^{-1}\cdot\text{s}^{-1}$ (Buxton et al. 1988)), and the decreasing oxidation potential of $\bullet\text{OH}$ with increasing pH (Zhao et al. 2004).

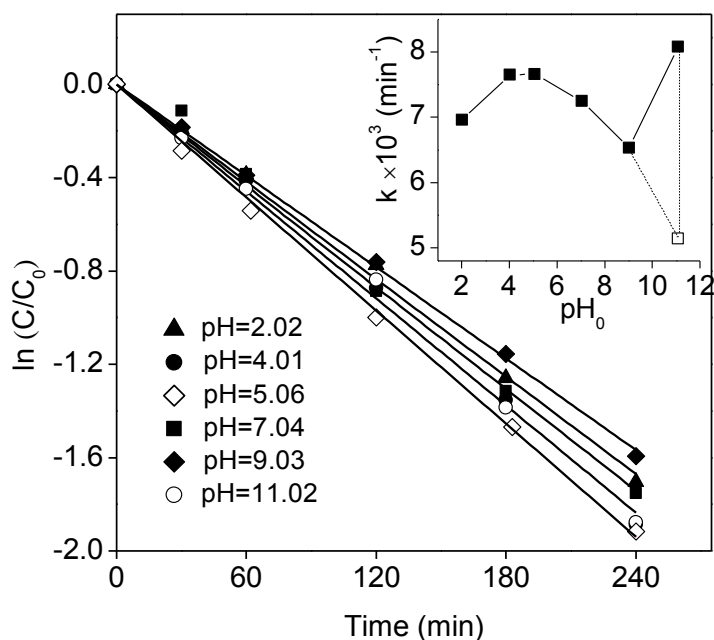


Figure 4-6: Effect of initial solution pH on DMP sonolysis ($[\text{DMP}]_0 = 0.05 \text{ mM}$; ultrasound: 400 kHz–120 W).

The lower DMP degradation rate at pH 2 compared to the rates at pH 4 and 5 is believed to be the effect of $\bullet\text{OH}$ radical scavenging by hydrogen sulphate ions ($k_{\text{OH}} \approx 1 \times 10^6 \text{ M}^{-1}\cdot\text{s}^{-1}$ (Buxton et al. 1988)), arising from the use of sulphuric acid to lower the pH in these tests (pKa of $\text{HSO}_4^- \approx 1.9$). At pH 4 and 5 the concentration of added sulphate is very low and therefore the extent of scavenging will be considerably less than at pH 2.

4.2.5. Effect of addition of hydrogen peroxide on DMP decomposition

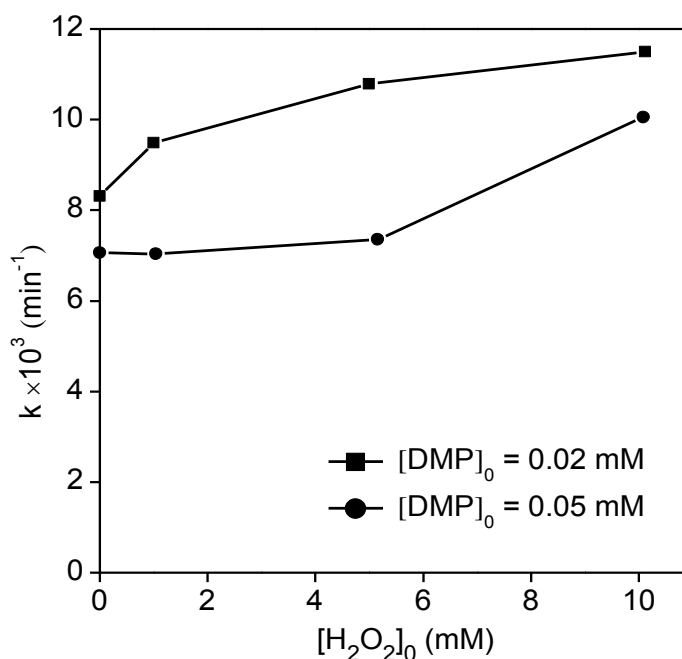


Figure 4-7: Influence of hydrogen peroxide dose on the DMP degradation rate (ultrasound: 400 kHz–120 W).

As discussed previously, hydrogen peroxide is generated during ultrasonic irradiation via reactions R 2-3, R 2-5, R 2-6, R 2-17, and R 2-22. The influence of H_2O_2 on the sonochemical degradation of a target compound is expected to be determined by its impact on the concentration of $\bullet\text{OH}$ in solution, and the direct or synergistic (with $\bullet\text{OH}$) reaction

between H_2O_2 and the compound. In the former case, the presence of H_2O_2 can have both a positive and negative effect on $[\bullet\text{OH}]$ in solution, in which $\bullet\text{OH}$ are generated directly from H_2O_2 sonolysis (Adewuyi 2001, Ku et al. 2005):



and where $\bullet\text{OH}$ radicals are scavenged by H_2O_2 , as described previously. Given the complexity of these related mechanisms, it is expected that the net effect of the presence of H_2O_2 on DMP degradation will depend on the prevailing reaction conditions. A previous study by the authors with a group of iodinated compounds (Ning et al. 2009) showed that the extent of compound degradation by ultrasound was significantly enhanced by the addition of H_2O_2 to the solution, but that the enhancement was significantly dependent on the compound concentration (i.e. much less at higher concentration).

In this study, the impact of H_2O_2 on DMP degradation was considered by the application of different H_2O_2 concentrations (0 – 10 mM) at the start of a sonolysis reaction lasting 180 min. Prior to these tests it was established that direct oxidation of DMP by H_2O_2 alone was not significant. The results of addition of hydrogen peroxide in the presence of ultrasound are shown in Figure 4-7, where in general H_2O_2 had a promoting effect on DMP degradation, which increased with the initial H_2O_2 concentration. As observed in the previous study mentioned above (Ning et al. 2009), the promoting effect of H_2O_2 was dependent on $[\text{DMP}]_0$, where the presence of moderate concentrations of H_2O_2 (< 5 mM) significantly enhanced the compound degradation rate of the 0.02 mM DMP solution, but gave very little enhancement in the case of 0.05 mM DMP solution. However, at the greatest H_2O_2 concentration (10 mM) the degradation rates for the two DMP concentrations were relatively close. It is believed that these effects reflect the relative concentrations

(molar ratio) of $\bullet\text{OH}$ and DMP in the solutions, and the relative contribution that H_2O_2 makes to $\bullet\text{OH}$ radical generation or scavenging. The accumulation of H_2O_2 during the sonolysis process within 3 h was less than 0.2 mM in a 0.05 mM DMP solution (see 5.2.2). Based on the results in Figure 4-7, under this low range of $[\text{H}_2\text{O}_2]$, the role of H_2O_2 is mainly a radical source rather than a radical scavenger.

4.2.6. Identification of reaction intermediates from DMP sonolysis

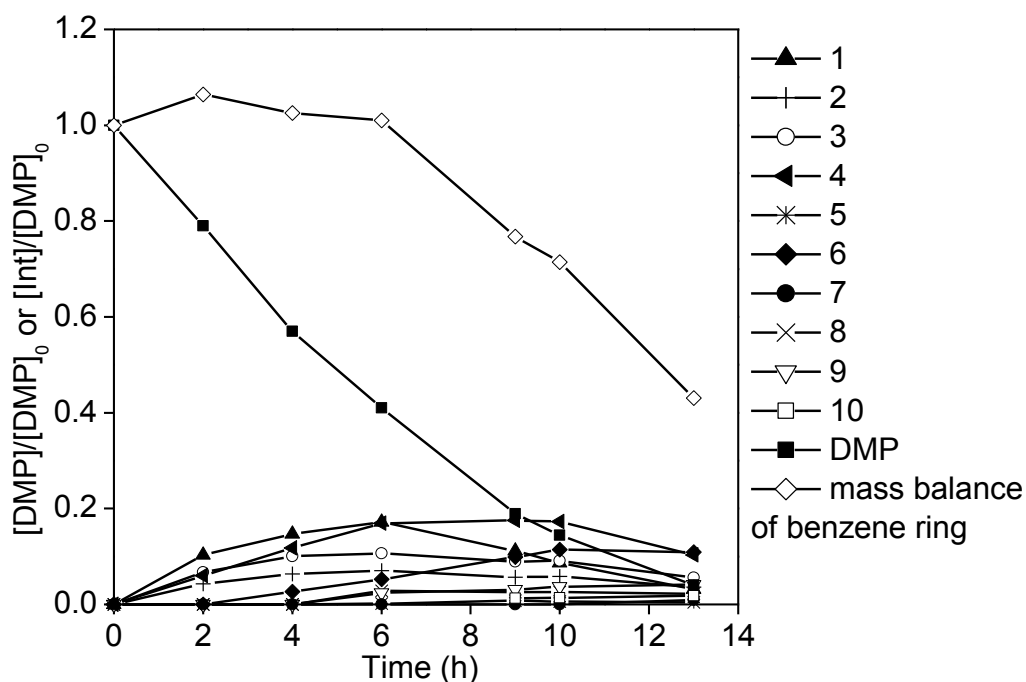


Figure 4-8: The concentration evolution of DMP and the detected sonolysis intermediates of DMP (ultrasound: 400 kHz–120 W; $C_0 = 0.25$ mM).

The ultrasonic degradation of DMP is mainly attributed to hydroxyl radical oxidation (see 4.2.3). However, the sonolytic process is slower compared to other $\bullet\text{OH}$ generating AOTs (e.g. Fenton, $\text{UV}/\text{H}_2\text{O}_2$) due to its distinct heterogeneous water-bubble interface which can repel hydrophilic compounds from the $\bullet\text{OH}$ concentrated area. It has been reported that the

efficiency of $\bullet\text{OH}$ scavenging in sonolysis process is correlated to the hydrophobicity of the solutes rather than the specific reactivity towards $\bullet\text{OH}$ in homogeneous solution (Henglein and Kormann 1985). E. Psillakis et al. have proved that the PAEs with higher hydrophobicity demonstrated greater sonolytic degradation efficiency (Psillakis et al. 2004). Therefore, reaction intermediates with more hydrophilic characteristics might have difficulties in competing $\bullet\text{OH}$ with their mother compound, DMP. The accumulation of these intermediates not only confirm this hypothesis, but also makes them easier to be detected. This explains why many new intermediates were reported in this study for the first time, because they were easily escaped from the detection in other AOTs.

The information of the identified intermediates is summarized in Table 4-2, and the evolution profile of the main intermediates is shown in Figure 4-8. For some intermediates the addition of one formate anion, $[\text{M} + 45]^-$, was observed due to the use of 0.1% formic acid as the mobile phase (Quang et al. 2006). All the intermediates detected in this study had shorter retention times than DMP, implying a higher polarity than their mother compound. The hydroxyl groups attached to the benzene ring readily participate in the $p-\pi$ conjugation effect, and therefore the electron density was increased. In addition, the carboxylic group was also beneficial for electron withdrawing, all resulting in a higher polarity of these intermediates. Many studies have reported hydroxylation in different AOTs involving the mechanism of $\bullet\text{OH}$ radicals (Rao and Chu 2009, Tay et al. 2011, Yuan et al. 2008b), and hydroxylated intermediates were also found in sonochemical reactions (Inoue et al. 2008). However, in the case of DMP, only mono- and bi-hydroxylated phthalates were reported by using other AOTs (Tay et al. 2011, Yuan et al. 2008b). The tri- and tetra-hydroxylated derivatives of DMP, the hydroxy-MMP (monomethyl phthalate),

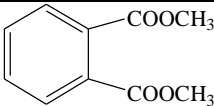
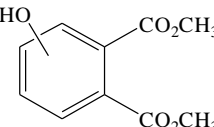
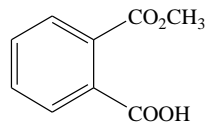
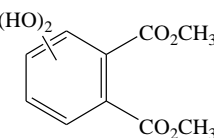
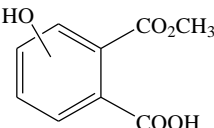
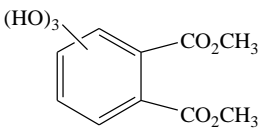
and hydroxy-PA (phthalic acid) are reported for the first time in this study. This is partly because LC/MS is more capable of detecting hydrophilic intermediates than GC/MS. Another reason, as mentioned above, is the slower generation of hydroxal radicals on the hydrophobic surface of bubbles resulting in the accumulation of the more hydrophilic intermediates in the solution.

As can be seen from Figure 4-8, compounds 1 – 4 were more abundant during the early period, but declined later after reaching a peak at 6 – 8 h. Compound 2 with evident LC signal hardly responded to MS detection (see Figure 4-9). With further degradation of these primary intermediates, secondary derivatives appeared and accumulated gradually (compounds 5 – 10). In addition, the dimethyl hydroxy-phthalate with more hydroxylated groups increased slower during the reaction, indicating that the hydroxylation potentially proceeded step by step. Hence, the degradation pathway of DMP sonolysis was proposed in Scheme 4-1. The degradation of DMP involved the hydroxylation of the aromatic ring, the oxidation of the aliphatic chains, or both. It should be noted that the intermediates of MMP and PA have been reported to be much less toxic than DMP (Jonsson and Baun 2003).

According to the mass balance as shown in Figure 4-8, 57% of detectable benzene ring structures were opened when 96% DMP was removed. However, no evident TOC removal was observed during this period (data not shown). This suggests the likely formation and accumulation of many aliphatic organics with higher hydrophilicity, accounting for the intact of TOC. If mineralization is one of the treatment objectives, other proper AOTs should be combined with ultrasound, such as UV irradiation (although DMP is inert toward direct photolysis (Chen et al. 2009b)) to improve the decomposition of the more

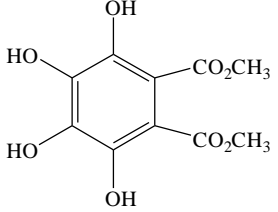
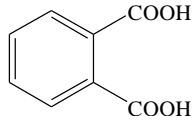
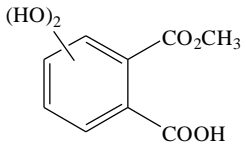
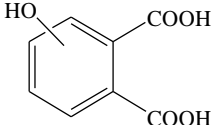
hydrophilic intermediates. S. Na et al. have proved that the mineralization of DEP was improved significantly when ultrasound was combined with UV irradiation, which might be also applicable for DMP degradation (Na et al. 2012a, Na et al. 2012b).

Table 4-2: Information of the identified intermediates from DMP sonolysis determined by LC/ESI-MS.

Compound Code	Retention Time (min)	Structural Formula	Formula	Molar Weight
DMP	54.35		$C_{10}H_{10}O_4$	194
1	50.20		$C_{10}H_{10}O_5$	210
2	47.62	unknown	unknown	unknown
3	45.90		$C_9H_8O_4$	180
4	43.23		$C_{10}H_{10}O_6$	226
5	41.95		$C_9H_8O_5$	196
6	39.85		$C_{10}H_{10}O_7$	242

(c.o.)

(b.f.)

7	38.35		$C_{10}H_{10}O_8$	258
8	36.78		$C_8H_6O_4$	166
9	33.42, 32.80		$C_9H_8O_6$	212
10	29.28		$C_8H_6O_5$	182

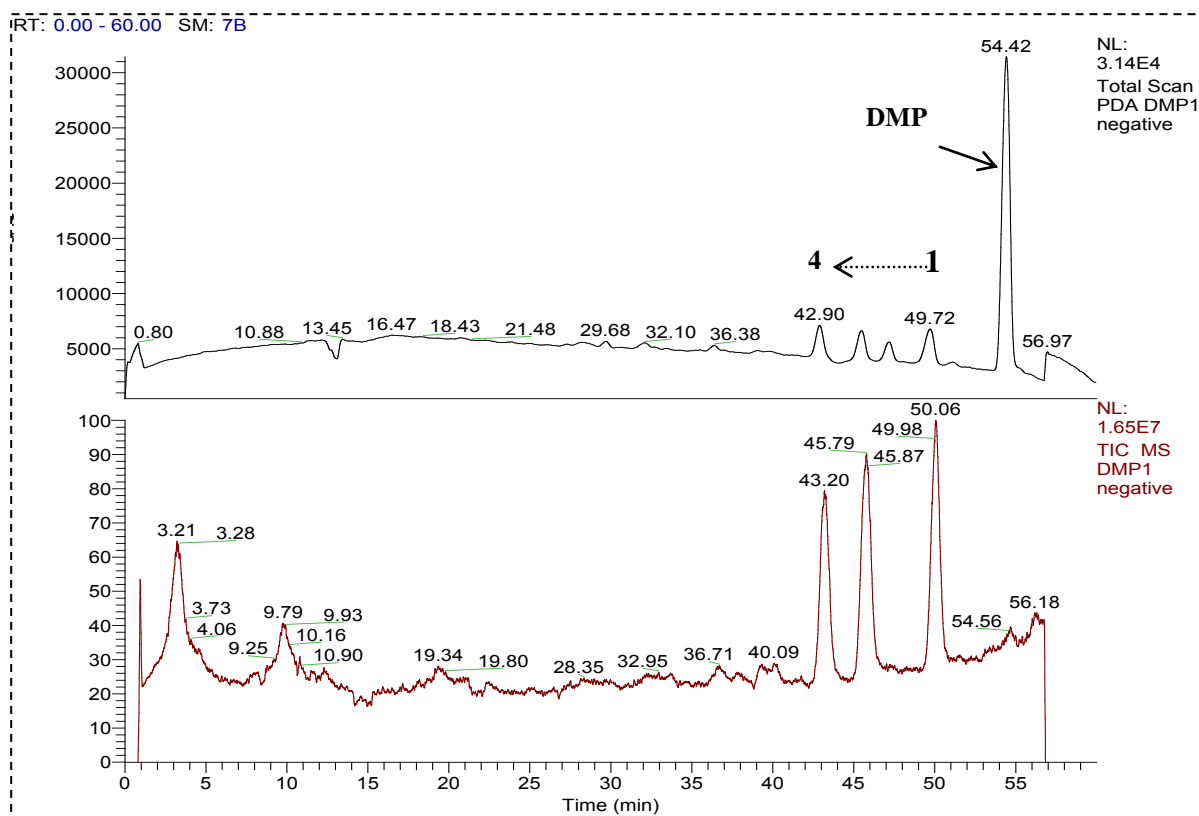
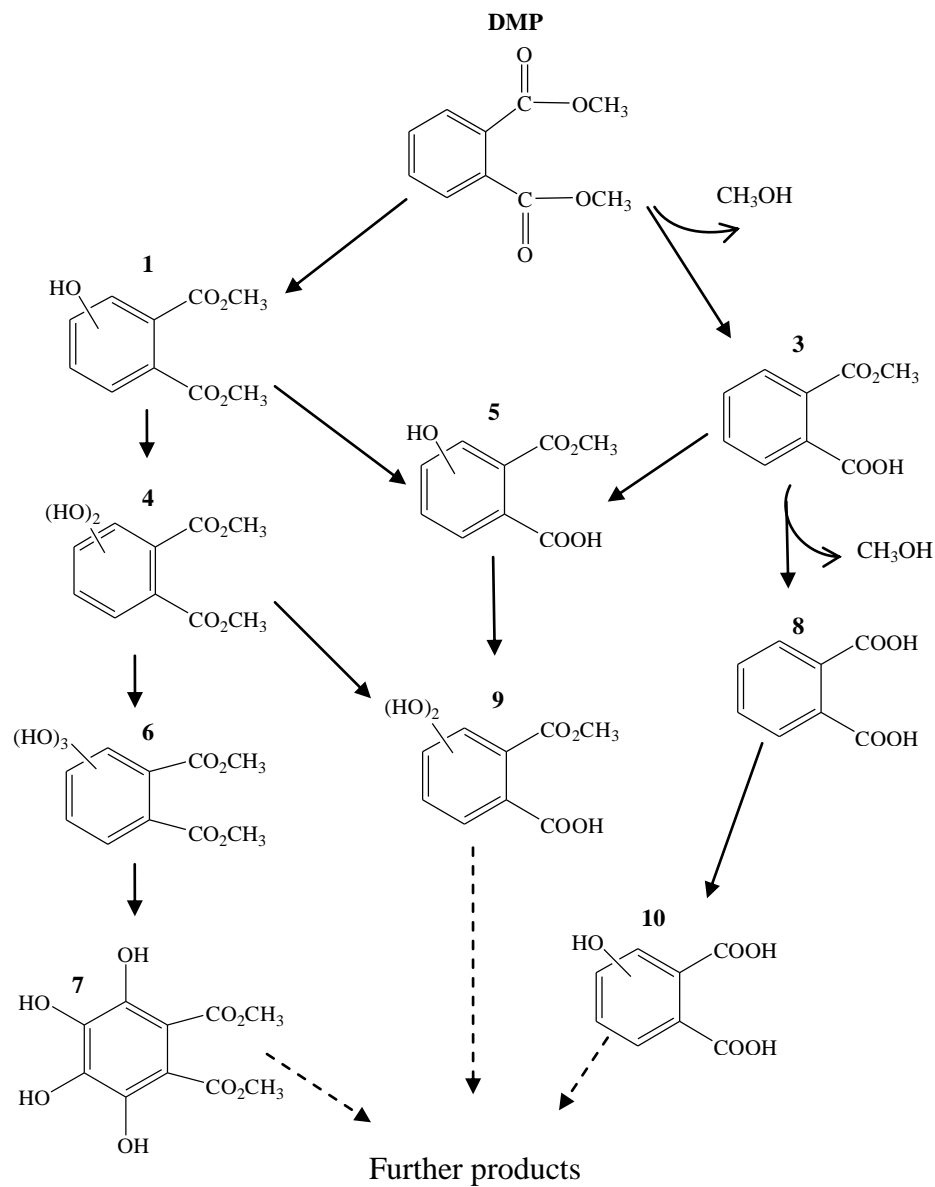


Figure 4-9: HPLC/ESI-MS chromatogram of DMP and its degradation intermediates after 4 h sonolysis (ultrasound: 400 kHz–120 W; $C_0 = 0.25$ mM).



Scheme 4-1: Degradation pathways of sonochemical degradation of DMP (Dashed arrows indicate reactions that require more than one step).

4.3. Chapter summary




In this chapter, DMP can be degraded by HFUS via reacting with $\bullet\text{OH}$ radicals, and the degradation follows pseudo first-order kinetics. The optimal performance corresponds to a frequency of 400 kHz. The degradation rate increased directly with the ultrasound power density, and decreased moderately with increasing pH in the range typically found in the environment (pH 5 – 9). Higher initial concentration results in a lower degradation rate. Both the hydroxylation of the benzene ring and the oxidation the aliphatic chain were found to be the dominating mechanisms of DMP sonolysis. In addition, the HFUS was found to be effective in degrading more hydrophobic DMP, but less efficient in degrading its more hydrophilic intermediates. All these findings may cast some light on understanding the mechanisms of the sonolytic processes and finding proper processes to improve the efficiency.

Chapter 5: Sonophotolytic Degradation of Dimethyl Phthalate: Analysis of the Synergistic Effect and Modeling.

The results chapter of a thesis is often simply a presentation of results, including tables, diagrams and a description of the findings. It is often done without any interpretation or discussion of the results, which often comes in a separate chapter. This chapter includes a discussion of both the results and the methodology chosen.

This chapter is very effective partly because the writer includes the following:

Structure:

Introduction		Section 5.1
Findings and Discussion on each set of parameters in turn		Section 5.2.1-5.2.5
New Model		Section 5.2.6
Summary		Section 5.3

Contents:

- Gives a clear overview of the topic (e.g. Section 5.1 paragraph 1).
- Develops the first paragraph of Section 1 in a logical way:
 - a. Background (e.g. first part sentence 1)
 - b. Problem (e.g. second part sentence 1)
 - c. Possible solution (e.g. sentence 2)
 - d. Evaluates possible solution (e.g. sentence 3)
 - e. Discusses the disadvantages of the possible solution (e.g. second part sentence 3)
 - f. Discusses the advantages of the possible solution (e.g. sentence 4)
 - g. Highlights a gap in knowledge (e.g. sentence 7).
- Outlines the content of the chapter (e.g. Section 5.1 paragraph 2)
- Compares the results to previous studies (e.g. Section 5.2.1, paragraph 1, final sentence)
- Highlights what has not been researched in other studies e.g. information...is scarce (e.g. Section 5.2.4, paragraph 1, sentence 2)

- Highlights the contribution of the findings to understanding of the topic (e.g. Section 5.3, final sentence)

Language

- Uses past simple tense and passive voice to describe the results e.g. *was found* (e.g. Section 5.2.1, paragraph 1, sentence 4).
- Uses empty subject with verb *note* e.g. it should be noted (e.g. Section 5.2.3 paragraph 3, sentence 1).
- Uses uncertain language when discussing possible reasons e.g. *Most likely resulting from* (e.g. Section 5.2.1 paragraph 1, sentence 3), *These results may suggest* (e.g. Section 5.2.5 paragraph 1, sentence 4)

To Consider

This chapter of the thesis is effective. However, it could be further improved in the following aspects.

💡 Check the real meaning of linking words e.g. *At last* does not mean finally and should not be used with that meaning (e.g. Section 5.3, final sentence).

💡 Provide a clear overview of what each section contains in the introductory section, e.g. Section 5.2.1 describes the results of the...Section 5.2.2 discusses these findings...

💡 Include a transitional statement at the end of the chapter that leads into the next chapter.

5. Chapter Five Sonophotolytic Degradation of Dimethyl Phthalate: Analysis of the Synergistic Effect and Modeling

5.1. Overview

Although US can achieve the degradation of refractory compounds, one of its shortcomings is its relatively low efficiency, mostly due to the inevitable recombination of generated radicals (*ca.* 80%) to form more stable molecules (e.g. H₂O₂, H₂O) (Stock et al. 2000), which reduces the effective contact between radicals and target contaminants. In order to counter these effects and enhance the oxidation performance by US, its combination with other AOTs (photocatalysis, Fenton process, ozonation, etc.) has been tested in an attempt to show either an additive or a synergistic benefit (Lesko et al. 2006, Peller et al. 2003, Stock et al. 2000, Torres et al. 2007). The hybrid technique of combining UV and US has been found to be beneficial in enhancing the degradation of target compounds but the majority of previous studies have been conducted under photocatalyst mediated conditions (Gogate et al. 2002, Hamdaoui and Naffrechoux 2008, Johnston and Hocking 1993), which has the disadvantage of incurring the additional costs of the catalysts and their final disposal. The combination of catalyst-free UV and US, however, has the advantage of avoiding the cost of the catalyst, the additional process complexity and the potential hazard of catalyst leaching into the aqueous environment. Currently, information regarding the US/UV process is relatively limited, and a similar conjecture of the auxiliary role of photolysis of the ultrasonically generated H₂O₂ is proposed (Torres et al. 2007). The degradation kinetics of US/UV process was always approximately considered as a first-order reaction (Na et al. 2012b, Rong et al. 2003). There is a need for more detailed

information concerning the exact role of H₂O₂ in the treatment reactions and a mechanistic model to describe the US/UV process.

The main interest of this chapter is to ascertain the main mechanism of the hybrid process of US/UV in the absence of any catalyst with DMP as a chosen probe. The contribution of H₂O₂ is examined both qualitatively and quantitatively, and a novel inverted S-curve degradation model is proposed to describe the hybrid process.

5.2. Results and discussion

5.2.1. Effect of UV light intensity

The DMP photo-decomposition with different UV light intensities (viz. different numbers of lamps) is shown in Figure 5-1, where pseudo first-order kinetics was assumed. As expected, the rate of compound degradation increased systematically with light intensity, but the extent of DMP degradation by photolysis alone was relatively minor. Thus, only 21.3% of DMP was eliminated after 150 min at the greatest applied light intensity (6 lamps), most likely resulting from the poor quantum yield at 253.7 nm. The photo-degradation of DMP was found to follow closely pseudo first-order kinetics and the rate constant (k) was linearly related with the light intensity (inset of Figure 5-1). The theoretical photodegradation rate of a specific compound can be expressed by the following relationship (Eq. 5-1) (Chan et al. 2010):

$$k = 2.303\phi I_{\lambda} \varepsilon_{\lambda} l \quad (5-1)$$

where ϕ is the quantum yield (mol·Einstein⁻¹), I_{λ} is the light intensity (Einstein·L⁻¹·s⁻¹), ε_{λ} is the compound molar absorptivity (L·mol⁻¹·cm⁻¹), and l is the light path (cm). This is

consistent with the experimentally observed linear correlation between k (min^{-1}) and the light intensity I_λ ($\text{Einstein}\cdot\text{L}^{-1}\cdot\text{s}^{-1}$), i.e. $k = 2.515 \times I_\lambda$ ($R^2 = 0.99$). By incorporating the regression equation with Eq. 5-1 and substituting the appropriate values, where ε_λ is $1.43 \times 10^3 \text{ L}\cdot\text{mol}^{-1}\cdot\text{cm}^{-1}$ (measured experimentally) and l is 1.8 cm, the quantum yield was determined to be $4.24 \times 10^{-4} \text{ mol}\cdot\text{Einstein}^{-1}$. A similarly low value for ϕ ($= 8.5 \times 10^{-4} \text{ mol}\cdot\text{Einstein}^{-1}$) was reported by Chen et al. (Chen et al. 2009b).

The effect of UV light intensity was also investigated for the combined US/UV process (see Figure 5-2). As with UV alone, the DMP degradation increased with UV light intensity, but the increase diminished at higher light intensities (more than 3 lamps) with the DMP degradation reaching a maximum, indicating that the UV irradiation was not a rate-limiting factor in the process (i.e. the system turns into a highly optical dilute condition, and the rate becomes less dependent on light intensity). It was clear that the combined US/UV process significantly improved the DMP degradation (98.4% in 120 min with 6 lamps) compared to that of solely US (57.4% in 120 min) or solely UV (16.6% in 120min with 6 lamps) processes. Thus, the effectiveness of the three processes could be summarized as: UV (6 lamps) < US < US/UV (6 lamps). It was evident that the nature of the DMP degradation kinetics by the combined US/UV process was different from that of US and UV alone. A distinct, and repeatable, lag phase (slower kinetics) appeared in the initial period (< 30 min), which was more obvious with higher light intensities. This indicated a departure from quasi-first order kinetics in which the decay curve had the form of an inverted S-curve; this will be discussed in more detail later. In all subsequent tests the maximum UV light intensity was applied (6 lamps) in order maximize the reactions and enable the fundamental mechanisms to be investigated.

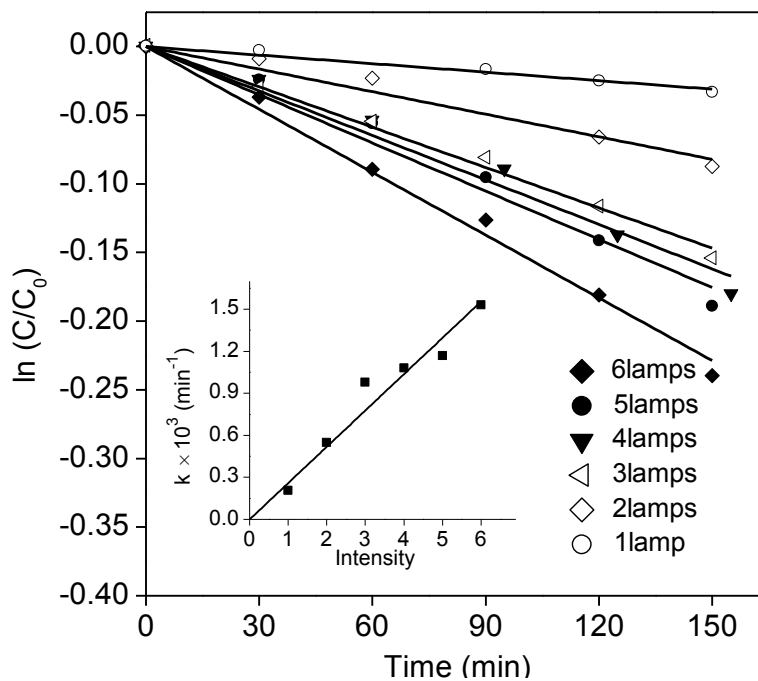


Figure 5-1: Effect of UV light intensity on DMP photolytic degradation ($C_0 = 0.05 \text{ mM}$, UV: $\lambda = 253.7 \text{ nm}$).

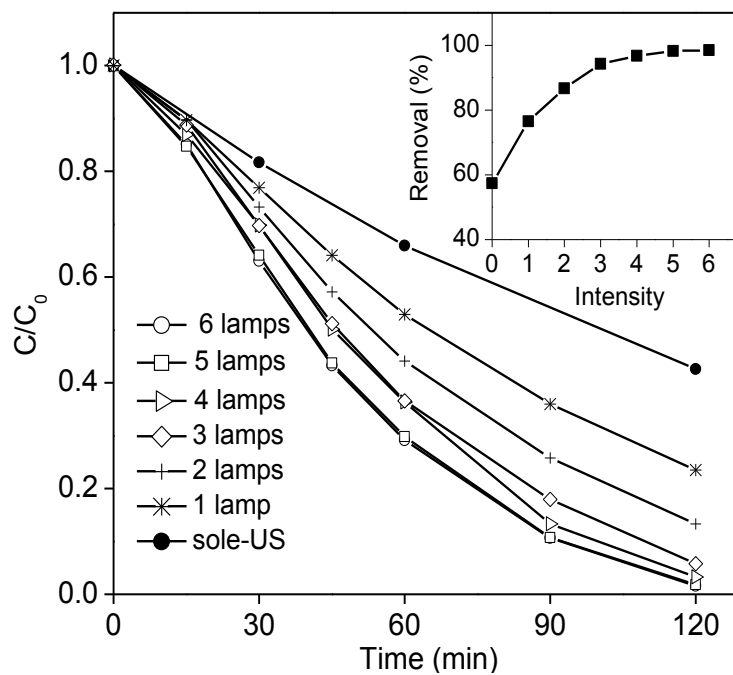


Figure 5-2: Effect of UV light intensity on DMP sonophotolytic degradation ($C_0 = 0.05 \text{ mM}$, UV: $\lambda = 253.7 \text{ nm}$, US: 400 kHz–120 W).

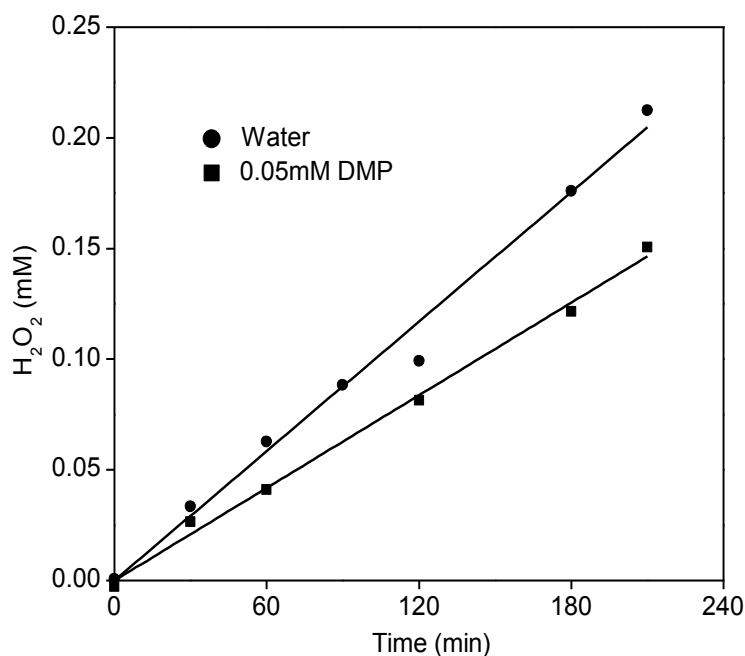
5.2.2. Formation of H₂O₂ during sonication

Figure 5-3: Variation of H₂O₂ concentration over sonication time (US: 400 kHz–120 W).

As has been established previously, H₂O₂ is produced during sonication by the interaction of US-generated radical species, either directly ($2\cdot\text{OH} \rightarrow \text{H}_2\text{O}_2$, $2\text{HO}_2\cdot \rightarrow \text{H}_2\text{O}_2 + \text{O}_2$) or with water molecules ($\text{O}\cdot + \text{H}_2\text{O} \rightarrow \text{H}_2\text{O}_2$) (Adewuyi 2001, Inoue et al. 2006). In this chapter, the formation of H₂O₂ during sonication was evaluated qualitatively and quantitatively both in pure water and 0.05 mM DMP solution, and the results are presented in Figure 5-3. The results showed that the concentration of H₂O₂ increased linearly with sonication time, and that the concentration increase in the 0.05 mM DMP solution was less than that in pure water, owing to the higher consumption of $\cdot\text{OH}$ radicals (the main precursor in forming H₂O₂) by DMP and its intermediates. Based on this result, the kinetics of H₂O₂ formation during sonolysis can be formulated as Eq. 5-2.

$$\frac{d[\text{H}_2\text{O}_2]}{dt} = k_1 \quad (5-2)$$

where k_1 was determined to be 6.97×10^{-4} and $9.75 \times 10^{-4} \text{ mM}\cdot\text{min}^{-1}$ for 0.05 mM DMP solution ($R^2 = 0.9980$) and pure water ($R^2 = 0.9951$), respectively.

5.2.3. DMP degradation by UV/H₂O₂ process

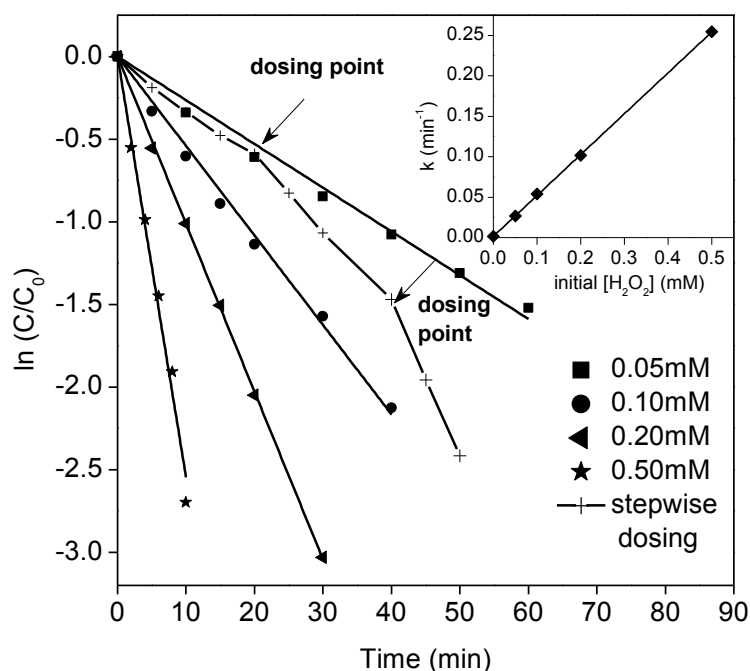


Figure 5-4: Degradation of DMP by UV/H₂O₂ process with different initial H₂O₂ concentrations and degradation of DMP by stepwise UV/H₂O₂ process (UV: $\lambda = 253.7 \text{ nm}$, 6 lamps, $[\text{DMP}]_0 = 0.05 \text{ mM}$).

Since the presence of H₂O₂ in the sonolysis process was confirmed, the combined process of US/UV also incorporates the advanced oxidation process of UV/H₂O₂. In order to ascertain the features of the UV/H₂O₂ process, the degradation of DMP directly by the UV/H₂O₂ process was investigated with various initial H₂O₂ concentrations, ranging from

0.05 to 0.50 mM (concentrations selected based on the results of the sonolytic experiment). The possible contribution of direct oxidation by H₂O₂ was found to be negligible from the results of control tests which showed there was no detectable change in DMP concentration in the presence of 30 mM H₂O₂ solution during 180 min. The results summarized in Figure 5-4 indicated that the DMP degradation followed pseudo first-order kinetics ($R^2 > 0.9950$) for each of the applied H₂O₂ concentrations. Thus, the DMP degradation by UV/H₂O₂ process can be expressed as:

$$-\frac{d[\text{DMP}]}{dt} = k_2[\text{DMP}] \quad (5-3)$$

where k_2 was 0.0265 min⁻¹ in the presence of only 0.05 mM initial H₂O₂, which is 18 times greater than that observed with UV alone (0.0015 min⁻¹). Thus, it can be concluded that DMP photo-degradation is accelerated substantially by the presence of H₂O₂, attributed mainly to the generation of hydroxyl radicals from the photo-decomposition of H₂O₂ (Chu 2001, Xu et al. 2009b).

The pseudo first-order rate constant (k_2) was found to increase linearly with the initial concentration of H₂O₂ (inset of Figure 5-4). The value of k_2 therefore can be further expanded to a more general rate expression including two reaction mechanisms as follows:

$$k_2 = k_3[\text{H}_2\text{O}_2]_0 + k_{\text{UV}} \quad (5-4)$$

where k_3 was determined to be 0.5060 mM⁻¹ min⁻¹ and the intercept (k_{UV}) is the direct photolysis rate constant ($[\text{H}_2\text{O}_2]_0 = 0$ mM), with the value of 0.0015 min⁻¹.

Hence, Eq. 5-3 can be re-written by substituting Eq. 5-4 as:

$$-\frac{d[\text{DMP}]}{dt} = \{k_3[\text{H}_2\text{O}_2]_0 + k_{\text{UV}}\}[\text{DMP}] \quad (5-5)$$

However, it should be noted that the concentration of H_2O_2 is replenished continuously in the US/UV process (Figure 5-3) rather than one-off feed. In order to clarify the kinetic property of DMP photolysis under the condition of a continuous supplement with H_2O_2 , stepwise-UV/ H_2O_2 was examined by stepwise dosing H_2O_2 (thrice in total), during the reaction (cross points in Figure 5-4). The reaction was initiated with 0.05 mM H_2O_2 , and then additional concentrations of 0.05 and 0.10 mM H_2O_2 were added at 20 and 40 min, respectively. For each resulting total H_2O_2 concentration (i.e. 0.05, 0.10 and 0.20 mM), the overall DMP degradation demonstrated first order kinetics and a stepwise increase in rate constant which was identical to the rate constant obtained when the same overall H_2O_2 concentration was added at the beginning of the reaction. From this, it was evident that the reaction rate was only dependent on the prevailing H_2O_2 concentration and was not sensitive to H_2O_2 consumption during the reaction.

In short, irrespective of the dosing pattern, the DMP decay rate in UV/ H_2O_2 process is mainly determined by the total dosage of H_2O_2 and pseudo first-order kinetics is applicable for the reaction span without any supplement with H_2O_2 . Thus, Eq. 5-4 could be restated as the rate constant of both one-off and stepwise UV/ H_2O_2 (at a certain moment t), where the $[\text{H}_2\text{O}_2]_0$ should be re-defined as the total dosage up to the moment t .

The consistent agreement with first-order kinetics in the DMP reactions with UV/ H_2O_2 (Figure 5-4) over periods up to 60 min indicated that the concentration of H_2O_2 during the

reactions was not limiting. Thus, although being consumed during the reaction, the H_2O_2 concentration, and thus the $\bullet\text{OH}$ radical concentration, was always in excess relative to the DMP concentration. From Eq. 5-1 the photolytic consumption of H_2O_2 can be estimated by assuming values for the quantum yield ($\phi = 0.98 \text{ mol}\cdot\text{Einstein}^{-1}$ (Hunt and Taube 1952)) and molar absorptivity ($\varepsilon_\lambda = 19.0 \text{ L}\cdot\text{mol}^{-1}\cdot\text{cm}^{-1}$ (Morgan et al. 1988)), giving a rate, k , of $8.0 \times 10^{-4} \text{ s}^{-1}$. This low value for the photolysis rate corresponds to a reduction of only 38% in H_2O_2 concentration over 10 min from an initial concentration of 0.5 mM, and hence supports the assumption that the concentration of H_2O_2 was not rate-limiting in the experiments.

By comparing the calculated initial rate of H_2O_2 consumption, where theoretically one mole of H_2O_2 produces two moles of $\bullet\text{OH}$ radicals ($k_{\text{OH}} = 2 \times 8.0 \times 10^{-4} \times [\text{H}_2\text{O}_2]_0, \text{ mM}\cdot\text{s}^{-1}$), and the experimentally measured initial rate of DMP degradation according to Eq. 5-5 (ignoring direct photolysis) under the corresponding conditions ($[\text{DMP}]_0 = 0.05 \text{ mM}$, $k_{\text{DMP}} = 0.5060/60 \times [\text{H}_2\text{O}_2]_0 \times 0.05, \text{ mM}\cdot\text{s}^{-1}$), the theoretical reaction stoichiometry ($\bullet\text{OH}$: DMP) was estimated to be 3.8 : 1.

5.2.4. Effect of initial solution pH

Solution pH is an important parameter influencing the efficiency of many AOTs. However, information regarding the effect of pH on the performance of the combined US/UV process is scarce. Figure 5-5 summarizes the results of the sonophotolytic degradation of DMP at different initial pH values, in the range from 2.44 to 10.89. The solid data points in the inset of Figure 5-5 depict the overall removal of DMP after 60 min under various initial pH.

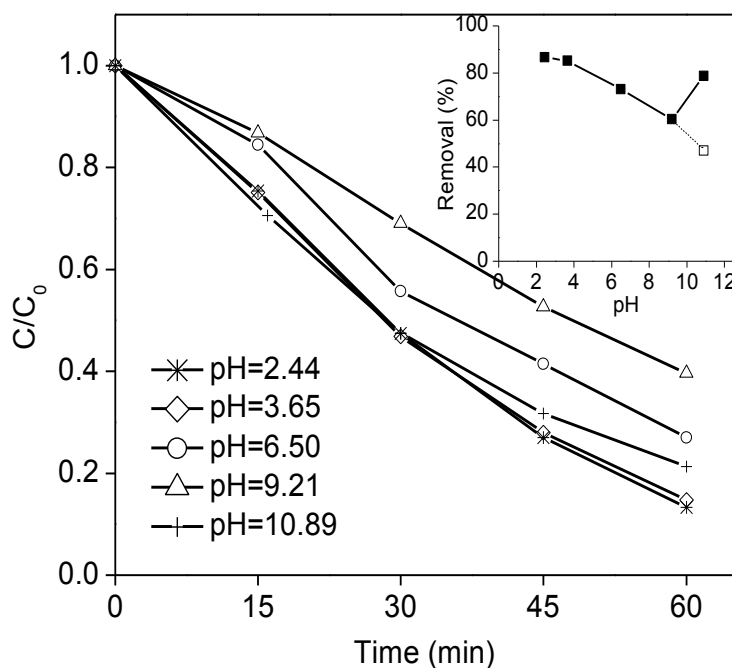


Figure 5-5: Effect of initial solution pH on DMP sonophotolytic ($[DMP]_0 = 0.05$ mM, UV: $\lambda = 253.7$ nm, 6 lamps, US: 400 kHz–120 W).

The results show a systematic reduction in DMP degradation with increasing pH, except at pH 10.89. An investigation of the hydrolysis of DMP over the same pH range showed no hydrolysis effects except under the strong basic conditions at pH 10.89, where 31.8% of DMP was hydrolyzed in 60 min. By excluding the hydrolysis effect, the hollow data point shown in the inset of Figure 5-5 is the net DMP removal by sonophotolysis which was consistent with the trend of decreasing DMP removal with increasing initial pH. Since DMP is a non-dissociating compound, the possible reasons for the decrease in DMP degradation with increasing pH are: (a) the decreasing oxidation potential of $\bullet\text{OH}$ with increasing pH (Buxton et al. 1988); (b) the rapid consumption of $\bullet\text{OH}$ in alkaline solution according to reaction R 5-1, where $k_{\text{forward}} = 1.2 \times 10^{10} \text{ M}^{-1}\cdot\text{s}^{-1}$ and $k_{\text{back}} = 9.3 \times 10^7 \text{ s}^{-1}$ (Hamdaoui and Naffrechoux 2008), and reaction R 5-2, owing to the presence of the

conjugate base of H_2O_2 , HO_2^- , in alkaline conditions ($\text{p}K_a = 11.6$), where the rate constant, $k_{\text{HO}_2^-}$ is $7.5 \times 10^9 \text{ M}^{-1}\cdot\text{s}^{-1}$ (cf. $k_{\text{H}_2\text{O}_2} = 2.7 \times 10^7 \text{ M}^{-1}\cdot\text{s}^{-1}$) (Buxton et al. 1988):



5.2.5. Sequential and simultaneous tests of US and UV

In order to examine the US/UV process in more detail and to confirm synergistic effects, DMP reactivity tests were conducted with the US and UV in series (in alternative order) and together. Thus, DMP solutions were first irradiated with UV (or US) for 120 min, and then transferred to undergo US (or UV) irradiation for a further 120 min. The results were compared with those of the combined US/UV process and can be seen in Figure 5-6. A rapid DMP degradation was achieved by the combined US/UV process with an almost complete elimination of DMP (> 98%) in 120 min, while the corresponding removal values for the individual US and UV processes were only 53.9% and 15.4%, respectively. These results suggest a synergistic, rather than additive, behavior in the combined US/UV process. For simplification, an approximate pseudo first-order rate constant of the combined process, $k_{\text{US/UV}}$, was calculated from the data and found to be 0.0238 min^{-1} . Consequently, a synergistic index could be determined as follows:

$$\text{Synergy Index} = \frac{k_{\text{US/UV}}}{k_{\text{UV}} + k_{\text{US}}} = \frac{0.0238}{0.0076 + 0.0015} = 2.6154 > 1$$

For the cases where the US and UV processes are applied in series, the residual DMP in the US pre-treated solution was totally removed by subsequent exposure to UV light for an

additional 120 min, whereas for the UV pre-treated solution 36.7% DMP still remained after 120 min of sonication. The greater degradation of DMP in the US→UV process indicates that photolysis of US generated products, particularly H₂O₂, accelerates the DMP degradation. The concentration of H₂O₂ in solution was monitored during the sequential and combined US/UV tests (Figure 5-7). In the case of the sequential US→UV arrangement it is evident that H₂O₂ accumulates continuously during the US phase and then is rapidly consumed in the following UV phase, via direct photolysis. In contrast, the build-up of H₂O₂ in the combined US/UV sonophotolytic process was much slower than that of the US alone, representing the balance between H₂O₂ generation (by US) and consumption (by UV).

While the experimental results indicated pseudo first-order kinetics for the degradation of DMP by sonolysis and photolysis separately, with respective rate constants of $k_{US} = 0.0076 \text{ min}^{-1}$ and $k_{UV} = 0.0015 \text{ min}^{-1}$, the degradation by sonophotolysis did not appear to obey first-order kinetics; this contrasts with the study by Rong et al. (Rong et al. 2003) which found that *p*-chlorophenol degradation by US, catalyst-free UV and their combination, all obeyed first-order kinetics. From the DMP degradation results shown in Figure 5-6, a slight lag phase was evident in the initial 30 min period, followed by a more rapid degradation until the DMP was nearly completely consumed. In order to explain this behavior a phenomenological model was developed which is described below.

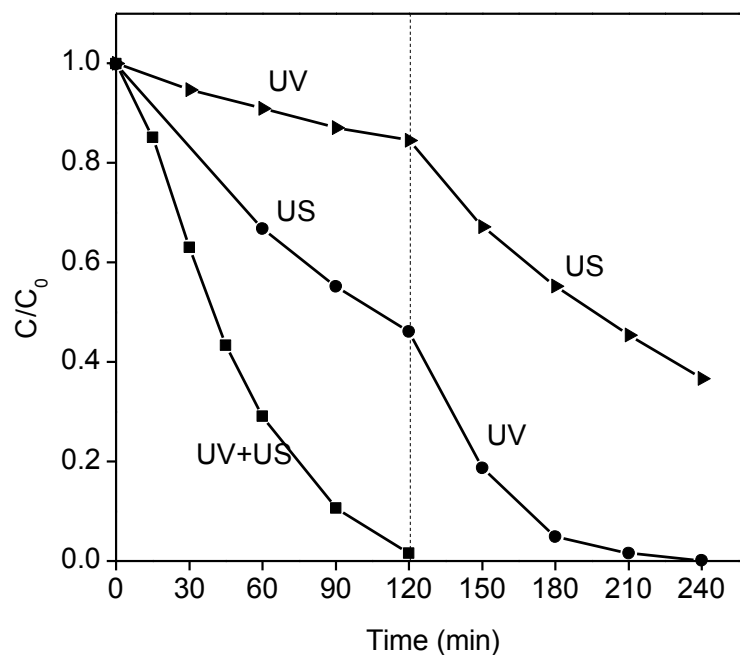


Figure 5-6: DMP degradation performance of sequential and simultaneous experiments using US: 400 kHz–120 W and UV: 253.7 nm, 6 lamps, $[DMP]_0 = 0.05$ mM.

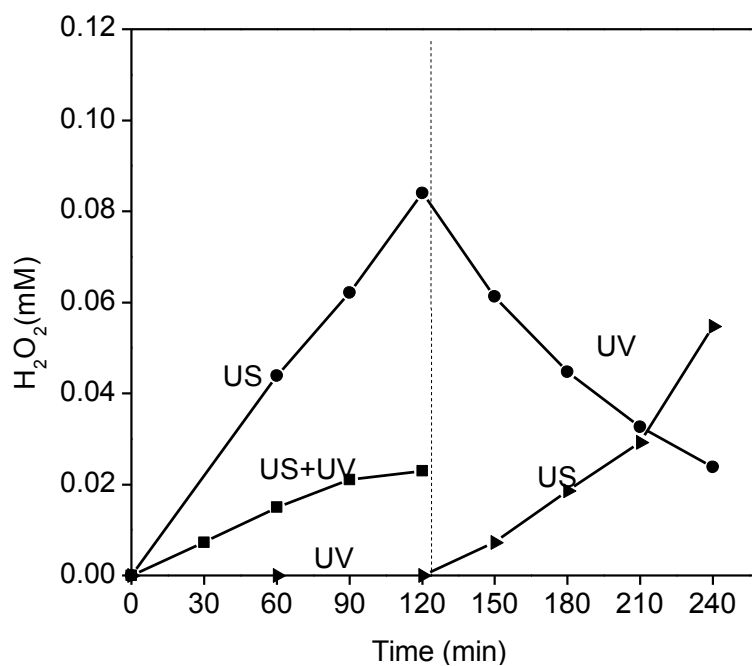


Figure 5-7: The variation of H_2O_2 concentration during the sequential and simultaneous tests using US: 400 kHz–120 W and UV: 253.7 nm, 6 lamps, $[DMP]_0 = 0.05$ mM.

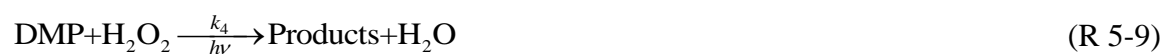
5.2.6. Modeling the sonophotolytic degradation of DMP

The main reactions involved in the sonophotolytic degradation of DMP are summarized as follows (R 5-3 – R 5-8):



where))) denotes the ultrasonic wave; the subscript))) denotes the products generated by ultrasonic irradiation; the $\cdot\text{X}$ in the bracket denotes all the possible intermediates leading to the formation of H_2O_2

To facilitate the modeling procedure, the US/UV process is divided into two dependent processes based on the above analysis, a US part and a UV/ H_2O_2 part, and the ultrasonically produced H_2O_2 linking the two parts. In this way, the above reactions can be simplified to:



where k_4 represents the rate constant of the UV/ H_2O_2 part in the US/UV process, and R 5-9

combines reaction R 5-5, R 5-7 and R 5-8.

In deriving the model, the following assumptions were made: (a) both the sonolytic and photolytic degradation of DMP follow pseudo first-order kinetics; (b) DMP degradation is principally by reactions R 5-4 and R 5-9 (i.e. DMP is oxidized by $\bullet\text{OH}$ radicals generated via either R 5-3 or R 5-7, in which the other minor oxidants, if any, contributing for DMP elimination are ignored); (c) the sonolytic degradation of DMP in the combined US/UV process (R 5-4) is not influenced by the UV process; (d) Eq. 5-4 is applicable to represent the DMP degradation via the UV/H₂O₂ process where the [H₂O₂]₀ term is defined as the total dosage up to moment t .

The overall DMP degradation rate by the US/UV process is therefore assumed to be the sum of reactions R 5-4 and R 5-9:

$$-\frac{d[\text{DMP}]}{dt} = k_{\text{US}}[\text{DMP}] + k_4[\text{DMP}] \quad (5-6)$$

It should be noted that the UV/H₂O₂ part in this process (the second term on the right-hand side of Eq. 5-6) is distinct from the traditional UV/H₂O₂ process as the supplementation of H₂O₂ is in a continuous mode by sonication rather than an one-off dosing at the beginning. From the observation of the stepwise UV/H₂O₂, DMP removal rate constants in UV/H₂O₂ process linearly depends on the total dosage of H₂O₂ regardless of the dosing manner (Figure 5-4). Additionally, the UV/H₂O₂ pathway in the US/UV process could be deemed as consisting of numerous tiny stepwise-UV/H₂O₂ processes and the instantaneous degradation rate (k_4) at moment t is assumed to be linearly related with the total provision

of H_2O_2 up to moment t based on Eq. 5-4, so the following equation could be obtained:

$$k_4 = k_3 \cdot (k_1 \cdot t) + k_{UV} \quad (5-7)$$

where $k_1 \cdot t$ is the H_2O_2 concentration generated by the US system up to time t (Eq. 5-2).

Combining Eq. 5-6 and Eq. 5-7 gives the following expression:

$$-\frac{d[\text{DMP}]}{dt} = k_{US}[\text{DMP}] + \{k_3 \cdot (k_1 \cdot t) + k_{UV}\}[\text{DMP}] \quad (5-8)$$

Using a definite integral of Eq. 5-8 to solve for the DMP concentration, C , gives:

$$\int_{C_0}^C -\frac{dC}{C} = \int_0^t \{(k_{US} + k_{UV}) + k_3 \cdot k_1 \cdot t\} dt \quad (5-9)$$

Finally, the following solution (empirical model) is obtained:

$$C = \exp \left[\ln C_0 - (k_{US} + k_{UV}) \cdot t - \frac{k_3 k_1 t^2}{2} \right], \text{ or}$$

$$\frac{C}{C_0} = \exp \left[-(k_{US} + k_{UV}) \cdot t - \frac{k_3 k_1 t^2}{2} \right] \quad (5-10)$$

where C is the DMP concentration at time t (mM); C_0 is the initial concentration of DMP (mM); k_{US} and k_{UV} are the pseudo first-order rate constants for the solely US and solely UV processes, respectively (min^{-1}); k_3 is the gradient shown in Figure 5-4 (inset) ($\text{mM}^{-1} \cdot \text{min}^{-1}$); k_1 is the gradient of the ultrasonically generated H_2O_2 ($\text{mM} \cdot \text{min}^{-1}$) (Eq. 5-2). By inspection the form of Eq. 5-10 satisfies the following limiting conditions: $t \rightarrow 0$, $C \rightarrow C_0$; and $t \rightarrow \infty$, $C \rightarrow 0$.

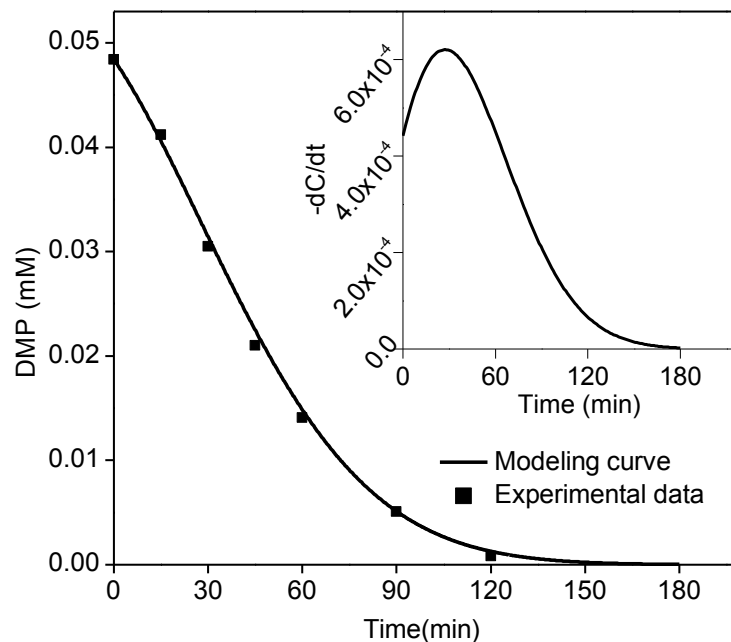


Figure 5-8: Modeling DMP degradation in the process of US/UV and comparison with the experimental data. (UV: 253.7 nm, 6 lamps; US: 400 kHz–120 W; $k_{US} = 0.0076 \text{ min}^{-1}$, $k_{UV} = 0.0015 \text{ min}^{-1}$, $k_3 = 0.5060 \text{ min}^{-1} \cdot \text{mM}^{-1}$, $k_1 = 6.97 \times 10^{-4} \text{ mM} \cdot \text{min}^{-1}$, $C_0 = 0.0484 \text{ mM}$).

A comparison between the model and experimental data is given in Figure 5-8, which demonstrated a good agreement, thereby supporting the assumptions that made in developing the model. It is believed that the model provides a useful representation of the interacting US/UV processes and reveals the synergetic role of H_2O_2 via the two characteristic constants, k_1 and k_3 . The derivative of Eq. 5-10, dC/dt , gives the rate of DMP degradation at any given reaction time, and this is shown graphically in the inset of Figure 5-8. The two phases of increasing and decreasing reaction rate are evident, where the first phase corresponds to the beneficial increase in H_2O_2 concentration, and the second phase corresponds to the declining DMP concentration; the value of dC/dt at time zero represents the term $C_0 \times (k_{US} + k_{UV})$, or the rate without the participation of H_2O_2 .

The maximum of the dC/dt curve, i.e. the inflection point on the $C-t$ curve, indicates the maximum degradation rate and the time at which this occurs. This critical point can be determined by the second derivative of Eq. 5-10, and the corresponding t_{\max} (critical time) and dC/dt_{\max} (critical rate) are given below:

$$t_{\max} = \frac{\sqrt{k_3 k_1} - (k_{US} + k_{UV})}{k_3 k_1} \quad (5-11)$$

$$\frac{dC}{dt}_{\max} = \sqrt{k_3 k_1} \times \exp \left[\left(\ln C_0 - \frac{1}{2} \right) + \frac{(k_{US} + k_{UV})^2}{2k_3 k_1} \right] \quad (5-12)$$

Using the experimental data and the above equations, the values for the critical time and maximum degradation rate were calculated to be 27.4 min and $6.21 \times 10^{-4} \text{ mM}\cdot\text{min}^{-1}$, respectively. It is evident that the position of the critical point and the shape of the degradation curve are determined by the efficiency of the two dominant mechanisms and the properties of the target compound.

For practice, the energy consumption of US, UV, and US/UV for 98% DMP removal was estimated to be 1.03, 1.52, and 0.31 kW·h, respectively. Apparently, the latter is more cost-effective in real applications.

5.3. Chapter summary


The property of the combinative process of US/UV has been investigated with DMP as a model compound. It is found that higher UV intensity is beneficial for both the photolysis and sonophotolysis of DMP, and acidic condition is more favorable for DMP sonophoto-decay. As for the combinative process of US and UV without the presence of any catalyst, a synergetic effect could be obtained with a synergetic index of 2.6. Furthermore, the role of the ultrasonically generated H_2O_2 has been examined qualitatively and quantitatively, and verified to be the main contributor to the synergistic effect of US/UV process. At last, a novel inverted S-curve model was proposed to predict the compound degradation kinetics in US/UV process, which could well explain the role of the H_2O_2 , and the formulas in determining the critical time and rate of the maximum conditions were also developed.

Chapter 6: Atrazine Degradation Using Chemical Free Process of US/UV: Analysis of the Heterogeneous Micro Environments and the Degradation Mechanisms

Chapter 7: Degradation of Dinbutyl Phthalate by a Homogeneous Sono-Photo Fenton Process with In-Situ Generated Hydrogen Peroxide

These chapters report on and discuss experimental results. Chapter 6 is organized in the following way and is very effective partly because the writer includes the following:

Structure

Introduction		Section 6.1
Findings and Discussion on each set of parameters in turn		Section 6.2
Summary		Section 6.3

Content

- Provides an overview of the section at the start of the chapter (e.g. Section 6.1).
- Organises the first paragraph to overview current knowledge:
 - Background (e.g. Section 6.1, paragraph 1, sentence 1)
 - Cites relevant sources (e.g. Section 6.1, paragraph 1, sentence 1)
 - Discusses the existing problem (e.g. Section 7.1 paragraph 1, sentence 2)
 - Highlights a gap in current knowledge (e.g. Section 7.1, paragraph 1, sentence 6)
 - Describes how the chapter will address the problem (e.g. Section 7.1, paragraph 1 final sentence)
- Outlines the content of the chapter in the second paragraph (e.g. Section 6.1, paragraph 2)
- Summarises the content and main findings of figures and tables in text (e.g. Section 7.2.1, paragraph 1, sentence 1-2)

- Organises reporting paragraphs in a logical way, e.g. Section 6.2.3 paragraph 2:
 - Sentence 1: Background
 - Sentence 2: Methodology used
 - Sentence 3: Findings
 - Sentence 4: Possible interpretation of findings
- Organises sections in a logical way (e.g. Section 6.2.4)
 - Paragraph 1: Background and problem
 - Possible solution 1
 - Previous studies citing sources
 - Paragraph 2: Possible solution 2
 - Lack of studies on this topic
 - Investigation
 - Findings
 - Paragraph 3: Explanation of findings

Language

- Uses objective language to report findings e.g. A pseudo first-order kinetics was observed (e.g. Section 6.2.1 paragraph 1, sentence 2)
- Compares findings to others in the literature e.g. *are consistent with those reported by* (e.g. Section 6.2.1 paragraph 1, sentence 3)
- Uses uncertain language when interpreting findings, e.g. *which could possibly explain* (e.g. Section 6.2.1, paragraph 2, sentence 4)

To Consider

This chapter of the thesis is effective. However, it could be further improved in the following aspects.

💡 Avoid using overly long paragraphs (e.g. Section 7.1 paragraph 1).

💡 Avoid overusing *In this chapter* at the start of a sentence. It is better to use *this chapter* as a subject, e.g. *This chapter explores...* (e.g. Section 7.3, paragraph 1, sentence 1).

6. Chapter Six Atrazine Degradation Using Chemical-Free Process of US/UV: Analysis of the Heterogeneous Micro- Environments and the Degradation Mechanisms

6.1. Overview

The photolytic degradation of ATZ has been reported before, and 2-hydroxyatrazine (OIET) was found to be the main intermediate (Chan and Chu 2005, Chen et al. 2009a, Torrents et al. 1997), accounting for more than 90% of ATZ decay (Chan and Chu 2005). Further degradation of OIET by photolysis is difficult and additional AOTs are needed to facilitate its degradation. The chemical-free US process may be a possible candidate for this. The mechanism of US and its competitive advantages have been discussed previously. A distinct feature of the US process is the heterogeneous micro-environment that exists between gas bubbles (generated from cavitation) and bulk solution (Okitsu et al. 2005), which is favorable for the degradation of more hydrophobic compounds (Henglein and Kormann 1985). In contrast, the relatively hydrophilic intermediates from the degradation of parent compounds have lower reactivity for competing radicals, so that their degradation will be restricted. The combination of UV and US may promote the degradation of these less hydrophobic intermediates via: (a) direct photolysis of the intermediates which cannot be efficiently degraded by US alone; and (b) producing additional hydroxyl radicals in the bulk solution by homolysis of the ultrasonically generated H_2O_2 (Torres et al. 2007).

Therefore, in this chapter, the sonolytic, photolytic, and sonophotolytic degradations of ATZ were investigated in detail. The existence of synergy in the US/UV process was

considered by applying the kinetic model proposed in Chapter Five to the observed sonopholytic degradation of ATZ. The heterogeneous micro-environments created by the application of 20 and 400 kHz US processes were examined for comparison, and the salt effects on these two different ultrasonic processes were also investigated. The intermediates of sonolytic, photolytic, and sonopholytic degradation of ATZ were identified via LC/ESI-MS analysis, and detailed degradation pathways of these processes were proposed.

6.2. Results and discussion

6.2.1. Kinetics of individual UV, US processes

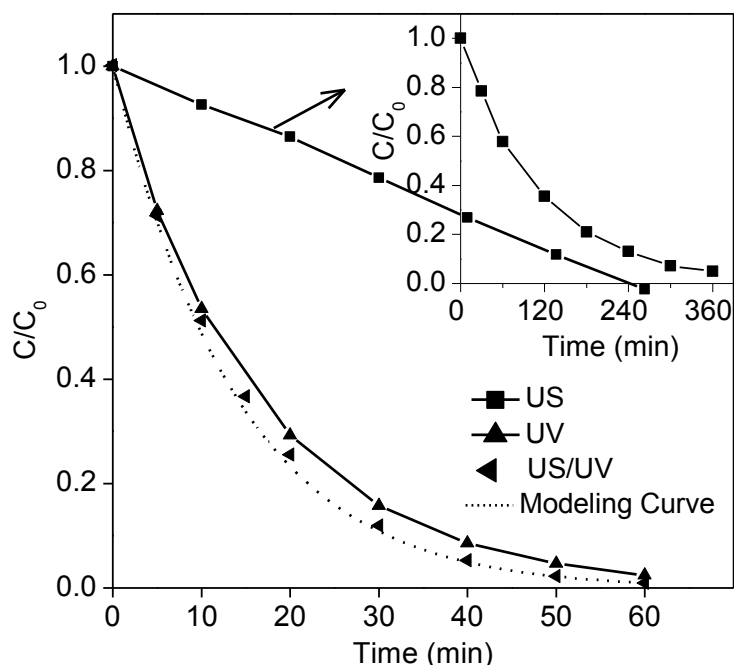


Figure 6-1: Performance of the photolytic, sonolytic, and sonopholytic degradation of ATZ ($[\text{ATZ}]_0 = 0.02 \text{ mM}$; UV: 253.7 nm, 1 lamp; US: 400 kHz, 0.03 W mL^{-1}).

The ATZ degradation by direct photolysis is shown in Figure 6-1, where 97.6% of ATZ was found to be removed within 60 min. A pseudo first-order kinetics was observed for the

photolytic degradation of ATZ, and the rate constant (k_{uv}) was determined to be $0.0617 \pm 0.0002 \text{ min}^{-1}$. The molar absorption coefficient (ϵ_{254}) and quantum yield ($\Phi_{ATZ,254}$) of ATZ were determined to be $3.39 \times 10^3 \text{ L}\cdot\text{mol}^{-1}\cdot\text{cm}^{-1}$ and $0.043 \pm 0.001 \text{ mol}\cdot\text{Einstein}^{-1}$, respectively, which are consistent with those reported previously by De Laat et al. (e.g. $\Phi_{ATZ,254} = 0.041 \pm 0.002$) (DeLaat et al. 1997). The molar absorption coefficient (ϵ_{254}) was experimentally determined based on Lambert-Beer's Law, i.e. $A = \epsilon_{254} \times b \times c$. Hence, A (absorbance) is linearly related to the concentration of ATZ (c) with a slope of $\epsilon_{254} \times b$. The optical path length (b) is known to be 1.0 cm, so the ϵ_{254} was determined to be $3.39 \times 10^3 \text{ L}\cdot\text{mol}^{-1}\cdot\text{cm}^{-1}$. The quantum yield ($\Phi_{ATZ,254}$) of ATZ could be calculated by Eq. 5-1.

The degradation of ATZ by US alone (400 kHz) is also shown in Figure 6-1 and a full scale curve is given in the figure inset. It was found that the sonolytic degradation of ATZ also followed pseudo first-order kinetics with a lower rate constant (k_{us}) of $0.0089 \pm 0.0003 \text{ min}^{-1}$. The mechanisms of aqueous ultrasound irradiation have been reported extensively (Gutierrez et al. 1991, Pang et al. 2011, Park et al. 2011, Seymour and Gupta 1997), and involve the formation and adiabatic collapse of cavitation bubbles which generate various radical species within the gaseous and solution phases, among which the hydroxyl radicals are the most abundant species; these are believed to be responsible for the degradation of many organic compounds in aqueous solution. Gutierrez et al. (Gutierrez et al. 1991) observed a steady state concentration of hydroxyl radicals of approximately 4 mM near the interface of the cavitating bubbles, which could possibly explain the observed first-order kinetics of ATZ sonolytic degradation.

6.2.2. Kinetics of sonophotolytic degradation of ATZ

The degradation performance of ATZ by the combined US/UV process is shown in Figure 6-1. The kinetics of ATZ sonophotolytic degradation was very close to a pseudo first-order reaction, as commonly adopted in several other studies (Na et al. 2012b, Rong et al. 2003). The same model proposed in Chapter Five (Eq. 5-10) was applied here, and was found to represent closely the ATZ degradation, as indicated in Figure 6-1.

$$\frac{C}{C_0} = \exp \left[-(k_{\text{US}} + k_{\text{UV}}) \cdot t - \frac{k_3 k_1 t^2}{2} \right] \quad (\text{Eq. 5-10 from 5.2.6})$$

where C is $[\text{ATZ}]_t$ (mM); C_0 is $[\text{ATZ}]_0$ (mM); k_{US} and k_{UV} are the respective pseudo first-order rate constants for the individual US and UV processes (min^{-1}); k_1 is the observed zero-order rate constant of H_2O_2 formation ($5.0 \times 10^{-4} \text{ mM} \cdot \text{min}^{-1}$) (see Figure 6-2, where the formation of H_2O_2 in both blank solution and solution with 0.02 mM ATZ was given. Good linear relationships were obtained from both conditions. The observed zero-order rate constants, i.e. k_1 , were determined to be $7.8 \times 10^{-4} \text{ mM} \cdot \text{min}^{-1}$ and $5.0 \times 10^{-4} \text{ mM} \cdot \text{min}^{-1}$ for blank water and 0.02 mM ATZ solution respectively); k_3 is the increase of pseudo first-order rate constants with per unit increase of $[\text{H}_2\text{O}_2]_0$ in the UV/ H_2O_2 process ($k_3 = 0.4548 \text{ mM}^{-1} \cdot \text{min}^{-1}$) (see Figure 6-3, where the constant k_3 is the slope of the inset curve.)

By substituting the above constants into Eq. 5-10, an equation similar to pseudo first-order but having a second term results (Eq. 6-1).

$$\ln \frac{[\text{ATZ}]_t}{[\text{ATZ}]_0} = -0.0706 \cdot t - 1.14 \times 10^{-4} t^2 \quad (6-1)$$

To further analyze the two terms on the right hand side, symbols IE and SE were used to

denote $-0.0706t$ and $-1.14 \times 10^{-4}t^2$, respectively, as shown in Eq. 6-2:

$$\ln \frac{[\text{ATZ}]_t}{[\text{ATZ}]_0} = \text{IE} + \text{SE} \quad (6-2)$$

where IE is the “individual effect” or arithmetic sum of the rate of the two individual processes (US and UV), and SE indicates the additional “synergetic effect” that is available only when UV and US coexist in the process, i.e. the higher the value of SE, the greater the synergetic effect. The temporal variation of IE, SE, and IE+SE for ATZ degradation are shown in Figure 6-4, with a longer time period given in the inset figure. As can be seen, the synergetic effect (SE) was insignificant for ATZ degradation (IE+SE) within the normal reaction time (the first 60 min), mainly because ATZ is much more sensitive to UV photolysis. However, the SE was predicted to be dominant after 600 min, as determined by calculation, so the significant influence of SE exists only when the reaction time is very long; for normal treatment operations, involving short irradiation times and low ATZ concentrations (beyond detection limit), it can be ignored, resulting in a pseudo first-order reaction. However, for the case of DMP studied previously, which is a UV insensitive chemical with a low k_{UV} , the corresponding value of SE exceeded IE after about 50 min (Figure 6-5), resulting in a noticeable inverted S decay curve. In addition, the shape of the kinetics curve is mainly determined by the position of the inflection point. According to the inflection point expression (Eq. 5-11), if $\sqrt{k_3 k_1}$ is greater than $(k_{\text{US}} + k_{\text{UV}})$, like DMP sonophotolysis, $t_{\text{max}} > 0$ and it will result in an observable inflection point, i.e. the degradation kinetics demonstrates as an inverted S-curve. However, if $\sqrt{k_3 k_1}$ is smaller than $(k_{\text{US}} + k_{\text{UV}})$, like ATZ sonophotolysis, $t_{\text{max}} < 0$ and the inflection point cannot be observed during the sampling period, which causes the degradation kinetics very similar to

a first-order reaction due to the insignificance of $\frac{k_3 k_1 t^2}{2}$ in Eq. 5-10.

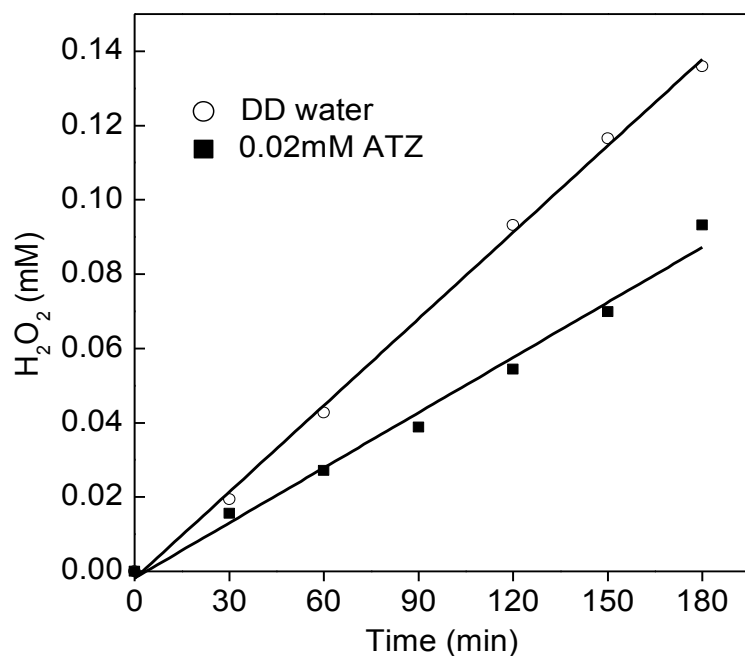


Figure 6-2: H₂O₂ formation in ultrasonic process in the presence or absence of ATZ.

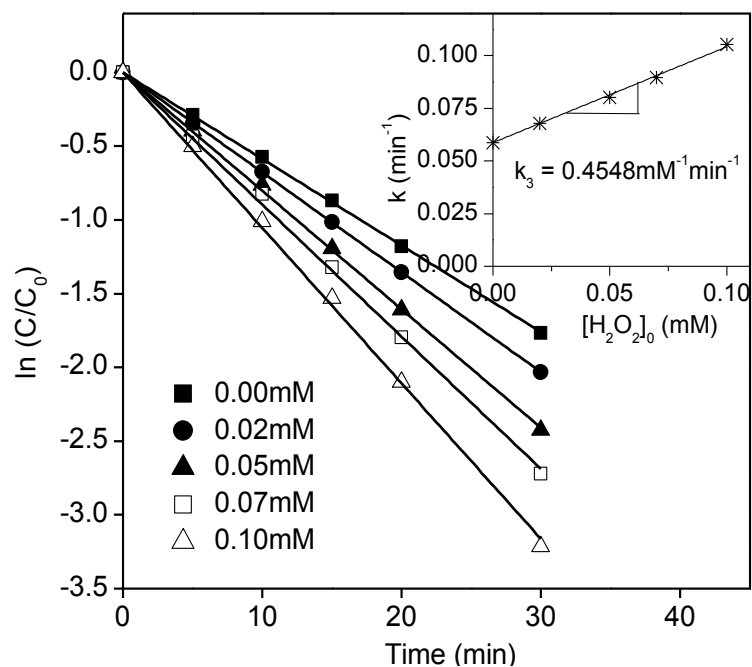


Figure 6-3: ATZ degradation in the UV/H₂O₂ process with different [H₂O₂]₀ ([ATZ]₀ = 0.02 mM).

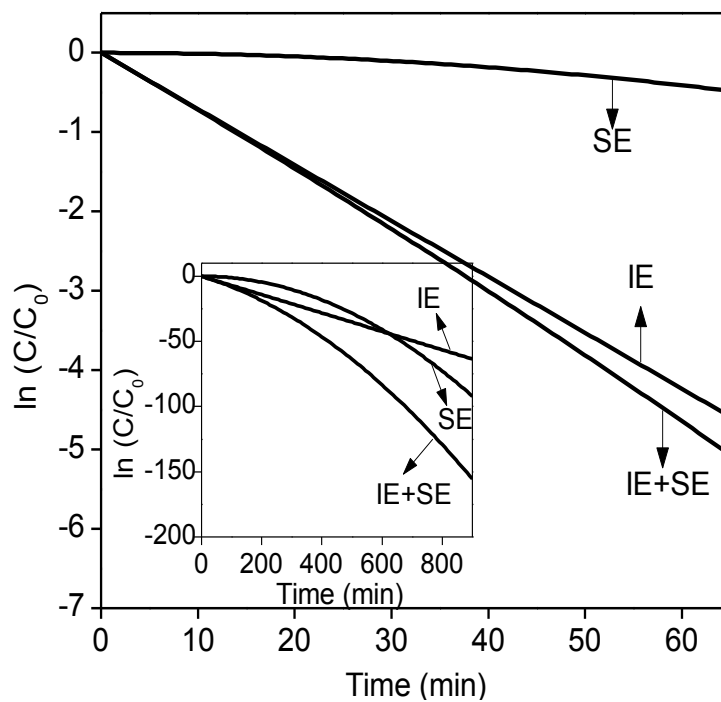


Figure 6-4: The application of kinetics model for the sonophotolytic degradation of ATZ ($IE = -0.0706t$; $SE = -1.14 \times 10^{-4}t^2$; 400 kHz).

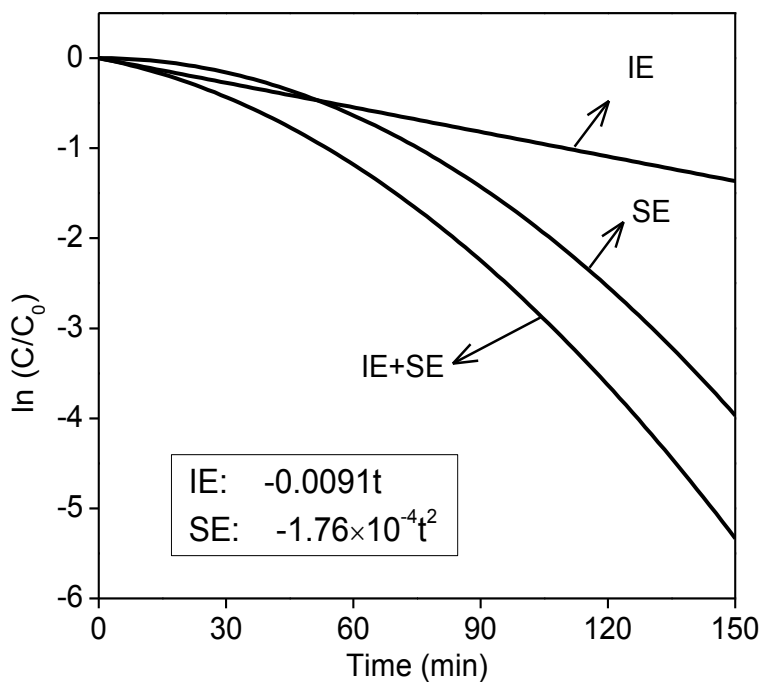
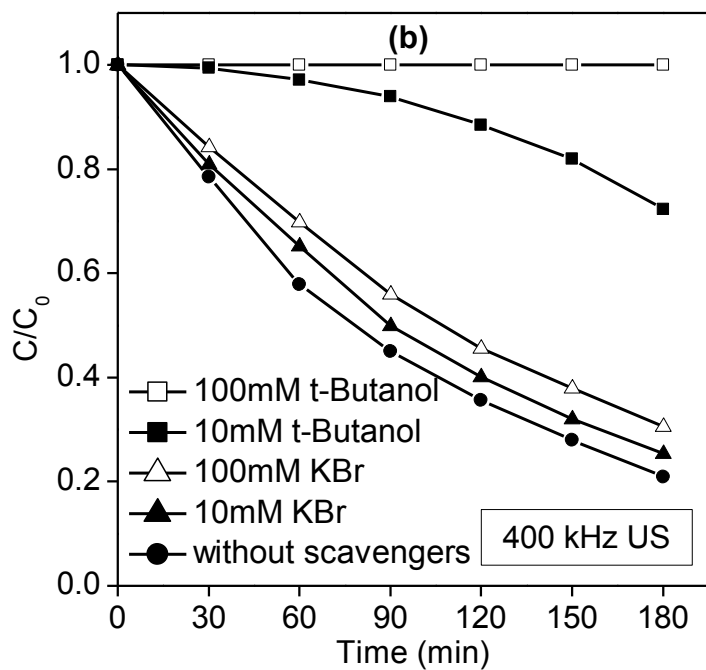
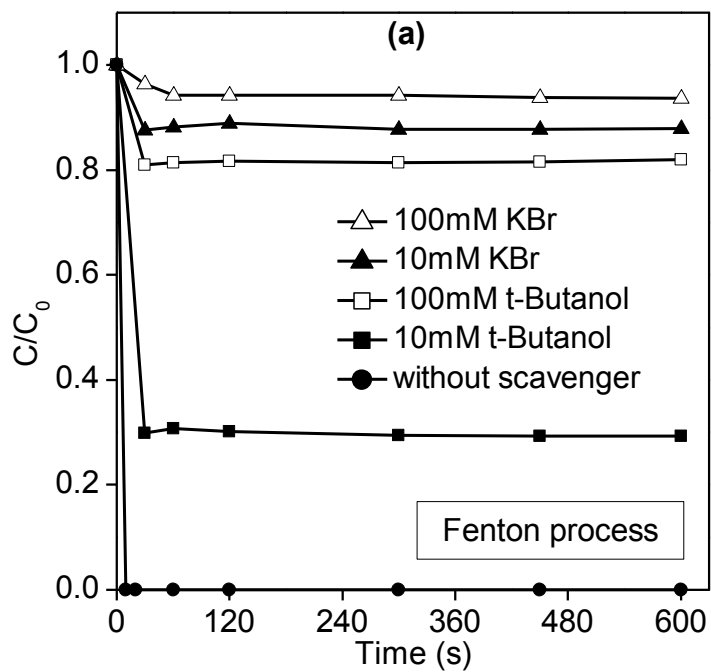


Figure 6-5: The application of kinetics model for the sonophotolytic degradation of DMP ($IE = -0.0091t$; $SE = -1.76 \times 10^{-4}t^2$, detailed data are shown in Chapter Five, 5.2.6).

6.2.3. Mechanisms of sonolytic degradation of ATZ

As proposed in previous studies, there are three potential reaction zones in aqueous sonochemistry, i.e. direct pyrolysis inside the cavitation bubbles, oxidation by radicals in the interfacial regions, and in the bulk solution (Pang et al. 2011). In order to clarify the mechanisms of sonolytic degradation of ATZ, two different types of radical scavengers, *t*-butanol and KBr, were used to investigate the possible reaction zones, and results are shown in Figure 6-6.

The *t*-butanol (TBA) is a frequently used radical scavenger in studies of US process, which is able to efficiently quench $\bullet\text{OH}$ radicals at the bubble interfaces (Henglein and Kormann 1985), whereas the ionic scavenger KBr remains in the bulk solution and can quench the radicals escaping to the bulk (Manousaki et al. 2004). To verify the quenching capacities of these two scavengers, homogeneous Fenton experiments (5 mM Fe^{2+} and 5 mM H_2O_2 , $\text{pH}_0 = 3.0$) were conducted in the presence of 10 mM and 100 mM of the two scavengers (see Figure 6-6 (a)). Results demonstrated that both TBA and KBr could quench the Fenton process to a substantial degree. It was evident that KBr had a superior quenching performance to *t*-butanol, and the difference in performance was more obvious at the lower concentration (10mM) of scavenger. The superior quenching capacity of KBr in homogeneous condition most likely resulted from the greater reaction rate between KBr and hydroxyl radicals ($k = 8.9 \times 10^{10} \text{ M}^{-1} \text{ s}^{-1}$) (Malesic et al. 2006) than that of TBA ($k = 5 \times 10^8 \text{ M}^{-1} \text{ s}^{-1}$) (Henglein and Kormann 1985).



(c.o.)

(b.f.)

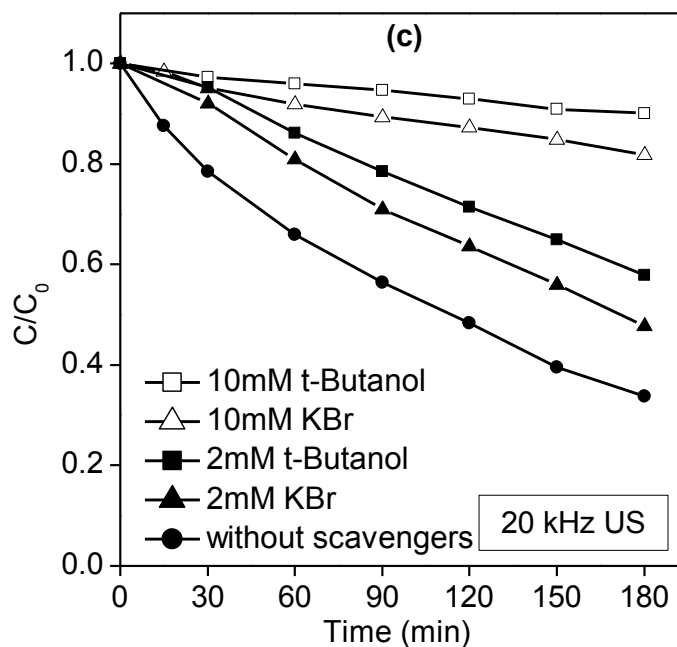


Figure 6-6: Effect of different radical scavengers on the sonodegradation of ATZ ($[ATZ]_0 = 0.02$ mM). (a) Fenton process (reference); (b) 400 kHz ultrasound; (c) 20 kHz ultrasound.

Figure 6-6 (b) shows ATZ degradation in 400 kHz US process in the presence of two radical scavengers. It can be seen that in contrast to the results of Fenton process, the presence of KBr had only minor inhibition on ATZ degradation. However, TBA remained as an effective radical scavenger, completely inhibiting ATZ degradation over a period of 180 min when 100 mM was present. These results suggest that under these conditions (400 kHz ultrasonic process, 0.03 W mL⁻¹), ATZ molecules mainly congregated and decayed at the gas bubble interfaces and only a small proportion of ATZ decayed in the bulk solution (i.e. radicals concentrate and react at the surface of bubbles). It was also worth noticing that, ATZ degradation in the presence of two scavengers followed different kinetics, where KBr showed a steady inhibition rate throughout the 180 min while TBA (10 mM) had a

complete inhibition initially and gradual weak inhibition in the later period. This could also be explained by the different physical properties of these two scavengers. With the depletion of TBA by the continuous generation of radicals, ATZ molecules would have more chances to contact with radicals at the interfaces leading to an increasingly faster degradation rate. However, the hydrophilic KBr residing in the bulk solution had much less chances to interfere with the reaction between ATZ molecules and radicals. Therefore, it was proposed that a good heterogeneous micro-environment was formed during ultrasonic oscillation in the 400 kHz US process, where different molecules located at their privileged sites in the gas-liquid environment based on their hydro-phobic/philic properties.

It was clear that the sonolytic degradation of ATZ was dominated by radical oxidation rather than pyrolysis since a high concentration of *t*-butanol totally suppressed ATZ degradation (Figure 6-6 (b)).

For comparison, a low frequency ultrasonic process (20 kHz) using TBA or KBr as radical scavengers was also investigated and results are shown in Figure 6-6 (c). Owing to the expected lower effectiveness of 20 kHz ultrasound, lower concentrations (2 and 10 mM) of scavengers were used. As was found at the higher US frequency (400 kHz), TBA displayed a greater quenching effect than KBr; however, the difference in the quenching effects of these two scavengers was not as marked as that of 400 kHz process. Furthermore, in the 20 kHz process, the concentrations of radical scavengers played more important roles than their hydro-phobic/philic properties, where 10 mM of both TBA and KBr had better quenching performances than 2 mM of them. These findings implied a poor heterogeneous micro-environment in the 20 kHz process, which means solutes for both ATZ and

scavengers (with different hydro-phobic/philic properties) were not adequately placed based on their physical properties comparing to that in the 400 kHz process. This might be because at low frequency, the “fragmentary transient cavitation bubbles”, which are responsible for the mechanical activity rather than chemical effect of ultrasound, are subjected to violent collapse and create shock wave damage to the surface (well known for its cleaning purpose) (Servant et al. 2001). These mechanical action might disturb the distribution of different solutes and lead to a relatively inferior heterogeneous micro-environment.

6.2.4. Salt effect on sonolytic degradation of ATZ

The degradation of solutes in the ultrasonic process has been reported to depend highly on their physicochemical properties (Henglein and Kormann 1985, Park et al. 2011). In general, compounds that are more hydrophobic (more volatile, less soluble, higher octanol-water partition coefficient, etc) generally have higher sonolytic degradation efficiencies (Park et al. 2011). One potential method to enhance the hydrophobicity of an organic compound and drive it towards the gas-liquid interface is to increase the salinity of the aqueous solution. Previous studies of the salt effect on sonolytic degradation efficiency have shown variable behavior. For example, Seymour et al. reported a salt-induced enhancement of sonolytic oxidation of aqueous pollutants (Seymour and Gupta 1997), while Manousaki et al. found an adverse effect of NaCl addition on the sonolytic degradation of a surfactant (Manousaki et al. 2004).

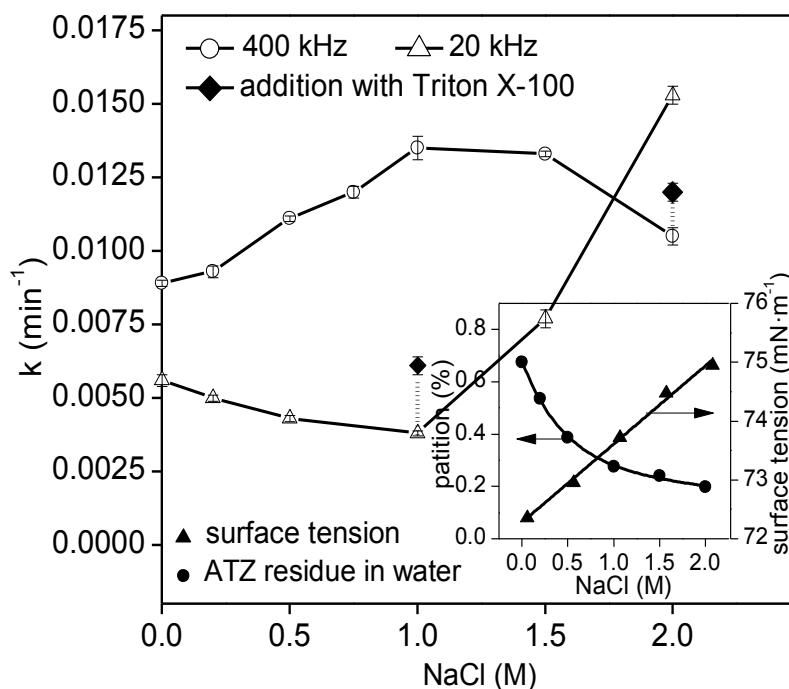


Figure 6-7: Effect of NaCl addition on ATZ sonodegradation (400 kHz and 20 kHz US processes). Inset: variation of ATZ partition (between aqueous and *n*-octanol phases) and surface tension with [NaCl] ([ATZ]₀ = 0.02 mM).

This variability may arise from different properties of the investigated compounds, and/or possibly different ultrasonic processes. So far, the information available regarding the salt effect on solute degradation in different types of ultrasonic processes is very limited. Therefore, the effect of NaCl addition on ATZ degradation was investigated using 20 and 400 kHz ultrasound and results are shown in Figure 6-7. It is evident that for both frequencies the first-order degradation rate varied with NaCl concentrations, but the variation was different for the two cases. For the 20 kHz process, a mild inhibition in degradation rate was observed for [NaCl] values up to 1.0 M, but there was a clear, systematic enhancement in rate with [NaCl] in the range 1.0 M < [NaCl] < 2.0 M. For the 400 kHz process, the ATZ decay rate was significantly different in that it increased steadily

with [NaCl] up to 1.0 M, but reduced systematically with [NaCl] in the range $1.0 \text{ M} < [\text{NaCl}] < 2.0 \text{ M}$.

The observed increase in degradation rate with salt concentration may be due to the increase in the hydrophobicity of ATZ. The results of ATZ partitioning between *n*-octanol and NaCl solution are shown in the inset of Figure 6-7. A 2 mL *n*-octanol and 5 mL ATZ solution (0.10 mM) with different [NaCl] were mixed vigorously for 20 min and settled for 1 h. The ATZ in the aqueous and *n*-octanol phase was quantified by LC and calculated by mass balance, respectively. It was clear that ATZ has a strong hydrophobic property ($\log K_{ow} = 2.61$) ((HSDB) 2007) and had a greater affinity for the organic phase when the water phase contained more NaCl, but the partition ratio (ATZ% in aqueous phase) approached a minimum level for $[\text{NaCl}] > 1.0 \text{ M}$. In general, the results are consistent with a previous study involving sonolysis which reported an approximately linear correlation between compound degradation rate and $\log K_{ow}$ (Park et al. 2011). Therefore, the observed improvement in compound degradation rate with [NaCl] at the two ultrasonic frequencies might be due to a “salting out” effect, whereby ATZ molecules were pushed towards the cavitation bubble interfaces and thereby exposed to the high radical concentrations.

Apart from the “salting out” effect, the surface tension of the solution is also an important factor influencing the ultrasonic nucleation process. The formation and retention of bubbles are more difficult at higher surface tension. The inset of Figure 6-7 shows the variation of surface tension coefficient with different [NaCl] and a positive correlation is observed. Thus, the contrary trends of the two effects (i.e. the “salting out” effect and surface tension) with increasing [NaCl] will mean that the actual compound degradation rate will depend on

the relative significance of the two effects, and this may be the reason for the variable results reported previously, and observed in this study.

The relative significance of the two effects may also be influenced by the different heterogeneous environments prevailing at two ultrasound frequencies, as discussed in Section 6.2.3. For the 400 kHz process, characterized as having a well-defined heterogeneous environment and relatively small gas bubble sizes (the bubble size has been shown to be inversely proportional to the ultrasonic frequency) (Pang et al. 2011), the ATZ degradation rate, k_{ATZ} , increased with [NaCl] up to 1.0 M reflecting the increasing hydrophobicity of ATZ. However, from a maximum k_{ATZ} at [NaCl] = 1.0 M, the k_{ATZ} gradually decreased systematically with [NaCl] greater than 1.0 M, indicating that the further minor increase in hydrophobicity (Figure 6-7 inset) was counteracted by a greater effect from the increase of surface tension. For the 20 kHz process, it is assumed that the larger cavitation bubble size made it more sensitive to surface tension variation. In addition, the 20 kHz process was found to have a poor heterogeneous distribution of solutes. Consequently, it is believed that for [NaCl] < 1.0 M, the surface tension effect dominated and the corresponding ATZ decay rate slightly decreased with [NaCl]. However, at higher [NaCl] (> 1.0 M), the “salting out” effect was increasingly dominant (ATZ molecules were pushed toward bubble surfaces) and the corresponding ATZ degradation rate was enhanced.

To support these assumptions, a nonionic surfactant, Triton X-100, was used to verify the surface tension effect in the US process. The critical micelle concentration (CMC) of Triton X-100 was determined to be 0.223 mM (see Figure 6-8), and the dosage of Triton X-100 was calculated based on the information given in Figure 6-8 and Figure 6-7 (inset), to

reduce the surface tension to that for the solution without the NaCl. As can be seen from Figure 6-7, a moderate increase of k_{ATZ} was observed for both US frequencies, which supports the assumed effects of surface tension in the test solutions with NaCl.

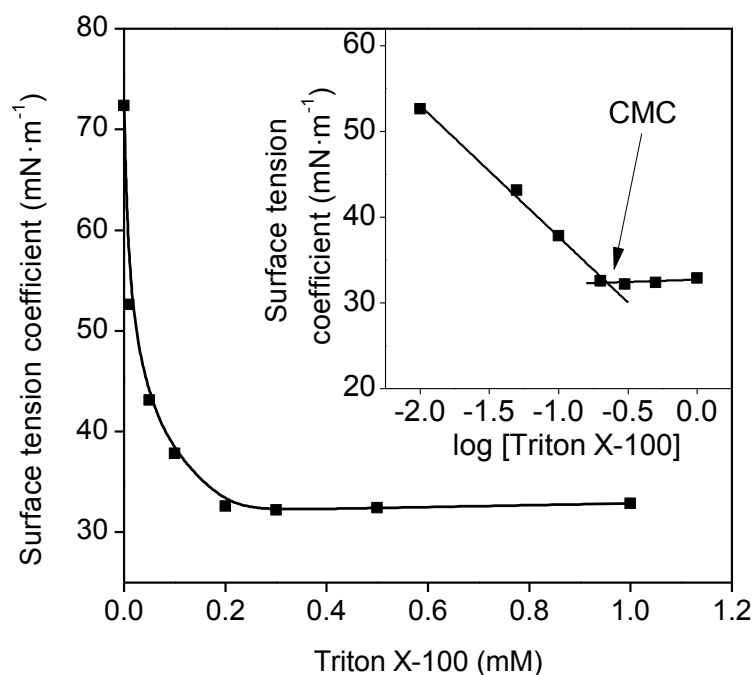


Figure 6-8: The determination of CMC value of Triton X-100.

The specific role of the chloride ion was considered. Chloride has been reported to form the less reactive chlorine-radical species ($\bullet\text{OH} + \text{H}^+ + \text{Cl}^- \leftrightarrow \text{Cl}\bullet + \text{H}_2\text{O}$, $\text{Cl}\bullet + \text{Cl}^- \leftrightarrow \text{Cl}_2\bullet^-$) (Yuan et al. 2012) in homogenous AOTs and have an inhibitory role owing to the futile consumption of hydroxyl radicals. For the US process this appears not to be the case since the chloride ion is restricted to the bulk-aqueous phase and cannot easily concentrate at the bubble surface due to its hydrophilic properties. Thus, no significant quenching effect was observed in the presence of NaCl, which was consistent with the minor quenching effect observed (at 400 kHz) in the presence of bromide (KBr) (see Figure 6-6).

6.2.5. UV absorption spectra

Changes in UV absorption spectra of ATZ solutions during UV and US irradiation are given in Figure 6-9. Obvious different degradation pathways were observed of these two processes. There are two principal absorption peaks displayed by ATZ, an intense peak at 222 nm and a weaker peak at 264 nm. In UV process, ATZ degraded rapidly in the first 30 min, and subsequently the absorption band near 222 nm was observed to progressively broaden and shift sideward. Further variation of the spectra after 50 min turned extremely slow, indicating further transformation of the photolytic intermediates was inefficient under 253.7 nm irradiation. During UV irradiation, the pH of ATZ solution decreased from 6.50 to 5.20 within 70 min. One principal intermediate of ATZ photolytic degradation was found to be OIET and the absorption spectra of standard OIET under neutral and acidic conditions are shown in the inset of Figure 6-9 (a); it is evident that the spectrum of OIET varied with solution pH. When the solution pH decreased from 6.50 to 5.20, the absorption maxima split sideward, which was in accordance with the observation of ATZ photolytic degradation. However, for the US process, a continuous change of the spectra was observed (see Figure 6-9 (b)), with the peak increasing in value and moving towards lower wavelengths, suggesting a steady and continual transformation of ATZ and its daughter compounds compared to that of UV photolysis.

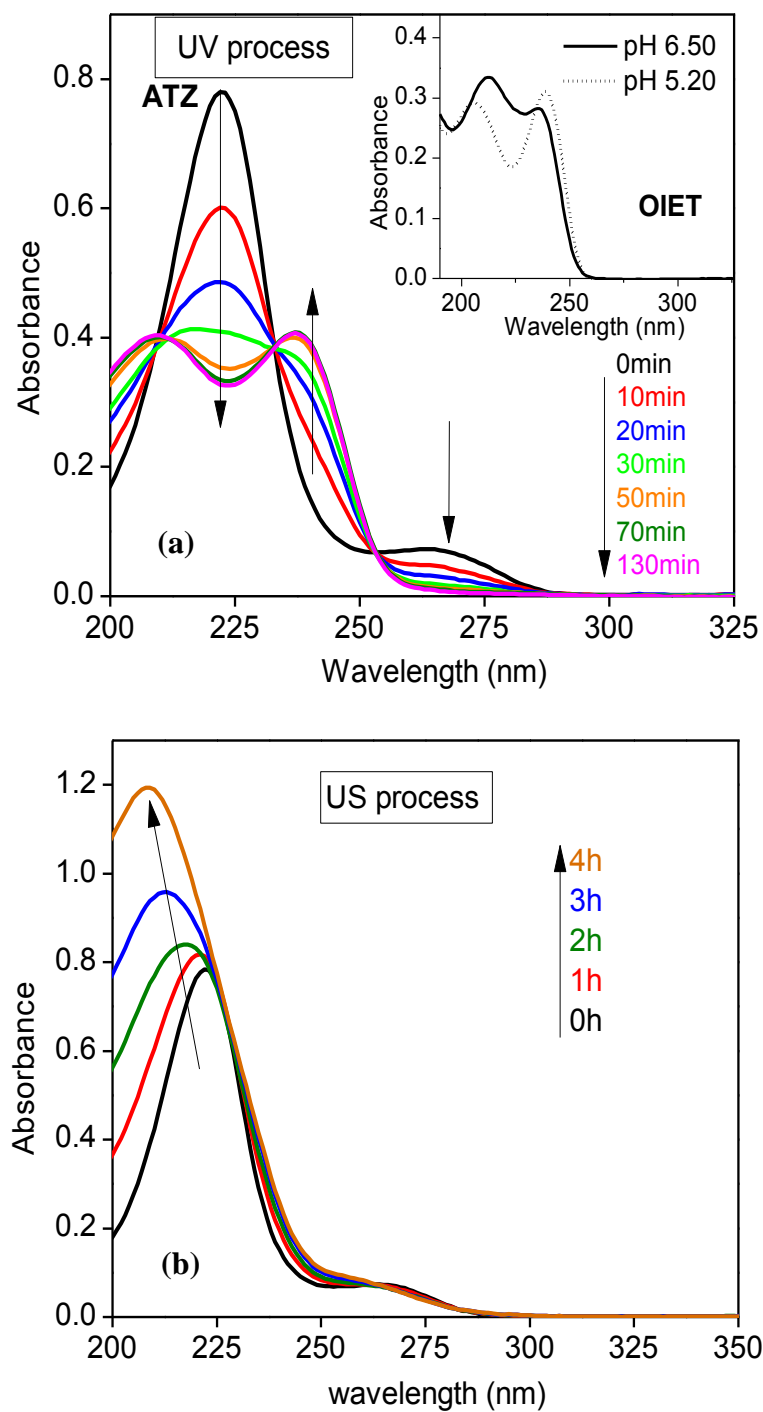


Figure 6-9: Variation of the UV absorption spectra of the reaction solution in the individual process of UV or US ($[ATZ]_0 = 0.02$ mM).

6.2.6. Identification of intermediates and degradation pathways

The information of ATZ and all the detected intermediates are listed in Table 6-1.

A summary of proposed ATZ degradation pathways for the UV, US and US/UV processes is given in Scheme 6-1. The photodegradation of ATZ and the evolution profiles of the primary intermediates (OIET, ODIT, ODET, CVVT) are shown in Figure 6-10. As indicated previously, the photodegradation of ATZ proceeded much faster than sonodegradation, and almost 95% of ATZ was converted to OIET; further photodegradation of OIET was very slow, which agreed with the observation of the UV absorption spectra variation (Figure 6-9 (a)). The dechlorination-hydrogenated product HIET was also observed in the early stages with obvious mass spectra (Figure 6-11), but its quantification by LC was difficult due to the trace amount. It is thus evident that the C-Cl bond was the most-likely reaction position under UV irradiation due to the longest bond length and relatively low bond polarity (Chen et al. 2009a). The secondary derivatives of OVAT and ODDT could be detected at the later stage with low concentrations. However, the end product of ammeline (Chen et al. 2009a) or cyanuric acid (Hequet et al. 2001) reported by others were not observed in this study even under a six-fold UV light intensity. In general, the mechanisms of ATZ photodegradation identified in this study mainly included dechlorination-hydroxylation (A - pathway as defined in Scheme 6-1), dechlorination-hydrogenation (F), alkylic oxidation (B), and alkylic olefination (E).

A separate test using OIET (0.02 mM) as the initial compound was conducted to examine its degradability under US, UV and US/UV processes, and results are shown in the inset of

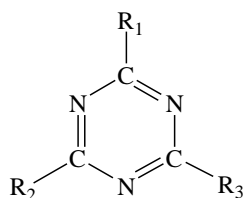
Figure 6-10. The sonolytic degradation of OIET was found to be much more efficient than photodegradation, in which 75% of OIET was degraded compared to only 5% by photolysis. In addition, the most efficient degradation of OIET (97%) was obtained from the US/UV process, mainly because of the supplementation of $\bullet\text{OH}$ radicals by H_2O_2 photolysis. So the OIET accumulated in the sole-UV process can be efficiently decomposed by incorporating US into the process.

Profiles of the major sonodegradation intermediates were shown in Figure 6-12, and the separated UV peaks of intermediates in the early, middle and end stages were given in Figure 6-13. It can be seen that the alkylic oxidation products (CDIT, CDET) and the dealkylation products (CIAT, CEAT) prevailed in the early stage and accumulated to their maximum in the middle stage, indicating the sonodegradation of ATZ was initiated by side chain oxidation. However, the primary intermediates began to decrease after 5 h, accompanied by the generation of secondary intermediates (e.g. ODDT, ODET, OIAT). The middle stage was characterized by the formation of hydroxylation products. It is worth noting that although the same hydroxylated intermediates were found in both UV and US involved processes (i.e. OIET, ODIT, and ODET of pathway A), their formation mechanisms are different. In the US process, their formation was mainly induced by $\bullet\text{OH}$ attacking at the C–Cl position and/or the alkylic side chains. In the end stage, the primary intermediates were mostly degraded and more polar intermediates (OEAT, CAAT, and OAAT, etc.), with retention time less than 20 min, appeared. The compound, ammeline (OAAT), was verified as the end product in the US and US/UV processes by using ammeline as the initial probe, and observing that no further degradation occurred. This might be because the strong hydrophilic nature of ammeline ($\log K_{ow} = -3.65$) ((HSDB)

2007) limited its contact with radicals surrounding the collapsed bubbles. In summary, the pathways of ATZ sonodegradation could be categorized as: alkylic oxidation (B), dechlorination-hydroxylation (A), alkylic hydroxylation (C), and dealkylation (D). Trace amounts of a special intermediate OOEIT were identified in this study for the first time. This is because of the special heterogeneous nature of the US process, which encourages the accumulation of relatively hydrophilic intermediates without them being oxidized immediately.

Judging from the intermediates identified in the US/UV process, it is suggested that the initial derivatives are mainly from photodegradation because k_{uv} is much greater than k_{us} . Subsequently, ultrasonic oxidation becomes the dominant process. However, fewer oxidative intermediates (12) were observed for the US/UV process compared to that for the US process (18), and the final product ammeline was observed in both processes. This implied that while the direct photolysis of intermediates was a minor effect at the later stages of treatment, UV irradiation could promote radical generation via H_2O_2 decomposition, thereby resulting in less accumulation of intermediates.

Table 6-1: Details of the indentified intermediates of ATZ degradation.



The following symbols are used in the nomenclature:

A, amino; **C**, chloro; **E**, ethylamino; **I**, isopropylamino; **O**, hydroxy; **T**, *s*-triazine ring; **D**, acetamido; **V**, vinylamino; **M**, methylamino; **H**, hydrogen (Hiskia et al. 2001).

(*c.o.*)

(b.f.)

Name	Retention Time (min)	[M+H] ⁺	MS ² spectrum ions	Detected Processes	R ₁	R ₂	R ₃
atrazine (CIET)	40.79	216	216,188,174,146,138, 132,104,96	UV, US, US/UV	Cl	NHC ₂ H ₅	NHCH(CH ₃) ₂
CVVT	35.20	198	198,156,128,114	UV, US/UV	Cl	NHCH=CH ₂	NHCH=CH ₂
COIOET	32.74	248	248,205	US	Cl	NHCH(OH)CH ₃	NHC(OH)(CH ₃) ₂
HIET	32.21	182	182,140	UV, US/UV	H	NHC ₂ H ₅	NHCH(CH ₃) ₂
CDIT	31.20	230	230,188,146,110	US, US/UV	Cl	NHCOCH ₃	NHCH(CH ₃) ₂
ODIT	30.55	212	212,170,128	UV, US/UV	OH	NHCOCH ₃	NHCH(CH ₃) ₂
COEIT	28.48	232	232,188,130	US	Cl	NHCH(OH)CH ₃	NHCH(CH ₃) ₂
CIAT	27.52	188	188,146,110	US	Cl	NH ₂	NHCH(CH ₃) ₂
OIET	25.73	198	198,170,156, 128,114	UV,US, US/UV	OH	NHC ₂ H ₅	NHCH(CH ₃) ₂
CDET	25.37	216	216,188,174,146	US, US/UV	Cl	NHC ₂ H ₅	NHCOCH ₃
CEAT	21.69	174	174,146,132	US	Cl	NHC ₂ H ₅	NH ₂
OOEIT	20.85	214	214,170	US	OH	NHCH(OH)CH ₃	NHCH(CH ₃) ₂
OVAT	19.61	154	154,112	UV, US/UV	OH	NHCH=CH ₂	NH ₂
ODDT	18.20	212	212,170	UV,US, US/UV	OH	NHCOCH ₃	NHCOCH ₃
CDAT	15.31	188	188,146	US	Cl	NHCOCH ₃	NH ₂
ODET	15.21	198	198,156,128	UV,US, US/UV	OH	NHC ₂ H ₅	NHCOCH ₃

(c.o.)

(b.f.)

ODAT	14.44	170	170,128,86	US, US/UV	OH	NHCOCH ₃	NH ₂
ODOIT	12.16	228	228,196	US	OH	NHCOCH ₃	NHC(OH)(CH ₃) ₂
CAAT	11.62	146	146,110,104	US	Cl	NH ₂	NH ₂
OEAT	9.48	156	156,128,114	US, US/UV	OH	NHC ₂ H ₅	NH ₂
OIAT	6.88	170	170,128,86	US	OH	NH ₂	NHCH(CH ₃) ₂
OIMT	6.33	184	184,114	US	OH	NHCH ₃	NHCH(CH ₃) ₂
ammeline (OAAAT)	4.89	128	128,86	US, US/UV	OH	NH ₂	NH ₂

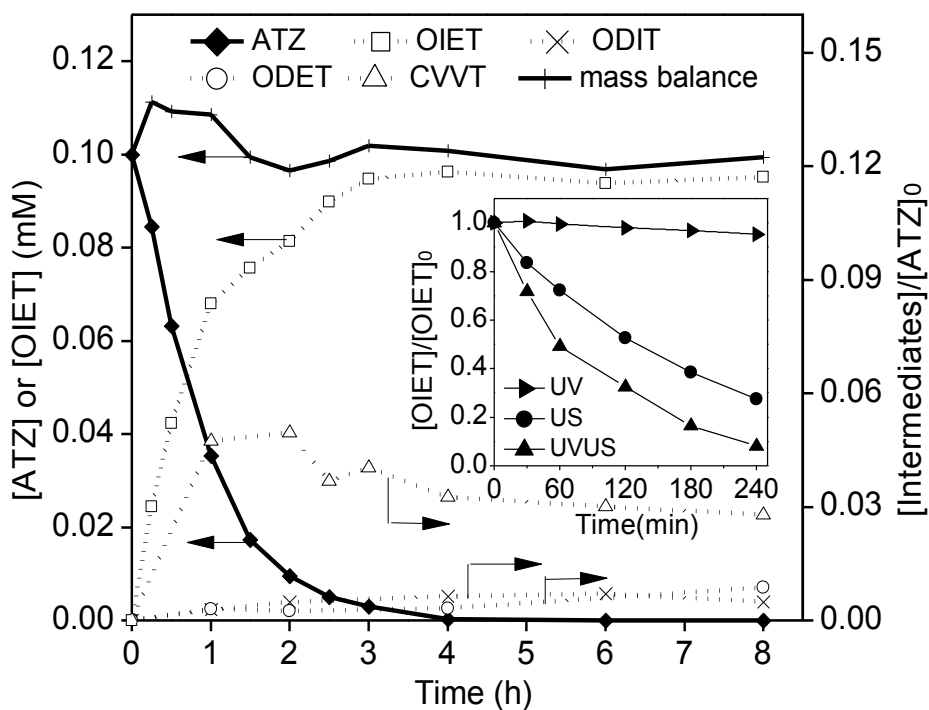
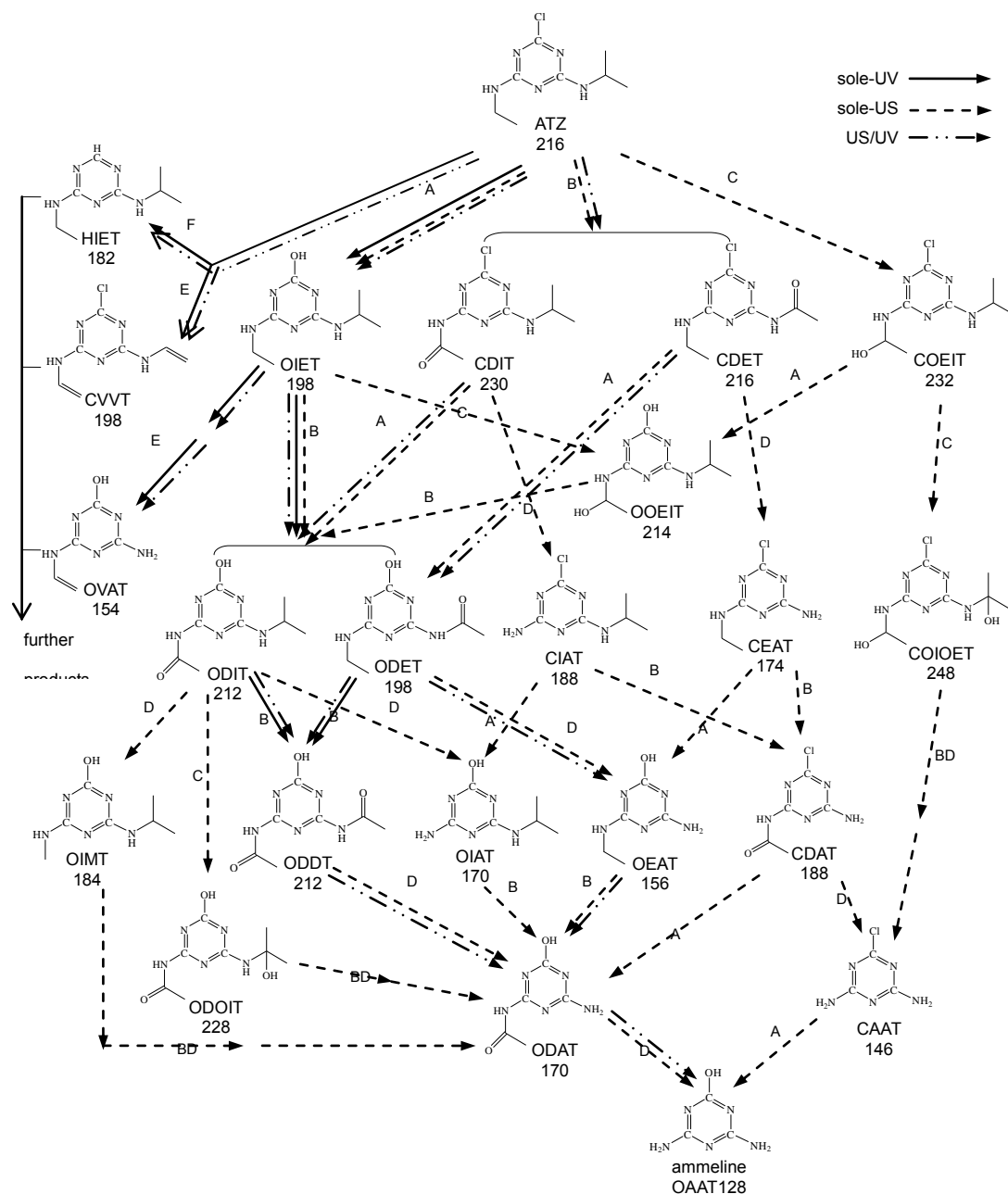


Figure 6-10: Temporal profiles of ATZ degradation and formation of principal intermediates in the photolytic process ($[ATZ]_0 = 0.1$ mM). Inset: OIET degradation under US, UV, US/UV processes ($[OIET]_0 = 0.02$ mM).



Scheme 6-1: Degradation pathways of ATZ for the UV, US, and US/UV processes. The double arrow denotes reaction more than one step.

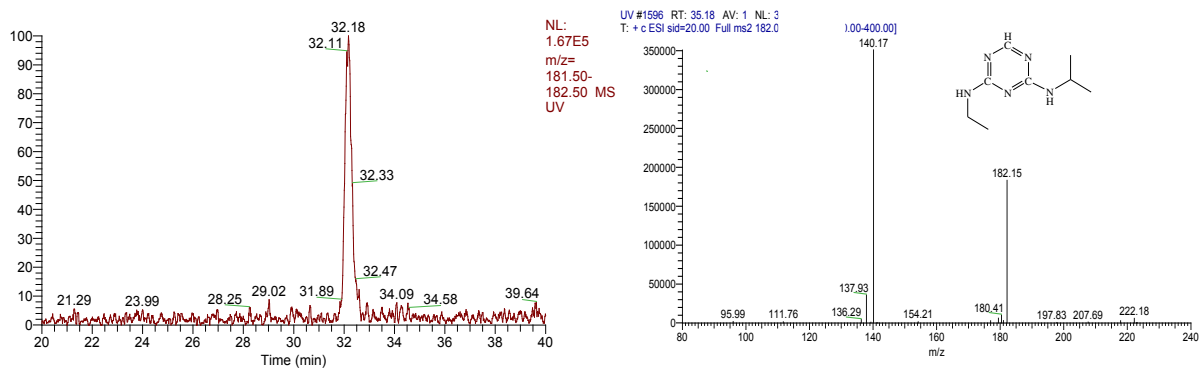
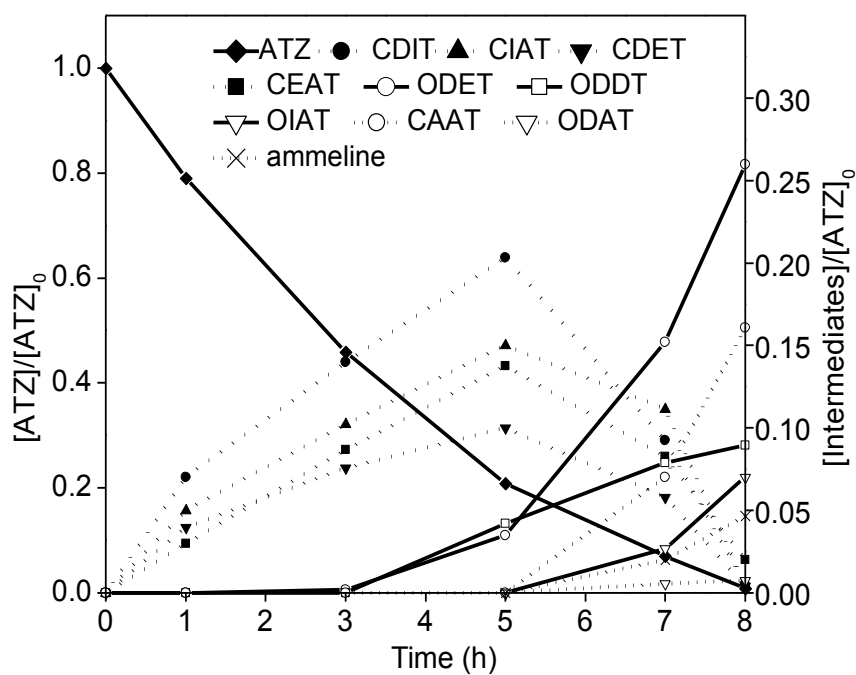


Figure 6-11: Mass spectra of HIET.

Figure 6-12: Temporal profiles of ATZ degradation and formation of principal intermediates in the sonolytic process ($[ATZ]_0 = 0.1 \text{ mM}$).

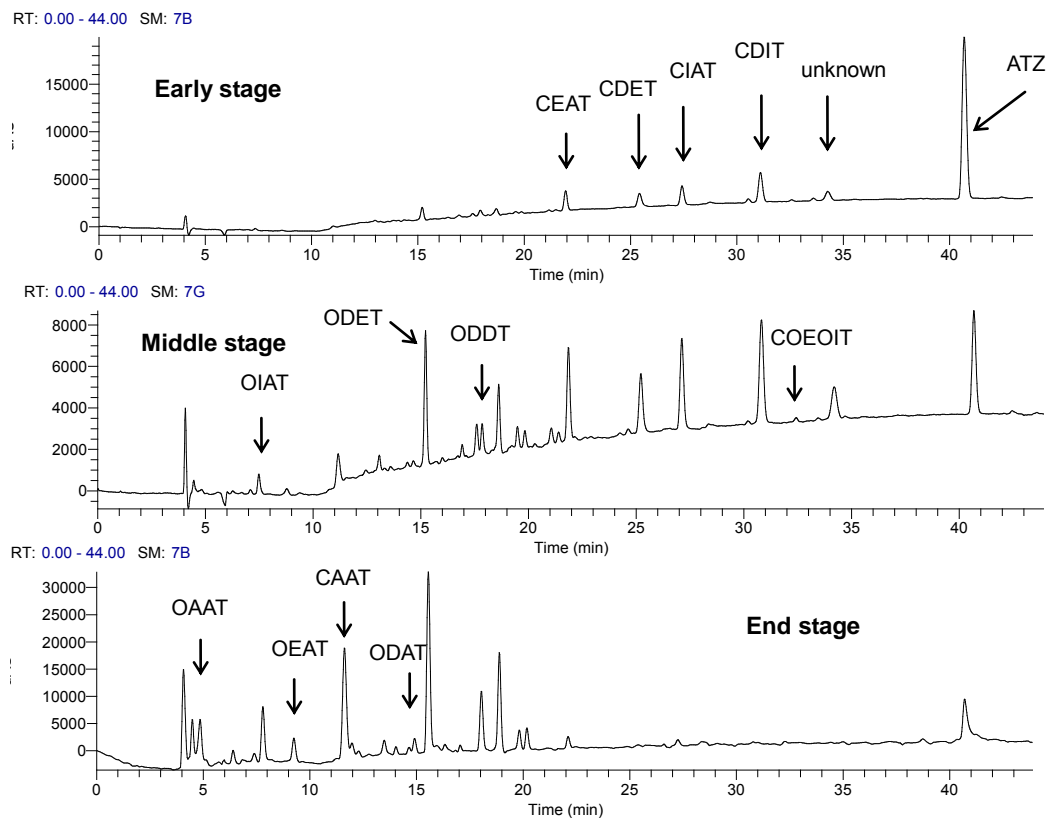


Figure 6-13: The separated HPLC peaks of the sonolytic degradation intermediates at the early, middle, and end stages.

6.2.7. Mineralization

The evolution profiles of TOC concentrations in the UV, US and US/UV processes are shown in Figure 6-14. The results showed that mineralization was not evident to any measurable degree in the UV process, but approximately 37% and 60% TOC was removed in the US and US/UV processes, respectively. By comparing the carbon content of ATZ (8) and ammeline (3), at most 62.5% TOC removal can be achieved, which is very close to the observed value of 60% in the US/UV process. Based on this evidence, ammeline appears to be the sole end-product of ATZ oxidation in the US/UV process, with the TOC reduction

due entirely to the oxidation and mineralization of ATZ side chains, and these carbons can be fully oxidized in the US/UV process.

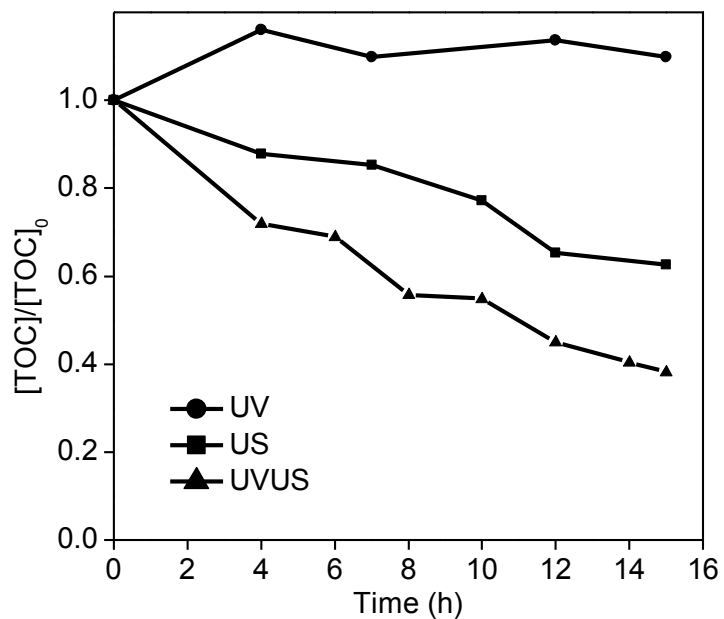


Figure 6-14: Evolution profiles of TOC concentration in the UV, US, and US/UV processes ($[\text{ATZ}]_0 = 0.1 \text{ mM}$).

6.3. Chapter summary

The relative effectiveness of US, UV and US/UV for the degradation of ATZ has been investigated and under the test conditions ATZ degradation by US was much less than by UV. The combination of UV and US was only slightly superior to UV and reaction modeling suggested there was only a minor synergistic effect, thus the kinetics of ATZ degradation can be described by a pseudo first-order model.

The mechanism of compound degradation by US was principally through radical attack at the cavitation bubble surfaces as indicated by the presence of different radical scavengers (*t*-butanol and KBr). ATZ degradation by sonolytic processes depended on the heterogeneous environment, which was found very different in the 400 and 20 kHz ultrasound systems. The better heterogeneous distribution of solutes in the former allowed a faster decay of hydrophobic compounds than that in the latter. Similarly, the presence of NaCl had different effects on the two ultrasound processes, mainly because the competition between “salting out” effect and surface tension, and they were again influenced by the different heterogeneous environment in the solution.

The OIET was found to be the most abundant intermediate in UV process, and the combination of UV and US facilitated its degradation. In the US/UV process, the photodegradation and sonolytic oxidation dominated the initial and later stage, respectively, and UV was found to promote radical generation. Ammeline was the sole end product of both the US and US/UV processes. The combined US/UV process also had the best mineralization performance. More than 60% TOC was removed via oxidation of the side

chains of ATZ.

7. Chapter Seven Degradation of Di-*n*-butyl Phthalate by a Homogeneous Sono-Photo-Fenton Process with In-Situ Generated Hydrogen Peroxide

7.1. Overview

The advantages of US and the sonochemical mechanisms have been discussed in considerable detail previously. One major drawback of the US process is its relatively low efficiency resulting from the inevitable recombination of the radicals produced (e.g. $\text{H}\cdot + \cdot\text{OH} \rightarrow \text{H}_2\text{O}$; $2\cdot\text{OH} \rightarrow \text{H}_2\text{O}_2$; $2\text{HO}_2\cdot \rightarrow \text{H}_2\text{O}_2 + \text{O}_2$ (Adewuyi 2001, Inoue et al. 2006)). As a result, hydrogen peroxide is a principal product of the sonochemical process which will accumulate in the reaction solution. Some processes have been combined with US to improve the degradation efficiency, such as US/UV/TiO₂ (Bahena et al. 2008), US/O₃ (Ji et al. 2012), and US/Fe₃O₄ (Huang et al. 2012), in which the sono-photolytic (US/UV) and homogeneous sono-Fenton (US/Fe²⁺) processes are two relatively simple and feasible combinations (Grcic et al. 2010, Xu et al. 2013a). A common feature of these two techniques is the utilization of hydrogen peroxide to provide additional hydroxyl radicals. Synergistic effects arising from the US/UV and the US/Fe²⁺ processes have been reported and the main mechanisms were found to be the photolyzing of ultrasonically produced hydrogen peroxide ($\text{H}_2\text{O}_2 + h\nu \rightarrow 2\cdot\text{OH}$) (see Chapter Five) and Fenton-like reaction ($\text{H}_2\text{O}_2 + \text{Fe}^{2+} \rightarrow \text{Fe}^{3+} + \text{OH}^- + \cdot\text{OH}$) (Torres et al. 2007), respectively. However, information regarding the hybrid process of homogeneous sono-photo-Fenton (US/UV/Fe²⁺) is still relatively limited, and especially concerning mutual synergistic mechanisms. Previously, Torres et al. examined the US/UV/Fe²⁺ process for the removal of bisphenol A and found it

was the most efficient technique compared to either the US/UV or US/Fe²⁺ process (Torres et al. 2007). Katsumata et al. also investigated the degradation of linuron by the US/UV/Fe²⁺ process and reported it was a useful and efficient technique (Katsumata et al. 2011). However, additional synergistic effects other than hydrogen peroxide reduction arising from combining the three parts (i.e. US, UV, and Fe²⁺) were not examined in these studies and the features of the inclusive processes were not discussed, which were investigated in the present study. In addition, most studies previously of the sono-Fenton process involved the application of hydrogen peroxide at the beginning of the reaction in order to enhance radical generation (Babuponnusami and Muthukumar 2012, Li et al. 2013b, Ma et al. 2010, Ninomiya et al. 2013), which obscured examination of the intrinsic properties of the US/Fe²⁺ process. Since the concentration of hydrogen peroxide increases gradually from zero during the sonochemical process (Xu et al. 2013a), the initiation and progress of H₂O₂-related reactions may differ significantly compared to the case where a high initial H₂O₂ dosage is added. In this chapter, the US/UV/Fe²⁺ process was investigated in detail without the external addition of hydrogen peroxide, but involving the generation of hydrogen peroxide in-situ from the US process as the exclusive source.

In this chapter, the sono-photo-Fenton process (US/UV/Fe²⁺) and its constituent processes (e.g. US/UV, US/Fe²⁺, UV/Fe²⁺) were investigated in detail using DBP as the probe compound. The synergistic mechanism of the hybrid process was analyzed and the effects of several reaction parameters (initial solution pH and Fe²⁺ dosage) were also evaluated.

7.2. Results and discussion

7.2.1. Comparison of US/UV/Fe²⁺ and related processes

The DBP degradation performance by the sono-photo-Fenton process (US/UV/Fe²⁺) and related control experiments is shown in Figure 7-1, and the pseudo first-order rate constants (k) of these processes are listed in Table 7-1. It was observed that DBP degradation generally followed pseudo first-order kinetics ($R^2 > 0.98$) except for the UV/Fe²⁺ process, for which an approximate k value for the initial 60 min of reaction was used for comparison (see Table 7-1). The results showed that the best degradation performance was obtained from the hybrid process of US/UV/Fe²⁺ ($k = 0.0638 \text{ min}^{-1}$), where DBP was completely degraded within 75 min. The relative degradation performance for the alternative processes was found to be in the order: US/UV/Fe²⁺ > US/Fe²⁺ > US/UV > US > UV/Fe²⁺ > UV. A synergistic effect was evident with the US/UV process in respect to the DBP degradation based on the rate constants, and a synergistic index (SI) was calculated to be 1.43 according to the values shown in Table 7-1 ($SI = 0.0410/(0.0234+0.0052) = 1.43$) (Xu et al. 2013a); where a $SI > 1$ indicates a synergistic effect. It was also found that the involvement of Fe²⁺ in the US/Fe²⁺, UV/Fe²⁺, and US/UV/Fe²⁺ processes substantially increased DBP degradation efficiencies compared to the corresponding processes without Fe²⁺ (i.e. US, UV, and US/UV), indicating the beneficial role of ferrous ions in the hybrid processes. It is significant to note that the DBP degradation rate was significantly enhanced by adding Fe²⁺ to the direct UV process (see Figure 7-1), which is an effect that has rarely been reported in other studies and will be discussed in more detail later. In addition, by comparing the rate constants of the various processes, where $k_{US/UV/Fe^{2+}} > k_{US/Fe^{2+}} + k_{UV} > k_{UV/Fe^{2+}} + k_{US}$, it can be inferred that there may be complex synergistic mechanisms present in the US/UV/Fe²⁺

process. A greater synergistic effect was observed by combining UV/Fe²⁺ with US (SI = 2.03) compared to the combination of US/Fe²⁺ and UV (SI = 1.33), which indicates the critical role of US, particularly in providing H₂O₂, in the hybrid process of US/UV/Fe²⁺. Moreover, the rate constant of the US/UV/Fe²⁺ process was less than the sum of the individual US/Fe²⁺ and UV/Fe²⁺ processes ($k_{\text{US/UV/Fe}^{2+}} < k_{\text{US/Fe}^{2+}} + k_{\text{UV/Fe}^{2+}}$), which is likely due to the competition of the limited (or deficient) H₂O₂ in the solution.

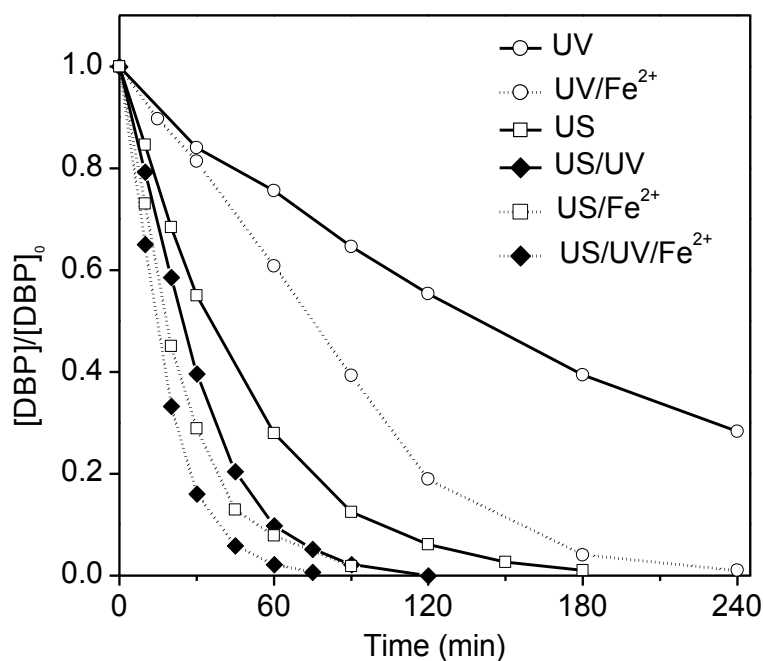


Figure 7-1: DBP degradation performance under different processes (conditions: $[\text{DBP}]_0 = 0.01 \text{ mM}$; $[\text{Fe}^{2+}]_0 = 0.1 \text{ mM}$; $[\text{pH}]_0 = 6.5 \pm 0.05$).

Table 7-1: The pseudo first-order rate constants of different processes

Process	US	UV	US/UV	US/Fe ²⁺	UV/Fe ²⁺	US/UV/Fe ²⁺
$k \text{ (min}^{-1}\text{)}$	0.0234	0.0052	0.0410	0.0428	0.0080	0.0638
R^2	0.9955	0.9953	0.9841	0.9934	0.9884	0.9946

7.2.2. H₂O₂ formation in US, UV, and US/UV processes

Since the only source of H₂O₂ in the reaction solutions was that formed in-situ during the sonochemical process, the accumulation of H₂O₂ was quantified in the US (both in blank water and 0.01 mM DBP solution), UV and US/UV processes, and the results are presented in Figure 7-2 (a). It can be seen the H₂O₂ concentration ([H₂O₂]) increased linearly with reaction time for the US processes in either blank water or the 0.01 mM DBP solution. The observed zero-order kinetics of H₂O₂ formation could be explained by the steady equilibrium between radical generation and consumption during the cavitation process. The slight difference in the formation rate between the 0.01 mM DBP solution ($k = 0.0007 \text{ mM}\cdot\text{min}^{-1}$) and blank water ($k = 0.0008 \text{ mM}\cdot\text{min}^{-1}$) was mainly the result of competition in the consumption of radicals through reactions with DBP molecules and the intermediates, instead of self-decomposition ($2\cdot\text{OH} \rightarrow \text{H}_2\text{O}_2$). As expected, H₂O₂ was not detected in UV photolysis, verifying that hydroxyl radicals, as the main precursor in forming H₂O₂, were not present and direct photolysis by UV was responsible for DBP degradation. The rate of H₂O₂ production was observed to be much less in the US/UV process due to the photo-decomposition of H₂O₂ as mentioned above, corresponding to a greater DBP degradation rate.

It was worth noting that the accumulation of H₂O₂ in the US/UV process also followed an approximate zero-order kinetics ($k = 3.4 \times 10^{-4} \text{ mM}\cdot\text{min}^{-1}$). To explain this, the photolysis of H₂O₂ under 254 nm UV irradiation was examined with different initial H₂O₂ concentrations ([H₂O₂]₀) and the results are shown in Figure 7-2 (b). The range of [H₂O₂]₀ studied (0.025 – 0.2 mM) was chosen based on the ultrasonically produced concentrations

determined previously, as shown in Figure 7-2 (a), in which 0.17 mM H_2O_2 was the maximum formed in the DBP solution after 240 min. It can be seen from Figure 7-2 (b) that, for a specific $[\text{H}_2\text{O}_2]_0$, the temporal decrease of $[\text{H}_2\text{O}_2]$ generally followed zero-order kinetics. The relationship between the zero-order rate constants (k_0) and $[\text{H}_2\text{O}_2]_0$ is also shown in Figure 7-2 (b) (inset), where it is evident that the degradation rate was positively correlated with $[\text{H}_2\text{O}_2]_0$, and higher the $[\text{H}_2\text{O}_2]_0$, faster the k_0 . However, the kinetics of H_2O_2 decomposition in the US/UV process was expected to be different from that in traditional UV/ H_2O_2 process because the H_2O_2 was supplied continuously (in-situ) in US/UV by sonochemical process rather than one-off dosing at the beginning. Therefore, H_2O_2 photolysis in the US/UV process could be approximately deemed as an integration of numerous transient processes and each individual process was like a traditional UV/ H_2O_2 but with different $[\text{H}_2\text{O}_2]_0$. In every time interval, the momentary decomposition rate of H_2O_2 should be dependent on the instantaneous $[\text{H}_2\text{O}_2]_t$ according to the results illustrated in Figure 7-2 (b). Whereas, the instantaneous $[\text{H}_2\text{O}_2]_t$ in the US/UV process kept a low level during the investigated time range (less than 0.083 mM, Figure 7-2 (a)), which indicated the decomposition rate of H_2O_2 was supposed to be of insignificant variation within this time range based on the results shown in Figure 7-2 (b). The accumulation of H_2O_2 in the US/UV process will be the net effect of its continuous generation from US and consumption, principally through UV photolysis. Consequently, the generation and decomposition of H_2O_2 in the US/UV process were both approximately at a constant rate, thereby resulting in an approximate zero-order kinetics of the accumulation of H_2O_2 .

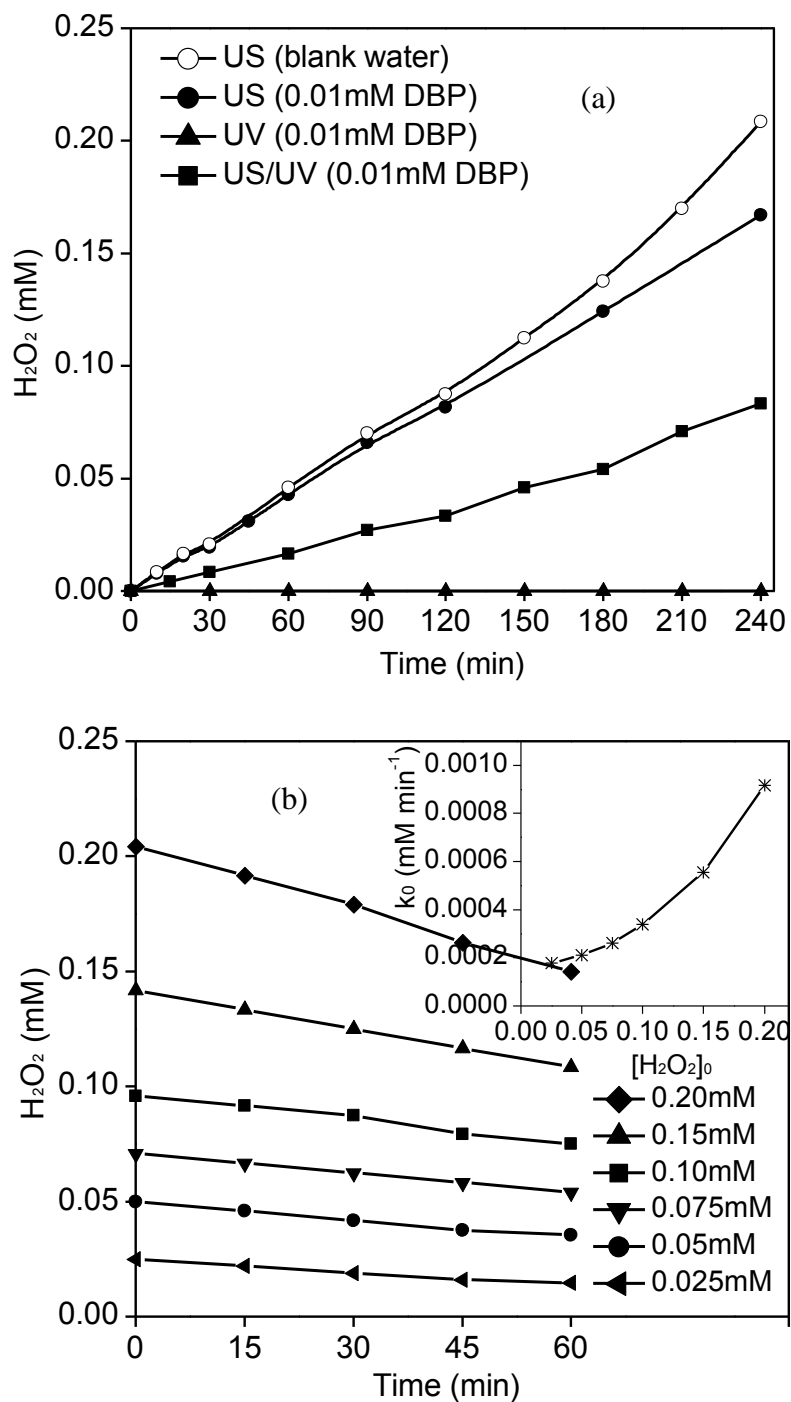


Figure 7-2: (a) Variation of H_2O_2 concentration with reaction time in the processes of US, UV, and US/UV ($[\text{DBP}]_0 = 0.01 \text{ mM}$; $[\text{Fe}^{2+}]_0 = 0.1 \text{ mM}$; $[\text{pH}]_0 = 6.5 \pm 0.05$); (b) Variation of H_2O_2 concentration under UV irradiation with different $[\text{H}_2\text{O}_2]_0$ ($[\text{DBP}]_0 = 0.01 \text{ mM}$; $[\text{Fe}^{2+}]_0 = 0.1 \text{ mM}$; $[\text{pH}]_0 = 6.5 \pm 0.05$; $[\text{H}_2\text{O}_2]_0 = 0.025 - 0.2 \text{ mM}$).

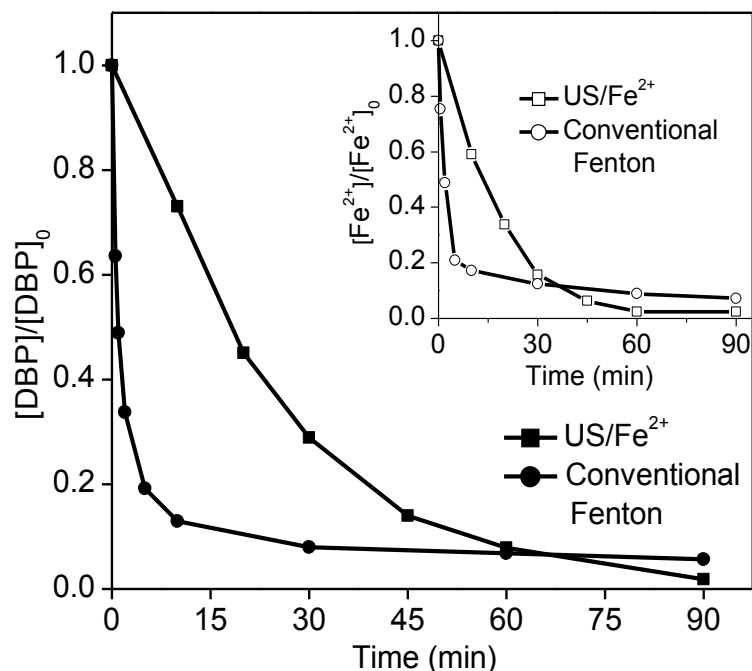
7.2.3. Properties of Sono-Fenton (US/Fe²⁺) process

Figure 7-3: Variation of DBP and Fe²⁺ concentrations with reaction time in the US/Fe²⁺ process and conventional Fenton process (conditions: $[DBP]_0 = 0.01$ mM; $[Fe^{2+}]_0 = 0.1$ mM; $[pH]_0 = 6.5 \pm 0.05$; $[H_2O_2]_0$ in conventional Fenton is 0.065 mM).

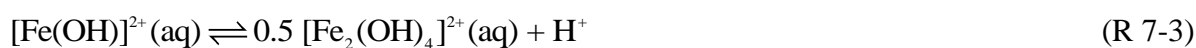
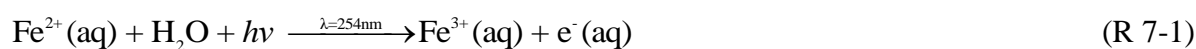
In order to examine the properties of the US/Fe²⁺ process, a control experiment with conventional Fenton's reagent was conducted for comparison; the results showing the temporal variation of [DBP] and [Fe²⁺] are shown in Figure 7-3. Since the accumulated H₂O₂ during the sonochemical process was determined to be 0.065 mM in 90 min (see Figure 7-2 (a)), the same concentration of H₂O₂ was added for the conventional Fenton process at the beginning to ensure an equivalent [H₂O₂] was available in the two processes. As can be seen from Figure 7-3, the DBP reaction kinetics was substantially different for the two reactions. In the conventional Fenton's reaction, a typical two-stage kinetics of a fast decay followed by a more gradual decay was observed. In contrast, the DBP

degradation in the US/Fe²⁺ process generally followed a pseudo first-order kinetics behaviour. With the Fenton's reaction, 87% DBP was degraded in the first 10 min in traditional Fenton, followed by a more gradual further degradation but a complete removal of DBP could not be achieved over 90 min. This behavior is mainly attributed to the unconstrained reaction (and generation of •OH) initially in the presence of excess H₂O₂ and Fe²⁺, followed by a more gradual phase caused by the rapid depletion of H₂O₂ (Chu et al. 2007). To minimize this effect, a stepwise-Fenton process was proposed by Chu et.al showing that a "stepwise-Fenton" could improve the performance of a conventional Fenton process by reducing the initial, peak concentration of H₂O₂, thereby decreasing the extent of futile (scavenging) reactions between the H₂O₂ and valuable •OH radicals (Chu et al. 2007). In comparison, the US/Fe²⁺ process further improves on the stepwise-Fenton in that it approximates to a continuous-dosing process, where the H₂O₂ is generated quasi-uniformly in solution and continuously by the US process. The results shown in Figure 7-3 suggested that DBP could be totally removed by the US/Fe²⁺ process over approximately 90 min and without a significant reduction in degradation rate. The inset of Figure 7-3 shows the variation of [Fe²⁺], where more than 80% of Fe²⁺ was transformed in the first 10 min in the conventional Fenton reaction, corresponding well with the rapid decay of DBP in this period; the subsequent slow transformation of the remaining Fe²⁺ was a clear indication of the deficiency of H₂O₂. However, for the US/Fe²⁺ process, almost all of Fe²⁺ could be exploited within 90 min by the continuous generation of H₂O₂. Thus, while acknowledging that the DBP reaction rate is not as rapid as conventional Fenton's reagent in the initial stages of the reaction, the sono-Fenton process is nevertheless more efficient in utilizing H₂O₂ and Fe²⁺, and does not require external H₂O₂ addition.

7.2.4. Synergistic effect of UV/Fe²⁺

As reported in Section 7.2.1, the incorporation of Fe²⁺ into the UV irradiation process substantially enhanced DBP degradation compared to UV photolysis alone. To examine the reasons for this, six UV lamps were employed in order to amplify the synergistic effect and shorten the reaction time to minimize possible side reactions of Fe²⁺. The results showing the temporal variation of [DBP] and [Fe²⁺] are given in Figure 7-4 (a) and (b), respectively. It was evident again that DBP degradation could be improved substantially by the presence of Fe²⁺ compared to UV irradiation alone. To examine whether synergistic mechanisms exist with UV/Fe²⁺, tests were carried out in the presence of a hydroxyl radical scavenger, either methanol (10 mM, $k = 9 \times 10^8 \text{ M}^{-1}\cdot\text{s}^{-1}$ (Henglein and Kormann 1985)) (organic scavenger) or KBr (10 mM, $k = 1.1 \times 10^{10} \text{ M}^{-1}\cdot\text{s}^{-1}$ (Moumeni and Hamdaoui 2012)) (inorganic scavenger). It can be seen from the results in the absence of Fe²⁺ (dotted lines in Figure 7-4 (a)) that both scavengers had little effect on DBP degradation by direct photolysis mainly because of the transparent properties of MeOH and KBr under 254 nm irradiation, and because hydroxyl radicals are not generated in this process. However, in the UV/Fe²⁺ process, DBP degradation was clearly inhibited by the presence of either MeOH or KBr, which suggested a synergistic effect by incorporating Fe²⁺ into the UV process which was most likely caused by the generation of hydroxyl radicals. It has been reported that Fe(II) can be transformed to Fe(III) by 254 nm UV via photodetachment under acidic or neutral conditions with the simultaneous release of a hydrated electron (e_{aq}^-) (R 7-1) (Airey and Dainton 1966, Braterman et al. 1984). From the results shown in Figure 7-4 (b), it was confirmed that there was no measurable auto-oxidation of Fe²⁺ by dissolved oxygen in the solution (from air via the solution surface), but conversion of Fe²⁺ was clearly

evident in both blank water and 0.01 mM DBP solution under UV₂₅₄ irradiation. It has been reported that the photo-oxidation product of ferric iron hydrolyses rapidly and mainly exists in the form of hydroxyl complexes in mildly acidic solution (R 7-2 – R 7-5) (Brateman et al. 1984), and these complexes are photosensitive and easily undergo photoreduction to give •OH and ferrous iron (Pignatello et al. 2006). The Fe(OH)²⁺ ion is dominant at pH 2.5 – 4.0, and it can be photo-reduced, whether or not in the presence of H₂O₂, according to R 7-6 (Brillas et al. 2009, Pignatello et al. 2006). Thus, the hydroxyl radicals generated in this way may be responsible for the DBP degradation observed.



In addition, the quantum yield of Fe²⁺ transition (R 7-1) was found to depend on solution pH (Brateman et al. 1984) and increased significantly by reducing the pH (Souza et al. 2013). This could explain the more rapid conversion of Fe²⁺ in the DBP solution than in blank water (see Figure 7-4 (b)), since the solution pH may reduce faster during the photolysis of DBP via the formation of organic acid intermediates.

Though both radical scavengers could suppress DBP degradation in the UV/Fe²⁺ process,

the effect of MeOH and KBr on Fe^{2+} conversion was very different (see Figure 7-4 (b)). In the presence of MeOH, Fe^{2+} was converted much more rapidly, thus leading to a deeper yellowish color by forming the ferric complex (R 7-2 – R 7-5) and the resulting “inner filter” effect blocks the UV transmittance, inducing a much slower DBP degradation than sole-UV irradiation as shown in Figure 7-4 (a) (Jortner and Stein 1962). In the presence of KBr it was found that the conversion of Fe^{2+} was restricted, which might be because the electron donating property and abundance of Br^- ($[\text{Br}^-]:[\text{Fe}^{2+}] = 100$) stabilized the electron of Fe^{2+} in the valence band through the formation of covalent-like Br-Fe-Br bonding. Furthermore, the facilitation of Fe^{2+} conversion in the presence of MeOH was likely due to the formation of formic acid and/or formate ion as the primary methanol- $\bullet\text{OH}$ oxidation product (Monod et al. 2000). It can be seen from Figure 7-4 (b), that the addition of a small amount of either formic acid (0.1 mM) or formate ion (0.1 mM) could significantly improve Fe^{2+} conversion. This is because the formic acid induced a lower pH and increased the quantum yield of Fe^{2+} transition (R 7-1) (Souza et al. 2013); and the formate ion can serve as an organic ligand to facilitate electron transfer of Fe^{2+} . The short lag phase of Fe^{2+} conversion initially in the presence of MeOH was therefore, most likely the result of a limited amount of formic acid/formate ion present and the relatively higher initial pH.

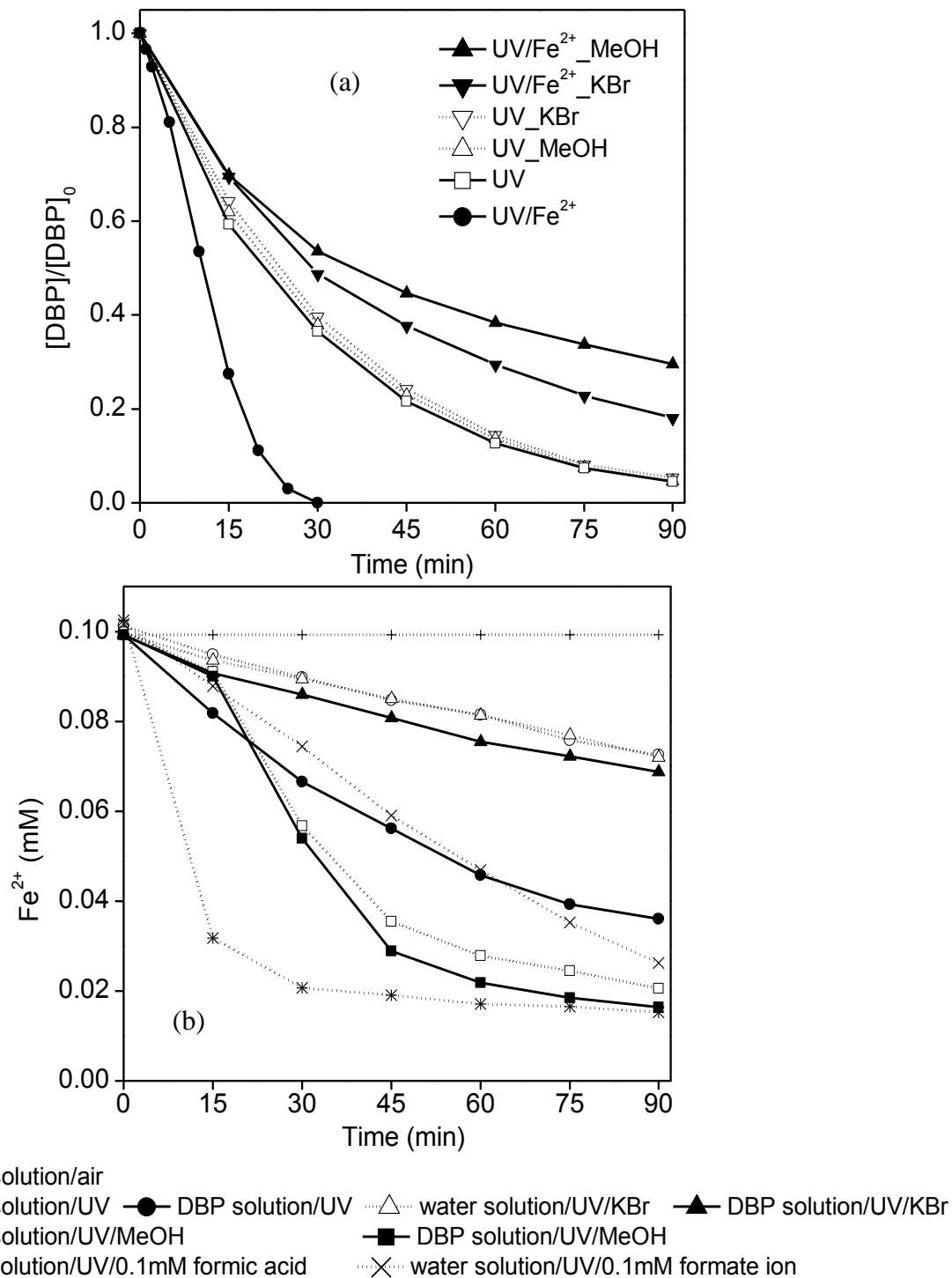


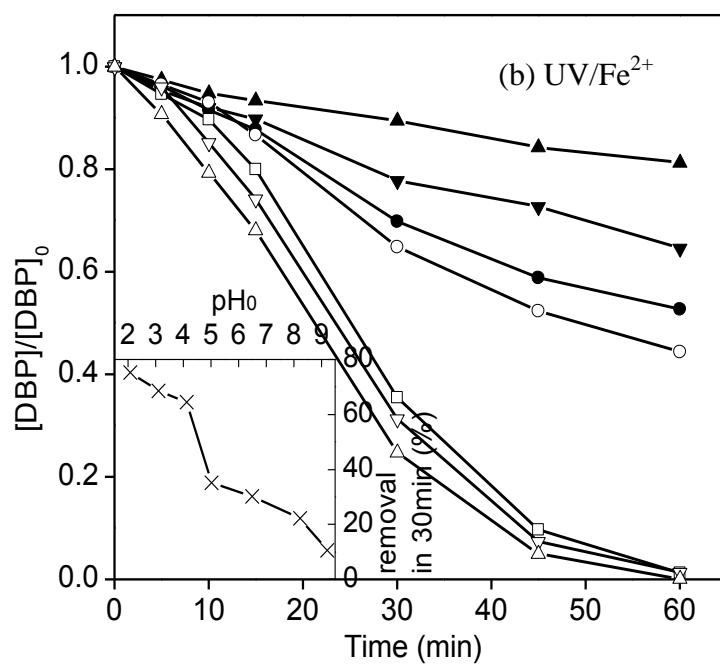
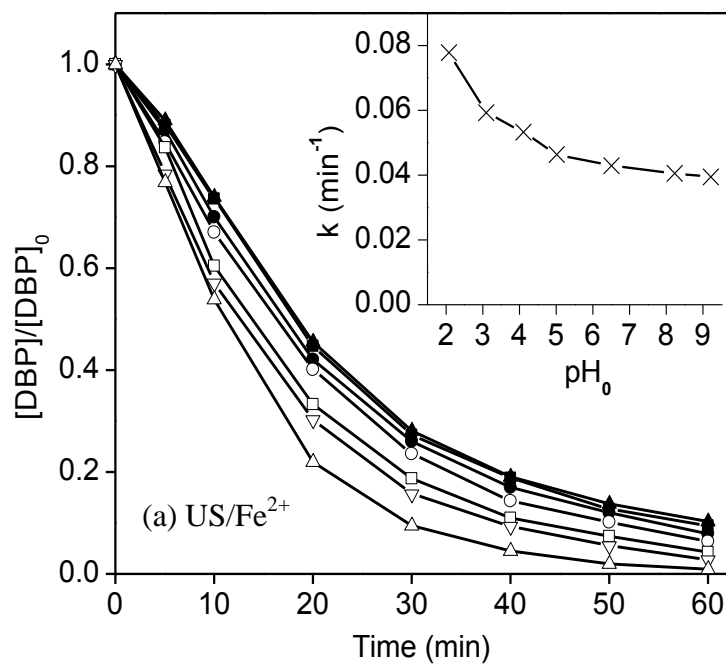
Figure 7-4: (a) Variation of DBP concentration in UV/ Fe^{2+} and related processes with/without radical scavengers; (b) Variation of $[Fe^{2+}]$ in the UV/ Fe^{2+} and related processes ($[DBP]_0 = 0.01$ mM; $[Fe^{2+}]_0 = 0.1$ mM; $[pH]_0 = 6.5 \pm 0.05$; $[MeOH]_0 = 10$ mM;

[KBr]₀ = 10 mM; Six UV₂₅₄ lamps; quartz beaker).

7.2.5. Effect of initial pH

It is well known that solution pH is a critical parameter influencing the efficiency of the conventional Fenton process (Burbano et al. 2005). Therefore, the effect of initial solution pH on the Fe²⁺-related processes involved in this study was examined in the pH range of 2.08 – 9.21, and the results are presented in Figure 7-5 (a) US/Fe²⁺; (b) UV/Fe²⁺; and (c) US/UV/Fe²⁺. It was found that the DBP degradation performance in these processes were significantly affected by solution pH and generally inversely related with pH₀. Specifically, in the US/Fe²⁺ process (Figure 7-5 (a)), the first-order rate constants increased systematically with the decrease of pH₀, which was possibly due to the higher oxidation potential of •OH at lower pH levels (Babuponnusami and Muthukumar 2012). In addition, the oxidation of Fe²⁺ in aqueous media is proportional to the [OH⁻]², so that the oxidation of Fe²⁺ and the further precipitation of insoluble ferric oxohydroxides are more significant at neutral and alkaline conditions, which therefore lowers the amount of Fe²⁺ available to take part in Fenton-type reactions (Burbano et al. 2005). It can be seen from Figure 7-5 (b) and (c) that the effect of pH₀ on UV/Fe²⁺ and US/UV/Fe²⁺ processes was more pronounced; for the UV/Fe²⁺ process the removal (%) of DBP at 30 min was used as a quantitative comparison as shown in the inset of Figure 7-5 (b). When the pH₀ was 4.11 and lower, the DBP removal increased dramatically, which is likely because the dominant ferric species of [Fe(OH)]²⁺ reaches its peak concentration at pH 3.0 – 4.0 and promotes •OH generation via R 7-6 (Brillas et al. 2009, Pignatello et al. 2006). In addition, the quantum yield of Fe²⁺ transition via R 7-1 reaches its maximum at about pH 2.0, which also facilitated the

formation of $[\text{Fe}(\text{OH})]^{2+}$ by increasing the concentration of Fe^{3+} and then promoting $\bullet\text{OH}$ generation. Therefore, the DBP decay is favorable at lower pH levels based on the above net effects.



(c.o.)

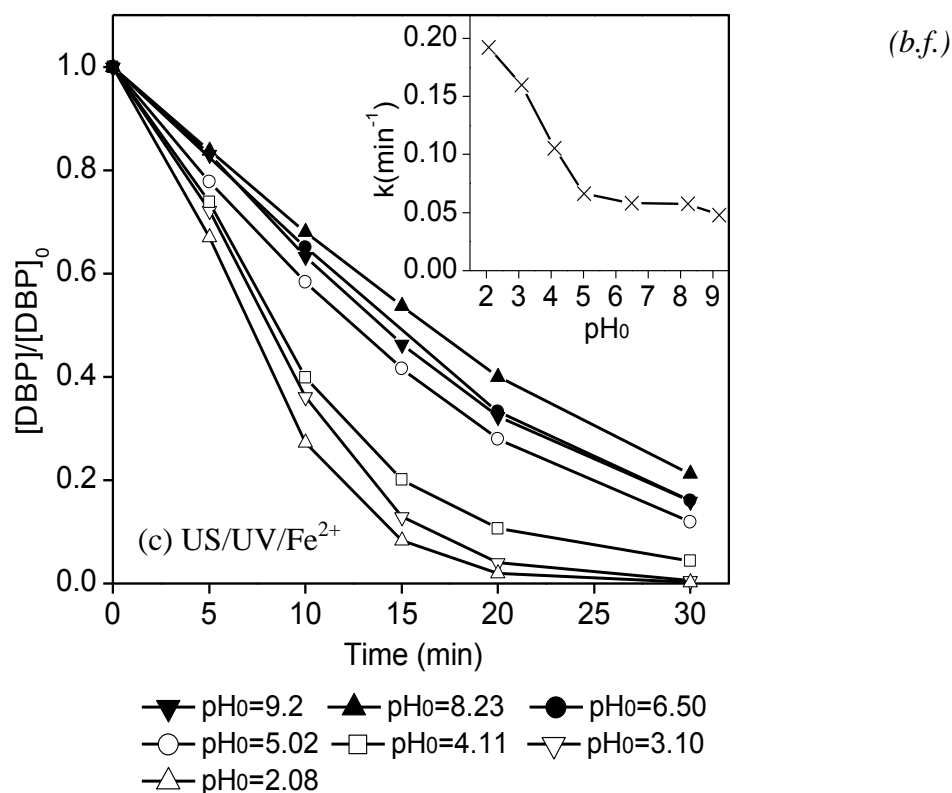


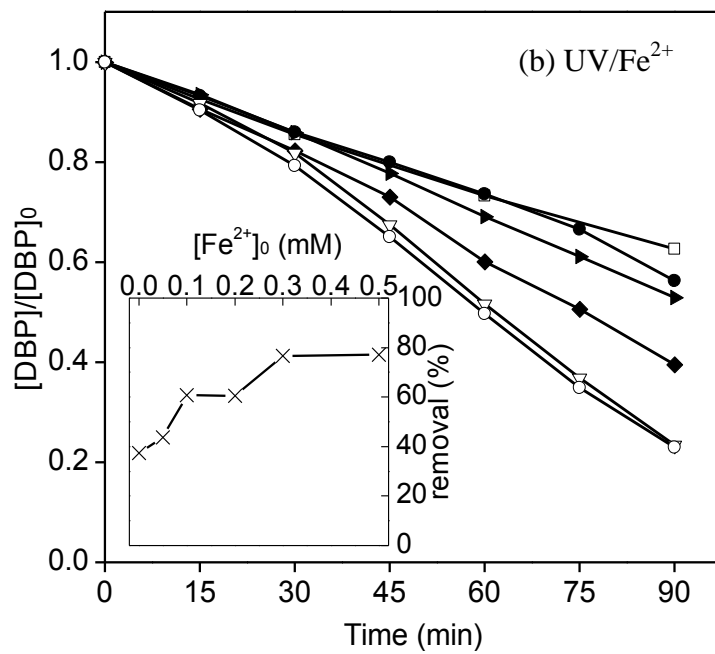
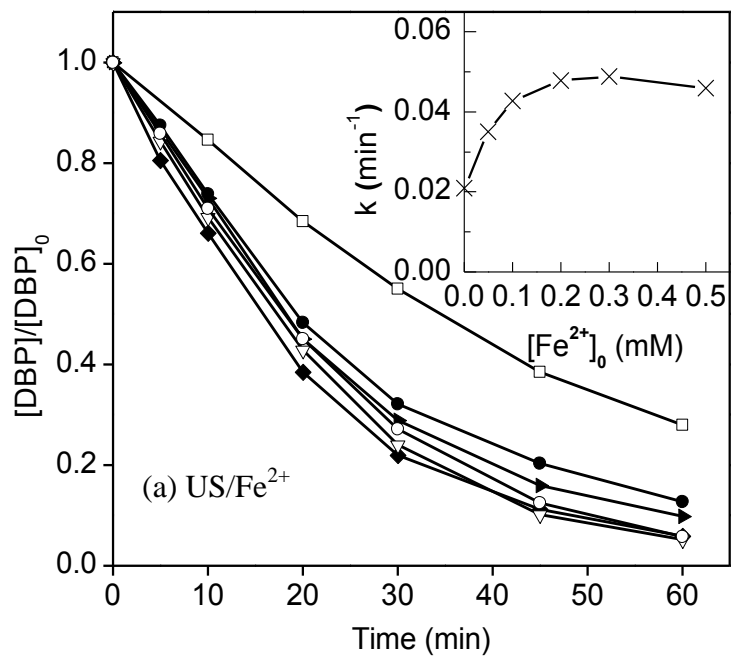
Figure 7-5: Effect of initial solution pH on DBP degradation in the processes of (a) US/Fe²⁺; (b) UV/Fe²⁺; (c) US/UV/Fe²⁺ (conditions: [DBP]₀ = 0.01 mM; [pH]₀ = 2.08 – 9.21; [Fe²⁺]₀ = 0.1 mM).

7.2.6. Effect of Fe²⁺ dosage

The effect of Fe²⁺ concentration (0 – 0.5 mM) on DBP degradation in the US/Fe²⁺, UV/Fe²⁺, and US/UV/Fe²⁺ processes is shown in Figure 7-6 (a), (b), and (c), respectively. It was observed that, in the US/Fe²⁺ process, increasing [Fe²⁺]₀ from 0 to 0.2 mM improved the DBP degradation, but further increase of [Fe²⁺]₀ (to 0.5 mM) resulted in a slight inhibition. This phenomenon could be explained by the limited amount of ultrasonically generated H₂O₂ at higher [Fe²⁺]₀. Thus, moderate increases of Fe²⁺ dosage can promote •OH generation while excessive Fe²⁺ would most probably result in radical scavenging

according to R 7-7. In the UV/Fe²⁺ process (Figure 7-6 (b)), DBP degradation increased systematically with Fe²⁺ dosage from 0 to 0.3 mM, but remained constant between 0.3 and 0.5 mM. As discussed in section 7.2.4 (R 7-1 – R 7-6), the presence of increasing amounts of Fe²⁺ can facilitate the formation of [Fe(OH)]²⁺ (R 7-1 and R 7-2), and subsequently •OH generation (R 7-6). However, higher concentrations of Fe²⁺ can simultaneously promote the formation of insoluble ferric oxohydroxides (R 7-1 – R 7-5), which can decrease the effective hydroxyl complexes of ferric iron and also limit the penetration of UV light. With the US/UV/Fe²⁺ hybrid process, the effect of Fe²⁺ concentration was more complicated with the DBP removal reaching a maximum at an Fe²⁺ concentration of 0.1 mM, and was substantially lower at the highest Fe²⁺ concentration (0.5 mM). In addition, it was evident from Figure 7-6 (c) that for [Fe²⁺]₀ > 0.1 mM, the rate of DBP degradation noticeably declined in the later period (~ 20 - 30 min). As well as the effects described above to explain the performance behaviour seen with the US/Fe²⁺ and UV/Fe²⁺ processes, which were equally applicable to the US/UV/Fe²⁺ process, there may be additional interactions present in US/UV/Fe²⁺ process to cause the distinct maximum in DBP degradation at a relatively low Fe²⁺ concentration. It is possible that the available H₂O₂ was limited due to the faster or parallel consumption by both Fe²⁺ and UV irradiation, so that the residual Fe²⁺ was more readily oxidized by •OH to form ferric iron (R 7-7) and therefore unavailable for the Fenton reaction. Thus, the lack of sufficient Fe²⁺ in the later stages of the reaction and the formation of a turbid solution (R 7-5), especially with higher [Fe²⁺]₀, may be responsible for the reduced DBP degradation rate in the later reaction period.





(c.o.)

(b.f.)

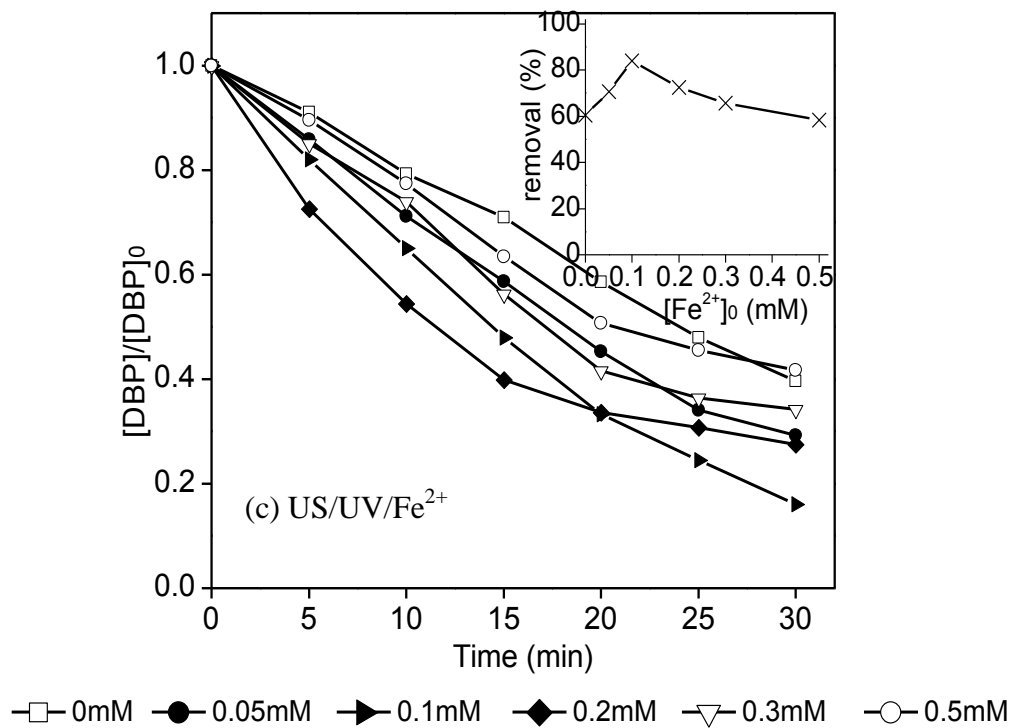


Figure 7-6: Effect of initial Fe^{2+} concentration on DBP degradation in the processes of (a) US/ Fe^{2+} ; (b) UV/ Fe^{2+} ; (c) US/UV/ Fe^{2+} (conditions: $[\text{DBP}]_0 = 0.01$ mM; $[\text{pH}]_0 = 6.5 \pm 0.05$; $[\text{Fe}^{2+}]_0 = 0 - 0.5$ mM).

7.3. Chapter summary


In this chapter, the homogeneous sono-photo-Fenton process (US/UV/Fe²⁺) was investigated by examining its treatment performance and those of its constituent processes using DBP as the probe. Clear synergistic effects were observed in the US/UV/Fe²⁺ process which led to it having the greatest impact on DBP degradation. The synergistic effects were found to be mainly due to the enhanced generation of •OH radicals via the following mechanisms: (a) a Fenton reaction from ultrasonically generated H₂O₂ in the presence of Fe²⁺; (b) the photo-decomposition of H₂O₂; and (c) the photo-decomposition of [Fe(OH)]²⁺ resulting from the Fe²⁺ photo-oxidation and hydrolyzation process. In addition, the sono-Fenton process was found to be more efficient in utilizing Fe²⁺ compared to the conventional Fenton process and the DBP degradation was more complete. The Fe²⁺-related processes involved in this study all had better performances at low pH. In general, a moderate increase of Fe²⁺ dosage could promote the efficiencies of the US/Fe²⁺, UV/Fe²⁺, and US/UV/Fe²⁺ processes, but an overdose could inhibit the treatment performance. The optimal dosage of Fe²⁺ for the US/UV/Fe²⁺ process was determined to be 0.1 mM under the conditions of this study.

Chapter 8: Sonopholytic Degradation of Phthalate Acid Esters in Water and Wastewater: Effects of Physicochemical Properties of the Compounds and Degradation Mechanisms.

Chapter 9: Efficient Degradation of Hydrophobic Nonylphenol in Solution by a Green Technology of Sonophotolysis.

These chapters report on and discuss experimental results. Chapter Eight is organised in the following way and is very effective partly because the writer includes the following:

Structure

Introduction		Section 8.1
Findings and Discussion on each set of parameters in turn		Section 8.2
Summary		Section 8.3

Content

- Gives an overview of the section at the start of the chapter (e.g. Section 8.1)
- Describes the background (e.g. Section 8.1 paragraph 1)
- Reports previous studies (e.g. Section 8.1 paragraph 2)
- Highlights the gap in current knowledge (e.g. Section 8.1, paragraph 2, final sentence)
- Outlines the chapter (e.g. Section 8.1, final paragraph)
- Develops paragraphs clearly, e.g. Section 9.2.1, paragraph 1:
 - Sentence 1 Background
 - Sentence 2 Investigation
 - Sentence 3 Main findings
 - Sentence 4 Interpretation of findings

Sentence 5-7 Additional findings

Sentence 8 Interpretation

Sentence 9-12 Other findings

- Refers to previous chapters e.g. *as described in Chapter Two* (e.g. Section 8.1, paragraph 1, sentence 1)
- Highlights unexpected results (e.g. Section 9.3, final paragraph)

Language

- Links paragraphs e.g. *In view of the above* (e.g. Section 8.1 paragraph 6, sentence 1)
- Uses formal expressions to explain purpose e.g. *to obtain insight into...* (e.g. Section 8.2.4, paragraph 1, sentence 1)

To Consider

This chapter of the thesis is effective. However, it could be further improved in the following aspects.

💡 Avoid using *some studies* (e.g. Section 8.1 paragraph 2). It is better to use a more academic word than some e.g. *a number of studies*.

💡 Avoid using spoken language e.g. *to know about* (e.g. Section 8.2.5 paragraph 1 line 1). It is better to use more formal terms e.g. *to discover*.

8. Chapter Eight Sonophotolytic Degradation of Phthalate Acid Esters in Water and Wastewater: Effects of Physicochemical Properties of the Compounds and Degradation Mechanisms

8.1. Overview

Among those theories proposed to explain the sonochemical situations, the “hot spot” theory is the most commonly adopted, which considers the sonochemical reaction as a heterogeneous reaction as described in Chapter Two and heat are produced from the cavitation bubbles (Okitsu et al. 2005, Serpone and Colarusso 1994). Therefore, organic compounds with different physicochemical properties are supposed to have different driving forces toward the bubble-liquid interfaces where the reactive radicals concentrate, which will further influence their degradation efficiencies.

Some studies have evaluated the effects of several physicochemical properties of compounds on their sonochemical degradation, such as octanol-water partition coefficient (K_{ow}), water solubility (S_w), vapor pressure (V_p), and Henry’s law constant (K_H) (Henglein and Kormann 1985, Nanzai et al. 2008, Park et al. 2011, Psillakis et al. 2004, Wu and Ondruschka 2005). However, all of these studies are limited to investigate the influence within the US process alone. In practice, the sonochemical process is better to combine with other AOTs to improve the cost-effectiveness, and the physicochemical properties of the interested compounds may also play an important role in the hybrid processes.

Compared to those hybrid processes involving chemical dosing (e.g. US/PMS (Li et al. 2013a), US/catalyst (Im et al. 2013), US/Fe²⁺ (Xu et al. 2014)), the combination of UV and US is an environmentally-friendly alternative. Synergistic effect was observed in the sonopholytic process (US/UV) and the principal synergistic mechanism was found to be the photodissociation of ultrasonically produced H₂O₂ ($\text{H}_2\text{O}_2 + \text{UV}_{254} \rightarrow 2\bullet\text{OH}$) (Xu et al. 2013a). So far, however, no studies have examined the relationship between physicochemical properties of the compounds and their degradation performance in US/UV process.

Furthermore, most of the previous investigations were conducted under pure water mediated conditions in the absence of any background solutes. However, AOTs are usually employed as tertiary wastewater treatment processes followed by secondary biological treatment, so that it is necessary and helpful to assess the interested AOTs using real wastewater as the matrix. The background TOC in the effluent is likely to influence the degradation of compounds with different physicochemical properties.

A group of PAEs with relatively shorter alkyl chain length and higher water solubility were selected as the probe compounds, including DMP, DEP, DBP and MMP. Many studies have been conducted trying to degrade one kind of PAEs using AOT methods (Huang et al. 2011, Hwang et al. 2011, Medellin-Castillo et al. 2013, Na et al. 2012b, Xu et al. 2013a, b, Xu et al. 2014), and a few studies have also compared the degradation performance of a group of PAEs (Psillakis et al. 2004, Wen et al. 2011, Yim et al. 2002). Although the physicochemical properties of different PAEs are sometimes used to explain their degradation performances, still little investigation is conducted in the US and/or US/UV

processes.

In view of the above, the sonolytic, sonophotolytic degradation of four PAEs (DMP, DEP, DBP, MMP) were investigated. The effects of physicochemical properties of compounds were evaluated using both pure water and real secondary effluent as water matrices. In addition, the degradation pathways of DBP were proposed based on the identified intermediates.

8.2. Results and discussion

8.2.1. Effect of physicochemical properties on PAE sonolysis

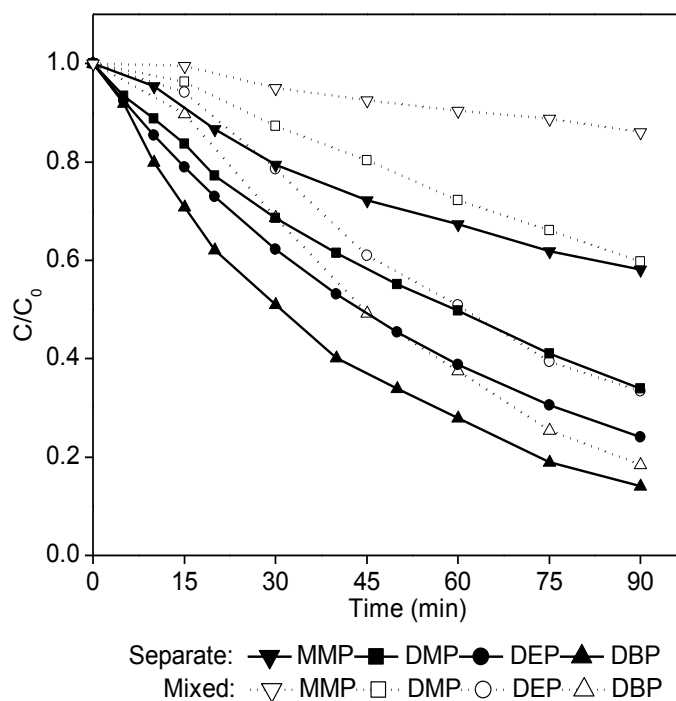


Figure 8-1: Temporal variation of PAE concentrations during the sonolysis process ($C_0 = 0.01$ mM, solid points: separate reaction, hollow points: mixed reaction).

The physicochemical parameters of selected PAEs are listed in Table 8-1, which were obtained from the United States National Library of Medicine (USNLM, <http://toxnet.nlm.nih.gov/>). The selected PAEs have similar chemical structures and demonstrate almost identical UV absorption bands and intensities as shown in Figure 3-5. The sonolytic degradation of PAEs separately or as a mixture was investigated and results are shown in Figure 8-1. It was found that, the sonolytic degradation of PAEs followed pseudo first-order kinetics and significant differences in efficiencies were observed. The degradation rate increased from MMP to DBP in both separate and mixed reactions. For each PAE, lower degradation rate and initial lag phase were found in the mixed reaction, which can be explained by the competition effect among different PAEs for the limited amount of radicals. It can be seen from Table 8-1, in general, PAEs with longer alkyl chains demonstrated larger $\text{Log}K_{ow}$, K_H , and smaller S_w (V_p shows irregularity based on USNLM), indicating increasing hydrophobicity and fugacity from MMP to DBP. The $\text{Log}K_{ow}$ and S_w are indicators of the hydrophobic and hydrophilic capacities of organic compounds, respectively; the V_p and K_H can be used to indicate the tendency of molecules to escape from liquid to gas phase. The detailed kinetic data are given in Table 8-2 and it was noted that different PAEs showed different extent of rate decrease in the mixed reaction, in which the decrease of 90 min removal rate for MMP, DMP, DEP, and DBP was 27.86%, 25.8%, 9.28%, and 4.38%, respectively. These results indicated that the more hydrophobic PAEs not only showed higher efficiencies when they were degraded alone, but also demonstrated stronger competitiveness with the presence of other competitors.

Table 8-1: Summary of the physicochemical properties of the investigated PAEs (Log K_{ow} : octanol-water partition coefficient; S_w , water solubility at 25 °C; V_p : vapor pressure at 25 °C; K_H : Henry's law constant at 25 °C; k_{OH} : •OH reaction rate constant at 25 °C) (USNLM, <http://toxnet.nlm.nih.gov/>).

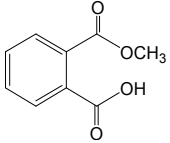
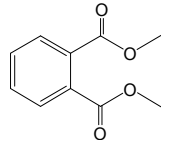
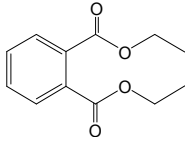
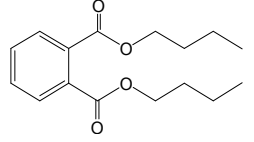
Name	Structure formula	Molecular formula	Molecular weight	Log K_{ow}	S_w (mg L ⁻¹)	V_p (mmHg)	K_H (atm m ³ mol ⁻¹)	k_{OH} (M ⁻¹ S ⁻¹)
MMP		C ₉ H ₈ O ₄	180.16	1.13	5960	1.84×10 ⁻⁴	6.99×10 ⁻¹⁰	5.47×10 ⁸
DMP		C ₁₀ H ₁₀ O ₄	194.18	1.60	4000	3.08×10 ⁻³	1.97×10 ⁻⁷	3.46×10 ⁸
DEP		C ₁₂ H ₁₄ O ₄	222.24	2.47	1080	2.1×10 ⁻³	6.1×10 ⁻⁷	2.09×10 ⁹
DBP		C ₁₆ H ₂₂ O ₄	278.34	4.9	13	2.01×10 ⁻⁵	1.81×10 ⁻⁶	5.59×10 ⁹

Table 8-2: The pseudo first-order rate constants and removal rate in 90 min of different PAEs in the sonolytic process, either in separate reaction or in mixed reaction ($C_0 = 0.01$ mM for each PAE).

Probes	Separate		Mixed		Difference	
	k_{us}	Removal ₉₀	k_{us}	Removal ₉₀	Δk	Δ Removal ₉₀
	(min ⁻¹)	(%)	(min ⁻¹)	(%)	(min ⁻¹)	(%)
MMP	0.0069	41.82	0.0016	13.96	0.0053	27.86
DMP	0.0120	66.04	0.0054	40.24	0.0066	25.8
DEP	0.0158	75.88	0.0117	66.60	0.0041	9.28
DBP	0.0218	85.94	0.0175	81.56	0.0043	4.38

To further illustrate the correlations between physicochemical parameters of PAEs and their sonolytic degradation performance, pseudo first-order rate constants (k) of both separate and mixed reactions were plotted as functions of various parameters in Figure 8-2. Continuous positive correlations were found between k and $\text{Log}K_{ow}$, K_H , and continuous negative correlation was found between k and S_w . In the case of V_p , except for MMP, k was generally inversely related to V_p . It is therefore concluded that the hydro-phobicity/philocity of PAEs characterized by $\text{Log}K_{ow}$ and S_w is a potent indicator of the sonolysis efficiency; the stronger hydrophobicity results in more efficient degradation. In contrast, parameters of K_H and V_p did not provide consistent results, which is most likely because the degradation regions of selected PAEs are near the bubble-liquid interfaces and in the bulk solution rather than inside the cavitation bubbles (see 8.2.2). A previous study (Nanzai et al. 2008)

has reported that the acceptable positive correlations between sonolysis rates and K_H , V_p were only obtained from the limited high ranges of about $10^{-4} \sim 10^{-1} \text{ atm m}^3 \text{ mol}^{-1}$ and $10^{-1} \sim 10^2 \text{ mmHg}$, respectively, which are much higher than the values in this study. Thus, the effects of physicochemical properties on sonolysis of organic compounds should also take into account of the dominant degradation mechanisms in sonolytic process.

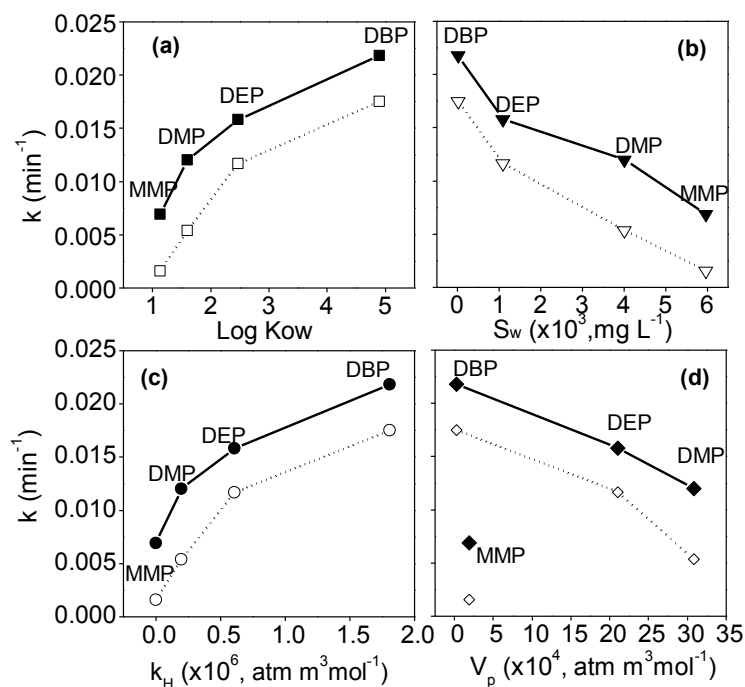


Figure 8-2: Correlation between the physicochemical parameters and the pseudo first-order rate constants of different PAEs ($C_0 = 0.01 \text{ mM}$, solid points: separate reaction, hollow points: mixed reaction).

8.2.2. Effect of radical scavengers on sonolytic degradation of PAEs

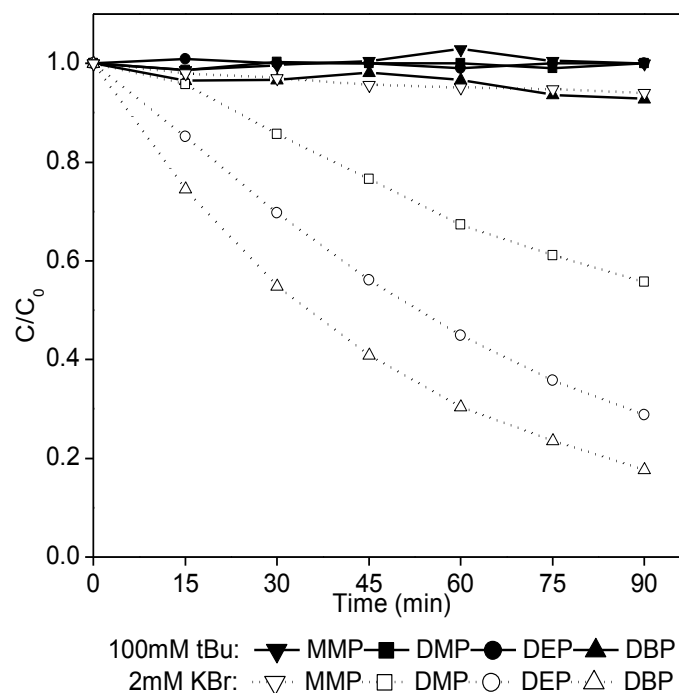


Figure 8-3: Effect of radical scavengers (100 mM tert-butanol or 2 mM KBr) on the sonolytic degradation of PAEs ($C_0 = 0.01$ mM).

Two different kinds of radical scavengers, TBA (100 mM) and KBr (2 mM), were used to investigate the mechanisms of PAEs sonolysis, and results are shown in Figure 8-3. TBA is an effective radical scavenger which is able to quench $\cdot\text{OH}$ radicals at the interfaces of cavitation bubbles (Henglein and Kormann 1985). It was found in Figure 8-3 that, 100 mM TBA could completely inhibit the sonolytic degradation of four PAEs, indicating that PAEs degradation mainly results from radical oxidation at the interfaces or in the aqueous phase rather than pyrolysis inside bubbles. The ionic scavenger of KBr is more likely to reside in the bulk solution and can quench the radicals escaping to the bulk (Manousaki et al. 2004). As can be seen from Figure 8-3, different extent of inhibition was observed for different

PAEs. The rate constants of different PAEs with or without the presence of KBr are given in Table 8-3. It was noted that the most hydrophilic compound, MMP, demonstrated the most significant inhibition by KBr ($\Delta k = 0.0061 \text{ min}^{-1}$), implying that MMP molecules were located farthest from the cavitation bubble and are most susceptible to KBr. However, the more hydrophobic DEP and DBP showed much less and similar inhibition ($\Delta k_{\text{DEP}} = 0.0023 \text{ min}^{-1}$, $\Delta k_{\text{DBP}} = 0.0024 \text{ min}^{-1}$), indicating their degradation regions were more close to bubble interfaces and less vulnerable to KBr. These results support that PAEs with more hydrophobicity are located nearer to the cavitation bubbles during the sonolysis process, corresponding to higher degradation efficiencies.

Table 8-3: The pseudo first-order rate constants (k_{us}) of different PAEs in the sonolytic degradation with or without the presence of KBr (2 mM) as a radical scavenger.

Compound	$k_{us} (\text{min}^{-1})$ (with KBr)	$k_{us} (\text{min}^{-1})$ (without KBr)	$\Delta k (\text{min}^{-1})$
MMP	0.0008	0.0069	0.0061
DMP	0.0064	0.0120	0.0056
DEP	0.0135	0.0158	0.0023
DBP	0.0194	0.0218	0.0024

8.2.3. Effect of physicochemical properties on PAE sonophotolytic degradation

Degradation of the investigated PAEs in both the photolytic and sonophotolytic processes is

shown in Figure 8-4, where the degradation generally followed pseudo first-order kinetics in both two processes. Significant increase of the degradation rates were found by combining US with UV for all PAEs. To scrutinize the degradation performance of different PAEs, the pseudo first-order rate constants and the synergistic index ($SI = k_{us/uv}/(k_{us} + k_{uv})$, where a $SI > 1$ indicates a synergistic effect) were summarized in Table 8-4. It is worth notice that increasingly weak synergistic effects were obtained from MMP to DBP with the increase of molecular hydrophobicity. In our previous study (Xu et al. 2013a), it was found that the synergistic effect in the hybrid US/UV process was mainly because of the sonochemical formation and photodecomposition of H_2O_2 to give birth to more $\bullet OH$ radicals. Furthermore, the photo-degradation of organic compound was accelerated substantially by the existence of even small amount of H_2O_2 (Xu et al. 2013a). In this study, the accumulation of H_2O_2 in solution during the sonochemical reactions was examined with the presence of either 0.01 mM MMP or 0.01 mM DBP, and results are shown in Figure 8-5. It can be seen that H_2O_2 concentration increasing in 0.01 mM DBP solution was less than that in 0.01 mM MMP solution, which resulted from the higher consumption rate of $\bullet OH$ radicals (the major precursor in forming H_2O_2) by DBP due to its stronger hydrophobicity as discussed in Section 8.2.1. On the contrary, the more hydrophilic MMP demonstrating slower sonochemical degradation efficiency produced greater accumulation of H_2O_2 and corresponding more significant synergistic effect in the US/UV process. Therefore, although the stronger hydrophobicity is beneficial for the sonochemical degradation of PAEs, it is adverse for obtaining remarkable synergistic effect in the sonopholytic process due to the less accumulation of H_2O_2 .

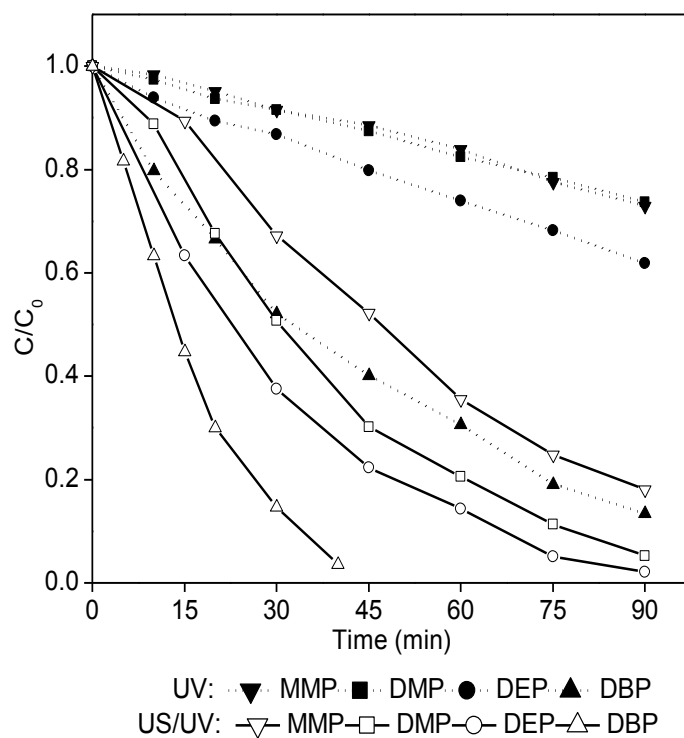


Figure 8-4: Temporal variation of PAEs concentrations during the photolytic and sonophotolytic processes ($C_0 = 0.01$ mM).

Table 8-4: The pseudo first-order rate constants of PAEs degradation in the sonolytic, photolytic, and sonophotolytic processes, and the synergistic index for different PAEs in the sonophotolytic processes.

Compound	k_{us} (min^{-1})	k_{uv} (min^{-1})	$k_{us/uv}$ (min^{-1})	Synergistic Index
MMP	0.0069	0.0032	0.0238	2.36
DMP	0.0120	0.0033	0.0293	1.92
DEP	0.0158	0.0052	0.0387	1.84
DBP	0.0218	0.0207	0.0712	1.68

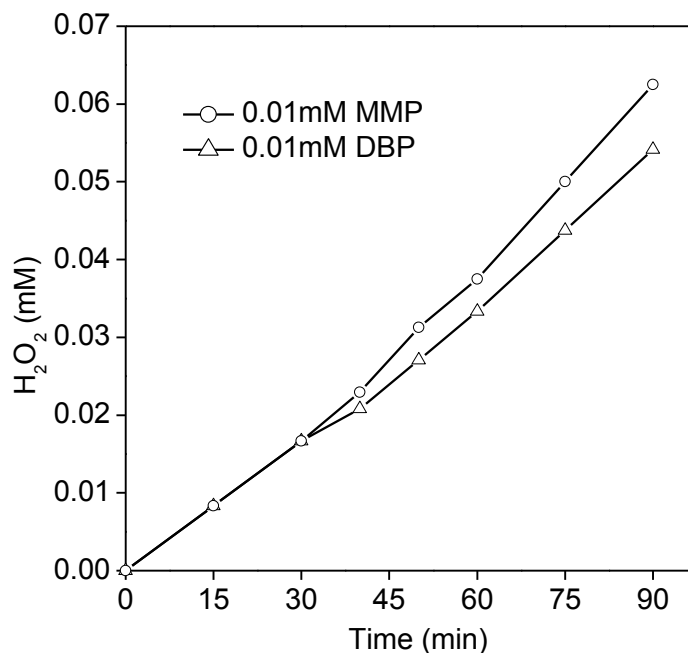


Figure 8-5: Formation of hydrogen peroxide in solution during the sonochemical reaction with the presence of either 0.01 mM MMP or 0.01 mM DBP.

8.2.4. Sonophotolytic degradation of PAEs in real wastewater

To obtain a further insight into how the sonophotolytic process works when applied to real effluents containing a variety of compounds, experiments were carried out using real secondary effluent as the water matrix. Typical parameters of the secondary effluent used in this study were given in Table 8-5, in which, soluble TOC in the wastewater was used as an indicator and different TOC concentrations were realized by diluting the wastewater in varying ratios. Figure 8-6 shows the variation of pseudo first-order rate constants of four PAEs mediated by different TOC concentrations. It was found that, the increase of background TOC led to the decrease of the sonophotolysis rate for all the PAEs. It is known that TOC in the secondary effluent indicates the presence of various organic species arising from both the unbiodegradable organic matter and the degradation products after the

biological treatment. Obviously, the presence of TOC in water inhibited the sonophotolytic degradation of PAEs mainly by competing for the limited radicals. For each PAE, the correlation between k_{effluent} and background TOC concentration ($[\text{TOC}]$) was found to follow quasi-exponential relationship (Eq. 8-1), where the constant K defined as the “inhibiting index” by background TOC was used to indicate the decreasing rate of k_{effluent} . Larger K value indicates more significant inhibition induced by background TOC. Moreover, it was also observed that the investigated PAEs demonstrated different magnitude of rate decrease, i.e. showing different K values, where MMP was subjected to the most serious inhibition and DBP was the least influenced. To elucidate more clearly the relationship between index K and the physicochemical properties of PAEs, the inset of Figure 8-6 plots the value $1/K$ of different PAEs as a function of $1/K_{\text{ow}}$ and an almost linear relationship was obtained, which was expressed in Eq. 8-2. Negative correlation was found between K and K_{ow} , which implied that the hydrophobicity of an organic compound was also crucial for its sonophotolysis in real application and the more hydrophobic compounds were more readily degraded and less influenced by other dissolved organic matters.

$$k_{\text{effluent}} = k_{\text{DDW}} \times e^{-K \times [\text{TOC}]} \quad (8-1)$$

$$1/K = 33.1 - 276.2 \times 1/K_{\text{ow}} \quad (8-2)$$

Combining Eq. 8-1 and Eq. 8-2 gives the following expression:

$$\ln \frac{k_{\text{effluent}}}{k_{\text{DDW}}} = \frac{K_{\text{ow}} \times [\text{TOC}]}{276.2 - 33.1 \times K_{\text{ow}}} \quad (8-3)$$

From Eq. 8-3, it is quantitatively revealed the relationship between the hydrophobicity of the investigated PAEs characterized by K_{ow} and the expected degradation rate mediated by

wastewater at a given soluble TOC concentration. This may provide a useful representation in predicting the sonopholytic degradation performance of organic compounds with different physicochemical properties for real application.

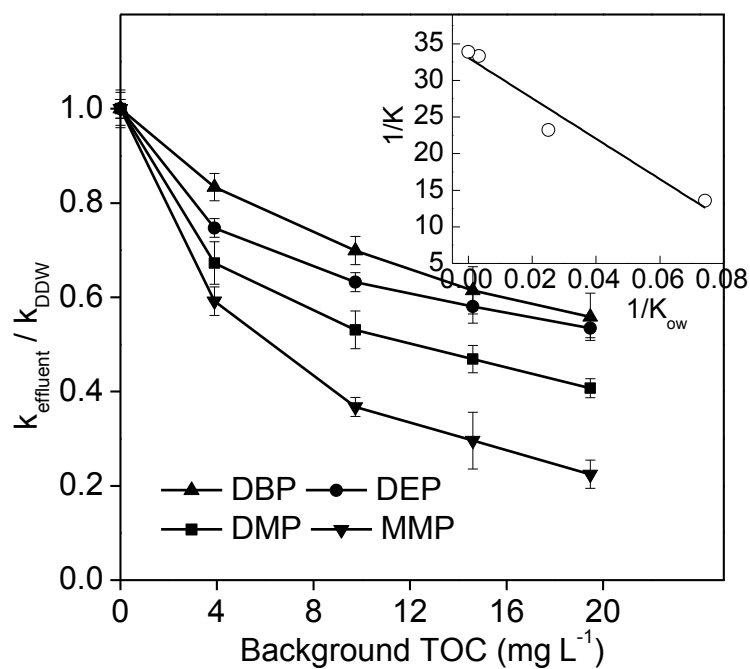


Figure 8-6: Variation of pseudo first-order rate constants (k) of different PAEs in the sonopholytic process mediated by different dissolved TOC concentrations from wastewater (inset: correlation between TOC inhibiting index K and K_{ow} of different PAEs).

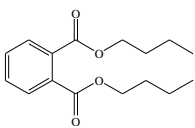
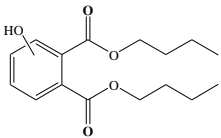
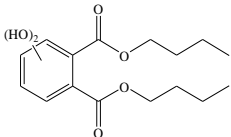
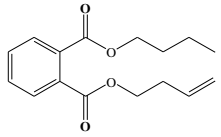
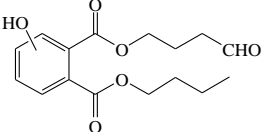
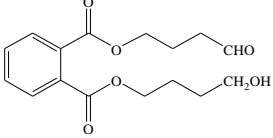
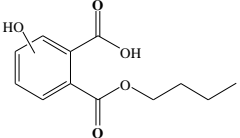
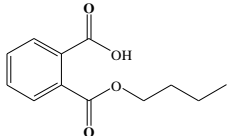
Table 8-5: Parameters of secondary effluent of domestic wastewater used in this study.

Parameter	COD* (mg L ⁻¹)	TOC* (mg L ⁻¹)	pH	NH ₄ ⁺ -N* (mg L ⁻¹)	NO ₃ ⁻ -N* (mg L ⁻¹)	TN* (mg L ⁻¹)
Value	23.42	18.77	7.96	0.48	4.00	6.33

* denotes soluble concentrations determined after filtration

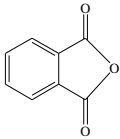
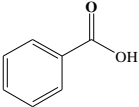
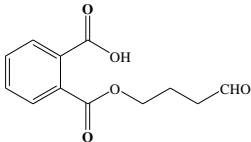
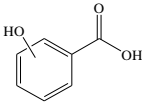
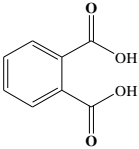
8.2.5. Degradation mechanisms of DBP

Table 8-6: Information of the identified intermediates from DBP degradation.

No.	Name	Structural formula	Retention time (min)	$\frac{[M+H]^+}{[M-H]^-}$ $\frac{[M]^+}{[M]^+}$	Ion mode	MS ² spectrum ions	Detected Processes
1	DBP		12.5	279.13	+	148.98, 205.02	US, UV, US/UV
2	hydroxy-DBP		11.4	293.17	-	162.98, 237.05	US, UV, US/UV
			11.3	295.09	+	164.94, 221.00	
3	di-hydroxy-DBP		10.6	311.10	+	148.97, 204.96	US,
4	1,2-benzenedicarboxylic acid, 1-(3-buten-1-yl) 2-butyl ester		10.1	277.10	+	148.96, 204.97	US, UV
5	1,2-benzenedicarboxylic acid, hydroxy, 1-(4-oxobutyl) 2-butyl ester		9.7	307.14	-	162.94, 237.04	US/UV
6	1,2-benzenedicarboxylic acid, 1-(4-oxobutyl) 2-hydroxybutyl ester		9.4	307.12	-	237.06	US/UV
7	hydroxy-MBP		6.5	237.06	-	162.93, 193.02	UV, US/UV
8	monobutyl phthalate (MBP)		6.9	221.07	-	177.03, 149.02	US, UV, US/UV

(c.o.)

(b.f.)

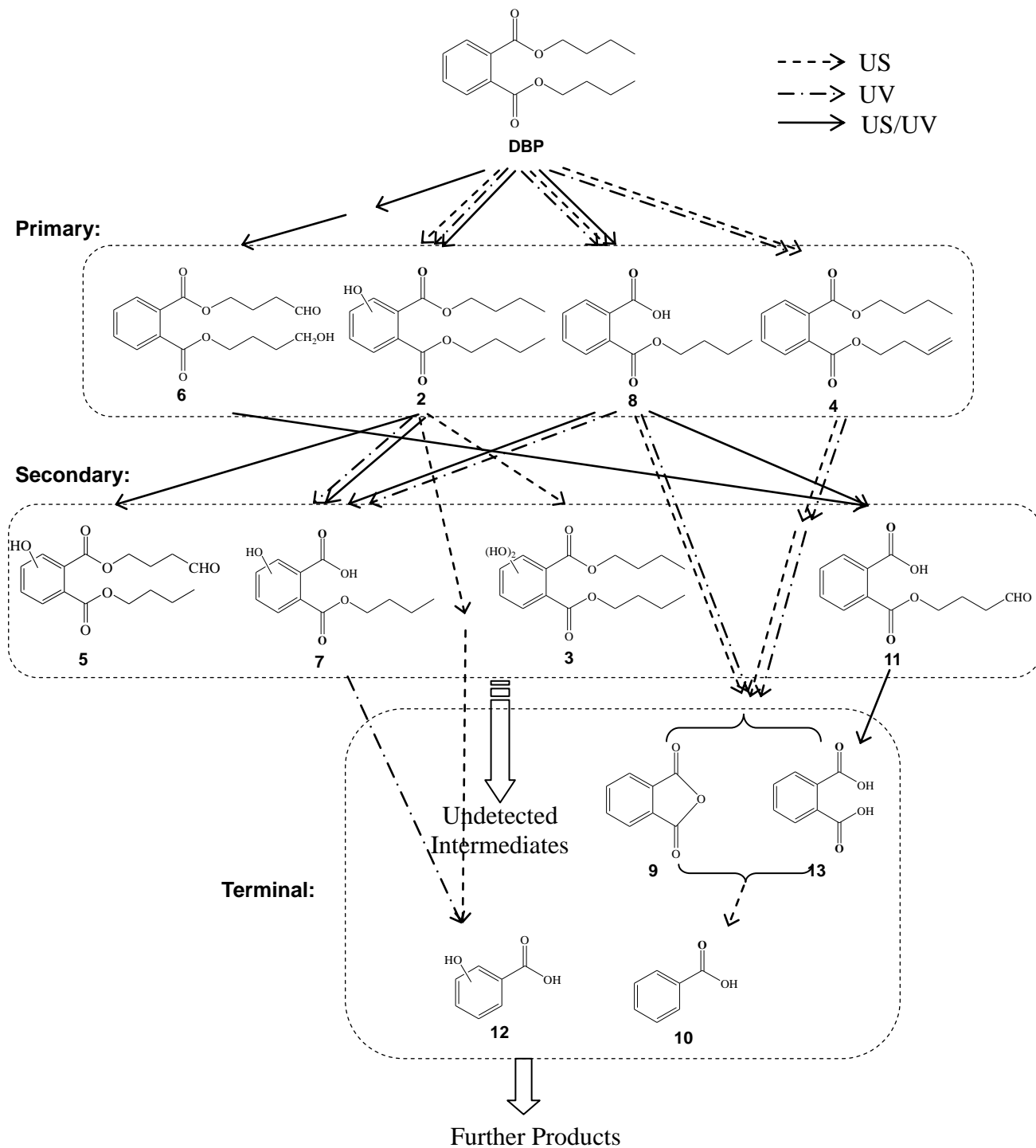
9	phthalic anhydride		4.0	148.96	+	167.85, 216.9	US, UV
10	benzoic acid (BA)		2.6	121.00	-	77.06	US
11	1,2-benzenedicarboxylic acid, 1-(4-oxobutyl) ester		2.3	235.03	-	87.04, 164.89	US/UV
12	hydroxy-BA		1.0	137.00	-	120.95	US
13	phthalic acid (PA)		0.9	164.98	-	121.02	US, UV, US/UV

To know about the reaction mechanisms of PAEs degradation, DBP was selected as a representative compound and its degradation was investigated in detail by analyzing LC/MS results and comparing the mass spectra with standard compounds. The identified intermediates from the sonolytic, photolytic, and sonophotolytic degradation of DBP are summarized in Table 8-6. A total of twelve intermediates were identified, eight for sonolysis, six for photolysis, and seven for sonophotolysis. The possible degradation pathways in related processes are proposed in Scheme 8-1, from which it was found that DBP degradation mainly occurred by oxidation reactions.

Three common intermediates (hydroxy-DBP, monobutyl phthalate (MBP), phthalic acid (PA)) were identified in all the involved processes (i.e. US, UV, US/UV), indicating the dominant pathways responsible for DBP degradation are hydroxylation of the aromatic ring and the butyl-scission of the aliphatic part. However, different abundance of hydroxy-DBP and MBP were generated in individual UV and US process, where hydroxy-DBP dominated in the US process while MBP prevailed in the UV process. The hydroxyl radicals responsible for DBP degradation in US process are strong electrophilic species (Marusawa et al. 2002), prone to attach to the benzene rings with high electron density, more likely to produce hydroxy-DBP. Whereas, the photolysis of DBP originates essentially from reactions involving the carbonyl groups rather than the aromatic ring (Balabanovich and Schnabel 1998, Lau et al. 2005). These two pathways were also reported in other studies investigating the degradation of other PAEs (Bajt et al. 2001, Lau et al. 2005, Xu et al. 2013b). In the sonolytic and photolytic process, dehydrogenation (intermediate 4) was also identified as a minor pathway in the early stage, which was not observed in the US/UV process, probably because of its weak reaction or being short-lived and escaping from sampling. However, a new pathway of oxidizing the alkyl carbon was observed in the US/UV process leading to the formation of aldehyde and alkanol derivatives (intermediate 6, 5, 11) which could not be detected in either individual US or UV process. This may be the result of larger amount of available hydroxyl radicals prevailing in the combined process than that in any individual process, making it possible of those minor reactions. In the late stage of DBP degradation, products with one aliphatic chain (intermediate 10, 12) were identified as the terminal products. Although ring-opening products were not detected, likely due to the limitation of detection method for strong polar and small molecular compounds (m.w. < 100), decrease of the terminal intermediates were

measured. Therefore, it can be assumed that further undetected intermediates even the mineralized products (CO_3^{2-} , HCO_3^-) may exist, of trace amount, in the reaction solution. To examine the mineralization performance of the involved processes, TOC concentration was measured (300 min for sole-US, sole-UV, and 90 min for US/UV). Results showed that the combined process of US/UV demonstrated the best mineralization efficiency with 17% TOC decrease in 90 min, compared to 4% decrease for sole-US and 11% decrease for sole-UV in 300 min. Obviously, the sonolytic process is most unfavorable in mineralizing DBP because of the heterogeneous generation of radicals. The stronger polarity of sonolysis products compared to DBP, as can be seen from the shorter retention time in LC analysis (Table 8-6), was disadvantageous for them to compete radicals surrounding the bubble-liquid interfaces and therefore their further mineralization were suppressed. By combining US with UV process, significant improvement was found in mineralizing DBP by either regenerating hydroxyl radicals in the bulk solution ($\text{H}_2\text{O}_2 + \text{UV}_{254} \rightarrow 2\cdot\text{OH}$ (Xu et al. 2013a)) or direct photolysis of the stronger polar intermediates.

Scheme 8-1: Degradation pathways of DBP for the US, UV, and US/UV processes (the double arrow denotes reaction requiring more than one step).



8.3. Chapter summary

The physicochemical properties of PAEs can not only influence their sonolysis efficiency, but also influence their sonopholytic degradation performance. The sonolytic degradation of investigated PAEs was found mainly by radical oxidation near the bubble-liquid interfaces and in the bulk solution rather than pyrolysis inside cavitation bubbles. Good correlation was found between sonolysis rates and hydrophobic/philic parameters ($\text{Log}K_{ow}$, S_w). The more hydrophobic PAEs not only demonstrated faster sonolysis rate but also exhibited stronger competitiveness in sonochemical reactions with the presence of other competitors. However, stronger hydrophobicity is adverse for PAEs to obtain remarkable synergistic effect in the sonopholytic process due to the less accumulation of H_2O_2 . Furthermore, the more hydrophobic PAEs also experienced less inhibition of the sonopholytic degradation by dissolved TOC in real wastewater. Both hydroxylation of the aromatic ring and butyl-scission of the aliphatic chain were found to be the principal mechanisms initiating the degradation of DBP. The combined process of US/UV also showed the highest efficiency in mineralizing DBP compared either sole-US or sole-UV process.

9. Chapter Nine Efficient Degradation of Hydrophobic Nonylphenol in Solution by a Green Technology of Sonophotolysis

9.1. Overview

Scarce information has been provided concerning NP degradation in high-frequency ultrasonic process and sonophotolytic process, the relevant results obtained in this study are expected to provide some useful information. In this study, the degradation of NP in solution was investigated using the green technology of sonophotolysis. The critical factor of solution pH and influence of nitrate ions (NO_3^-) were investigated in detail. The degradation mechanisms under different conditions were also investigated by identifying intermediates based on UPLC/ESI-MS analysis.

9.2. Results and discussion

9.2.1. Optimization of synergistic effect

Previous studies have shown that synergistic effect may exist between sonochemical process and UV irradiation, and the synergistic mechanism was found primarily due to the photolysis of ultrasonically generated hydrogen peroxide ($\text{H}_2\text{O}_2 + h\nu \rightarrow 2 \text{OH}$) (Xu et al. 2013a). In order to obtain the best synergistic performance, NP degradation by sonolysis, photolysis, and sonophotolysis were examined and different UV light intensities were applied. NP degradation in the investigated processes were found all following pseudo first-order kinetics and the rate constants of different processes were summarized in Table 9-1. It

was found that NP degraded fast by direct sonolysis with a half life of < 30 min ($k_{US} = 0.0264 \text{ min}^{-1}$), much faster compared to other compounds investigated previously (Xu et al. 2013a, b). This can be owing to the strong hydrophobicity of the long alkyl chain of NP, which makes NP molecules more favorably enter into the bubble-liquid interfaces where the effective radicals concentrate. It was also found that both the photolytic (k_{UV}) and sonophotolytic ($k_{US/UV}$) degradation rates increased with UV light intensities. However, the synergistic index (SI) calculated by Eq. 9-1 and used to quantify the synergistic effect of sonophotolytic process demonstrated variable trends. Although the SI values at different light intensities were all higher than one, indicating the existence of synergistic effect, the optimum situation with SI value of 1.133 was only obtained when two lamps were employed and either higher or lower light intensities decreased the SI. Figure 9-1 shows NP degradation profiles in involved processes under the optimal synergistic condition, where 96.2% of NP was degraded within 1 h by sonophotolysis. The influence of UV light intensity on the synergistic effect of the sonophotolytic process is expected to be the result from the balance between available H_2O_2 and photon intensity. The generation of H_2O_2 was found as a pseudo zero-order reaction (Xu et al. 2013a), and the rate constant was determined to be $4 \times 10^{-4} \text{ mM}\cdot\text{min}^{-1}$ for 0.01 mM NP solution in this study. With UV light below the optimal dose (< 2 lamps), the “optical dilute” condition made light intensity as the rate-limiting factor; radical increase by increasing light intensity made more significant improvement of NP degradation. With higher light dose (> 2 lamps), systems turned to “optical dense” for the limited amount of H_2O_2 , and the insufficiency of H_2O_2 restricted further increase of the synergistic effect. Therefore, two UV lamps were applied in following investigations to keep the optimum synergistic performance and prevent energy waste as well.

$$\text{Synergistic Index} = \frac{k_{\text{US/UV}}}{k_{\text{US}} + k_{\text{UV}}} \quad (9-1)$$

Table 9-1: Pseudo first-order rate constants of NP degradation in photolytic and sonophotolytic processes and the corresponding synergistic index at different UV light intensities (ref. $k_{\text{US}} = 0.0264 \text{ min}^{-1}$).

No. of UV lamps	1	2	3	4	5	6
$k_{\text{UV}} (\text{min}^{-1})$	0.0111	0.0181	0.0262	0.0321	0.0358	0.0445
$k_{\text{US/UV}} (\text{min}^{-1})$	0.0382	0.0504	0.0530	0.0601	0.0633	0.0724
Synergistic Index	1.019	1.133	1.008	1.027	1.018	1.021

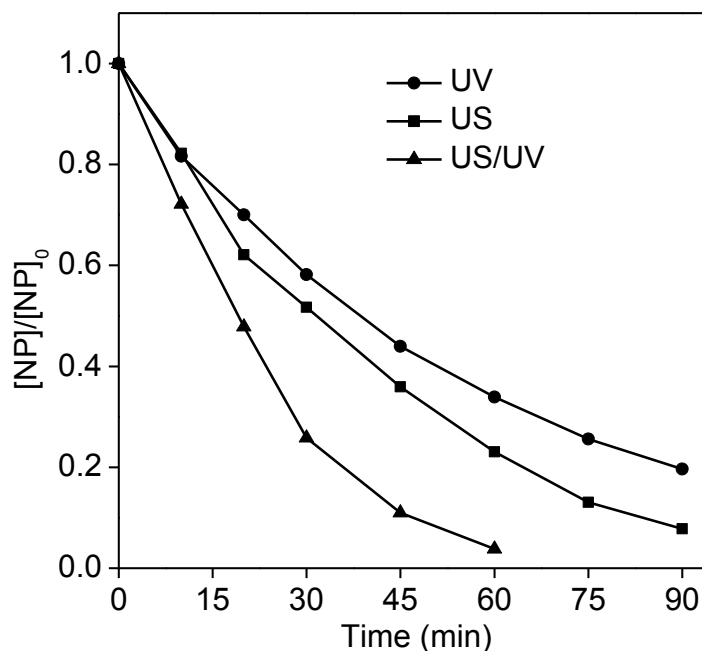


Figure 9-1: Temporal variation of NP concentrations in the sonolytic, photolytic and sonophotolytic degradation processes ($C_0 = 0.01 \text{ mM}$, UV: 2 lamps).

9.2.2. Effect of initial solution pH

The solution pH plays different roles in various AOT processes, and the influence of initial solution pH on the sonophotolysis of NP was evaluated in a wide range of 2.89 – 11.12. Results are shown in Figure 9-2, in which initial pH of 6.54 represents the control experiment without pH adjustment. It can be seen that NP degradation rate was affected substantially by solution pH, where in general the lower efficiency was obtained from near neutral to weakly acidic and basic conditions (6.5 – 8.7), and strongly acidic and basic conditions were found advantageous for NP degradation. It is known that NP is a dissociating compound with pKa value of 10.25 (USNLM), which implies that almost complete NP was protonated at pH 2.89 compared to ca. 3% dissociated at pH 8.70 (lowest efficiency). Since the anionic form of NP was more hydrophilic compared to NP molecules, acceleration by acidification could be partially resulting from the enhancement of hydrophobicity of NP by protonation of the phenolic moiety (Ince et al. 2009, Kidak and Ince 2006), leading to larger potentials of NP molecules migrating towards the bubble-liquid interfaces. Besides, the oxidation potential of hydroxyl radicals, which were verified to be responsible for NP sonolysis by using methanol as the radical scavenger, increased with decreasing pH (Xu et al. 2013b, Zhao et al. 2004). Furthermore, the scavenging of hydroxyl radicals by hydroxide ions (Eq. 9-2) also inhibited the sonolysis efficiency of NP at more basic conditions (Buxton et al. 1988). Moreover, the reaction between hydroxyl radicals and the conjugate base of H₂O₂ (pKa = 11.6), HO₂⁻ (Eq. 9-3), could accelerate the dissociation of H₂O₂ (Eq. 9-4), which was believed to decrease the synergistic effect of NP sonophotolysis.

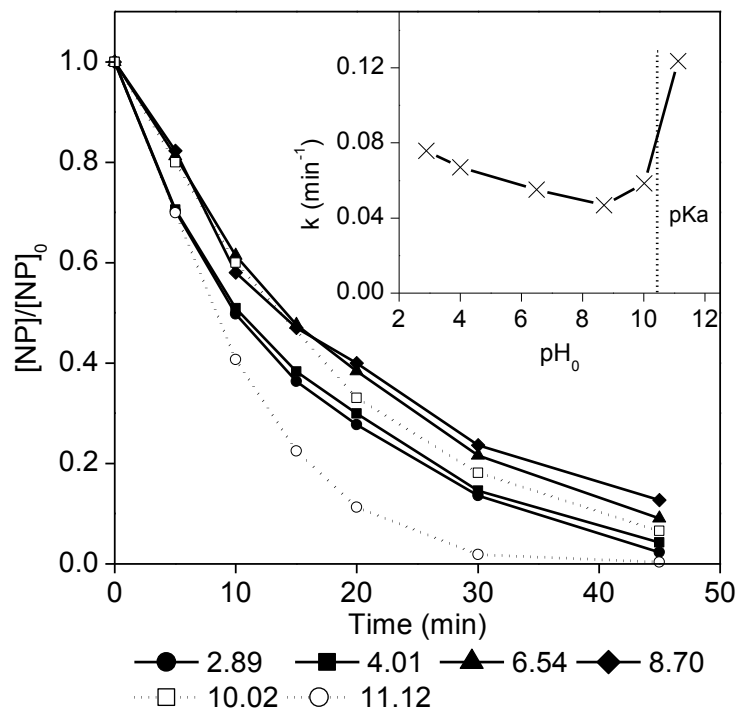
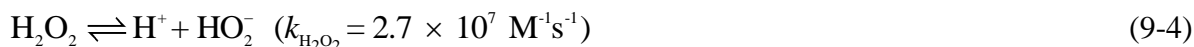
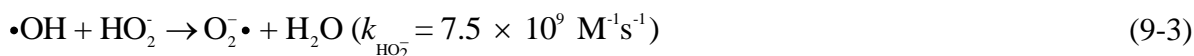


Figure 9-2: Effect of initial solution pH on the sonopholytic degradation of NP ($C_0 = 0.01$ mM; UV: 2 lamps).

The drastic acceleration of NP sonophotolysis at pH 11.12 could be explained by the substantial deprotonation (> 88%) of the phenolic moiety to produce phenolate. The negatively charged phenolate is more hydrophilic compared to the uncharged nonyl moiety and more preferable to remain in the bulk solution (Gultekin et al. 2009, Ince et al. 2009). Therefore, two moieties with significantly different K_{ow} simulate the surfactant properties and pull against each other at the bubble-liquid interfaces. It is possible that such opposite

forces of the two moieties of NP facilitated the cleavage of the covalent bond between them (Gultekin et al. 2009). This hypothesis was supported by the fact that nonanoic acid as an intermediate could only be detected at $\text{pH}_0 = 11.12$ condition but not at near neutral conditions (control experiment) (see Figure 9-3).

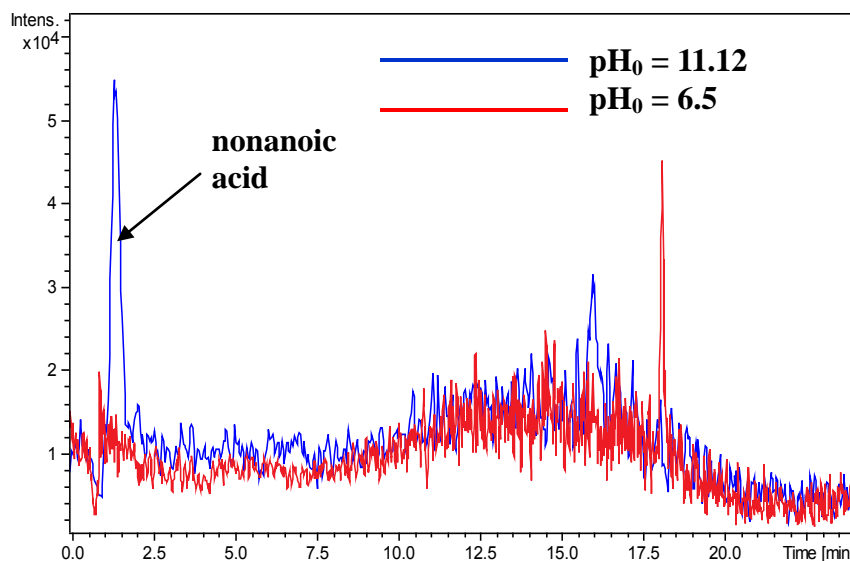


Figure 9-3: The extracted ion chromatogram of nonanoic acid ($[\text{M-H}]^- = 157.2$) of the 60 min reaction solution in the sonopholytic process at $\text{pH}_0 = 11.12$ and $\text{pH}_0 = 6.5$ (control experiment) conditions.

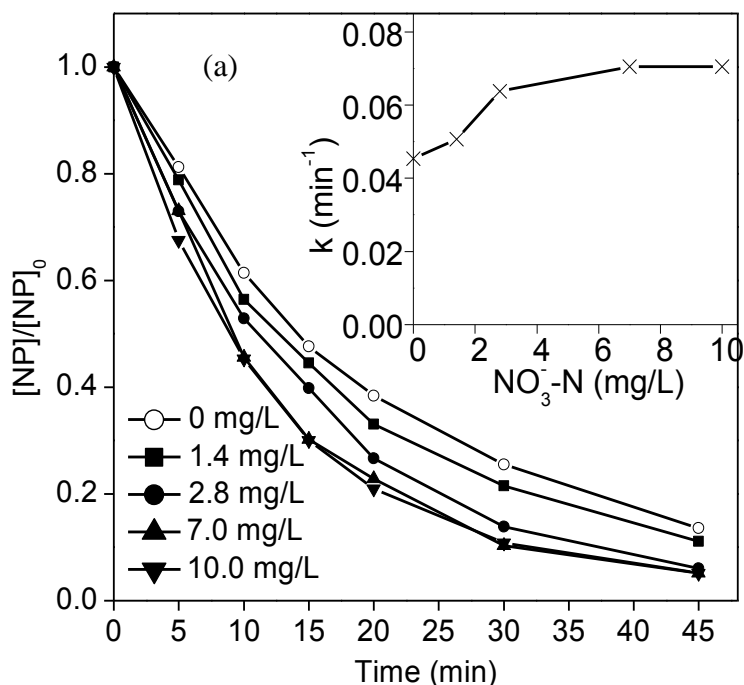
9.2.3. Effect of nitrate on sonophotolysis of NP

Since AOTs are potentially applied as post-tertiary wastewater treatment procedures (Agullo-Barcelo et al. 2013, Chong et al. 2012), the constituents in secondary wastewater effluent may influence the performance of subsequent AOTs. Apart from non-biodegradable COD, nitrate (NO_3^-), as a product of nitrification, is also a commonly seen species present in the secondary effluent because of nitrification, constituting the major part

of discharged TN. Hereby, the influence of nitrate (NO_3^-) on NP sonophotolysis was investigated in the range of $0 - 10 \text{ mg L}^{-1} \text{ NO}_3^- \text{-N}$, which was selected based on the discharged TN concentrations in secondary effluent of eight wastewater treatment plants in Hong Kong (DSD). Results are shown in Figure 9-4 (a), where nitrate had a positive effect on NP sonophotolysis within the investigated concentrations. Figure 9-4 (b) and (c) also respectively showed NP degradation in individual sonolytic and photolytic processes mediated by different nitrate concentrations. It was found that nitrate significantly improved NP photolysis, while affected little on the sonolytic degradation, implying that the positive role of nitrate in NP sonophotolysis was mainly by facilitating its photolytic degradation. This could also be supported by the equivalent increase of degradation rate constants of NP sonophotolysis ($\Delta k = 0.025 \text{ min}^{-1}$) and photolysis ($\Delta k = 0.025 \text{ min}^{-1}$) with $10 \text{ mg L}^{-1} \text{ NO}_3^- \text{-N}$ applied.

The UV absorption spectra of nitrate are given in Figure 9-5, which absorbs light in the UV range ($\lambda < 350 \text{ nm}$) with a strong band at 205 nm ($\pi \rightarrow \pi^*$) and a weak band at 302 nm ($n \rightarrow \pi^*$). Two primary photochemical processes of nitrate under UV irradiation have been reported (Wagner et al. 1980, Zaviska et al. 2014, Zepp et al. 1987) (Eq. 9-5, 9-6), and the $\text{O}^- \bullet$ is rapidly protonated to its conjugate acid, $\bullet\text{OH}$ (Eq. 9-7), which can react with organic compounds than does atomic oxygen (Zepp et al. 1987). In order to examine the role of nitrate in NP photolysis, methanol was used as a hydroxyl radical scavenger, and NP degradation by direct photolysis was used as the control test. It can be seen from Figure 9-6 that methanol had little effect on NP photolysis due to its transparency under 254 nm irradiation. However, it is clearly observed that acceleration of NP photolysis by the presence of $10 \text{ mg L}^{-1} \text{ NO}_3^- \text{-N}$ was mostly inhibited by applying 20 mM MeOH , indicating

that the acceleration was mainly due to the generation of additional hydroxyl radicals. In addition, the active species of NO_2^\bullet (Eq. 9-6) was also found involving in the reaction with NP since the minor intermediates with nitro group addition to the aromatic ring (Intermediate 5, 6, 7 in Table 9-2, see 9.2.4) were detected in the presence of nitrate, which was supposed to be another pathway for the acceleration of [NP] decrease and also explain the incomplete quenching by applying 20 mM methanol.



(c.o.)

(b.f.)

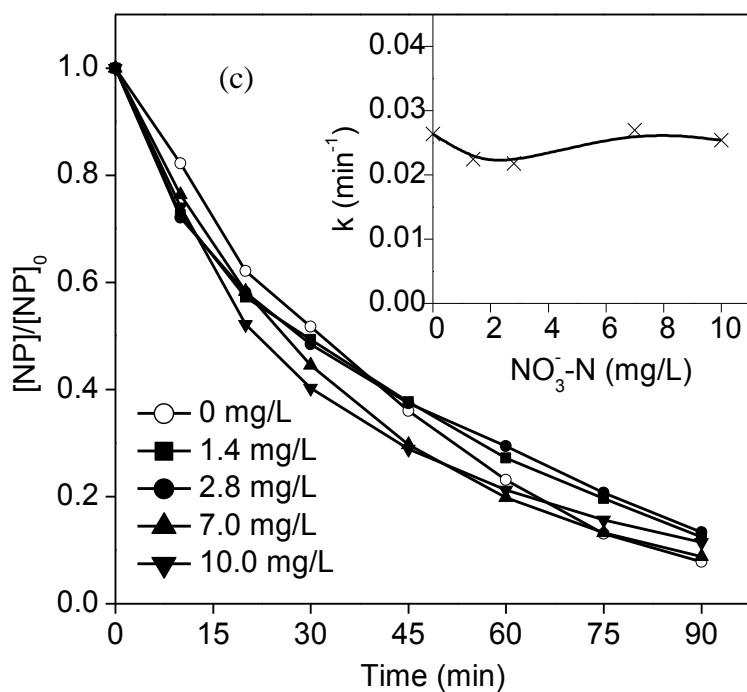
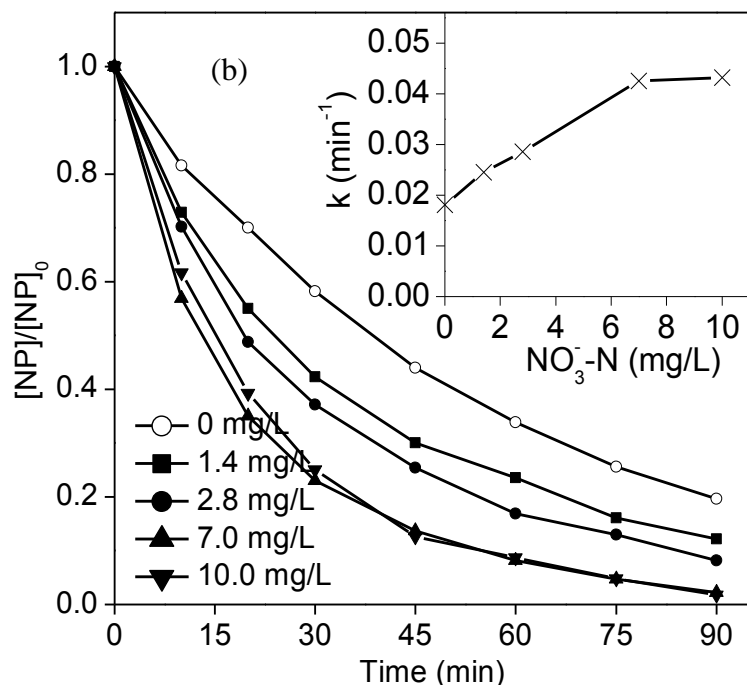


Figure 9-4: Effect of nitrate on NP degradation in sonophotolytic, sonolytic, and photolytic processes.

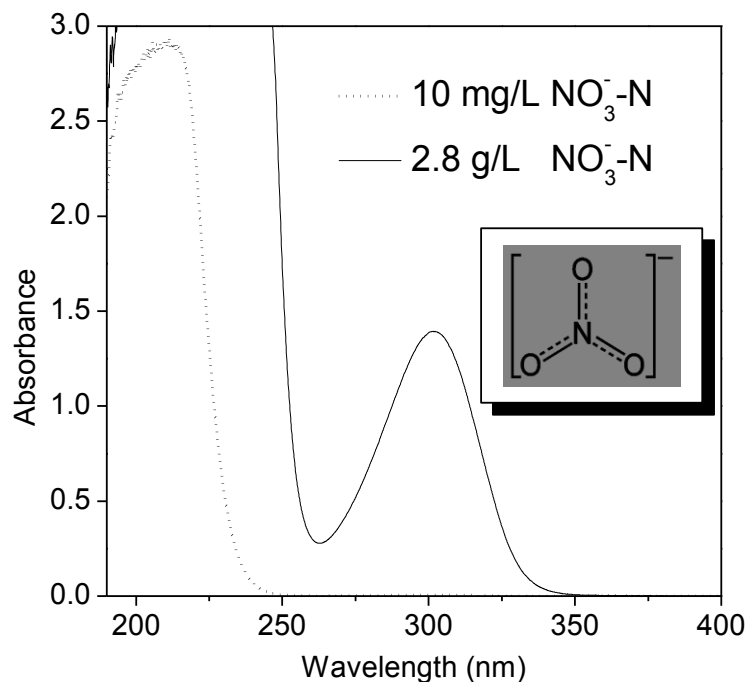


Figure 9-5: The UV absorption spectra of nitrate in different concentrations.

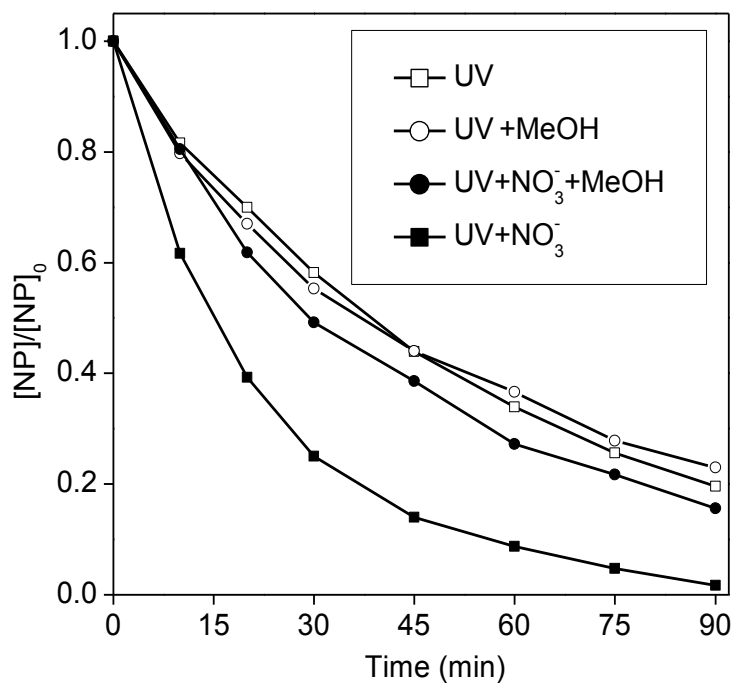
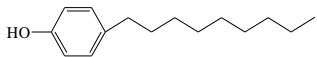
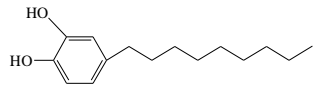
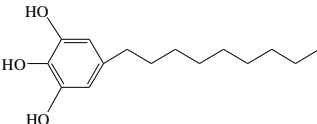


Figure 9-6: Effect of hydroxyl radical scavenger on NP photolytic degradation under different conditions ($C_0 = 0.01$ mM, $[\text{NO}_3^-$ -N] = 10 mg L^{-1} , $[\text{MeOH}] = 20$ mM).

9.2.4. Reaction mechanism and degradation product of NP sonophotolysis under different conditions

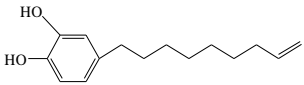
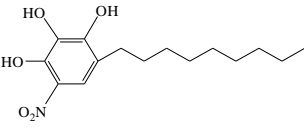
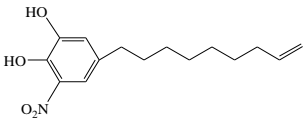
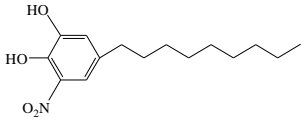
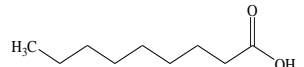
The products of NP degradation by AOTs have rarely been reported in previous studies. Neamtu et al. reported several intermediates (phenol, 1,4-dihydroxybenzene, and 1,4-benzoquinone) based on HPLC method (Neamtu and Frimmel 2006), and Li et al. (Li et al. 2013c) detected only one intermediate (4-nonylcatechol) by GC/MS analysis. In this study, determination and quantification of the primary degradation products were performed by UPLC/ESI-MS, which avoids solvent extraction and sample derivatization procedures frequently used in GC/MS pretreatment, and may have the chance to observe some new intermediates.

Table 9-2: Summarization of the identified intermediates of NP sonophotolysis determined by LC/ESI-MS.

Compound code	Structural formula	Formula	Retention time (min)	[M-H] ⁻	Conditions
1		C ₁₅ H ₂₄ O	23.4	219.23	–
2		C ₁₅ H ₂₄ O ₂	22.0	235.27	Normal NO ₃ ⁻ pH 11.15
3		C ₁₅ H ₂₄ O ₃	19.2	251.28	Normal

(c.o.)

(b.f.)

4		$C_{15}H_{22}O_2$	20.7	233.25	Normal NO_3^- pH 11.15
5		$C_{15}H_{23}NO_5$	20.4	296.28	NO_3^-
6		$C_{15}H_{21}NO_4$	20.2	278.28	NO_3^-
7		$C_{15}H_{23}NO_4$	21.5	280.29	NO_3^-
8		$C_9H_{18}O_2$	1.3	157.20	pH 11.15

The detected intermediates of NP sonophotolysis under different conditions (normal condition: neutral pH_0 without NO_3^- ; $pH_0 = 11.15$ without NO_3^- ; neutral pH_0 with 10 mg L^{-1} NO_3^-) are summarized in Table 9-2. It was found that three intermediates were identified in normal condition, five were detected in the presence of nitrate, and three were observed at strong basic condition. Besides, almost all the detected intermediates were observed with m/z ratio bigger than 219 (Intermediate 2 – 7), implying that those were the primary intermediates and mainly formed by the attack of $\bullet OH$ and $NO_2\bullet$ radicals on the aromatic ring. The temporal variation of NP and the identified intermediates under normal condition was provided in Figure 9-7. It was noted that, within the sampling period (90 min), TOC demonstrated no detectable decrease and the theoretical mass balance curve was given

based on the assumption that no mineralization occurred during the process. By comparing the theoretical mass balance curve with initial formation rate of hydroxy-NP (m/z 235), it was noticed that NP degradation was principally initiated by the formation of hydroxy-NP. The other two intermediates (3, 4) generated more slowly and demonstrated similar variation trends, which were considered to be the further derivatives of hydroxy-NP and their formation was limited by the concentration of hydroxy-NP. Although mineralization was not observed within 90 min, the detected intermediates all demonstrated further degradation, which indicated the formation of other organic products escaping from the detection method used in this study.

Based on the above analysis, the degradation pathways of NP sonophotolysis under different conditions were proposed in Scheme 9-1. It was observed that at strong basic condition, the oxidizing power in the process decreased as analyzed in 9.2.2, and therefore the minor product of di-hydroxy-NP was not detected at this condition while the scission product of nonanoic acid was observed in trace amount due to the deprotonation of NP. The dehydrogenation product of 4, 6 were detected in both normal and nitrate present conditions, which was also observed in the degradation of DBP (see Chapter Eight). At conditions with the formation of $\bullet\text{OH}$ radicals in the process, the NP degradation was all supposed to be initiated by the formation of hydroxy-NP. However, the small-molecule intermediates such as phenol mentioned by Neamtu et al. (Neamtu and Frimmel 2006) were not detected in this study.

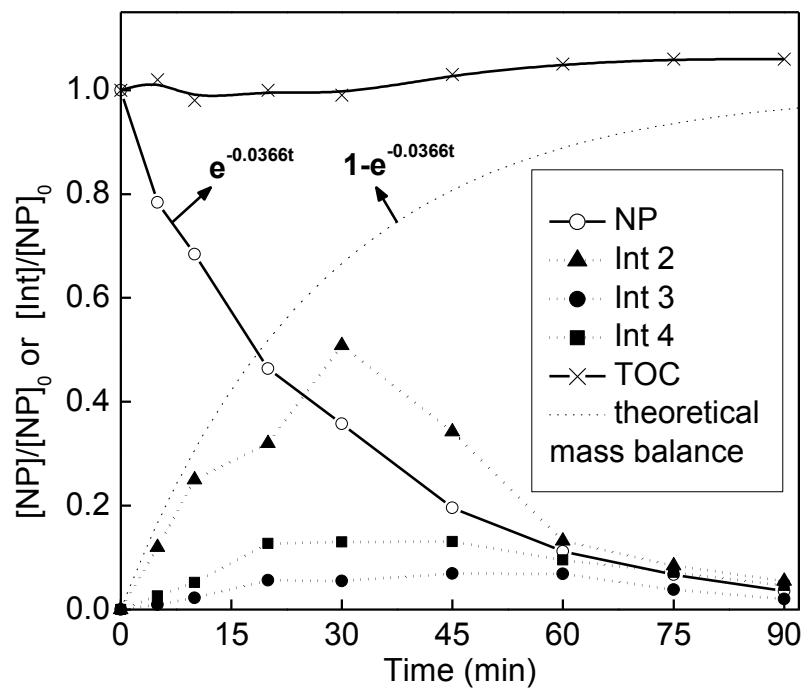
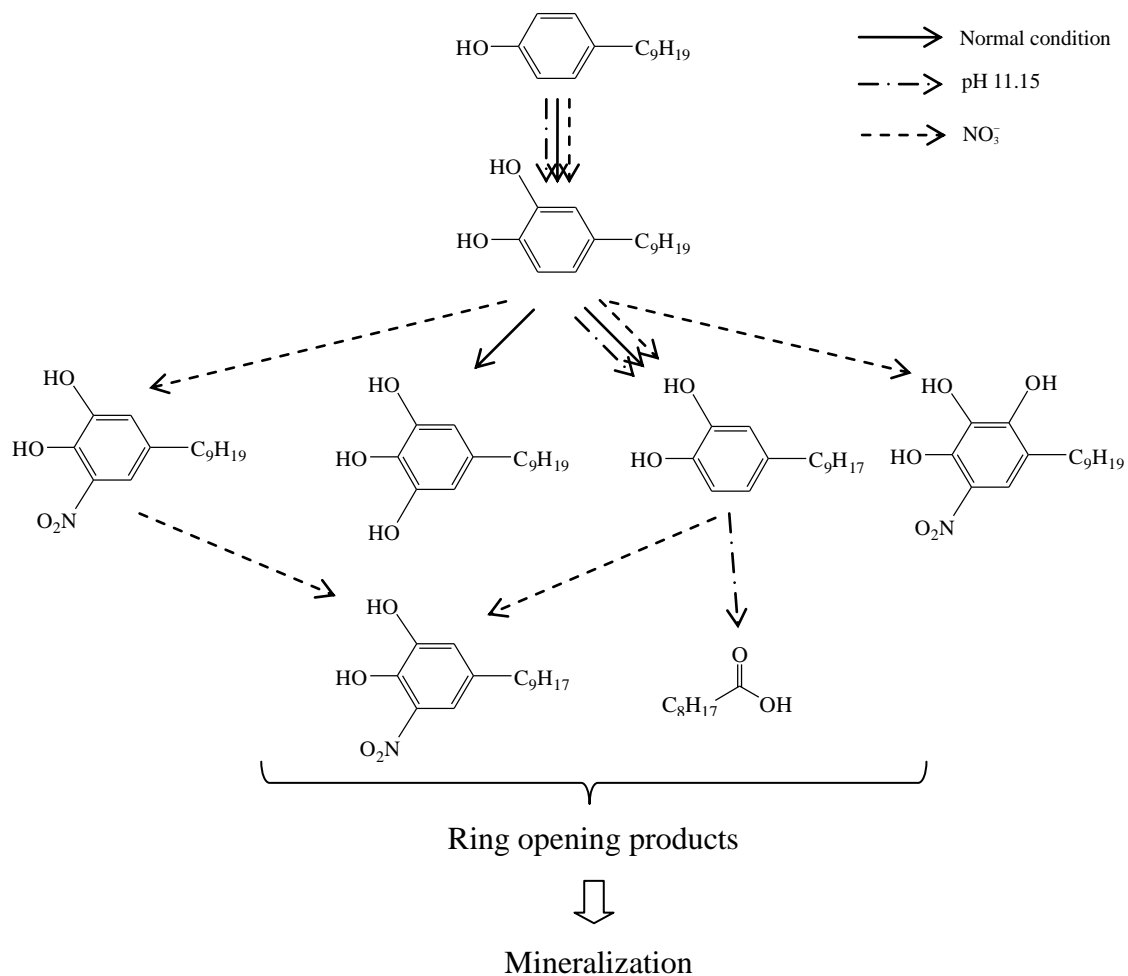


Figure 9-7: Temporal profiles of NP degradation and formation of primary intermediates in the sonophotolytic process ($[NP]_0 = 0.015$ mM, UV: 2 lamps, $pH_0 = 6.5$).

Scheme 9-1: Degradation pathways of NP sonophotolysis under different conditions (normal condition: neutral pH₀ without NO₃⁻; pH₀ = 11.15 without NO₃⁻; neutral pH₀ with 10 mg L⁻¹ NO₃⁻).



9.3. Chapter summary

In this chapter, the degradation of NP by sonophotolysis was investigated by evaluating several critical parameters and examining the degradation mechanisms under different conditions. Results showed that NP degraded faster compared to other investigated compounds in this thesis mainly due to its strong hydrophobicity. The best synergistic performance was obtained from applying two UV lamps, either higher or lower light intensity decreased the synergistic efficiency. Solution pH played important roles on the sonophotolysis of NP by influencing the existing form of NP in the solution. In addition, nitrate was found demonstrating positive effect on NP sonophotolysis at the range of 0 – 10 mg L⁻¹ NO₃⁻-N, and the acceleration mechanisms were found to be as a photosensitizer and also the reaction between NO₂⁻ • radicals and NP molecules. Finally, the degradation mechanism of NP sonophotolysis was observed to be the attack of •OH radicals mainly on the aromatic ring, and the reaction was supposed to be initiated by the formation of hydroxy-NP. Mineralization was not observed within the sampling period.

Chapter 10: Conclusions and Recommendations

The final chapter of a thesis summarizes the main findings of the research. It often also includes comments on limitations of the study, future work, how the findings will help both the academic field and the wider community.

This chapter is very effective partly because the writer includes the following:

Structure

(Introduction)		Not included
	↓	
Conclusions (and summary of main findings)		Section 10.1
	↓	
Limitations		Section 10.2
(Summary)		Not included

Content

- Introduces the chapter with a short summary paragraph that briefly outlines the thesis and states the contributions made in the final sentence (e.g. Section 10.1)
- Summarises each of the four research chapters with one paragraph for each chapter
- Develops paragraphs logically, e.g. Section 10.1 paragraph 4:
 - Sentence 1 Topic sentence
 - Sentence 2-4 Main findings
 - Sentence 4-5 Interpretation of findings
 - Sentence 5-8 Additional findings
- States limitations of the study (e.g. Section 10.2, sentence 1)

To Consider

This chapter of the thesis is effective. However, it could be further improved in the following aspects.

💡 Highlight the uniqueness of the research

💡 Avoid starting every paragraph with a linking word (e.g. Section 10.2 paragraph 2-

5).

💡 Use positive language to explain why the results are important.

💡 Compare results with other studies.

💡 Explain how the results fill a gap in knowledge.

💡 Explain how the result will contribute the academic field.

💡 End with a summary paragraph that includes a one sentence overall summary of the thesis followed by highlighting the importance of future studies in this field.

💡 Discuss what future work is needed.

💡 Use separate paragraphs to outline limitations and to suggest areas for further research. Discuss limitations in greater detail.

10. Chapter Ten Conclusions and Recommendations

10.1. Conclusions

In this thesis, an environmentally friendly AOT process of US/UV, which was effective without external additive, was set up and investigated in depth by examining the degradation performance of different EDCs, including DMP, DBP, ATZ, and NP. Results showed that the US/UV process could efficiently realize the degradation of different types of organic compounds. Although the results were based on lab-scale experiments, real wastewater was also involved as the water matrix to reveal the influence. It is believed that the results obtained in this study may help to predict and explain the practical issues under specific conditions, so as to assist the development and/or optimization of the pilot-scale and full-scale US/UV system.

Firstly, the prototype US/UV unit with its optimum situation was set up by evaluating the critical parameters. Generally, in the US process, the optimal performance was obtained from a frequency of 400 kHz, and the degradation rate increased directly with the ultrasonic power density. Higher initial concentration resulted in a lower degradation rate constant. In the UV-related process, higher UV light intensity was beneficial for both the photolytic and sonophotolytic degradation performance. Thus, a prototype US/UV unit consisting of a 400 kHz ultrasonic system with its maximum input power of 120 W and a photolytic system at 253.7 nm was set up accordingly.

Meanwhile, significant synergistic effect ($SI = 2.61$) was observed in the US/UV process

when investigating the sonophotolysis of DMP. The ultrasonically generated hydrogen peroxide was decomposed under UV₂₅₄ irradiation to reimburse hydroxyl radicals, which was verified to be the principal mechanism for the system synergy. The sonolytic and photolytic degradation of the investigated compounds all followed pseudo first-order kinetics, while their sonophotolysis exhibited variable kinetics. A novel inverted S-curve model clearly illustrating both the “individual effect” and the “synergistic effect” was developed and found to successfully describe the sonophotolytic process and the degradation of different probe compounds. Different relative weight of “individual effect” and “synergistic effect” for different compounds resulted in their characteristic performance in sonophotolytic degradation.

Furthermore, the heterogeneous feature of sonochemical process due to the presence of cavitation bubbles was investigated from different aspects. ATZ degradation by sonolytic processes depended on the heterogeneous environment, which was found very different in the 400 and 20 kHz ultrasound systems. The better heterogeneous distribution of solutes in the former allowed a faster decay of hydrophobic compounds than that in the latter. Similarly, the presence of NaCl had different effects on the two ultrasonic processes, mainly because of the competition between “salting out” effect and surface tension, and they were again influenced by the different heterogeneous environments in the solution. Due to the heterogeneous property of the sonochemical process, the physicochemical properties of PAEs, especially the hydrophobic/philic parameters ($\text{Log}K_{ow}$, S_w), played an important role on their sonolytic degradation. The more hydrophobic PAEs not only demonstrated faster sonolysis rate but also exhibited stronger competitiveness in sonochemical reactions with the presence of other competitors. However, stronger hydrophobicity was adverse for PAEs

to obtain remarkable synergistic effect in the sonopholytic process due to the less accumulation of hydrogen peroxide. Besides, the more hydrophobic PAEs also experienced less inhibition by dissolved TOC in real wastewater in the sonopholytic degradation.

Moreover, the presence of background species (e.g. radical scavengers, H_2O_2 , Fe^{2+} , NO_3^-) made significant influence on related processes. The application of methanol and *t*-butanol could completely inhibit the sonolytic degradation of the investigated compounds, implying that the mechanism of sonolysis of these compounds was mainly by radical oxidation rather than pyrolysis. The weak quenching ability of KBr in the sonolytic process indicated that the degradation region of relevant compounds was predominately surrounding the bubble-liquid interfaces and much less happening in the bulk solution. It was also noted that the more hydrophilic compound demonstrated more significant inhibition by KBr, suggesting the further location from the cavitation bubbles. The addition of hydrogen peroxide in the sonolytic process could increase the radical generation to some extent, but significantly promoted the degradation efficiency in UV process even with little amount. The presence of Fe^{2+} in solution gave rise to a homogeneous sono-photo-Fenton (US/UV/ Fe^{2+}) process, and the clear synergistic effects were found mainly due to the enhanced generation of $\bullet\text{OH}$ radicals via: (a) a Fenton reaction from ultrasonically generated H_2O_2 in the presence of Fe^{2+} ; (b) the photo-decomposition of H_2O_2 ; and (c) the photo-decomposition of $[\text{Fe}(\text{OH})]^{2+}$ resulting from the Fe^{2+} photo-oxidation and hydrolyzation process. In addition, the sono-Fenton process was found to be more efficient in utilizing Fe^{2+} compared to the conventional Fenton process and the DBP degradation was more complete. Nitrate demonstrated positive effect on NP sonophotolysis and the acceleration mechanisms were found to be as a photosensitizer and also the reaction between $\text{NO}_2^- \bullet$ radicals and NP

molecules.

Finally, by identifying the degradation intermediates using LC/ESI-MS, the degradation mechanisms of the investigated compounds were explored. It was found that both hydroxylation of the aromatic ring and oxidation of the aliphatic chain were verified to be the common mechanisms initiating the sonolytic degradation of the involved compounds. It was also noted that the ultrasonic process was effective and non-selective in degrading more hydrophobic target compounds, but less efficient in degrading their more hydrophilic intermediates. Individual UV process was more selective in degrading organic compounds. Whereas, the incorporation of UV into US process could promote the degradation of probe compounds and those hydrophilic intermediates by either direct photolysis or producing additional $\bullet\text{OH}$ radicals. The combined US/UV process was found to be most efficient in preventing the accumulation of degradation intermediates. The results of TOC variation demonstrated that the sonolytic process was disadvantageous for the mineralization of organic compounds because of its inefficiency in degrading hydrophilic intermediates. The best mineralization performance was obtained from the US/UV process.

10.2.Limitations of this study and recommendations for future work

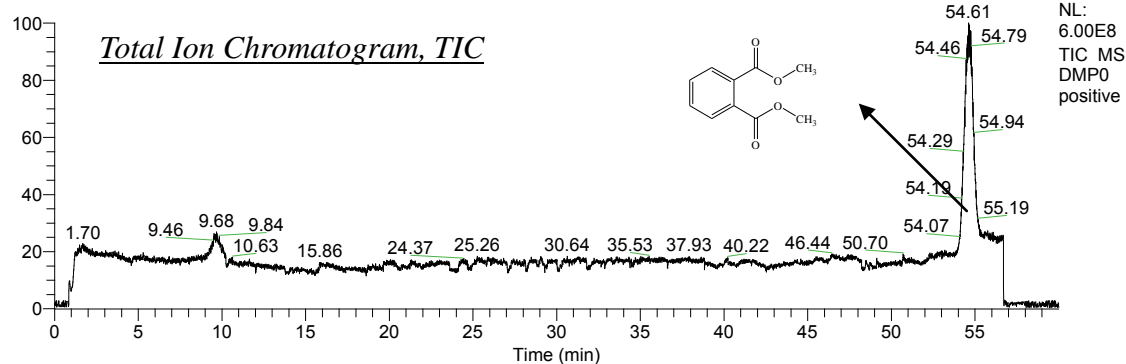
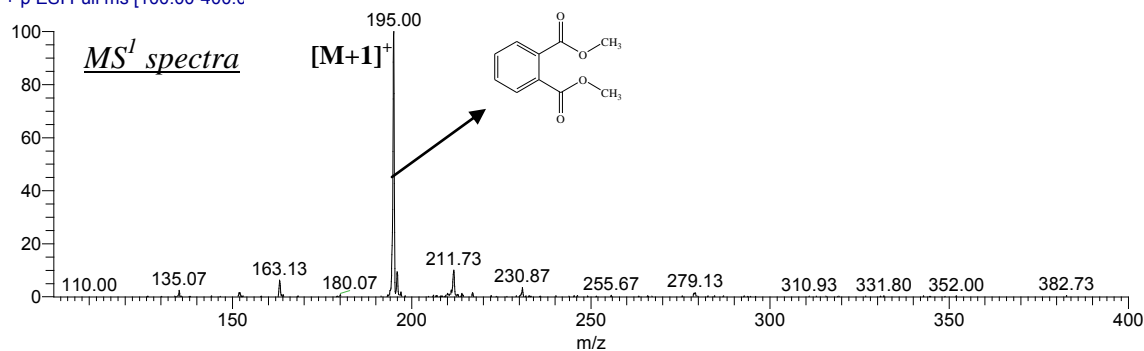
In this study, experiments were conducted in lab-scale batch reactors, which was impractical for real application. In future work, experiments in pilot-scale are needed to amend the results obtained under idealized conditions. In addition, from a practical point of view, the continuous flow reactors should be used in full-scale treatment, therefore reactor design including both the configuration of ultrasound and the layout of UV lamps will be a

critical factor determining the performance of the US/UV process. Furthermore, more experiments based on real wastewater are recommended for future work, which will facilitate the estimation of practical operation performance.

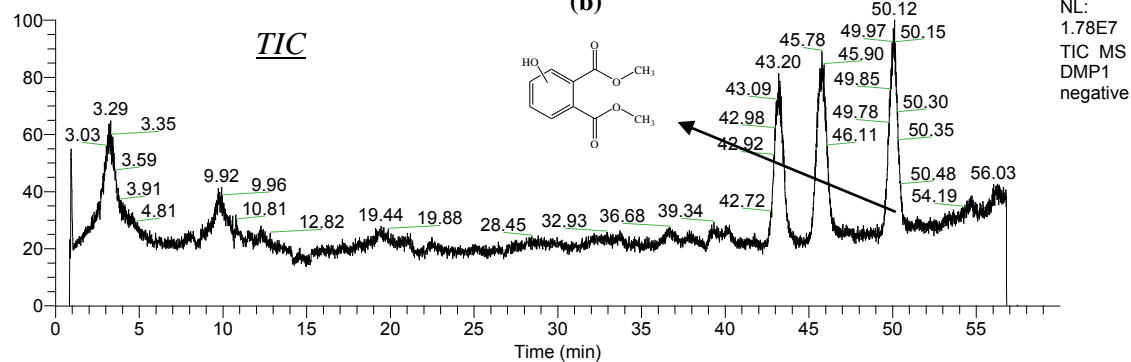
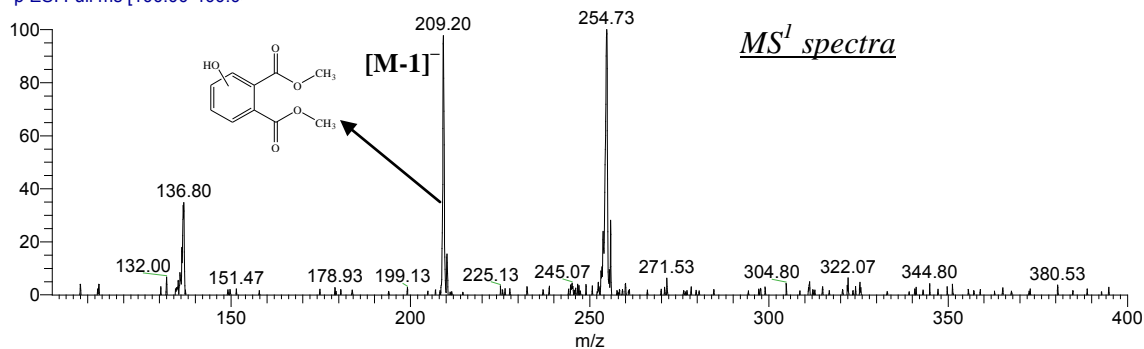
Appendix I: Mass spectra of DMP and its major intermediates

(a)

RT: 0.00 - 59.99

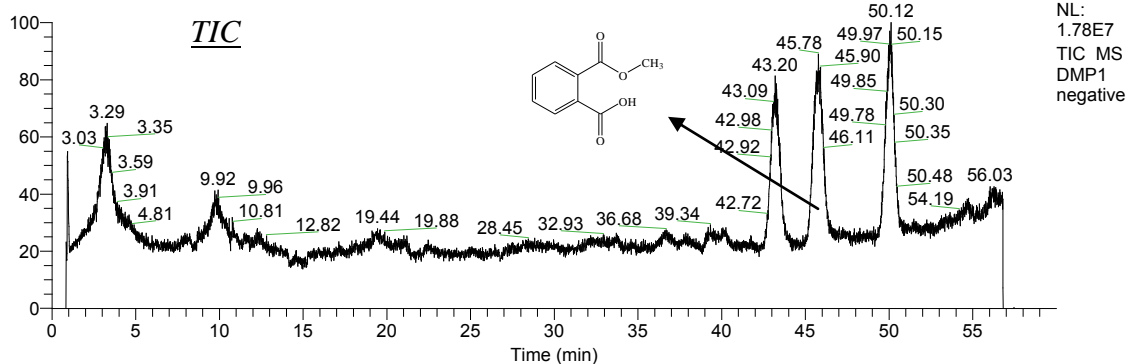
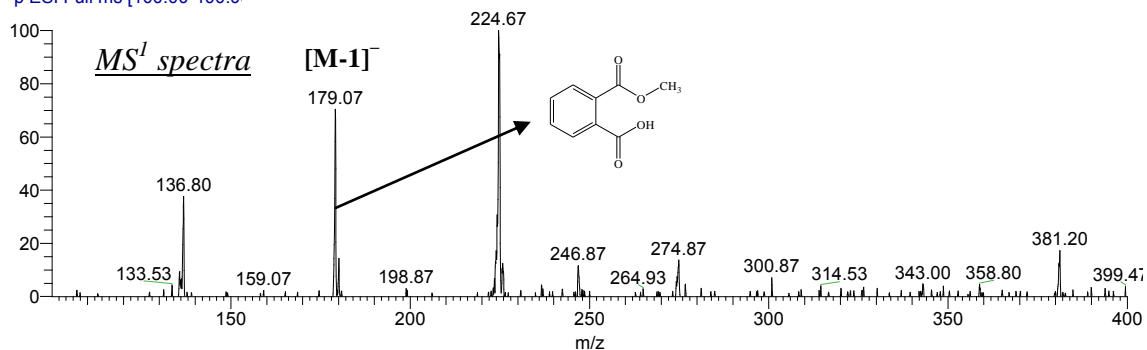
DMP0 positive #6296 RT: 54.64 AV: 1 NL: 5.17E7
T: + p ESI Full ms [100.00-400.0]

RT: 0.00 - 60.00

DMP1 negative #4953 RT: 50.02 AV: 1 NL: 5.04E5
T: - p ESI Full ms [100.00-400.0]

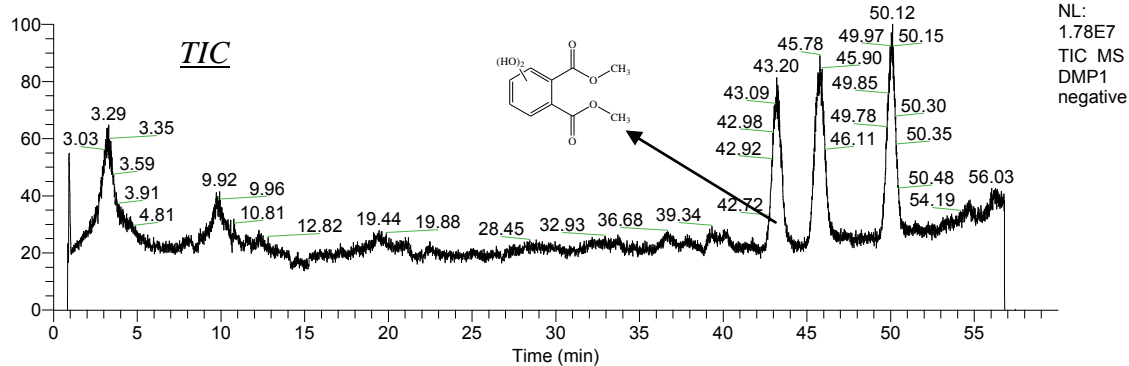
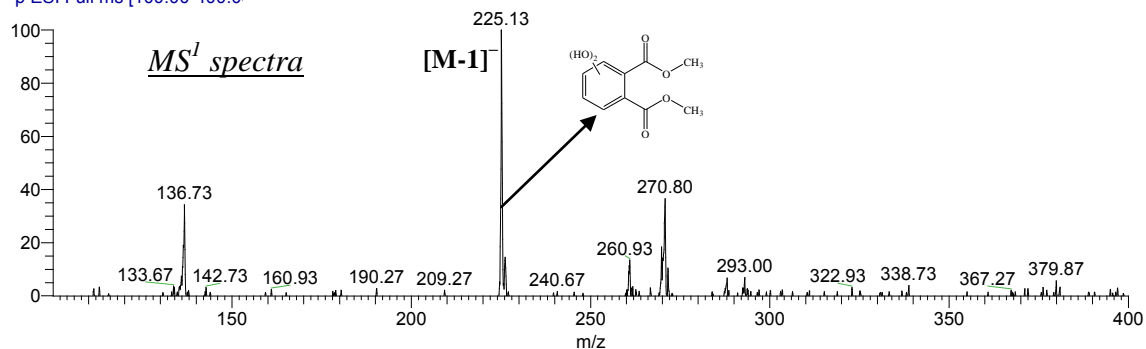
(c)

RT: 0.00 - 60.00

DMP1 negative #4507 RT: 45.70 AV: 1 NL: 5.45E5
T: - p ESI Full ms [100.00-400.0]

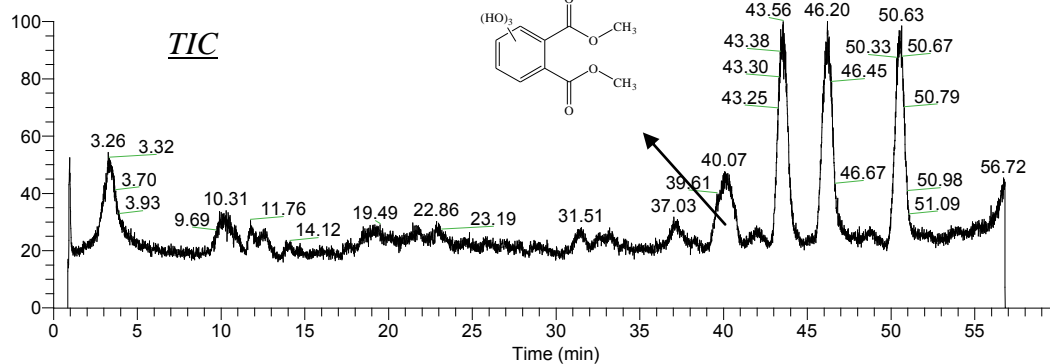
(d)

RT: 0.00 - 60.00

DMP1 negative #4256 RT: 43.27 AV: 1 NL: 6.46E5
T: - p ESI Full ms [100.00-400.0]

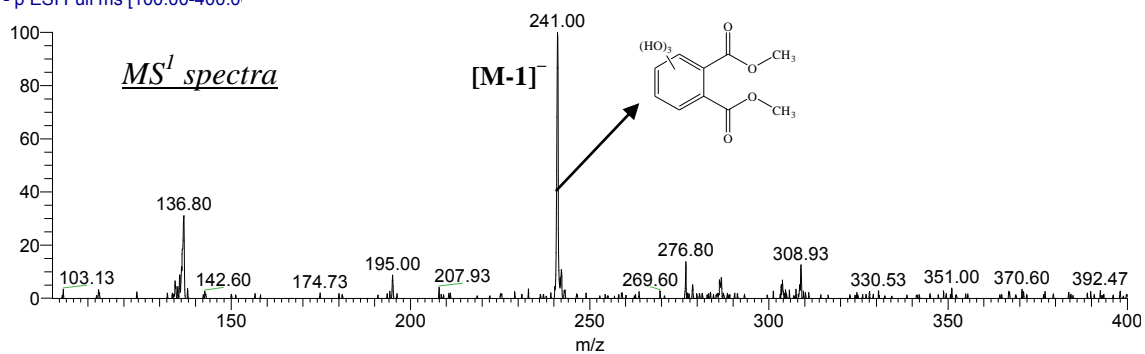
(e)

RT: 0.00 - 60.00

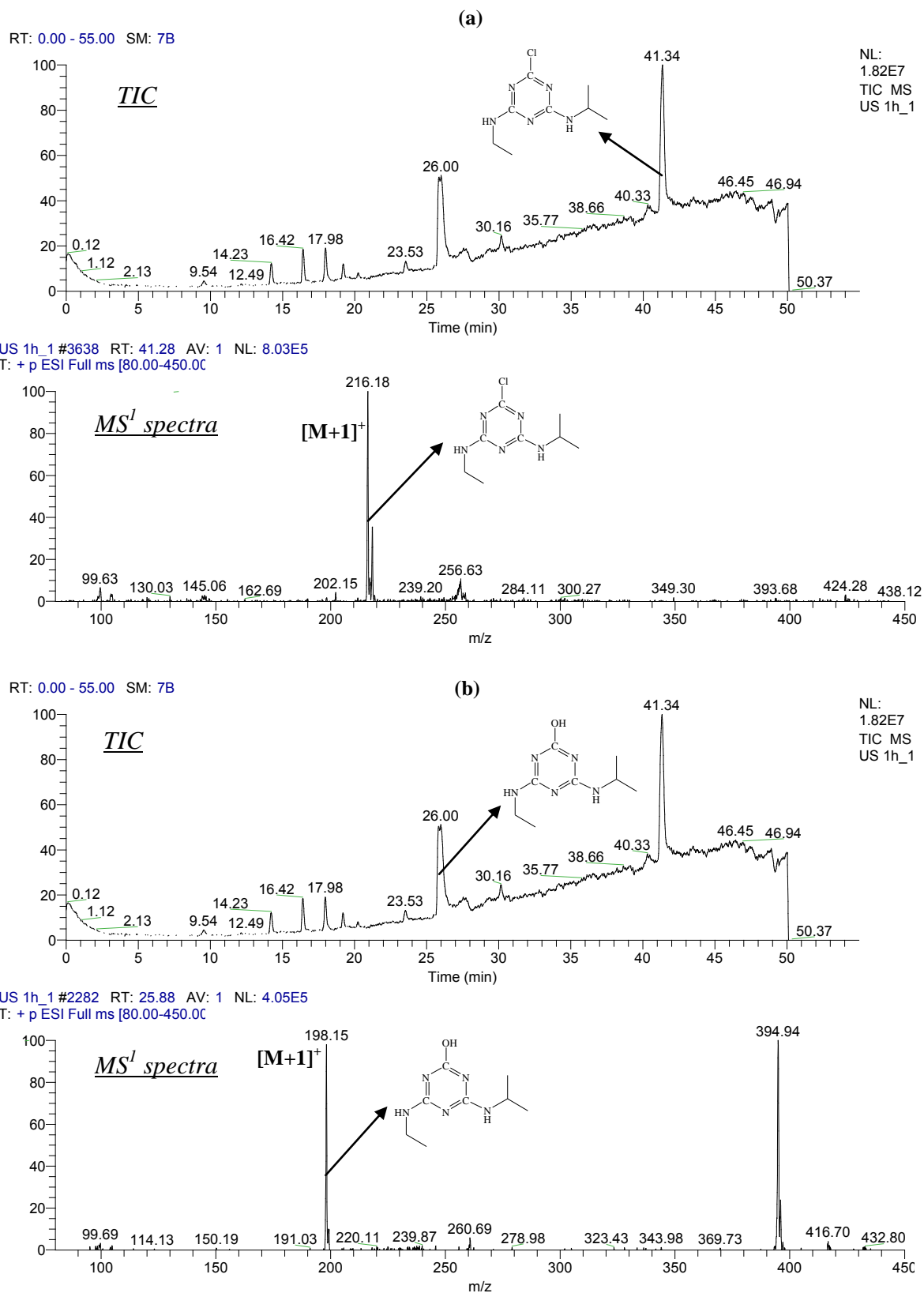


DMP2 negative #4096 RT: 40.12 AV: 1 NL: 4.65E5

T: -p ESI Full ms [100.00-400.0]

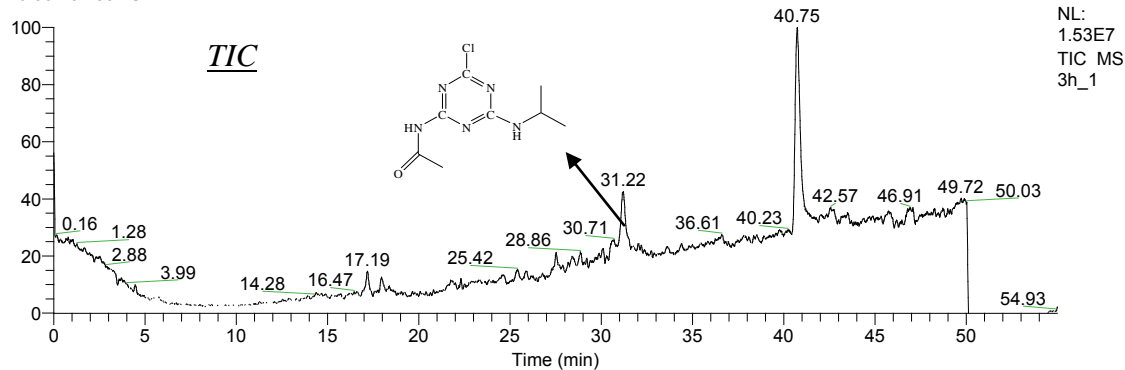
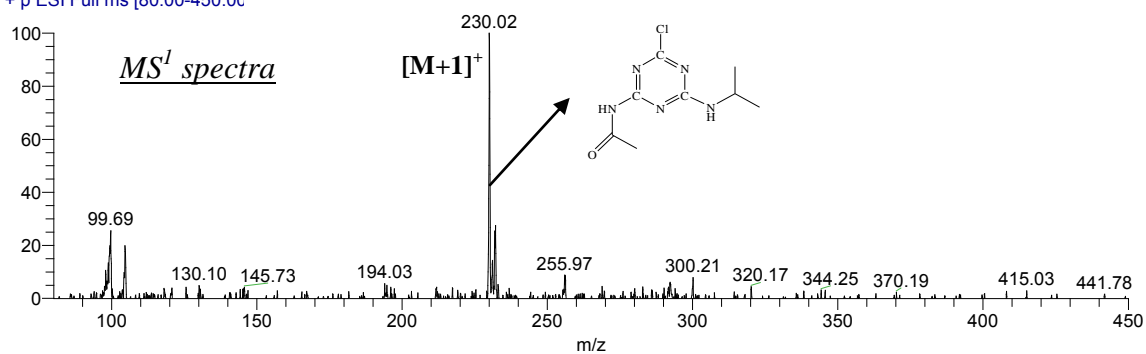


Appendix II: Mass spectra of ATZ and its major intermediates



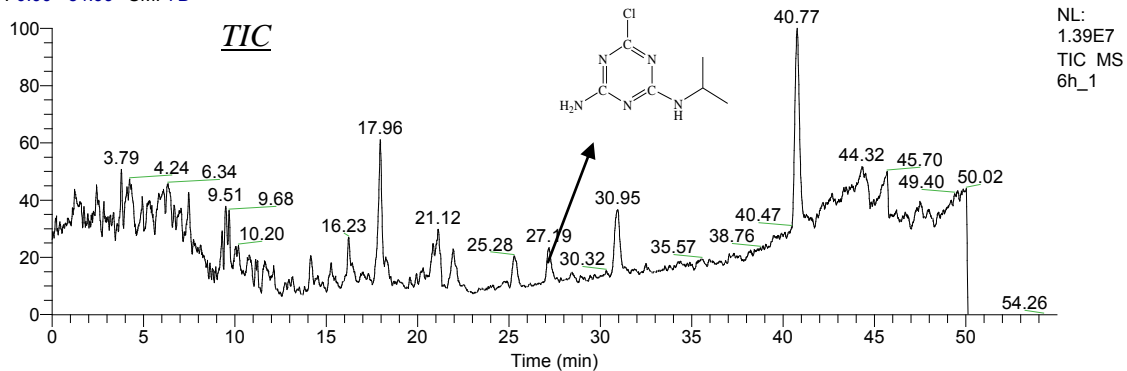
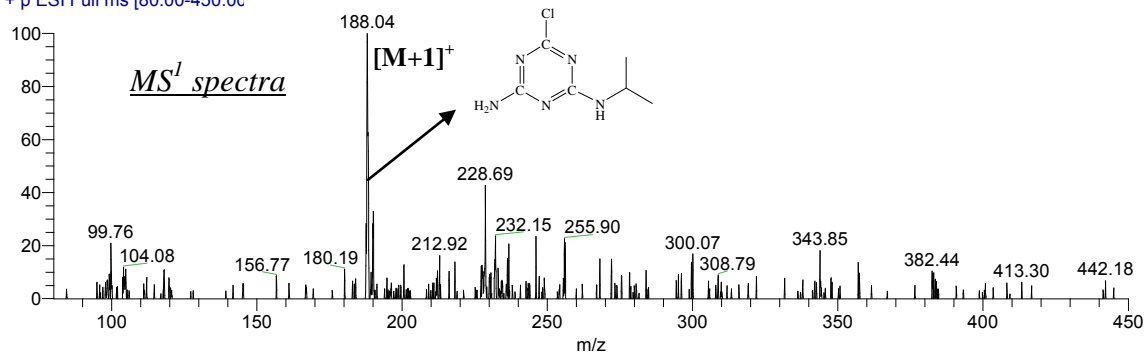
(c)

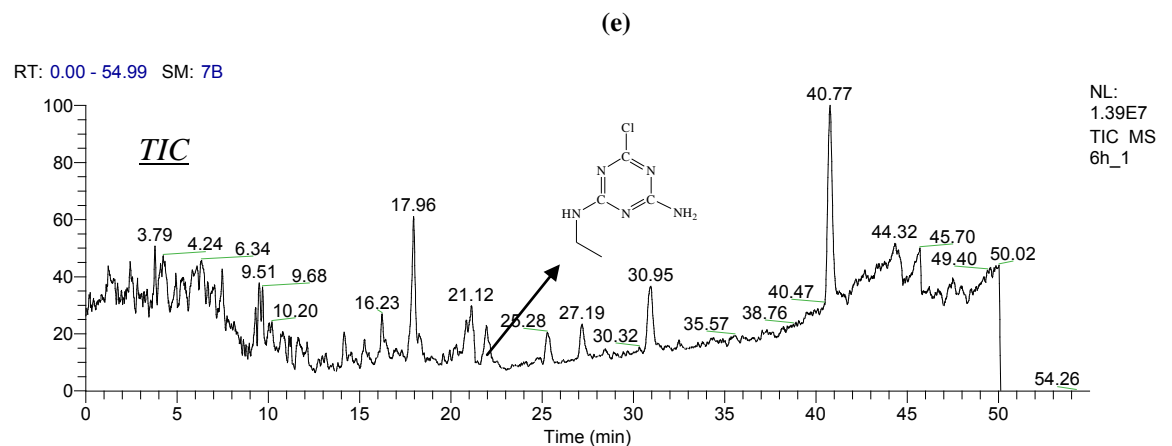
RT: 0.00 - 54.99 SM: 7B

3h_1 #2744 RT: 31.13 AV: 1 NL: 2.31E5
T: + p ESI Full ms [80.00-450.00]

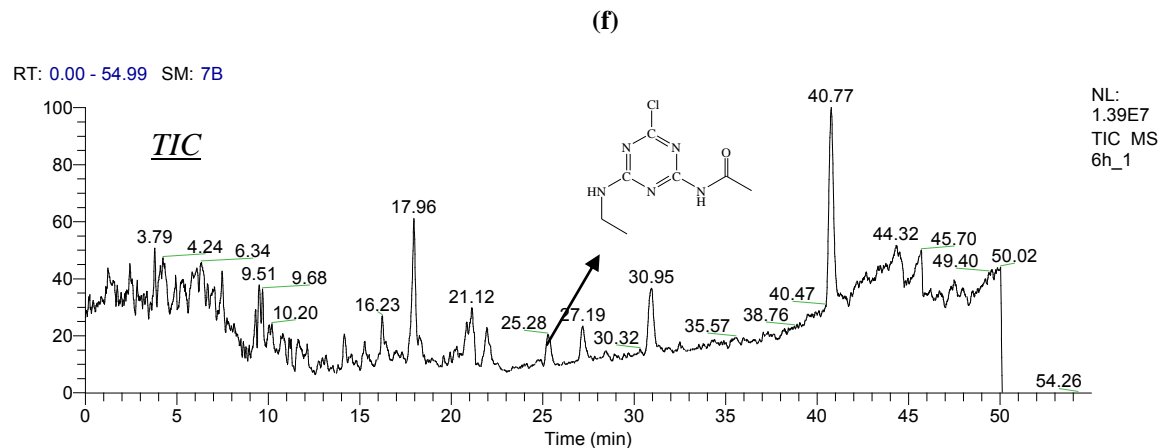
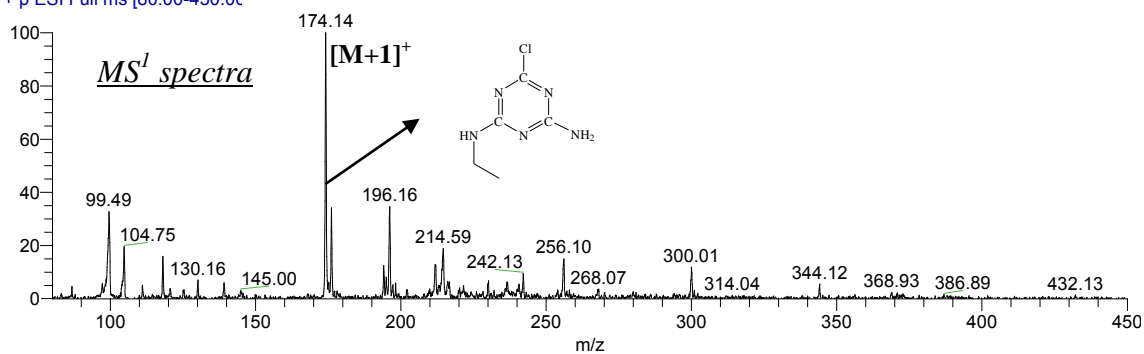
(d)

RT: 0.00 - 54.99 SM: 7B

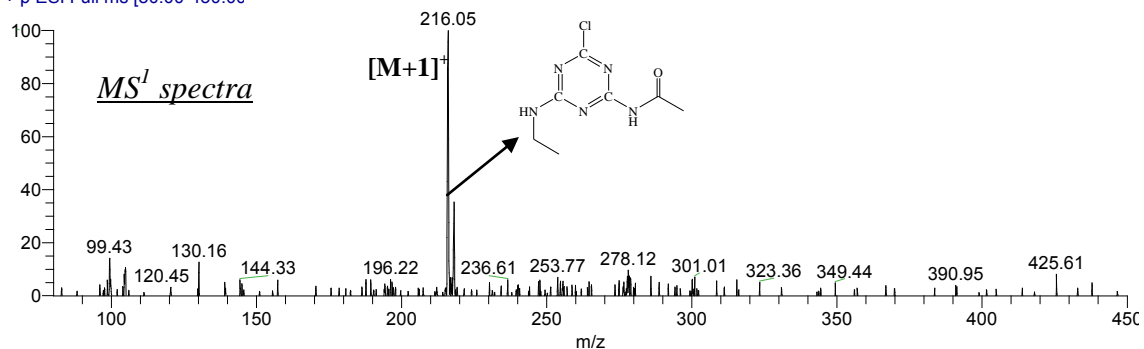
6h_1 #2405 RT: 27.30 AV: 1 NL: 6.05E4
T: + p ESI Full ms [80.00-450.00]



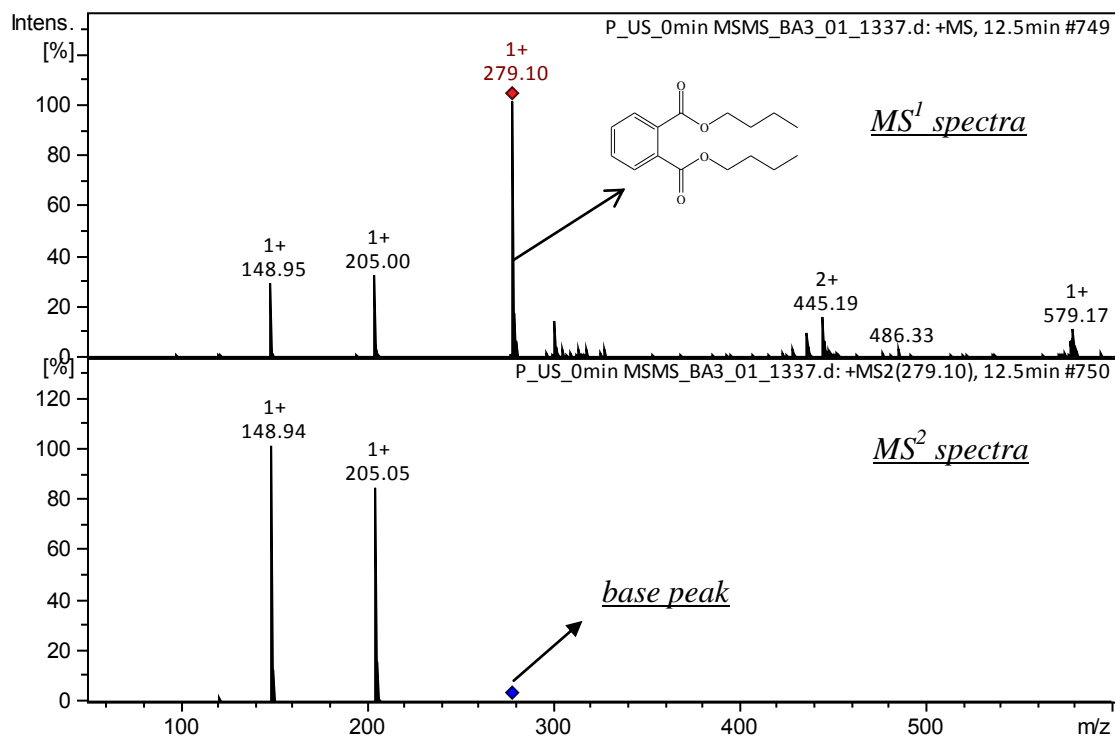
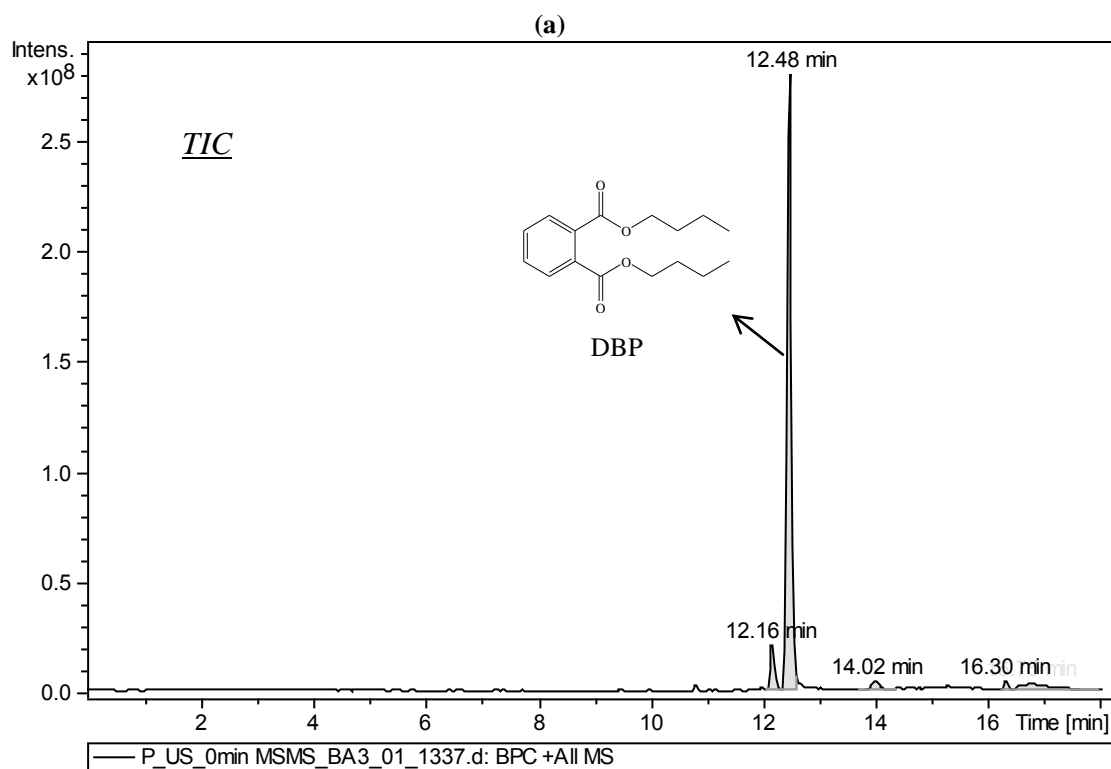
6h_1 #1925-1961 RT: 21.85-22.26 AV: 37 NL: 4.14E4
T: + p ESI Full ms [80.00-450.00]



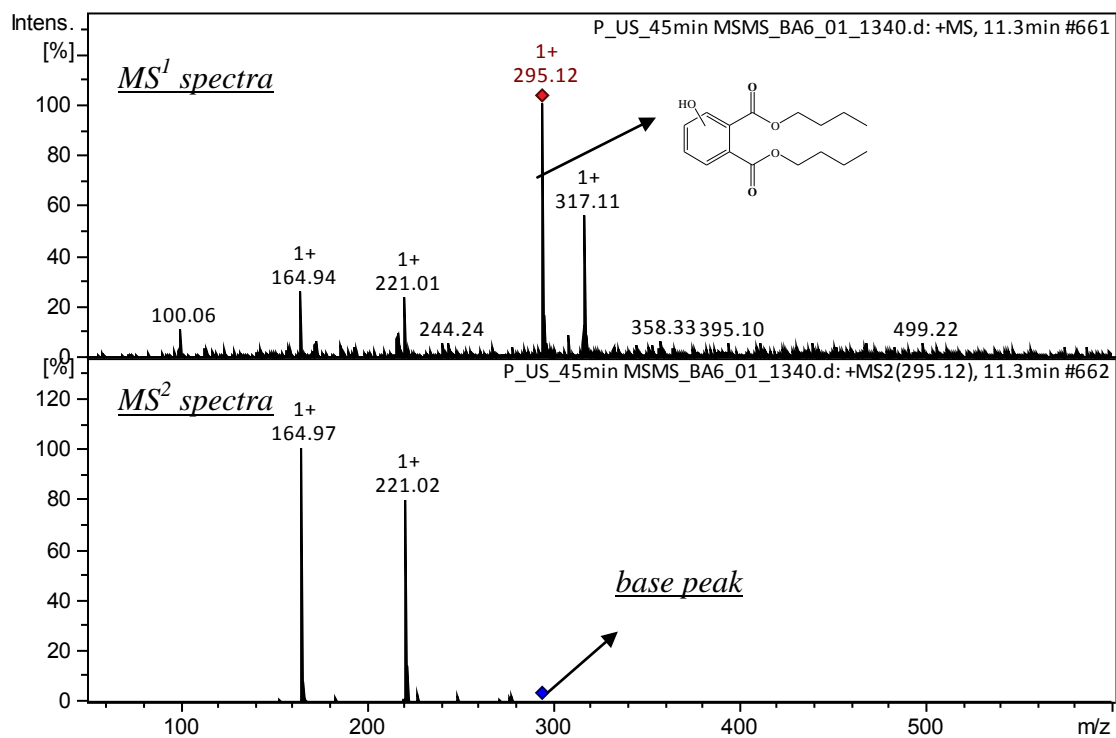
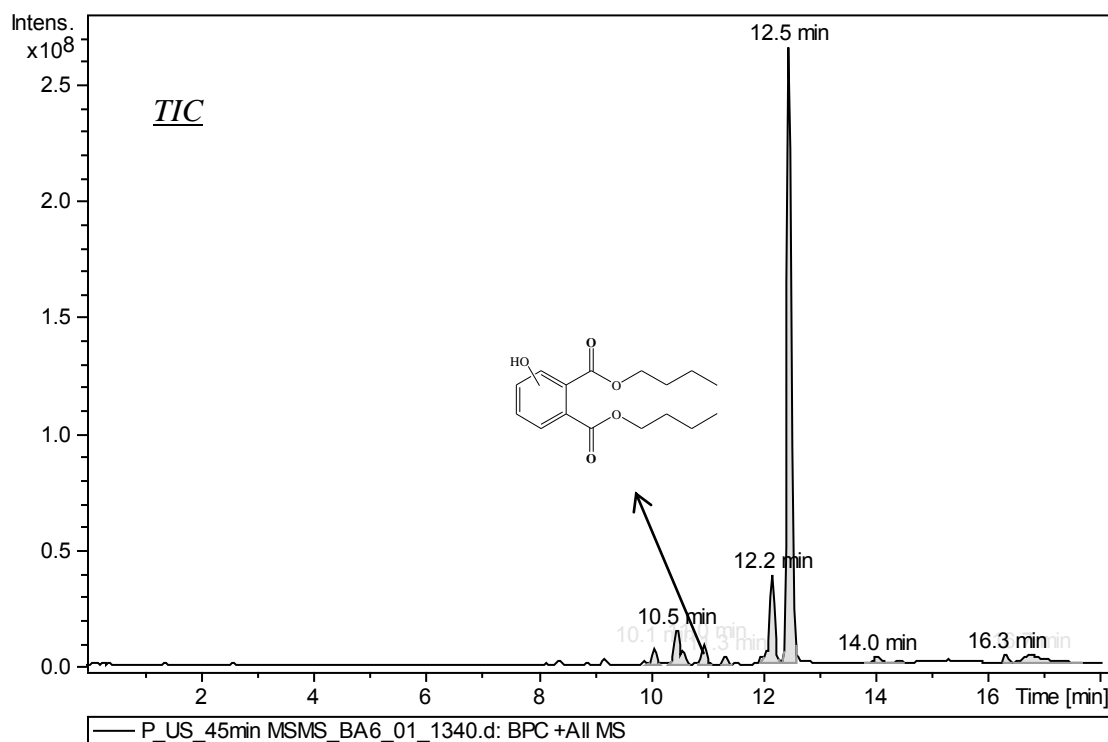
6h_1 #2221 RT: 25.21 AV: 1 NL: 1.05E5
T: + p ESI Full ms [80.00-450.00]



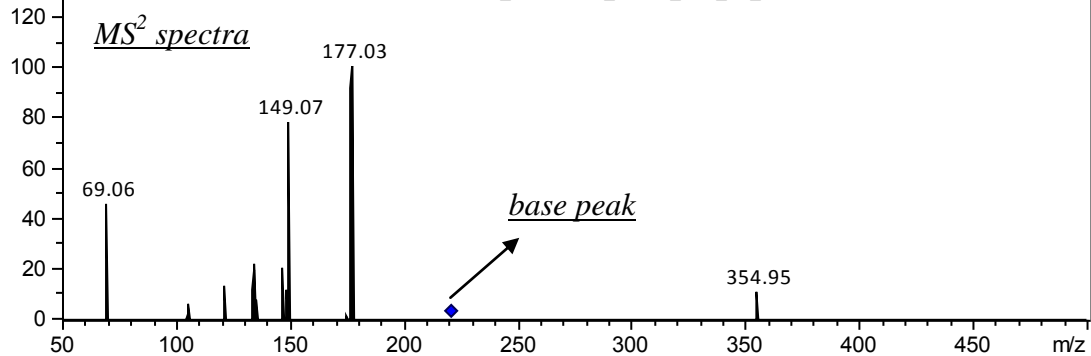
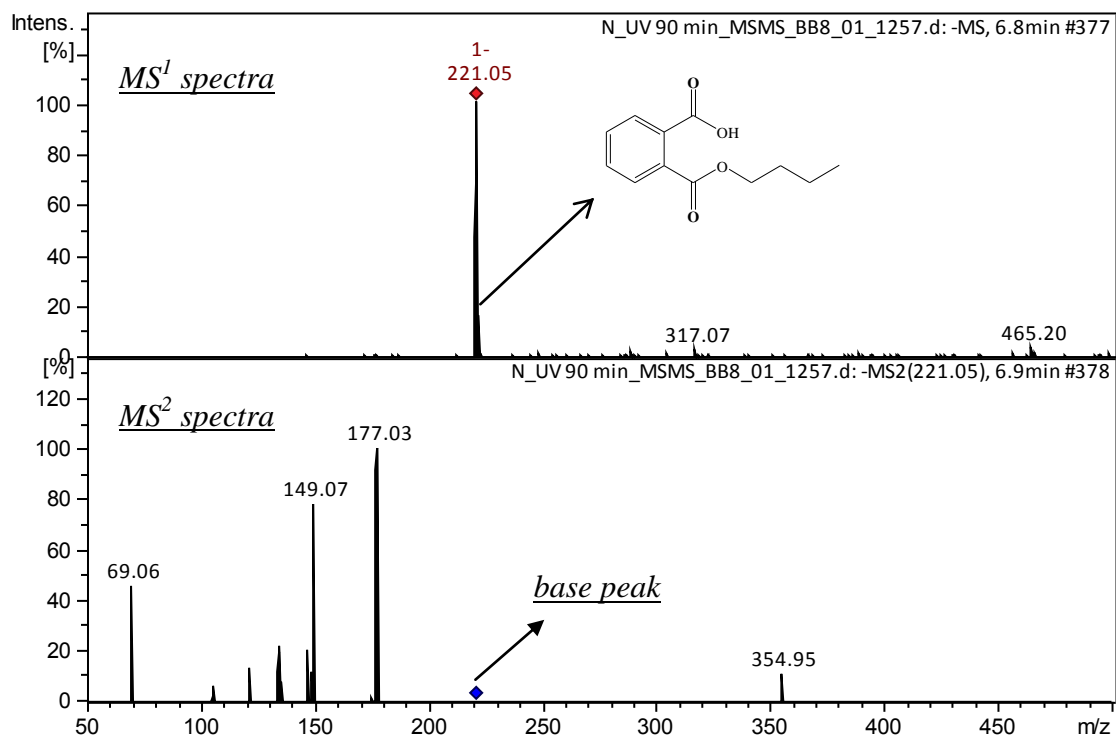
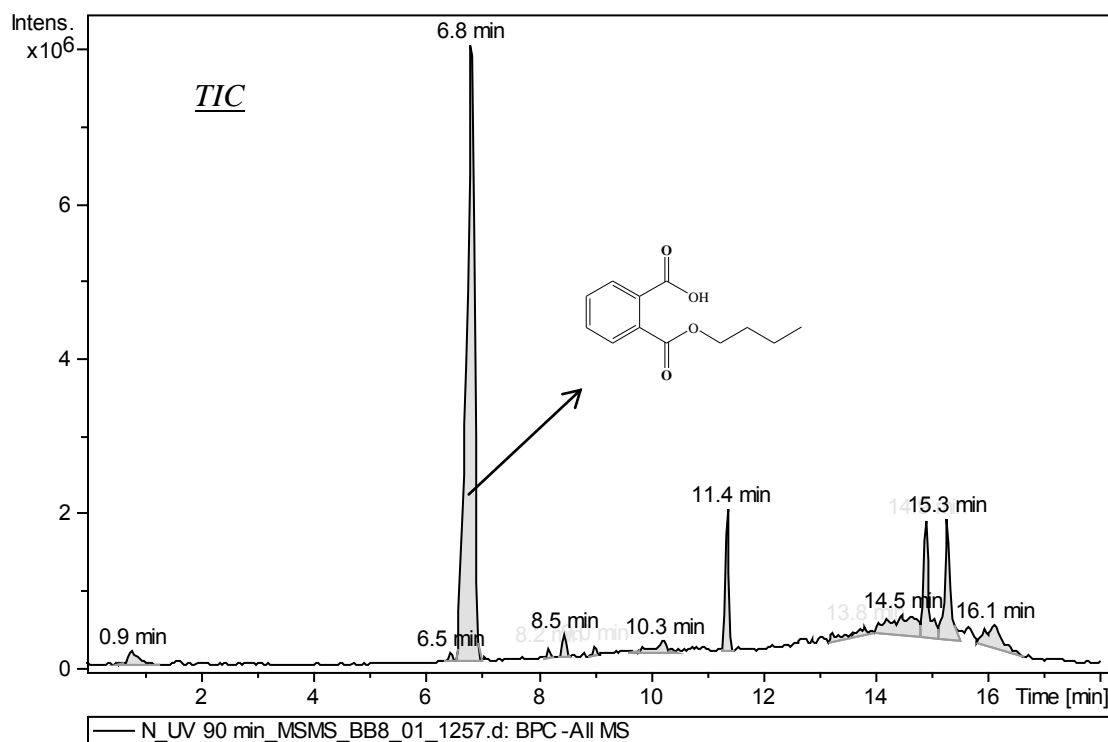
Appendix III: Mass spectra of DBP and its major intermediates



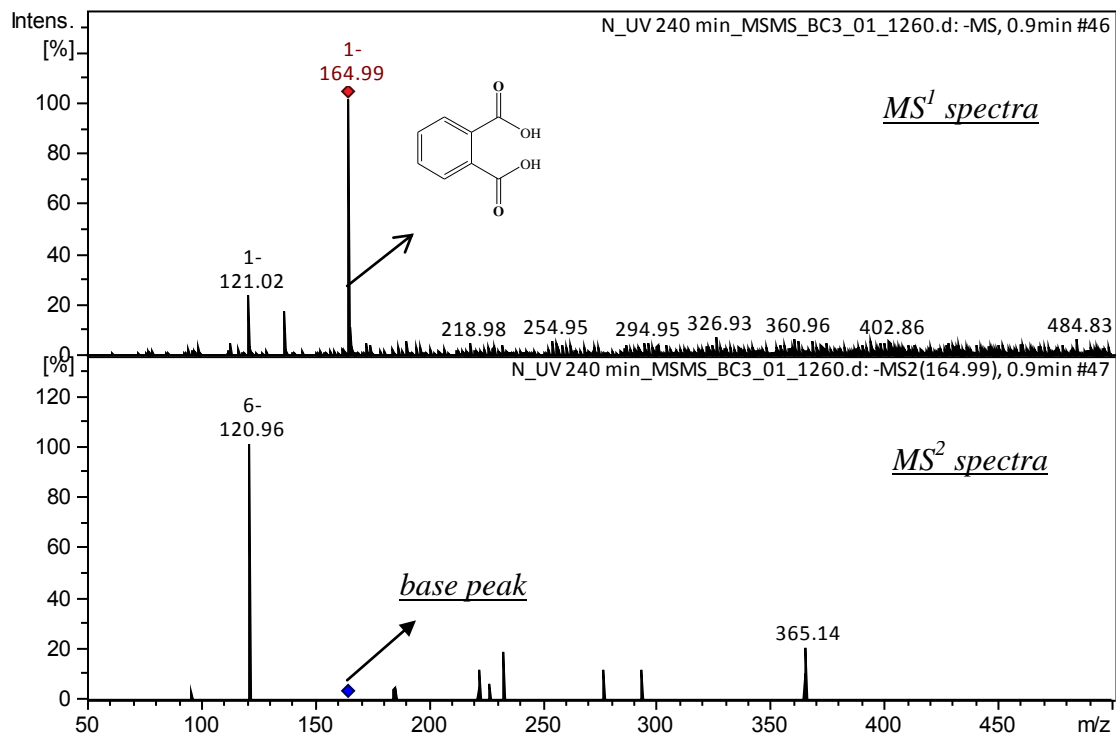
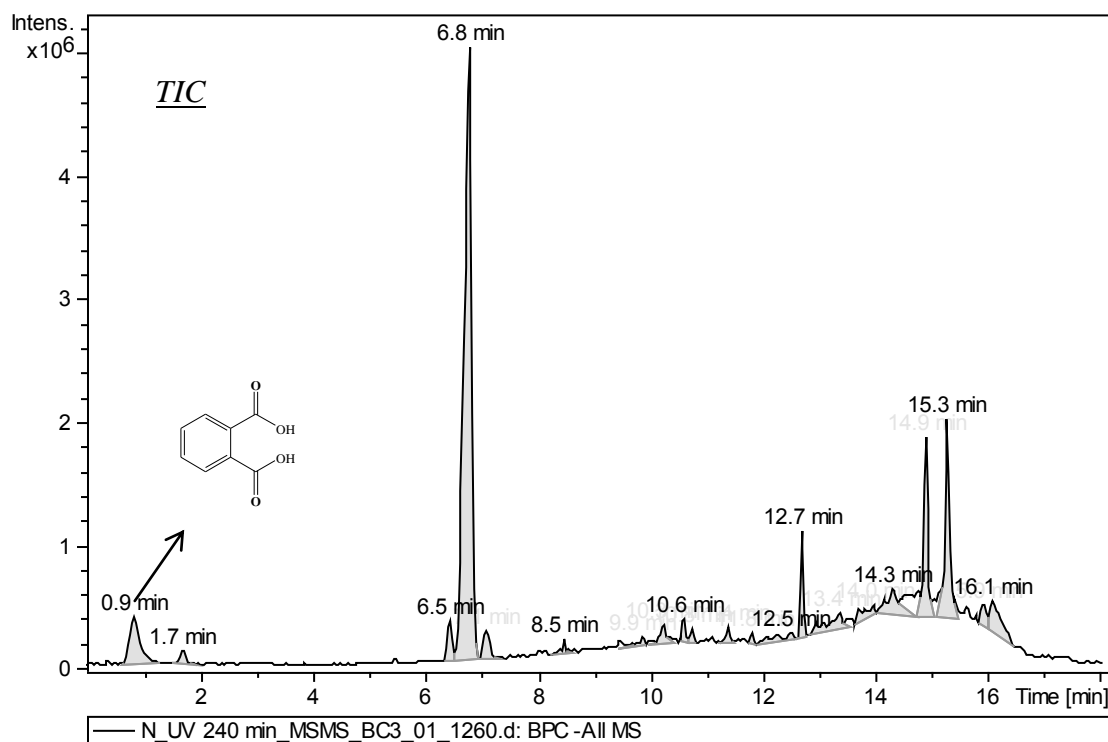
(b)



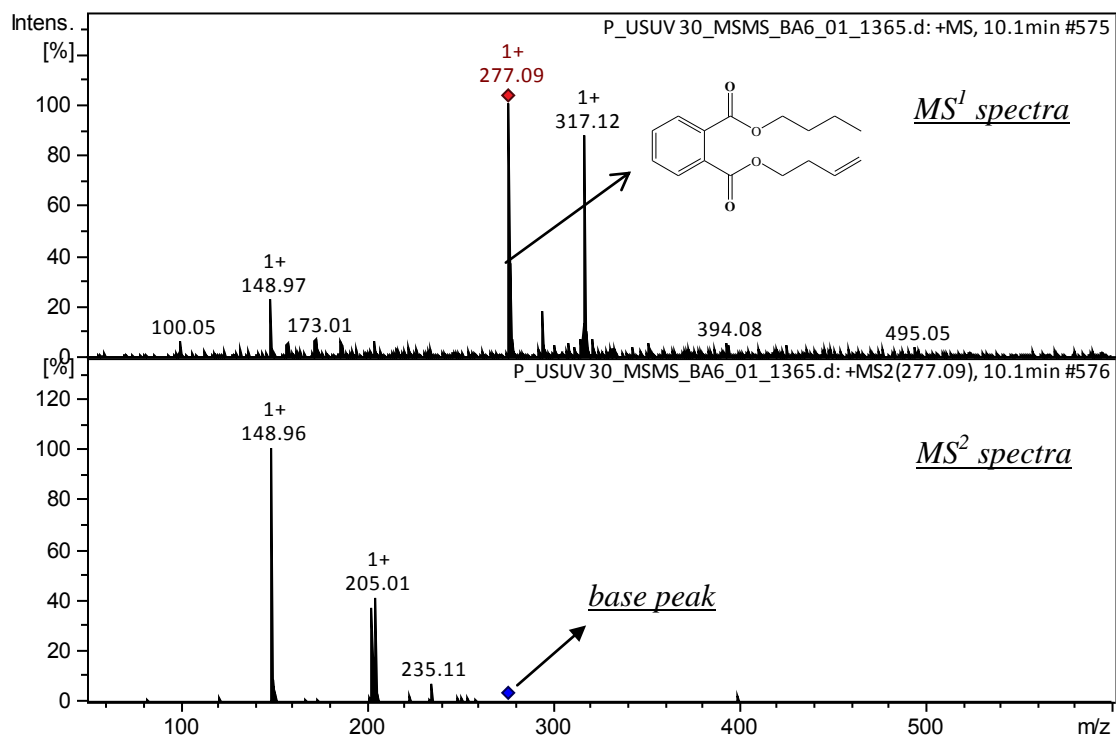
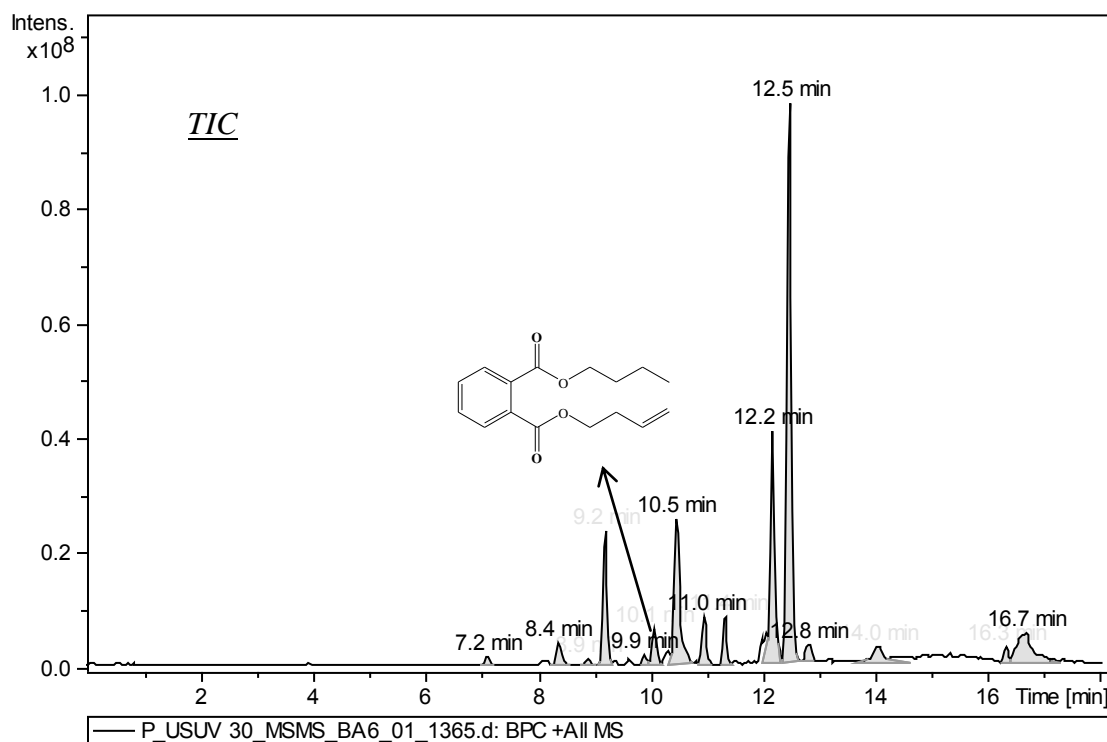
(c)

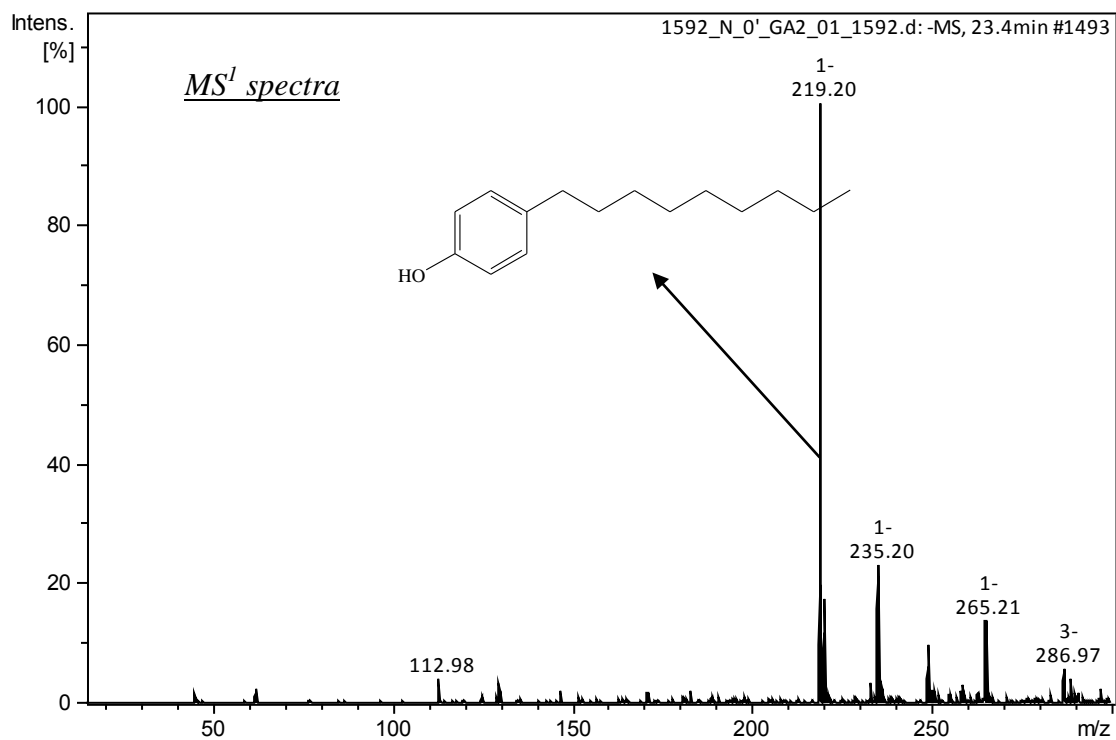
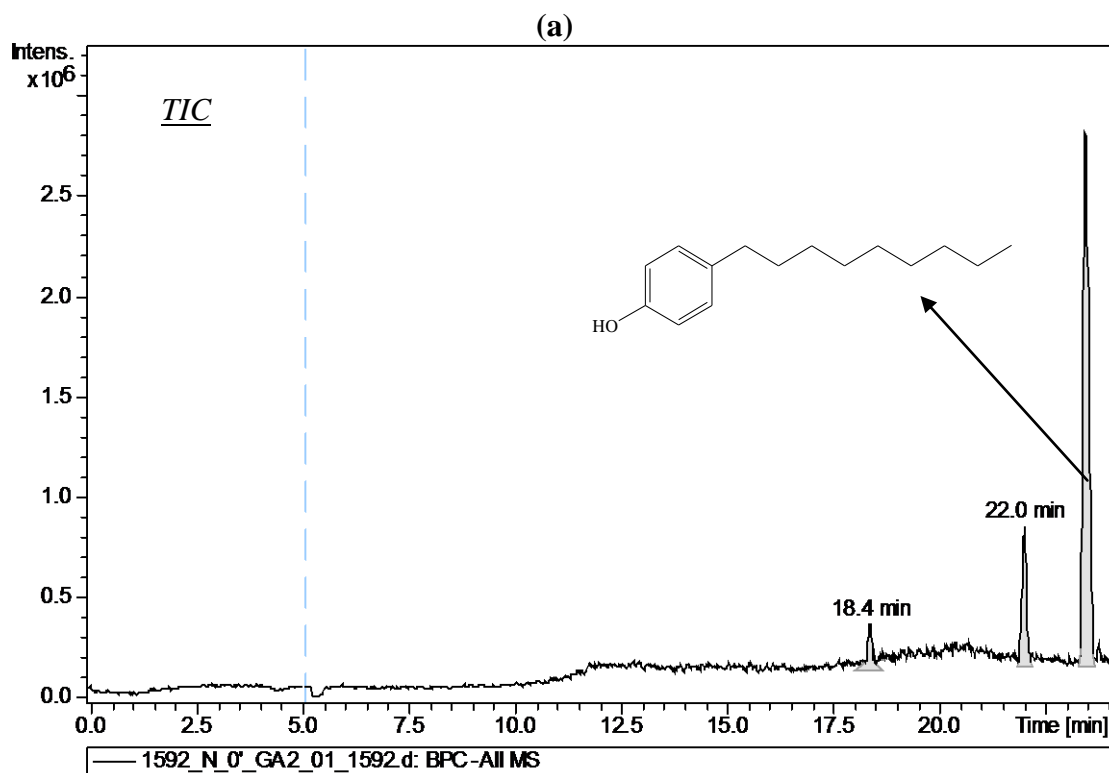


(d)

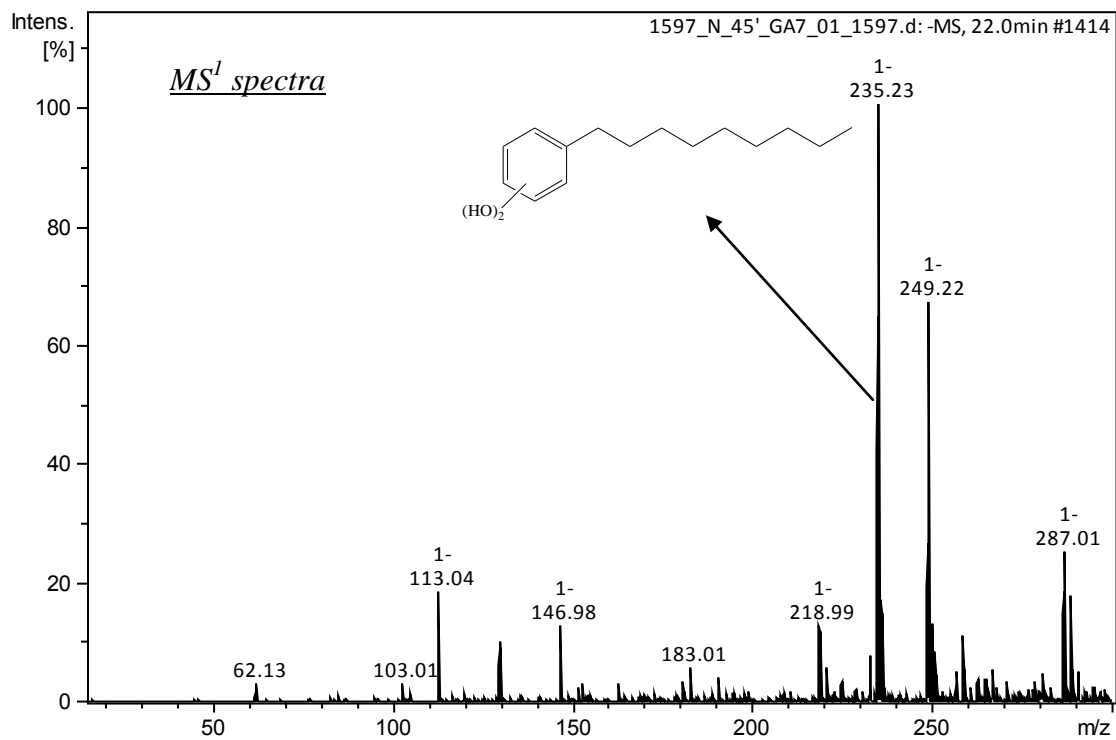
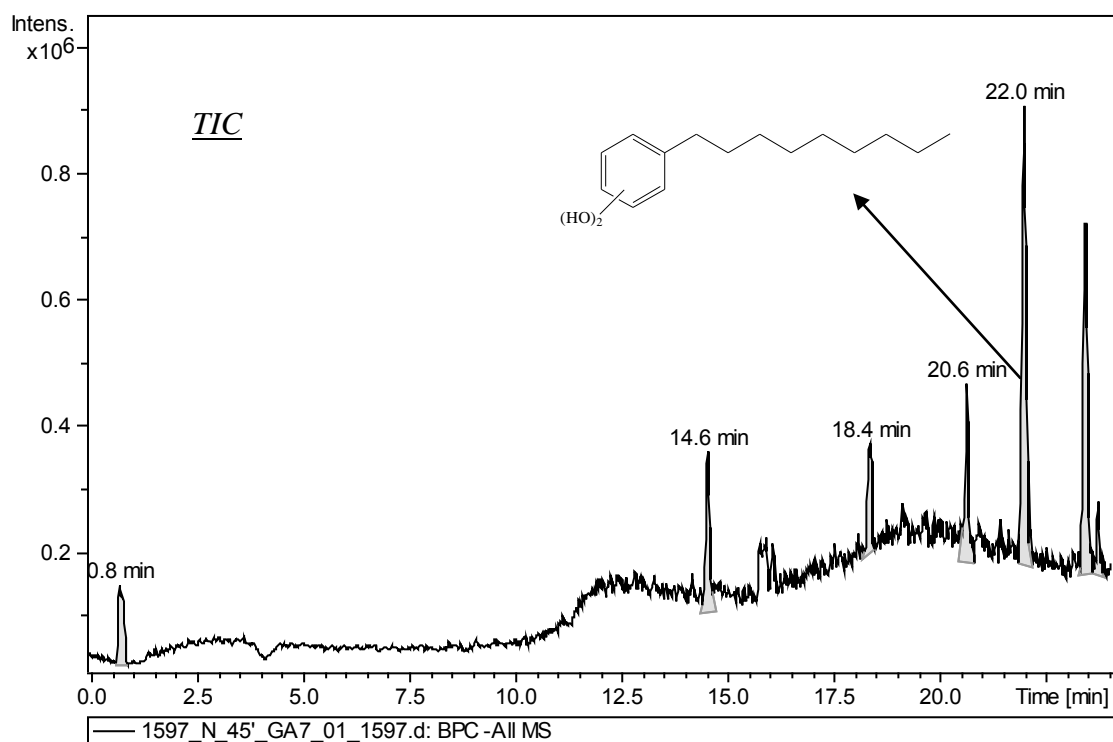


(e)

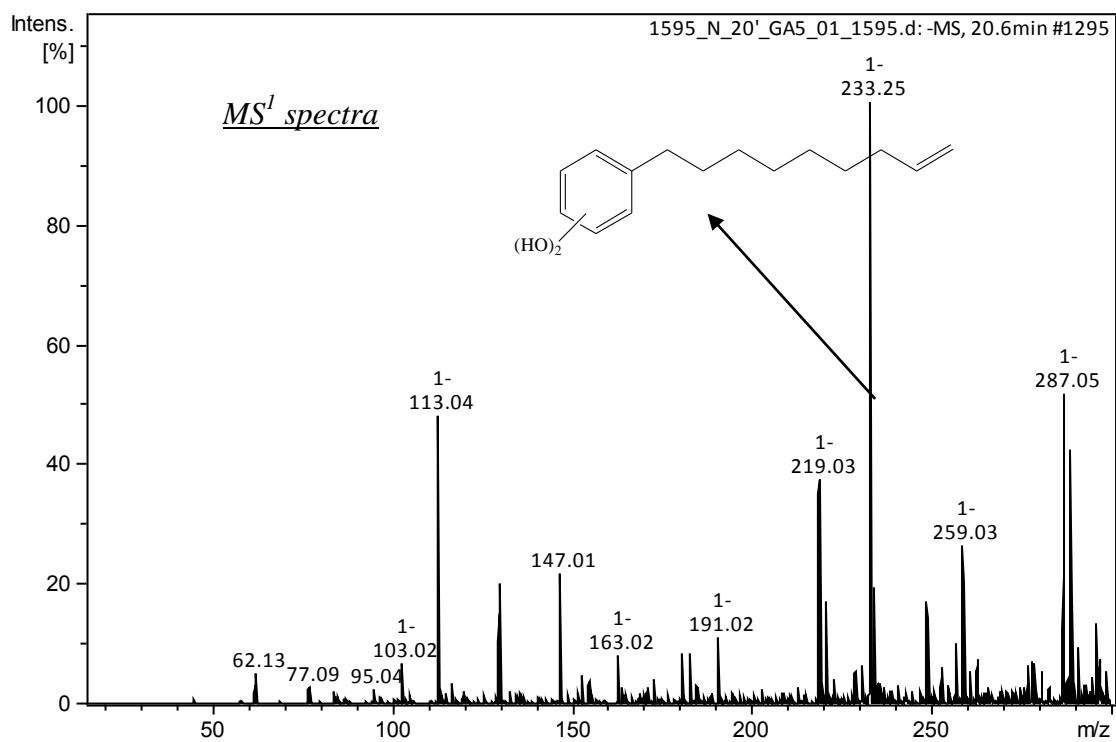
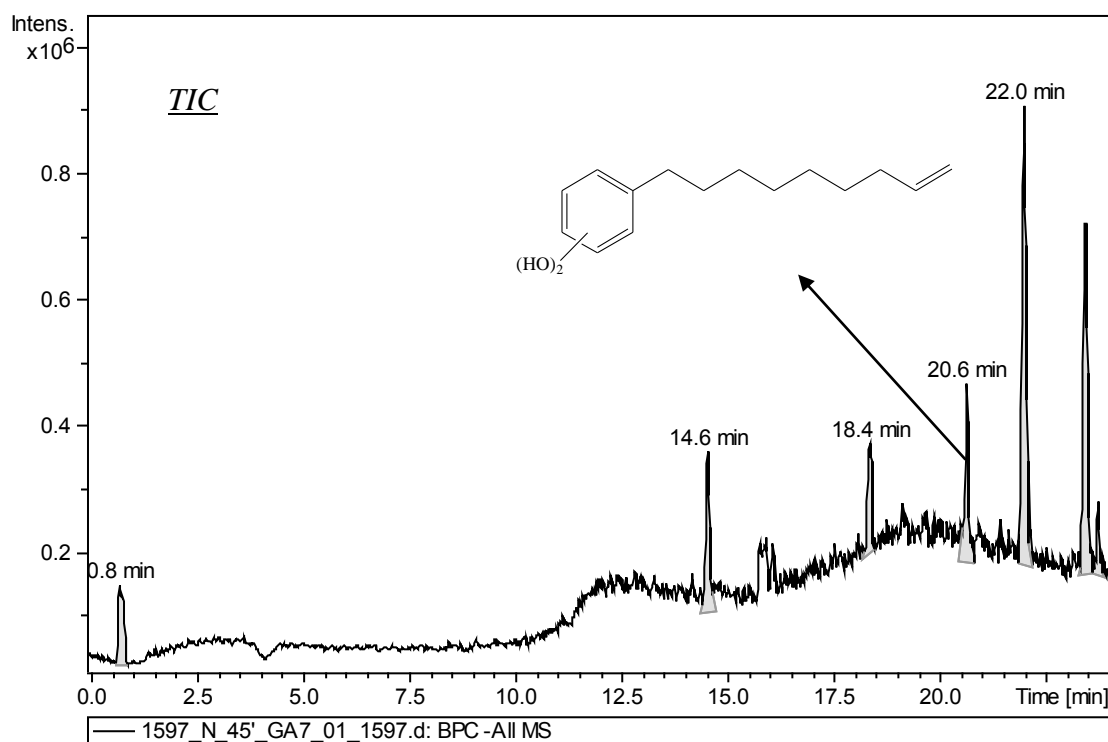


Appendix IV: Mass spectra of NP and its major intermediates

(b)



(c)



References

- (HSDB), H.S.D.B. (2007) <http://toxnet.nlm.nih.gov>.
- Adams, C.D. and Randtke, S.J. (1992) Ozonation by-products of atrazine in synthetic and natural-waters. *Environmental Science & Technology* 26(11), 2218-2227.
- Adeyuyi, Y.G. (2001) Sonochemistry: Environmental science and engineering applications. *Industrial & Engineering Chemistry Research* 40(22), 4681-4715.
- Agullo-Barcelo, M., Polo-Lopez, M.I., Lucena, F., Jofre, J. and Fernandez-Ibanez, P. (2013) Solar Advanced Oxidation Processes as disinfection tertiary treatments for real wastewater: Implications for water reclamation. *Applied Catalysis B-Environmental* 136, 341-350.
- Ahel, M., Scully, F.E., Hoigne, J. and Giger, W. (1994) Photochemical degradation of nonylphenol and nonylphenol polyethoxylates in natural-waters. *Chemosphere* 28(7), 1361-1368.
- Airey, P.L. and Dainton, F.S. (1966) The Photochemistry of Aqueous Solutions of Fe (II). I. Photoelectron Detachment from Ferrous and Ferrocyanide Ions. *Proceedings of the Royal Society of London. Series A, Mathematical and Physical Sciences* 291(1426), 340-352.
- Al-Momani, F., Touraud, E. and Thomas, O. (2004) VUV photolysis of commercial textile dyes: Kinetic study and UV sensitivity. *Afinidad* 61(510), 129-133.
- Argese, E., Marcomini, A., Miana, P., Bettiol, C. and Perin, G. (1994) Submitochondrial particle response to linear alkylbenzene sulfonates, nonylphenol polyethoxylates and their biodegradation derivatives. *Environmental Toxicology and Chemistry* 13(5), 737-742.

- Arnold, S.M., Hickey, W.J. and Harris, R.F. (1995) Degradation of atrazine by fentons reagent - condition optimization and product quantification. *Environmental Science & Technology* 29(8), 2083-2089.
- Ayyildiz, O., Sanik, S. and Ileri, B. (2011) Effect of ultrasonic pretreatment on chlorine dioxide disinfection efficiency. *Ultrasonics Sonochemistry* 18(2), 683-688.
- Babuponnusami, A. and Muthukumar, K. (2012) Advanced oxidation of phenol: A comparison between Fenton, electro-Fenton, sono-electro-Fenton and photo-electro-Fenton processes. *Chemical Engineering Journal* 183, 1-9.
- Bahena, C.L., Martinez, S.S., Guzman, D.M. and Hernandez, M.D.T. (2008) Sonophotocatalytic degradation of alazine and gesaprim commercial herbicides in TiO₂ slurry. *Chemosphere* 71(5), 982-989.
- Bajt, O., Mailhot, G. and Bolte, M. (2001) Degradation of dibutyl phthalate by homogeneous photocatalysis with Fe(III) in aqueous solution. *Applied Catalysis B-Environmental* 33(3), 239-248.
- Bajt, O., Zita, J., Novotna, P., Krysa, J. and Jirkovsky, J. (2008) Photocatalytic degradation of dibutyl phthalate: Effect of catalyst immobilization. *Journal of Solar Energy Engineering-Transactions of the Asme* 130(4).
- Balabanovich, A. and Schnabel, W. (1998) On the photolysis of phthalic acid dimethyl and diethyl ester: a product analysis study. *Journal of Photochemistry and Photobiology a-Chemistry* 113(2), 145-153.
- Belluck, D.A., Benjamin, S.L. and Dawson, T. (1991) Groundwater contamination by atrazine and its metabolites - risk assessment, policy, and legal implications. *Acs Symposium Series* 459, 254-273.
- Bianchi, C.L., Pirola, C., Ragaini, V. and Selli, E. (2006) Mechanism and efficiency of

- atrazine degradation under combined oxidation processes. *Applied Catalysis B-Environmental* 64(1-2), 131-138.
- Bintein, S. and Devillers, J. (1996) Evaluating the environmental fate of atrazine in France. *Chemosphere* 32(12), 2441-2456.
- Borras, N., Oliver, R., Arias, C. and Brillas, E. (2010) Degradation of Atrazine by Electrochemical Advanced Oxidation Processes Using a Boron-Doped Diamond Anode. *Journal of Physical Chemistry A* 114(24), 6613-6621.
- Braterman, P.S., Cairnsmith, A.G., Sloper, R.W., Truscott, T.G. and Craw, M. (1984) Photo-oxidation of iron(ii) in water between pH 7.5 and 4.0. *Journal of the Chemical Society-Dalton Transactions* (7), 1441-1445.
- Brillas, E., Sires, I. and Oturan, M.A. (2009) Electro-Fenton Process and Related Electrochemical Technologies Based on Fenton's Reaction Chemistry. *Chemical Reviews* 109(12), 6570-6631.
- Burbano, A.A., Dionysiou, D.D., Suidan, M.T. and Richardson, T.L. (2005) Oxidation kinetics and effect of pH on the degradation of MTBE with Fenton reagent. *Water Research* 39(1), 107-118.
- Buxton, G.V., Greenstock, C.L., Helman, W.P. and Ross, A.B. (1988) Critical-review of rate constants for reactions of hydrated electrons, hydrogen-atoms and hydroxyl radicals ($\text{OH}^\cdot/\text{O}^\cdot$) in aqueous-solution. *Journal of Physical and Chemical Reference Data* 17(2), 513-886.
- Cesaro, A. and Belgiorno, V. (2013) Sonolysis and ozonation as pretreatment for anaerobic digestion of solid organic waste. *Ultrasonics Sonochemistry* 20(3), 931-936.
- Chainikova, E., Safiullin, R., Spirikhin, L. and Erastov, A. (2013) Synthesis of nitrogen-containing heterocyclic compounds by photooxidation of aromatic azides.

- Tetrahedron Letters 54(17), 2140-2142.
- Chan, K.H. and Chu, W. (2003) Modeling the reaction kinetics of Fenton's process on the removal of atrazine. *Chemosphere* 51(4), 305-311.
- Chan, K.H. and Chu, W. (2005) Atrazine removal by catalytic oxidation processes with or without UV irradiation Part II: an analysis of the reaction mechanisms using LC/ESI-tandem mass spectrometry. *Applied Catalysis B-Environmental* 58(3-4), 165-174.
- Chan, T.W., Graham, N.J.D. and Chu, W. (2010) Degradation of iopromide by combined UV irradiation and peroxydisulfate. *Journal of Hazardous Materials* 181(1-3), 508-513.
- Chan, Y.J., Chong, M.F., Law, C.L. and Hassell, D.G. (2009) A review on anaerobic-aerobic treatment of industrial and municipal wastewater. *Chemical Engineering Journal* 155(1-2), 1-18.
- Chen, C., Yang, S.G., Guo, Y.P., Sun, C., Gu, C.G. and Xu, B. (2009a) Photolytic destruction of endocrine disruptor atrazine in aqueous solution under UV irradiation: Products and pathways. *Journal of Hazardous Materials* 172(2-3), 675-684.
- Chen, Y.H., Chen, L.L. and Shang, N.C. (2009b) Photocatalytic degradation of dimethyl phthalate in an aqueous solution with Pt-doped TiO₂-coated magnetic PMMA microspheres. *Journal of Hazardous Materials* 172(1), 20-29.
- Chen, Y.H., Shang, N.C. and Hsieh, D.C. (2008) Decomposition of dimethyl phthalate in an aqueous solution by ozonation with high silica zeolites and UV radiation. *Journal of Hazardous Materials* 157(2-3), 260-268.
- Chen, Y.L., Ai, Z.H. and Zhang, L.Z. (2012) Enhanced decomposition of dimethyl phthalate via molecular oxygen activated by Fe@Fe₂O₃/AC under microwave

- irradiation. *Journal of Hazardous Materials* 235, 92-100.
- Cheung, J.K.H., Lam, R.K.W., Shi, M.Y. and Gu, J.D. (2007) Environmental fate of endocrine-disrupting dimethyl phthalate esters (DMPE) under sulfate-reducing condition. *Science of the Total Environment* 381(1-3), 126-133.
- Chiha, M., Hamdaoui, O., Baup, S. and Gondrexon, N. (2011) Sonolytic degradation of endocrine disrupting chemical 4-cumylphenol in water. *Ultrasonics Sonochemistry* 18(5), 943-950.
- Chiou, C.S., Chen, Y.H., Chang-Tang, C., Chang, C.Y., Shie, J.L. and Li, Y.S. (2006a) Photochemical mineralization of di-n-butyl phthalate with $\text{H}_2\text{O}_2/\text{Fe}^{3+}$. *Journal of Hazardous Materials* 135(1-3), 344-349.
- Chiou, C.S., Shie, J.L., Chang, C.Y., Liu, C.C. and Chang, C.T. (2006b) Degradation of di-n-butyl phthalate using photoreactor packed with TiO_2 immobilized on glass beads. *Journal of Hazardous Materials* 137(2), 1123-1129.
- Chong, M.N., Sharma, A.K., Burn, S. and Saint, C.P. (2012) Feasibility study on the application of advanced oxidation technologies for decentralised wastewater treatment. *Journal of Cleaner Production* 35, 230-238.
- Chowdhury, P. and Viraraghavan, T. (2009) Sonochemical degradation of chlorinated organic compounds, phenolic compounds and organic dyes - A review. *Science of the Total Environment* 407(8), 2474-2492.
- Chu, W. (2001) Modeling the quantum yields of herbicide 2,4-D decay in UV/ H_2O_2 process. *Chemosphere* 44(5), 935-941.
- Chu, W., Chan, K.H., Kwan, C.Y. and Choi, K.Y. (2007) Degradation of atrazine by modified stepwise-Fenton's processes. *Chemosphere* 67(4), 755-761.
- Chu, W. and Rao, Y.F. (2012) Photocatalytic oxidation of monuron in the suspension of

- WO₃ under the irradiation of UV-visible light. *Chemosphere* 86(11), 1079-1086.
- Chu, W., Wang, Y.R. and Leung, H.F. (2011) Synergy of sulfate and hydroxyl radicals in UV/S₂O₈²⁻/H₂O₂ oxidation of iodinated X-ray contrast medium iopromide. *Chemical Engineering Journal* 178, 154-160.
- Cintas, P. and Luche, J.L. (1999) Green chemistry - The sonochemical approach. *Green Chemistry* 1(3), 115-125.
- Dantas, R.F., Rossiter, O., Teixeira, A.K.R., Simoes, A.S.M. and da Silva, V.L. (2010) Direct UV photolysis of propranolol and metronidazole in aqueous solution. *Chemical Engineering Journal* 158(2), 143-147.
- Dargnat, C., Blanchard, M., Chevreuil, M. and Teil, M.J. (2009) Occurrence of phthalate esters in the Seine River estuary (France). *Hydrological Processes* 23(8), 1192-1201.
- de la Casa-Resino, I., Valdehita, A., Soler, F., Navas, J.M. and Perez-Lopez, M. (2012) Endocrine disruption caused by oral administration of atrazine in European quail (*Coturnix coturnix coturnix*). *Comparative Biochemistry and Physiology C-Toxicology & Pharmacology* 156(3-4), 159-165.
- DeLaat, J., Berger, P., Poinot, T., Leitner, N.K.V. and Dore, M. (1997) Modeling the oxidation of atrazine by H₂O₂/UV. Estimation of kinetic parameters. *Ozone-Science & Engineering* 19(5), 395-408.
- Derco, J., Valickova, M., Silharova, K., Dudas, J. and Luptakova, A. (2013) Removal of selected chlorinated micropollutants by ozonation. *Chemical Papers* 67(12), 1585-1593.
- DSD, H.K.
http://www.dsd.gov.hk/EN/Sewerage/Sewage_Treatment_Facilities/Effluent_Quality_of_Major_Sewage_Treatment_Works/index.html.

- Dukkanci, M. and Gunduz, G. (2006) Ultrasonic degradation of oxalic acid in aqueous solutions. *Ultrasonics Sonochemistry* 13(6), 517-522.
- Duran, A., Monteagudo, J.M., Sanmartin, I. and Gomez, P. (2013) Homogeneous sonophotolysis of food processing industry wastewater: Study of synergistic effects, mineralization and toxicity removal. *Ultrasonics Sonochemistry* 20(2), 785-791.
- Emeline, A.V., Zhang, X., Murakami, T. and Fujishima, A. (2012) Activity and selectivity of photocatalysts in photodegradation of phenols. *Journal of Hazardous Materials* 211, 154-160.
- Esplugas, S., Bila, D.M., Krause, L.G.T. and Dezotti, M. (2007) Ozonation and advanced oxidation technologies to remove endocrine disrupting chemicals (EDCs) and pharmaceuticals and personal care products (PPCPs) in water effluents. *Journal of Hazardous Materials* 149(3), 631-642.
- Fang, J.Y., Ling, L. and Shang, C. (2013) Kinetics and mechanisms of pH-dependent degradation of halonitromethanes by UV photolysis. *Water Research* 47(3), 1257-1266.
- Fernandez-Cegri, V., de la Rubia, M.A., Raposo, F. and Borja, R. (2012) Impact of ultrasonic pretreatment under different operational conditions on the mesophilic anaerobic digestion of sunflower oil cake in batch mode. *Ultrasonics Sonochemistry* 19(5), 1003-1010.
- Field, E.A., Price, C.J., Sleet, R.B., George, J.D., Marr, M.C., Myers, C.B., Schwetz, B.A. and Morrissey, R.E. (1993) Developmental toxicity evaluation of diethyl and dimethyl phthalate in rats. *Teratology* 48(1), 33-44.
- Gao, Y.Q., Gao, N.Y., Deng, Y., Gu, J.S., Gu, Y.L. and Zhang, D. (2013) Factor affecting sonolytic degradation of sulfamethazine in water. *Ultrasonics Sonochemistry* 20(6),

1401-1407.

- Garcia-Lopez, E., Marci, G., Serpone, N. and Hidaka, H. (2007) Photoassisted oxidation of the recalcitrant cyanuric acid substrate in aqueous ZnO suspensions. *Journal of Physical Chemistry C* 111(49), 18025-18032.
- Goel, M., Hu, H.Q., Mujumdar, A.S. and Ray, M.B. (2004) Sonochemical decomposition of volatile and non-volatile organic compounds - a comparative study. *Water Research* 38(19), 4247-4261.
- Gogate, P.R., Mujumdar, S. and Pandit, A.B. (2002) A sonophotochemical reactor for the removal of formic acid from wastewater. *Industrial & Engineering Chemistry Research* 41(14), 3370-3378.
- Gorner, H. (2011) Photoreduction of nitro-1,4-naphthoquinones in solution. *Journal of Photochemistry and Photobiology a-Chemistry* 224(1), 135-140.
- Graymore, M., Stagnitti, F. and Allinson, G. (2001) Impacts of atrazine in aquatic ecosystems. *Environment International* 26(7-8), 483-495.
- Grcic, I., Obradovic, M., Vujevic, D. and Koprivanac, N. (2010) Sono-Fenton oxidation of formic acid/formate ions in an aqueous solution: From an experimental design to the mechanistic modeling. *Chemical Engineering Journal* 164(1), 196-207.
- Guan, Y.H., Ma, J., Li, X.C., Fang, J.Y. and Chen, L.W. (2011) Influence of pH on the Formation of Sulfate and Hydroxyl Radicals in the UV/Peroxymonosulfate System. *Environmental Science & Technology* 45(21), 9308-9314.
- Gultekin, I. and Ince, N.H. (2006) Degradation of aryl-azo-naphthol dyes by ultrasound, ozone and their combination: Effect of alpha-substituents. *Ultrasonics Sonochemistry* 13(3), 208-214.
- Gultekin, I. and Ince, N.H. (2007) Synthetic endocrine disruptors in the environment and

- water remediation by advanced oxidation processes. *Journal of Environmental Management* 85(4), 816-832.
- Gultekin, I., Tezcanli-Guyer, G. and Ince, N.H. (2009) Degradation of 4-n-nonylphenol in Water by 20 kHz Ultrasound. *Journal of Advanced Oxidation Technologies* 12(1), 105-110.
- Gutierrez, M., Henglein, A. and Ibanez, F. (1991) Radical scavenging in the sonolysis of aqueous-solutions of Γ^- , Br^- , and N^{3-} . *Journal of Physical Chemistry* 95(15), 6044-6047.
- Hamdaoui, O. and Naffrechoux, E. (2008) Sonochemical and photosonochemical degradation of 4-chlorophenol in aqueous media. *Ultrasonics Sonochemistry* 15(6), 981-987.
- Hasegawa, K., Ito, T., Maeda, M. and Kagaya, S. (2001) A TiO_2 -suspended continuous flow photoreactor system combined with the separation of TiO_2 particles by coagulation for the photocatalytic degradation of dibutyl phthalate. *Chemistry Letters* (9), 890-891.
- He, H.Z., Yu, J., Chen, G.K., Li, W.Y., He, J.B. and Li, H.S. (2012) Acute toxicity of butachlor and atrazine to freshwater green alga *Scenedesmus obliquus* and cladoceran *Daphnia carinata*. *Ecotoxicology and Environmental Safety* 80, 91-96.
- He, Y.H., Grieser, F. and Ashokkumar, M. (2011) Kinetics and Mechanism for the Sonophotocatalytic Degradation of p-Chlorobenzoic Acid. *Journal of Physical Chemistry A* 115(24), 6582-6588.
- Henglein, A. (1987) Sonochemistry - historical developments and modern aspects. *Ultrasonics* 25(1), 6-16.
- Henglein, A. and Kormann, C. (1985) Scavenging of oh radicals produced in the sonolysis

- of water. *International Journal of Radiation Biology* 48(2), 251-258.
- Hequet, V., Gonzalez, C. and Le Cloirec, P. (2001) Photochemical processes for atrazine degradation: Methodological approach. *Water Research* 35(18), 4253-4260.
- Hiskia, A., Ecke, M., Troupis, A., Kokorakis, A., Hennig, H. and Papaconstantinou, E. (2001) Sonolytic, photolytic, and photocatalytic decomposition of atrazine in the presence of polyoxometalates. *Environmental Science & Technology* 35(11), 2358-2364.
- Hoffmann, M.R., Hua, I. and Hochemer, R. (1996) Application of ultrasonic irradiation for the degradation of chemical contaminants in water. *Ultrasonics Sonochemistry* 3(3), S163-S172.
- Horikoshi, S. and Hidaka, H. (2003) Non-degradable triazine substrates of atrazine and cyanuric acid hydrothermally and in supercritical water under the UV-illuminated photocatalytic cooperation. *Chemosphere* 51(2), 139-142.
- Hua, I., Hochemer, R.H. and Hoffmann, M.R. (1995) Sonolytic hydrolysis of p-nitrophenyl acetate - the role of supercritical water. *Journal of Physical Chemistry* 99(8), 2335-2342.
- Huang, H.B., Leung, D.Y.C., Kwong, P.C.W., Xiong, J. and Zhang, L. (2013) Enhanced photocatalytic degradation of methylene blue under vacuum ultraviolet irradiation. *Catalysis Today* 201, 189-194.
- Huang, R.H., Yan, H.H., Li, L.S., Deng, D.Y., Shu, Y.H. and Zhang, Q.Y. (2011) Catalytic activity of Fe/SBA-15 for ozonation of dimethyl phthalate in aqueous solution. *Applied Catalysis B-Environmental* 106(1-2), 264-271.
- Huang, R.X., Fang, Z.Q., Yan, X.M. and Cheng, W. (2012) Heterogeneous sono-Fenton catalytic degradation of bisphenol A by Fe₃O₄ magnetic nanoparticles under neutral

- condition. *Chemical Engineering Journal* 197, 242-249.
- Hunt, J.P. and Taube, H. (1952) The photochemical decomposition of hydrogen peroxide. quantum yields, tracer and fractionation effects. *Journal of the American Chemical Society (U.S.)* 74, 5999-6002.
- Huston, P.L. and Pignatello, J.J. (1999) Degradation of selected pesticide active ingredients and commercial formulations in water by the photo-assisted Fenton reaction. *Water Research* 33(5), 1238-1246.
- Hwang, A., Na, S., Ha, J. and Khim, J. (2011) Degradation of Diethyl Phthalate by Sono-Fenton Process and its Dependence on the Power Density. *Japanese Journal of Applied Physics* 50(7).
- Igarashi, S. (1976) Spectrophotometric determination of nitrate nitrogen using thymol. *Bunseki Kagaku* 25(1), 62-65.
- Im, J.K., Heo, J., Boateng, L.K., Her, N., Flora, J.R.V., Yoon, J., Zoh, K.D. and Yoon, Y. (2013) Ultrasonic degradation of acetaminophen and naproxen in the presence of single-walled carbon nanotubes. *Journal of Hazardous Materials* 254, 284-292.
- Ince, N.H., Gultekin, I. and Tezcanli-Guyer, G. (2009) Sonochemical destruction of nonylphenol: Effects of pH and hydroxyl radical scavengers. *Journal of Hazardous Materials* 172(2-3), 739-743.
- Inoue, M., Masuda, Y., Okada, F., Sakurai, A., Takahashi, I. and Sakakibara, M. (2008) Degradation of bisphenol A using sonochemical reactions. *Water Research* 42(6-7), 1379-1386.
- Inoue, M., Okada, F., Sakurai, A. and Sakakibara, M. (2006) A new development of dyestuffs degradation system using ultrasound. *Ultrasonics Sonochemistry* 13(4), 313-320.

- Inumaru, K., Murashima, M., Kasahara, T. and Yamanaka, S. (2004) Enhanced photocatalytic decomposition of 4-nonylphenol by surface-organografted TiO₂: a combination of molecular selective adsorption and photocatalysis. *Applied Catalysis B-Environmental* 52(4), 275-280.
- Ji, G.D., Zhang, B.L. and Wu, Y.C. (2012) Combined ultrasound/ozone degradation of carbazole in APG(1214) surfactant solution. *Journal of Hazardous Materials* 225, 1-7.
- Jin, X., Li, Z.F., Xie, L.L., Zhao, Y. and Wang, T.T. (2013) Synergistic effect of ultrasonic pre-treatment combined with UV irradiation for secondary effluent disinfection. *Ultrasonics Sonochemistry* 20(6), 1384-1389.
- Johnston, A.J. and Hocking, P. (1993) Ultrasonically accelerated photocatalytic waste treatment. *Acs Symposium Series* 518, 106-118.
- Jonsson, S. and Baun, A. (2003) Toxicity of mono- and diesters of o-phthalic esters to a crustacean, a green alga, and a bacterium. *Environmental Toxicology and Chemistry* 22(12), 3037-3043.
- Jortner, J. and Stein, G. (1962) The photochemical evolution of hydrogen from aqueous solutions of ferrous ions. Part I. The reaction mechanism at low pH. *The Journal of Physical Chemistry* 66(7), 1258-1264.
- Joseph, C.G., Puma, G.L., Bono, A., Taufiq-Yap, Y.H. and Krishnaiah, D. (2011) Operating parameters and synergistic effects of combining ultrasound and ultraviolet irradiation in the degradation of 2,4,6-trichlorophenol. *Desalination* 276(1-3), 303-309.
- Kaneco, S., Katsumata, H., Suzuki, T. and Ohta, K. (2006) Titanium dioxide mediated photocatalytic degradation of dibutyl phthalate in aqueous solution - kinetics,

- mineralization and reaction mechanism. *Chemical Engineering Journal* 125(1), 59-66.
- Kardos, N. and Luche, J.L. (2001) Sonochemistry of carbohydrate compounds. *Carbohydrate Research* 332(2), 115-131.
- Katsumata, H., Kobayashi, T., Kaneco, S., Suzuki, T. and Ohta, K. (2011) Degradation of linuron by ultrasound combined with photo-Fenton treatment. *Chemical Engineering Journal* 166(2), 468-473.
- Kidak, R. and Ince, N.H. (2006) Effects of operating parameters on sonochemical decomposition of phenol. *Journal of Hazardous Materials* 137(3), 1453-1457.
- Kim, S.J., Park, H.W., Yu, S.Y., Kim, J.S., Ha, J.M., Youn, J.P., An, Y.R., Oh, M.J., Kim, Y.J., Ryu, J.C. and Hwang, S.Y. (2009) Toxicogenomic Effect of Liver-toxic Environmental Chemicals in Human Hepatoma Cell Line. *Molecular & Cellular Toxicology* 5(4), 310-316.
- Kimura, T., Sakamoto, T., Leveque, J.M., Sohmiya, H., Fujita, M., Ikeda, S. and Ando, T. (1996) Standardization of ultrasonic power for sonochemical reaction. *Ultrasonics Sonochemistry* 3(3), S157-S161.
- Kohtani, S., Koshiko, M., Kudo, A., Tokumura, K., Ishigaki, Y., Toriba, A., Hayakawa, K. and Nakagaki, R. (2003) Photodegradation of 4-alkylphenols using BiVO_4 photocatalyst under irradiation with visible light from a solar simulator. *Applied Catalysis B-Environmental* 46(3), 573-586.
- Kondo, K., Murakami, N., Ye, C., Tsubota, T. and Ohno, T. (2013) Development of highly efficient sulfur-doped TiO_2 photocatalysts hybridized with graphitic carbon nitride. *Applied Catalysis B-Environmental* 142, 362-367.
- Ku, Y., Tu, Y.H. and Ma, C.M. (2005) Effect of hydrogen peroxide on the decomposition of

- monochlorophenols by sonolysis in aqueous solution. *Water Research* 39(6), 1093-1098.
- Lahnsteiner, F., Berger, B., Grubinger, F. and Weismann, T. (2005) The effect of 4-nonylphenol on semen quality, viability of gametes, fertilization success, and embryo and larvae survival in rainbow trout (*Oncorhynchus mykiss*). *Aquatic Toxicology* 71(4), 297-306.
- Lau, T.K., Chu, W. and Graham, N. (2005) The degradation of endocrine disruptor di-n-butyl phthalate by UV irradiation: A photolysis and product study. *Chemosphere* 60(8), 1045-1053.
- Lepoint, T. and Mullie, F. (1994) What exactly is cavitation chemistry. *Ultrasonics Sonochemistry* 1(1), S13-S22.
- Lesko, T., Colussi, A.J. and Hoffmann, M.R. (2006) Sonochemical decomposition of phenol: Evidence for a synergistic effect of ozone and ultrasound for the elimination of total organic carbon from water. *Environmental Science & Technology* 40(21), 6818-6823.
- Li, B.Z., Li, L., Lin, K.F., Zhang, W., Lu, S.G. and Luo, Q.S. (2013a) Removal of 1,1,1-trichloroethane from aqueous solution by a sono-activated persulfate process. *Ultrasonics Sonochemistry* 20(3), 855-863.
- Li, H.Y., Qu, J.H. and Liu, H.J. (2006) Removal of a type of endocrine disruptors-di-n-butyl phthalate from water by ozonation. *Journal of Environmental Sciences-China* 18(5), 845-851.
- Li, L.S., Zhu, W.P., Chen, L., Zhang, P.Y. and Chen, Z.Y. (2005) Photocatalytic ozonation of dibutyl phthalate over TiO₂ film. *Journal of Photochemistry and Photobiology a-Chemistry* 175(2-3), 172-177.

- Li, Y.G., Hsieh, W.P., Mahmudov, R., Wei, X.M. and Huang, C.P. (2013b) Combined ultrasound and Fenton (US-Fenton) process for the treatment of ammunition wastewater. *Journal of Hazardous Materials* 244, 403-411.
- Li, Y.X., Duan, X.Y., Li, X.G. and Zhang, D.H. (2013c) Photodegradation of nonylphenol by simulated sunlight. *Marine Pollution Bulletin* 66(1-2), 47-52.
- Li, Z.F., Zhao, X., Deng, F.R., Jin, X. and Wu, H. (2012) *Manufacturing Science and Technology*, Pts 1-8. Fan, W. (ed), pp. 3786-3791.
- Lim, M.H., Kim, S.H., Kim, Y.U. and Khim, J. (2007) Sonolysis of chlorinated compounds in aqueous solution. *Ultrasonics Sonochemistry* 14(2), 93-98.
- Lorimer, J.P. and Mason, T.J. (1987) *Sonochemistry* .1. the physical aspects. *Chemical Society Reviews* 16(2), 239-274.
- Ma, Y.S., Sung, C.F. and Lin, J.G. (2010) Degradation of carbofuran in aqueous solution by ultrasound and Fenton processes: Effect of system parameters and kinetic study. *Journal of Hazardous Materials* 178(1-3), 320-325.
- Madge, B.A. and Jensen, J.N. (2002) Disinfection of wastewater using a 20-kHz ultrasound unit. *Water Environment Research* 74(2), 159-169.
- Mahamuni, N.N. and Adewuyi, Y.G. (2010) Advanced oxidation processes (AOPs) involving ultrasound for waste water treatment: A review with emphasis on cost estimation. *Ultrasonics Sonochemistry* 17(6), 990-1003.
- Malesic, J., Kolar, J., Strlic, M. and Polanc, S. (2006) The influence of halide and pseudo-halide antioxidants in Fenton-like reaction systems. *Acta Chimica Slovenica* 53(4), 450-456.
- Manousaki, E., Psillakis, E., Kalogerakis, N. and Mantzavinos, D. (2004) Degradation of sodium dodecylbenzene sulfonate in water by ultrasonic irradiation. *Water Research*

38(17), 3751-3759.

- Mao, Z., Zheng, X.F., Zhang, Y.Q., Tao, X.X., Li, Y. and Wang, W. (2012) Occurrence and Biodegradation of Nonylphenol in the Environment. *International Journal of Molecular Sciences* 13(1), 491-505.
- Margulis, M.A. (1992) Fundamental-aspects of sonochemistry. *Ultrasonics* 30(3), 152-155.
- Martinez-Zapata, M., Aristizabal, C. and Penuela, G. (2013) Photodegradation of the endocrine-disrupting chemicals 4n-nonylphenol and triclosan by simulated solar UV irradiation in aqueous solutions with Fe(III) and in the absence/presence of humic acids. *Journal of Photochemistry and Photobiology a-Chemistry* 251, 41-49.
- Marusawa, H., Ichikawa, K., Narita, N., Murakami, H., Ito, K. and Tezuka, T. (2002) Hydroxyl radical as a strong electrophilic species. *Bioorganic & Medicinal Chemistry* 10(7), 2283-2290.
- Mason, T.J., Lorimer, J.P. and Bates, D.M. (1992) Quantifying sonochemistry - casting some light on a black art. *Ultrasonics* 30(1), 40-42.
- Medellin-Castillo, N.A., Ocampo-Perez, R., Leyva-Ramos, R., Sanchez-Polo, M., Rivera-Utrilla, J. and Mendez-Diaz, J.D. (2013) Removal of diethyl phthalate from water solution by adsorption, photo-oxidation, ozonation and advanced oxidation process (UV/H₂O₂, O₃/H₂O₂ and O₃/activated carbon). *Science of the Total Environment* 442, 26-35.
- Molkenthin, M., Olmez-Hanci, T., Jekel, M.R. and Arslan-Alaton, I. (2013) Photo-Fenton-like treatment of BPA: Effect of UV light source and water matrix on toxicity and transformation products. *Water Research* 47(14), 5052-5064.
- Monod, A., Chebbi, A., Durand-Jolibois, R. and Carlier, P. (2000) Oxidation of methanol by hydroxyl radicals in aqueous solution under simulated cloud droplet conditions.

- Atmospheric Environment 34(29-30), 5283-5294.
- Morgan, M.S., Vantrieste, P.F., Garlick, S.M., Mahon, M.J. and Smith, A.L. (1988) Ultraviolet molar absorptivities of aqueous hydrogen-peroxide and hydroperoxyl ion. *Analytica Chimica Acta* 215(1-2), 325-329.
- Moumeni, O. and Hamdaoui, O. (2012) Intensification of sonochemical degradation of malachite green by bromide ions. *Ultrasonics Sonochemistry* 19(3), 404-409.
- Mylchreest, E., Sar, M., Cattley, R.C. and Foster, P.M.D. (1999) Disruption of androgen-regulated male reproductive development by Di(n-butyl) phthalate during late gestation in rats is different from flutamide. *Toxicology and Applied Pharmacology* 156(2), 81-95.
- Na, S., Ahn, Y.G., Cui, M. and Khim, J. (2012a) Significant diethyl phthalate (DEP) degradation by combined advanced oxidation process in aqueous solution. *Journal of Environmental Management* 101, 104-110.
- Na, S., Jinhua, C., Cui, M. and Khim, J. (2012b) Sonopholytic diethyl phthalate (DEP) degradation with UVC or VUV irradiation. *Ultrasonics Sonochemistry* 19(5), 1094-1098.
- Naddeo, V., Landi, M., Belgiorno, V. and Napoli, R.M.A. (2009) Wastewater disinfection by combination of ultrasound and ultraviolet irradiation. *Journal of Hazardous Materials* 168(2-3), 925-929.
- Nanzai, B., Okitsu, K., Takenaka, N., Bandow, H. and Maeda, Y. (2008) Sonochemical degradation of various monocyclic aromatic compounds: Relation between hydrophobicities of organic compounds and the decomposition rates. *Ultrasonics Sonochemistry* 15(4), 478-483.
- Neamtu, M. and Frimmel, F.H. (2006) Photodegradation of endocrine disrupting chemical

- nonylphenol by simulated solar UV-irradiation. *Science of the Total Environment* 369(1-3), 295-306.
- Nelieu, S., Kerhoas, L. and Einhorn, J. (2000) Degradation of atrazine into ammeline by combined ozone/hydrogen peroxide treatment in water. *Environmental Science & Technology* 34(3), 430-437.
- Neppolian, B., Kim, Y., Ashokkumar, M., Yamashita, H. and Choi, H. (2010) Preparation and properties of visible light responsive $ZrTiO_4/Bi_2O_3$ photocatalysts for 4-chlorophenol decomposition. *Journal of Hazardous Materials* 182(1-3), 557-562.
- Nikolopoulos, A.N., Igglessi-Markopoulou, O. and Papayannakos, N. (2006) Ultrasound assisted catalytic wet peroxide oxidation of phenol: kinetics and intraparticle diffusion effects. *Ultrasonics Sonochemistry* 13(1), 92-97.
- Ning, B., Graham, N.J.D. and Lickiss, P.D. (2009) A comparison of ultrasound-based advanced oxidation processes for the removal of X-ray contrast media. *Water Science and Technology* 60(9), 2383-2390.
- Ning, B., Graham, N.J.D. and Zhang, Y.P. (2007a) Degradation of octylphenol and nonylphenol by ozone - Part I: Direct reaction. *Chemosphere* 68(6), 1163-1172.
- Ning, B., Graham, N.J.D. and Zhang, Y.P. (2007b) Degradation of octylphenol and nonylphenol by ozone - Part II: Indirect reaction. *Chemosphere* 68(6), 1173-1179.
- Ninomiya, K., Takamatsu, H., Onishi, A., Takahashi, K. and Shimizu, N. (2013) Sonocatalytic-Fenton reaction for enhanced OH radical generation and its application to lignin degradation. *Ultrasonics Sonochemistry* 20(4), 1092-1097.
- O'Sullivan, D.W. and Tyree, M. (2007) The kinetics of complex formation between Ti(IV) and hydrogen peroxide. *International Journal of Chemical Kinetics* 39(8), 457-461.
- Okitsu, K., Iwasaki, K., Yobiko, Y., Bandow, H., Nishimura, R. and Maeda, Y. (2005)

- Sonochemical degradation of azo dyes in aqueous solution: a new heterogeneous kinetics model taking into account the local concentration of OH radicals and azo dyes. *Ultrasonics Sonochemistry* 12(4), 255-262.
- Orton, F., Lutz, I., Kloas, W. and Routledge, E.J. (2009) Endocrine Disrupting Effects of Herbicides and Pentachlorophenol: In Vitro and in Vivo Evidence. *Environmental Science & Technology* 43(6), 2144-2150.
- Oturan, N., Brillas, E. and Oturan, M.A. (2012) Unprecedented total mineralization of atrazine and cyanuric acid by anodic oxidation and electro-Fenton with a boron-doped diamond anode. *Environmental Chemistry Letters* 10(2), 165-170.
- Pang, Y.L., Abdullah, A.Z. and Bhatia, S. (2011) Review on sonochemical methods in the presence of catalysts and chemical additives for treatment of organic pollutants in wastewater. *Desalination* 277(1-3), 1-14.
- Park, J.S., Her, N.G. and Yoon, Y. (2011) Sonochemical Degradation of Chlorinated Phenolic Compounds in Water: Effects of Physicochemical Properties of the Compounds on Degradation. *Water Air and Soil Pollution* 215(1-4), 585-593.
- Pelizzetti, E., Maurino, V., Minero, C., Carlin, V., Pramauro, E., Zerbinati, O. and Tosato, M.L. (1990) Photocatalytic degradation of atrazine and other s-triazine herbicides. *Environmental Science & Technology* 24(10), 1559-1565.
- Peller, J., Wiest, O. and Kamat, P.V. (2003) Synergy of combining sonolysis and photocatalysis in the degradation and mineralization of chlorinated aromatic compounds. *Environmental Science & Technology* 37(9), 1926-1932.
- Perez, M.H., Penuela, G., Maldonado, M.I., Malato, O., Fernandez-Ibanez, P., Oller, I., Gernjak, W. and Malato, S. (2006) Degradation of pesticides in water using solar advanced oxidation processes. *Applied Catalysis B-Environmental* 64(3-4), 272-281.

- Petrier, C., David, B. and Laguian, S. (1996) Ultrasonic degradation at 20 khz and 500 khz of atrazine and pentachlorophenol in aqueous solution: Preliminary results. *Chemosphere* 32(9), 1709-1718.
- Petrier, C. and Francony, A. (1997) Ultrasonic waste-water treatment: incidence of ultrasonic frequency on the rate of phenol and carbon tetrachloride degradation. *Ultrasonics Sonochemistry* 4(4), 295-300.
- Petrier, C., Lamy, M.F., Francony, A., Benahcene, A., David, B., Renaudin, V. and Gondrexon, N. (1994) Sonochemical degradation of phenol in dilute aqueous-solutions - comparison of the reaction-rates at 20-khz and 487-khz. *Journal of Physical Chemistry* 98(41), 10514-10520.
- Phyu, Y.L., Palmer, C.G., Warne, M.S., Dowse, R., Mueller, S., Chapman, J., Hose, G.C. and Lim, R.P. (2013) Assessing the Chronic Toxicity of Atrazine, Permethrin, and Chlorothalonil to the Cladoceran *Ceriodaphnia cf. dubia* in Laboratory and Natural River Water. *Archives of Environmental Contamination and Toxicology* 64(3), 419-426.
- Pignatello, J.J., Oliveros, E. and MacKay, A. (2006) Advanced oxidation processes for organic contaminant destruction based on the Fenton reaction and related chemistry. *Critical Reviews in Environmental Science and Technology* 36(1), 1-84.
- Pilli, S., Bhunia, P., Yan, S., LeBlanc, R.J., Tyagi, R.D. and Surampalli, R.Y. (2011) Ultrasonic pretreatment of sludge: A review. *Ultrasonics Sonochemistry* 18(1), 1-18.
- Psillakis, E., Mantzavinos, D. and Kalogerakis, N. (2004) Monitoring the sonochemical degradation of phthalate esters in water using solid-phase microextraction. *Chemosphere* 54(7), 849-857.
- Quang, C.Y., Kocan, G., Tang, D., Fast, D.M. and Michael, S.M. (2006) Development of an

- LC-ESI-MS-MS method with formate anion attachment for detecting neutral molecules in rat plasma. *American Laboratory* 38(10), 26-+.
- Rahman, M.F., Yanful, E.K., Jasim, S.Y., Bragg, L.M., Servos, M.R., Ndiougue, S. and Borikar, D. (2010) Advanced Oxidation Treatment of Drinking Water: Part I. Occurrence and Removal of Pharmaceuticals and Endocrine-Disrupting Compounds from Lake Huron Water. *Ozone-Science & Engineering* 32(4), 217-229.
- Rao, Y.F. and Chu, W. (2009) Reaction Mechanism of Linuron Degradation in TiO₂ Suspension under Visible Light Irradiation with the Assistance of H₂O₂. *Environmental Science & Technology* 43(16), 6183-6189.
- Rao, Y.F. and Chu, W. (2010) Degradation of linuron by UV, ozonation, and UV/O₃ processes-Effect of anions and reaction mechanism. *Journal of Hazardous Materials* 180(1-3), 514-523.
- Rao, Y.F. and Chu, W. (2013) Visible Light-Induced Photodegradation of Simazine in Aqueous TiO₂ Suspension. *Industrial & Engineering Chemistry Research* 52(38), 13580-13586.
- Ren, Y.M., Dong, Q., Feng, J., Ma, J., Wen, Q. and Zhang, M.L. (2012) Magnetic porous ferrosinell NiFe₂O₄: A novel ozonation catalyst with strong catalytic property for degradation of di-n-butyl phthalate and convenient separation from water. *Journal of Colloid and Interface Science* 382, 90-96.
- Rong, L., Yasuda, K., Nakamura, M., Kato, N., Kawakami, K. and Kitaide, Y. (2003) Decomposition of p-chlorophenol in aqueous solution by combination of ultrasound and ultraviolet light. *Journal of Chemical Engineering of Japan* 36(9), 1045-1049.
- Sadik, W. and Shama, G. (2002) UV-induced decolourization of an azo dye by homogeneous advanced oxidation processes. *Process Safety and Environmental*

- Protection 80(B6), 312-316.
- Segura, Y., Molina, R., Martinez, F. and Melero, J.A. (2009) Integrated heterogeneous sono-photo Fenton processes for the degradation of phenolic aqueous solutions. *Ultrasonics Sonochemistry* 16(3), 417-424.
- Serpone, N. and Colarusso, P. (1994) Sonochemistry .1. effects of ultrasounds on heterogeneous chemical-reactions - a useful tool to generate radicals and to examine reaction-mechanisms. *Research on Chemical Intermediates* 20(6), 635-679.
- Servant, G., Laborde, J.L., Hita, A., Caltagirone, J.P. and Gerard, A. (2001) Spatio-temporal dynamics of cavitation bubble clouds in a low frequency reactor: comparison between theoretical and experimental results. *Ultrasonics Sonochemistry* 8(3), 163-174.
- Seymour, J.D. and Gupta, R.B. (1997) Oxidation of aqueous pollutants using ultrasound: Salt-induced enhancement. *Industrial & Engineering Chemistry Research* 36(9), 3453-3457.
- Shang, D.Y., Macdonald, R.W. and Ikonomou, M.G. (1999) Persistence of nonylphenol ethoxylate surfactants and their primary degradation products in sediments from near a municipal outfall in the strait of Georgia, British Columbia, Canada. *Environmental Science & Technology* 33(9), 1366-1372.
- Sharma, V.K., Graham, N.J.D., Li, X.Z. and Yuan, B.L. (2010) Ferrate(VI) enhanced photocatalytic oxidation of pollutants in aqueous TiO₂ suspensions. *Environmental Science and Pollution Research* 17(2), 453-461.
- Shawaqfeh, A.T. and Al Momani, F.A. (2010) Photocatalytic treatment of water soluble pesticide by advanced oxidation technologies using UV light and solar energy. *Solar Energy* 84(7), 1157-1165.

- Shen, O.X., Du, G.Z., Sun, H., Wu, W., Jiang, Y., Song, L. and Wang, X.R. (2009) Comparison of in vitro hormone activities of selected phthalates using reporter gene assays. *Toxicology Letters* 191(1), 9-14.
- Short, P. and Colborn, T. (1999) Pesticide use in the US and policy implications: A focus on herbicides. *Toxicology and Industrial Health* 15(1-2), 240-275.
- Sivakumar, M. and Gedanken, A. (2004) Insights into the sonochemical decomposition of Fe(CO)(5): theoretical and experimental understanding of the role of molar concentration and power density on the reaction yield. *Ultrasonics Sonochemistry* 11(6), 373-378.
- Snyder, S.A., Westerhoff, P., Yoon, Y. and Sedlak, D.L. (2003) Pharmaceuticals, personal care products, and endocrine disruptors in water: Implications for the water industry. *Environmental Engineering Science* 20(5), 449-469.
- Soares, A., Guieysse, B., Jefferson, B., Cartmell, E. and Lester, J.N. (2008) Nonylphenol in the environment: A critical review on occurrence, fate, toxicity and treatment in wastewaters. *Environment International* 34(7), 1033-1049.
- Song, W.H., Teshiba, T., Rein, K. and O'Shea, K.E. (2005) Ultrasonically induced degradation and detoxification of microcystin-LR (cyanobacterial toxin). *Environmental Science & Technology* 39(16), 6300-6305.
- Soto, A.M., Justicia, H., Wray, J.W. and Sonnenschein, C. (1991) Para-nonyl-phenol - an estrogenic xenobiotic released from modified polystyrene. *Environmental Health Perspectives* 92, 167-173.
- Souza, F.L., Saez, C., Canizares, P., Motheo, A.J. and Rodrigo, M.A. (2013) Sonoelectrolysis of Wastewaters Polluted with Dimethyl Phthalate. *Industrial & Engineering Chemistry Research* 52(28), 9674-9682.

- Stackelberg, P.E., Gibs, J., Furlong, E.T., Meyer, M.T., Zaugg, S.D. and Lippincott, R.L. (2007) Efficiency of conventional drinking-water-treatment processes in removal of pharmaceuticals and other organic compounds. *Science of the Total Environment* 377(2-3), 255-272.
- Staples, A., Adams, W.J., Parkerton, T.F., Gorsuch, J.W., Biddinger, G.R. and Reinert, K.H. (1997a) Aquatic toxicity of eighteen phthalate esters. *Environmental Toxicology and Chemistry* 16(5), 875-891.
- Staples, C.A., Guinn, R., Kramarz, K. and Lampi, M. (2011) Assessing the Chronic Aquatic Toxicity of Phthalate Ester Plasticizers. *Human and Ecological Risk Assessment* 17(5), 1057-1076.
- Staples, C.A., Peterson, D.R., Parkerton, T.F. and Adams, W.J. (1997b) The environmental fate of phthalate esters: A literature review. *Chemosphere* 35(4), 667-749.
- Stock, N.L., Peller, J., Vinodgopal, K. and Kamat, P.V. (2000) Combinative sonolysis and photocatalysis for textile dye degradation. *Environmental Science & Technology* 34(9), 1747-1750.
- SUN Shiping, Xing Darong, Zhang Lan, Ai Younian, Fu Xuehong and Qingjuan, Z. (2007) Determination of nitrate-N in water by 2-isopropyl-5-methylphenol spectrophotometry. *Journal of Environment and Health* 24(4), 256-257.
- Suslick, K.S. (1990) Sonochemistry. *Science* 247(4949), 1439-1445.
- Suslick, K.S., Hammerton, D.A. and Cline, R.E. (1986) The sonochemical hot-spot. *Journal of the American Chemical Society* 108(18), 5641-5642.
- Taherian, S., Entezari, M.H. and Ghows, N. (2013) Sono-catalytic degradation and fast mineralization of p-chlorophenol: $\text{La}_{0.7}\text{Sr}_{0.3}\text{MnO}_3$ as a nano-magnetic green catalyst. *Ultrasonics Sonochemistry* 20(6), 1419-1427.

- Tappin, A.D., Loughnane, J.P., McCarthy, A.J. and Fitzsimons, M.F. (2012) Removal of atrazine from river waters by indigenous microorganisms. *Environmental Chemistry Letters* 10(1), 89-96.
- Tay, K.S., Rahman, N.A. and Bin Abas, M.R. (2011) Fenton degradation of dialkylphthalates: products and mechanism. *Environmental Chemistry Letters* 9(4), 539-546.
- Ternes, T.A. (1998) Occurrence of drugs in German sewage treatment plants and rivers. *Water Research* 32(11), 3245-3260.
- Thompson, L.H. and Doraiswamy, L.K. (1999) Sonochemistry: Science and engineering. *Industrial & Engineering Chemistry Research* 38(4), 1215-1249.
- Torrents, A., Anderson, B.G., Bilbouljian, S., Johnson, W.E. and Hapeman, C.J. (1997) Atrazine photolysis: Mechanistic investigations of direct and nitrate mediated hydroxy radical processes and the influence of dissolved organic carbon from the Chesapeake Bay. *Environmental Science & Technology* 31(5), 1476-1482.
- Torres, R.A., Petrier, C., Combet, E., Carrier, M. and Pulgarin, C. (2008) Ultrasonic cavitation applied to the treatment of bisphenol A. Effect of sonochemical parameters and analysis of BPA by-products. *Ultrasonics Sonochemistry* 15(4), 605-611.
- Torres, R.A., Petrier, C., Combet, E., Moulet, F. and Pulgarin, C. (2007) Bisphenol A mineralization by integrated ultrasound-UV-iron (II) treatment. *Environmental Science & Technology* 41(1), 297-302.
- U.S. Environmental Protection Agency, E.
http://www.epa.gov/pesticides/reregistration/atrazine/atrazine_update.htm#cancer.
- U.S. Environmental Protection Agency, E. (1997) Special report on environmental

- endocrine disruption: an effects assessment and analysis. Washington, D.C. Office of Research and Development, EPA/630/R-696/012.
- U.S. Environmental Protection Agency, U.S.E. (1999a) Integrated Risk Information System (IRIS) on Di-n-butyl Phthalate. National Center for Environmental Assessment, Office of Research and Development Washington, DC.
- U.S. Environmental Protection Agency, U.S.E. (1999b) Integrated Risk Information System (IRIS) on Dimethyl Phthalate. National Center for Environmental Assessment, Office of Research and Development Washington, DC.
- USNLM United States National Library of Medicine. <http://toxnet.nlm.nih.gov/>.
- Vieno, N.M., Harkki, H., Tuhkanen, T. and Kronberg, L. (2007) Occurrence of pharmaceuticals in river water and their elimination a pilot-scale drinking water treatment plant. *Environmental Science & Technology* 41(14), 5077-5084.
- Vincent, M.D. and Sneddon, J. (2009) Nonylphenol: An overview and its determination in oysters and wastewaters and preliminary degradation results from laboratory experiments. *Microchemical Journal* 92(1), 112-118.
- Wagner, I., Strehlow, H. and Busse, G. (1980) Flash-photolysis of nitrate ions in aqueous-solution. *Zeitschrift Fur Physikalische Chemie-Wiesbaden* 123(1), 1-33.
- Wang, J.L. and Xu, L.J. (2012) Advanced Oxidation Processes for Wastewater Treatment: Formation of Hydroxyl Radical and Application. *Critical Reviews in Environmental Science and Technology* 42(3), 251-325.
- Wang, Y., Hu, H.Y., Zhao, M.M., Zhao, J.S., Yin, D.D., Sun, X.F., Liu, S.Y., Gao, Q.H., Yu, L.F. and Hao, L.Y. (2013) Nonylphenol disrupts the cardio-protective effects of 17 beta-estradiol on ischemia/reperfusion injury in isolated hearts of guinea pig. *Journal of Toxicological Sciences* 38(5), 731-740.

- Wayne, C.E. and Wayne, R.P. (1996) *Photochemistry*, Oxford University Press, Oxford ; New York.
- Weavers, L.K., Malmstadt, N. and Hoffmann, M.R. (2000) Kinetics and mechanism of pentachlorophenol degradation by sonication, ozonation, and sonolytic ozonation. *Environmental Science & Technology* 34(7), 1280-1285.
- Wen, G., Ma, J., Liu, Z.Q. and Zhao, L. (2011) Ozonation kinetics for the degradation of phthalate esters in water and the reduction of toxicity in the process of O₃/H₂O₂. *Journal of Hazardous Materials* 195, 371-377.
- Wols, B.A. and Hofman-Caris, C.H.M. (2012) Review of photochemical reaction constants of organic micropollutants required for UV advanced oxidation processes in water. *Water Research* 46(9), 2815-2827.
- Wong, C.C. and Chu, W. (2003) The direct photolysis and photocatalytic degradation of alachlor at different TiO₂ and UV sources. *Chemosphere* 50(8), 981-987.
- Wu, H., Li, Z.F., Jin, X., Zhao, X. and Deng, F.R. (2012) *Materials Science and Information Technology*, Pts 1-8. Zhang, C.S. (ed), pp. 4751-4756.
- Wu, Z.L. and Ondruschka, B. (2005) Roles of hydrophobicity and volatility of organic substrates on sonolytic kinetics in aqueous solutions. *Journal of Physical Chemistry A* 109(29), 6521-6526.
- Xiong, S.F., Yin, Z.L., Yuan, Z.F., Yana, W.B., Yang, W.Y., Liu, J.J. and Zhang, F. (2012) Dual-frequency (20/40 kHz) ultrasonic assisted photocatalysis for degradation of methylene blue effluent: Synergistic effect and kinetic study. *Ultrasonics Sonochemistry* 19(4), 756-761.
- Xu, B., Gao, N.Y., Cheng, H.F., Xia, S.J., Rui, M. and Zhao, D.D. (2009a) Oxidative degradation of dimethyl phthalate (DMP) by UV/H₂O₂ process. *Journal of*

- Hazardous Materials 162(2-3), 954-959.
- Xu, B., Gao, N.Y., Cheng, H.F., Xia, S.J., Rui, M. and Zhao, D.D. (2009b) Oxidative degradation of dimethyl phthalate (DMP) by UV/H₂O₂ process. *Journal of Hazardous Materials* 162(2-3), 954-959.
- Xu, L., Yang, X., Guo, Y.H., Ma, F.Y., Guo, Y.N., Yuan, X. and Huo, M.X. (2010a) Simulated sunlight photodegradation of aqueous phthalate esters catalyzed by the polyoxotungstate/titania nanocomposite. *Journal of Hazardous Materials* 178(1-3), 1070-1077.
- Xu, L.J., Chu, W. and Graham, N. (2013a) Sonophotolytic degradation of dimethyl phthalate without catalyst: Analysis of the synergistic effect and modeling. *Water Research* 47(6), 1996-2004.
- Xu, L.J., Chu, W. and Graham, N. (2013b) A systematic study of the degradation of dimethyl phthalate using a high-frequency ultrasonic process. *Ultrasonics Sonochemistry* 20(3), 892-899.
- Xu, L.J., Chu, W. and Graham, N. (2014) Degradation of di-n-butyl phthalate by a homogeneous sono-photo-Fenton process with in situ generated hydrogen peroxide. *Chemical Engineering Journal* 240(0), 541-547.
- Xu, X.R., Li, H.B. and Gu, J.D. (2007) Photocatalytic reduction of hexavalent chromium and degradation of di-N-butyl phthalate in aqueous TiO₂ suspensions under ultraviolet light irradiation. *Environmental Technology* 28(9), 1055-1061.
- Xu, Z.W., Zhang, W.M., Lv, L., Pan, B.C., Lan, P. and Zhang, Q.X. (2010b) A New Approach to Catalytic Degradation of Dimethyl Phthalate by a Macroporous OH-Type Strongly Basic Anion Exchange Resin. *Environmental Science & Technology* 44(8), 3130-3135.

- Yan, H.H., Lu, P., Pan, Z.Q., Wang, X., Zhang, Q.Y. and Li, L.S. (2013) Ce/SBA-15 as a heterogeneous ozonation catalyst for efficient mineralization of dimethyl phthalate. *Journal of Molecular Catalysis a-Chemical* 377, 57-64.
- Yanagisawa, I., Oyama, T., Serponet, N. and Hidaka, H. (2008) Successful Scission of a Recalcitrant Triazinic Ring. The Photoassisted Total Breakup of Cyanuric Acid in Ozonized TiO₂ Aqueous Dispersions in the Presence of an Electron Acceptor (H₂O₂). *Journal of Physical Chemistry C* 112(46), 18125-18133.
- Yim, B., Nagata, Y. and Maeda, Y. (2002) Sonolytic degradation of phthalic acid esters in aqueous solutions. Acceleration of hydrolysis by sonochemical action. *Journal of Physical Chemistry A* 106(1), 104-107.
- Yin, X., Han, P.F., Lu, X.P. and Wang, Y.R. (2004) A review on the dewaterability of bio-sludge and ultrasound pretreatment. *Ultrasonics Sonochemistry* 11(6), 337-348.
- Ying, G.G., Williams, B. and Kookana, R. (2002) Environmental fate of alkylphenols and alkylphenol ethoxylates - a review. *Environment International* 28(3), 215-226.
- Yuan, B.L., Li, X.Z. and Graham, N. (2008a) Aqueous oxidation of dimethyl phthalate in a Fe(VI)-TiO₂-UV reaction system. *Water Research* 42(6-7), 1413-1420.
- Yuan, B.L., Li, X.Z. and Graham, N. (2008b) Reaction pathways of dimethyl phthalate degradation in TiO₂-UV-O₂ and TiO₂-UV-Fe(VI) systems. *Chemosphere* 72(2), 197-204.
- Yuan, R.X., Ramjaun, S.N., Wang, Z.H. and Liu, J.S. (2012) Photocatalytic degradation and chlorination of azo dye in saline wastewater: Kinetics and AOX formation. *Chemical Engineering Journal* 192, 171-178.
- Zaviska, F., Drogui, P., El Hachemi, E.M. and Naffrechoux, E. (2014) Effect of nitrate ions on the efficiency of sonophotochemical phenol degradation. *Ultrasonics*

- Sonochemistry 21(1), 69-75.
- Zepp, R.G., Hoigne, J. and Bader, H. (1987) Nitrate-induced photooxidation of trace organic-chemicals in water. *Environmental Science & Technology* 21(5), 443-450.
- Zhai, Q.Q., Bo, T. and Hu, G.X. (2011) High photoactive and visible-light responsive graphene/titanate nanotubes photocatalysts: Preparation and characterization. *Journal of Hazardous Materials* 198, 78-86.
- Zhang, W.J., Bai, J.W. and Li, R.Y. (2010) *Environment Materials and Environment Management* Pts 1-3. Du, Z.Y. and Sun, X.B. (eds), pp. 2158-2161.
- Zhao, L., Ma, J. and Zhai, X.D. (2010) Enhanced mechanism of catalytic ozonation by ultrasound with orthogonal dual frequencies for the degradation of nitrobenzene in aqueous solution. *Ultrasonics Sonochemistry* 17(1), 84-91.
- Zhao, X.K., Yang, G.P., Wang, Y.J. and Gao, X.C. (2004) Photochemical degradation of dimethyl phthalate by Fenton reagent. *Journal of Photochemistry and Photobiology a-Chemistry* 161(2-3), 215-220.
- Zhao, Y., Li, Z.F. and Zhang, Y. (2013) *Progress in Environmental Science and Engineering*, Pts 1-4. Xu, Q.J., Ju, Y.H. and Ge, H.H. (eds), pp. 1735-1738.